

# Cladding Embrittlement during Postulated Loss-of-Coolant Accidents

Manuscript Completed: May 20, 2008 DRAFT  
Date Published:

Prepared by  
Michael Billone, Yong Yan, Tatiana Burtseva, Rob Daum

Nuclear Engineering Division  
Argonne National Laboratory  
9700 South Cass Avenue  
Argonne, IL 60439

H. Scott, NRC Project Manager

**Prepared for**  
**Division of Fuel, Engineering and Radiological Research**  
**Office of Nuclear Regulatory Research**  
**U. S. Nuclear Regulatory Commission**  
**Washington, DC 20555**  
**NRC JCN N6281**



DRAFT

This page is intentionally left blank.

## Abstract

---

The effect of fuel burnup on the embrittlement of various cladding alloys was examined with laboratory tests conducted under conditions relevant to loss-of-coolant accidents (LOCAs). The cladding materials tested were Zircaloy-4, Zircaloy-2, ZIRLO, M5, and E110. Tests were performed with specimens sectioned from as-fabricated cladding, from prehydrided (surrogate for high-burnup) cladding, and from high-burnup fuel rods which had been irradiated in commercial reactors. The tests were designed to determine for each cladding material the ductile-to-brittle transition as a function of steam oxidation temperature, weight gain due to oxidation, hydrogen content, pre-transient cladding thickness, and pre-transient corrosion-layer thickness. For short, defueled cladding specimens oxidized at 1000-1200°C, ring compression tests were performed to determine post-quench ductility at  $\leq 135^\circ\text{C}$ . The effect of breakaway oxidation on embrittlement was also examined for short specimens oxidized at 800-1000°C. Among other findings, embrittlement was found to be sensitive to fabrication processes – especially surface finish – but insensitive to alloy constituents for these dilute zirconium alloys used as cladding materials. It was also demonstrated that burnup effects on embrittlement are largely due to hydrogen that is absorbed in the cladding during normal operation. Some tests were also performed with longer, fueled-and-pressurized cladding segments subjected to LOCA-relevant heating and cooling rates. Recommendations are given for types of tests that would identify LOCA conditions under which embrittlement would occur.

DRAFT

This page is intentionally left blank.

## Foreword

---

Fuel rod cladding is the first barrier for retention of fission products, and the structural integrity of the cladding ensures coolable core geometry. In the early 1990s, new data from foreign research programs showed degraded cladding behavior for high-burnup fuel under certain postulated accident conditions. It thus became clear that extrapolation from a low-burnup data base needed to be reassessed for regulatory purposes.

One of NRC's central regulations used in plant licensing deals with postulated loss-of-coolant accidents (LOCAs); a portion of that regulation was based on data from unirradiated cladding material. The regulations in 10 CFR 50.46(b) specify criteria derived from tests with unirradiated Zircaloy cladding to limit the peak cladding temperature and the maximum cladding oxidation. These two limits are known as embrittlement criteria. Their purpose is to prevent cladding embrittlement during a LOCA, thus ensuring that the general core geometry will be maintained and be coolable.

In the mid-1990s, NRC sponsored a cooperative research program at Argonne National Laboratory to reassess these limits for the possible effects of fuel burnup. The program's industry partners included the Electric Power Research Institute, Framatome ANP (now AREVA), Westinghouse, and Global Nuclear Fuel; in general, the industry partners were responsible for providing precharacterized high-burnup fuel rods and unirradiated archive tubing for testing. NRC also maintained coordination through the program with the Department of Energy, the Institute for Radiological Protection and Nuclear Safety in France, the French Atomic Energy Commission, the Japan Atomic Energy Agency, the Halden Reactor Project in Norway, and the Russian Research Center's Kurchatov Institute.

Because 10 CFR 50.46 only applies to two of the earlier cladding alloys, case-by-case reviews and frequent license exemptions are required for two newer alloys. The research in this program has addressed these alloy-related issues, as well as burnup-related issues.

This report provides test results and related models and correlations that could be used to establish a technical basis for revision of 10 CFR 50.46(b). Other aspects of LOCA behavior, such as heat source redistribution and ballooning size, are also being investigated in this research program, but this report presents only those results that are relevant to cladding embrittlement.

Brian W. Sheron, Director  
Office of Nuclear Regulatory Research  
U.S. Nuclear Regulatory Commission

DRAFT

This page is intentionally left blank.

## Contents

---

Abstract .....	iii
Foreword .....	v
Contents .....	vii
Figures .....	xiii
Tables .....	xxxi
Executive Summary .....	xxxviii
Acknowledgments .....	xl
Acronyms and Abbreviations .....	xlii
Symbols .....	xliv
1 Introduction .....	1
1.1 Cladding materials .....	1
1.2 Transient phase transformations .....	2
1.3 Oxidation equations .....	5
1.4 Embrittlement mechanisms .....	7
1.4.1 Beta-layer embrittlement by oxygen .....	7
1.4.2 Beta-layer thinning .....	7
1.4.3 Localized hydrogen-induced embrittlement in the balloon region .....	7
1.4.4 Hydrogen-enhanced beta-layer embrittlement by oxygen .....	7
1.4.5 General hydrogen-induced embrittlement from breakaway oxidation .....	7
1.4.6 Oxygen pickup from the cladding inner surface .....	8
2 Materials, Test Methods, and Procedures .....	9
2.1 Description of cladding alloys and high-burnup fuel segments .....	9
2.2 Oxidation and quench tests with short defueled cladding samples .....	12

2.3	Ductility determination using ring-compression tests.....	23
2.4	LOCA integral tests with fueled-and-pressurized samples .....	27
3	Results for As-fabricated Cladding Alloys .....	31
3.1	Zircaloy-4.....	31
3.1.1	Post-quench ductility of 17×17 Zry-4 oxidized at 1000°C, 1100°C, and 1200°C .....	31
3.1.2	Post-quench ductility of 15x15 Zry-4 oxidized at 1200°C.....	42
3.1.3	Breakaway oxidation time for 15×15 Zry-4 samples oxidized at 800-1015°C .....	51
3.2	Zircaloy-2.....	64
3.2.1	Post-quench ductility of 10×10 Zry-2 oxidized at 1000°C and 1200°C ....	65
3.2.2	Breakaway oxidation time for 10×10 Zry-2 samples oxidized at 970-1000°C .....	74
3.3	ZIRLO.....	76
3.3.1	Post-quench ductility of 17×17 ZIRLO oxidized at 1000°C, 1100°C, and 1200°C .....	76
3.3.2	Breakaway oxidation time for 17×17 ZIRLO samples oxidized at 800-1015°C .....	93
3.4	M5.....	96
3.4.1	Post-quench ductility of 17×17 M5 oxidized at 1000°C, 1100°C, and 1200°C .....	96
3.4.2	Breakaway oxidation time for 17×17 M5 samples oxidized at 1000°C ...	115
3.5	Effects of surface conditions on cladding performance .....	115
3.5.1	Effects of surface conditions on HBR-type Zry-4 and modern cladding alloys .....	116
3.5.2	Effects of surface conditions on E110 tubing and cladding .....	120
3.6	Effects of quench temperature on post-quench ductility.....	138

3.6.1	Effects of quench temperature on post-quench ductility of 17×17 Zry-4.....	138
3.6.2	Effects of quench temperature on post-quench ductility of 17×17 ZIRLO .....	140
3.6.3	Effects of quench temperature on post-quench ductility of 17×17 M5....	142
3.7	Summary of results for as-fabricated cladding .....	143
4	Results for Prehydrided Cladding Alloys .....	146
4.1	Prehydrided Zircaloy-4 oxidized at 1200°C and quenched at 800°C.....	147
4.1.1	Post-quench ductility of prehydrided 17×17 Zry-4 oxidized at 1200°C .....	150
4.1.2	Post-quench ductility of prehydrided HBR-type 15×15 Zry-4 oxidized at 1200°C .....	152
4.2	Effects of quench temperature on post-quench ductility.....	162
4.3	Discussion on cooling rate and quench temperature effects .....	173
4.4	Summary of post-quench ductility results for prehydrided Zry-4 .....	173
5	Results for High-Burnup Zry-4, ZIRLO, and M5.....	175
5.1	Results for high-burnup H. B. Robinson 15×15 Zry-4 .....	175
5.1.1	Characterization of high-burnup H. B. Robinson 15×15 Zry-4 .....	175
5.1.2	Results of two-sided oxidation tests for high-burnup HBR 15×15 Zry-4.....	187
5.1.3	Results of one-sided oxidation tests for high-burnup HBR 15×15 Zry-4.....	212
5.2	Results for high-burnup 17×17 ZIRLO cladding.....	229
5.3	Results for high-burnup 17×17 M5 cladding.....	229

6	LOCA Integral Test Results.....	230
6.1	As-fabricated 9×9 Zry-2 oxidized at 1204°C.....	230
6.1.1	Ballooning and burst.....	230
6.1.2	Oxidation and hydrogen pickup due to secondary hydriding.....	237
6.1.3	Post-quench ductility for unirradiated LOCA integral samples.....	241
6.2	High-burnup Limerick BWR 9×9 Zircaloy-2 oxidized at 1204°C.....	244
6.2.1	Ballooning and burst of high-burnup samples.....	244
6.2.2	Oxidation and hydrogen pickup due to secondary hydriding for high-burnup samples.....	252
6.2.3	Post-quench ductility of high-burnup samples.....	256
6.3	Cladding inner-surface oxygen pickup from fuel-cladding bond and fuel.....	257
7	Conclusions and Recommendations.....	262
7.1	Beta-layer embrittlement of unirradiated cladding.....	262
7.2	Beta-layer thinning of unirradiated cladding.....	264
7.3	Localized embrittlement in a balloon.....	264
7.4	Hydrogen-enhanced beta-layer embrittlement.....	264
7.5	Breakaway oxidation.....	272
7.6	Oxygen pickup from the cladding inside diameter (ID).....	272
7.7	Recommendations.....	273
7.7.1	Circumferential and axial variations in hydrogen content.....	273
7.7.2	Enbrittlement oxidation level as a function of hydrogen content for high-burnup cladding.....	273
7.7.3	Assessment of prehydrided cladding as a surrogate for high-burnup cladding.....	273
7.7.4	Sensitivity of breakaway oxidation to sample preparation and test conditions.....	274

References.....	275
Appendix A.....	279

---

DRAFT

DRAFT

This page is intentionally left blank.

## Figures

---

1.	Free energy of formation of oxides of alloy constituents and some impurities [8,9].....	3
2.	Schematic of cladding temperature during a LOCA.....	4
3.	Qualitative diagram of oxygen concentration in Zircaloy cladding exposed at high temperature (>980°C) to steam on the outside surface and cooled to room temperature. OD and ID are outer and inner diameters, respectively.....	5
4.	Unirradiated Zircaloy-2 after oxidation in steam at 1200°C for 600 seconds. Scale marker indicates for 200-µm length.....	5
5.	Diffusion couple character of oxygen sources and cladding metal.....	8
6.	Overview of the out-of-cell LOCA integral test apparatus. The in-cell unit is located at Workstation 6 of the Alpha-Gamma Hot Cell Facility (AGHCF) behind the hot-cell shield and seal windows. H. B. Robinson high-burnup Zry-4 oxidation/quench tests, as well as Limerick high-burnup integral tests, were conducted in the AGHCF. Following closure of the AGHCF to programmatic work on January 13, 2006, the in-cell apparatus was no longer available and the out-cell apparatus was moved to a different laboratory. A third apparatus was installed in Cell#4 of the Irradiated Materials Laboratory for performing oxidation-and-quench of high-burnup ZIRLO and M5 cladding samples.....	15
7.	Schematic of oxidation kinetics, oxidation-quench, and LOCA integral test apparatus; test train and sample are shown for LOCA integral testing.....	16
8.	Test train for conducting one-sided steam-oxidation kinetics tests in-cell using ≈25-mm-long Zircaloy cladding samples: a) test train within quartz tube; and b) enlarged view of sample region along the test train showing alumina spacers to inhibit Zircaloy-Inconel interaction and zirconia washers to minimize steam leakage to the sample inner surface.....	17
9.	Test train design for two-sided oxidation tests with four holes drilled into the Inconel holder below the sample (left) for steam ingress and four holes drilled into the holder above the sample for steam egress. Also shown are the three thermocouples permanently welded to the Inconel holder just above the sample.....	18
10.	Thermal benchmark results from two tests, each with two TCs welded onto as-fabricated, HBR-type 15×15 Zry-4 cladding. Test HBRU#20 had TCs welded onto the sample at 0° and 120°, while test HBRU#29 had TCs welded onto a new sample at 0° and 240°. The sample hold temperature is 1204±10°C, where 1204°C is the average of the three TC readings and ±10°C is the standard deviation.....	20
11.	Thermal benchmark results with as-fabricated 17×17 ZIRLO sample. Repeating this test following the growth of inner- and outer-surface oxide layers decreased the first peak during the heating ramp to <1200°C and decreased the overshoot during the early part of the hold time to ≈1200°C; the controller parameters used to generate this thermal history can be used for in-cell tests with high-burnup ZIRLO and M5 cladding samples.....	22

12.	Ring-compression load-displacement data at room temperature for Zry-4 oxidized to 20% CP-ECR (20.3% ECR based on measured weight gain) at 1100°C. The sample fractured into four pieces. The offset strain (0.455 mm) is the distance along the displacement axis between the loading slope (blue) and the unloading slope (green). .....	23
13.	Load-displacement results from RT compression and unloading of an 8-mm-long ring of HBR-type 15×15 Zry-4 cladding. ....	25
14.	Photograph of ring compression sample supported by the fixed flat plate and loaded by the moveable, load-train platen for the Instron 8511. Not shown in the photograph is the control thermocouple which is located at the bottom inner surface of the ring. Also, thermocouples that rest against the side walls of the sample have been moved down to obtain a better image of the sample. ....	27
15.	LOCA integral test train assembly and quartz tube. The 300-mm-long specimen is filled with zirconia pellets with a stack length of ≈270 mm. The quartz tube has an outer diameter of 50 mm, a wall thickness of 1.5 mm, and a length of 686 mm (27 inches).....	28
16.	Schematic of the thermal history used for LOCA integral tests. Zirconia-filled, as-fabricated cladding samples are tested out-of-cell, and fueled high-burnup cladding samples are tested in-cell. ....	30
17.	Thermal benchmark results for the 1000±10°C oxidation tests. The sample used was from the 0.57-mm-wall validation lot of M5, which has the same inner and outer diameter as 17×17 Zry-4 and ZIRLO. Quench at 800°C is not shown in this figure. ....	32
18.	Thermal benchmark results for the 1100±2°C oxidation tests. The sample used was from the 0.57-mm-wall validation lot of M5, which has the same inner and outer diameter as 17×17 Zry-4 and ZIRLO. Quench at 800°C is not shown in this figure. ....	33
19.	Post-test appearance of Zry-4 samples compressed at RT and 0.0333 mm/s: (a) samples oxidized at 1000°C and (b) samples oxidized at 1100°C. ECR values below each sample are calculated using the Cathcart-Pawel weight gain correlation. ....	35
20.	Thermal benchmark results (Test Train #1) for oxidation of 17×17 alloys at 1200±5°C. The sample used for this benchmark was 17×17 Zry-4 with a wall thickness of 0.57 mm. Quench is not shown in this figure.....	38
21.	Thermal benchmark results (current test train) for oxidation of 17×17 alloys at 1200±5°C. The sample used for this benchmark was 17×17 ZIRLO with a wall thickness of 0.57 mm. Quench is not shown in this figure.....	39
22.	Offset (a) and permanent (b) strains vs. CP-ECR for 17×17 Zry-4 oxidized at 1200°C, cooled at ≈13°C/s to 800°C, quenched, and ring-compressed at RT and 135°C.....	41
23.	Thermal benchmark (HBRU#5A) results for first test train used to oxidize HBR-type 15×15 low-tin Zry-4. The hold temperature based on two sample-welded TCs is 1200±17°C. ....	43

24.	RT microhardness across prior-beta layer for 1200°C-oxidized HBR-type 15×15 Zry-4. ....	46
25.	Measured vs. predicted weight gain for two lots of HBR-type 15×15 low-tin Zry-4 oxidized at 1204±10°C and quenched at 800°C.....	48
26.	Offset strain vs. CP-ECR and ring-compression test temperature for two lots of HBR-type 15×15 low-tin Zry-4 oxidized at 1204±10°C, cooled at ≈11°C/s to 800°C, and quenched.....	48
27.	Thermal benchmark results for belt-polished 15×15 low-tin Zry-4 with a hold temperature of ≈1190°C. Data-generating tests were conducted by increasing the holder control TC setting by 10°C to give a hold temperature of 1200°C.....	49
28.	Offset strain vs. CP-ECR for 15×15 and 17×17 Zry-4 samples oxidized at 1200°C, cooled at ≈11°C/s to 800°C, and quenched. Ring compression tests were conducted at 135°C and 0.0333-mm/s displacement rate. Nominal offset strain for ductile-to-brittle transition ECR is 2%. ....	50
29.	Breakaway-oxidation time vs. oxidation temperature determined from the trend curves presented by Leistikow and Schanz [19,20] for Zry-4 weight gain vs. time.....	52
30.	Results of thermal benchmark test with HBR-type 15×15 low-tin Zry-4. Measured weight gain is within 1% of the CP-predicted weight gain. Hold temperature is 992±9°C at 78 s and 984±10°C at 1500 s, beyond the temperature-ramp initiation.....	54
31.	Results of first thermal benchmark test with belt-polished 15×15 low-tin Zry-4. Measured weight gain is within 6% of the CP-predicted weight gain. Hold temperature is 1000±12°C at 95 s and 986±10°C at 1500 s, beyond the temperature-ramp initiation. ....	55
32.	Results of second thermal benchmark test with belt-polished 15×15 low-tin Zry-4. Initial overshoot temperature is 1012±7°C, and long-time hold temperature is 986±12°C. Results are based on the readings of three TCs welded to the sample 120° apart.....	57
33.	Low magnification (left) of inner- and outer-surface oxide layers for HBR-type 15×15 low-tin Zry-4 oxidized at ≈1000°C for 159 s; higher magnification (right) of the outer-surface oxide layer illustrating the smooth boundary between oxide and metal. ....	58
34.	Low magnification (left) of inner- and outer-surface oxide layers for HBR-type 15×15 low-tin Zry-4 oxidized at 984±10°C for 3600 s; higher magnification (right) of the outer-surface oxide layer showing the wavy boundary between oxide and metal, which is a precursor to breakaway. ....	59
35.	Low magnification (left) of inner- and outer-surface oxide layers for HBR-type 15×15 low-tin Zry-4 oxidized at 984±10°C for 5400 s; higher magnification (right) of outer-surface oxide layer showing cracks in monoclinic oxide layer formed during the transition to breakaway oxidation. ....	59

36.	Low magnification (left) of inner- and outer-surface oxide layers for belt-polished 15×15 low-tin Zry-4 oxidized at ≈1000°C for 135 s; higher magnification (right) of outer-surface oxide layer showing the smooth boundary between oxide and metal. ....	60
37.	Low magnification (left) of inner- and outer-surface oxide layers for belt-polished 15×15 low-tin Zry-4 oxidized at 986±12°C for 5400 s (BPZ4#13); higher magnification (right) of outer-surface oxide layer showing wavy metal-oxide interface and initiation of breakaway oxidation. ....	61
38.	Images of belt-polished 15×15 sample BPZ4#18: (a) appearance of outer surface of sample showing local breakaway along a longitudinal strip; (b) inner and outer oxide layers showing pre-breakaway morphology of inner-surface oxide layer and post-breakaway morphology of outer-surface oxide layer; and (c) high magnification of outer-surface oxide layer. ....	62
39.	Breakaway-oxidation data for HBR-type (0.3-μm surface roughness) and belt-polished (0.1-μm surface roughness) 15×15 Zry-4 oxidized in the same apparatus at 985±12°C. Based on the ANL 200-wppm-hydrogen-pickup criterion, breakaway oxidation time is ≈3800 s for HBR-type 15×15 Zry-4 and ≈5000 s for belt-polished (BP) 15×15 Zry-4. ....	63
40.	Measured vs. CP-model-predicted Xi (oxide + alpha) layers after steam-oxidation tests (300, 600, and 1200 s at ≈1204°C) with irradiated (LOI 6-8) and unirradiated (LOU 11-13) Zry-2. ....	64
41.	Thermal benchmark results for 10×10 Zry-2 at 1000°C target temperature. Average hold temperature is 1009±7°C. Hold temperature after 2000 s from ramp initiation is 1005±8°C. For oxidation tests, the control TC was lowered by ≈5°C to give a long-time hold temperature of 1000±8°C. ....	66
42.	Comparison of measured and CP-predicted weight gains for Zr-lined 10x10 Zry-2 and 17x17 Zry-4 oxidized at 1000°C. ....	67
43.	Micrographs of 10×10 Zry-2 sample oxidized at 1000°C to 10% CP-ECR: (a) one of eight cross-sectional arc lengths, (b) outer Zry-2 surface, and (c) inner Zr-liner surface. ....	68
44.	Thermal history for 10×10 Zry-2 oxidation tests at 1200±6°C. The raw data for the sample TC readings were corrected based on calibrating these TCs to an ANL NIST-calibrated TC. Also shown are the three TC readings for the holder TCs (Series 1-3). ....	70
45.	Comparison of measured and CP-predicted weight gains for 10x10 Zry-2 and 17x17 Zry-4 oxidized at 1200°C, cooled at ≈13°C/s to 800°C, and quenched at 800°C. ....	71
46.	Metallographic images of 10×10 Zry-2 sample oxidized at 1200°C to 10% CP-ECR: (a) cross section (one of 8 orientations), (b) outer Zry-2 surface, and (c) inner Zr-lined surface. ....	72
47.	Metallographic images of 10×10 Zry-2 sample oxidized at 1200°C to 17% CP-ECR: (a) cross section (one of 8 orientations), (b) outer Zry-2 surface, and (c) inner Zr-lined surface ....	73

48.	Post-quench ductility (offset strain) vs. CP-ECR for Westinghouse 17x17 Zry-4, AREVA 15x15 Zry-4, and 10x10 Zr-lined Zry-2, all oxidized at 1200°C, cooled at ≈11-13°C/s to 800°C, and quenched at 800°C. Ring-compression test temperature was 135°C. ....	74
49.	Comparison of Cathcart-Pawel model predictions to ANL sample weight gain data for irradiated (Limerick) Zry-2 after steam oxidation at ≈1000°C for test times of 1200 s, 3600 s, and 6000 s. ....	75
50.	Comparison between weight gain data for ZIRLO and Zry-4 and weight gain predicted by the Cathcart-Pawel (CP) correlation for samples oxidized (two-sided) in steam at 1000°C (a) and 1100°C (b). Data correspond to CP-ECR values of 5, 10, 15, 17, and 20%. ....	77
51.	Post-quench ductility vs. measured (a) and CP-predicted (b) ECR for ZIRLO and Zry-4 oxidized at 1000°C, cooled at ≈10°C/s to 800°C, and quenched. Ductility is based on offset strain determined from ring-compression data for tests conducted at RT and 0.0333-mm/s displacement rate. ....	80
52.	Post-quench ductility vs. CP-predicted ECR for ZIRLO and Zry-4 oxidized at 1100°C, cooled at ≈10°C/s to 800°C, and quenched. Ductility is based on offset strain determined from ring-compression data for tests conducted at RT and 0.0333-mm/s displacement rate. ....	81
53.	Post-test appearance of ZIRLO ring-compression samples tested at room temperature and 0.0333 mm/s: (a) samples oxidized at 1000°C and (b) samples oxidized at 1100°C. ECR values are calculated using the Cathcart-Pawel weight gain correlation. ....	81
54.	Metallography of as-polished Zry-4 (a) and ZIRLO (b) oxidized in steam at 1000°C for ≈3360 s, cooled at ≈10°C/s to 800°C, and water quenched. Measured ECR values are 22.4% for Zry-4 and 18.0% for ZIRLO. ....	83
55.	High-magnification images of etched ZIRLO sample following oxidation at 1000°C for 3360 s to 20% CP-ECR. The outer-surface oxide layer (a) is tetragonal, but the wavy oxide-metal interface indicates a precursor to breakaway oxidation. The inner-surface oxide layer (b) is thicker, has lateral cracks, appears to be monoclinic, and is in breakaway oxidation. The hydrogen pickup through the inner surface is ≈100 wppm. ....	84
56.	Metallography of etched Zry-4 (a) and ZIRLO (b) oxidized in steam at 1100°C for ≈1070 s to 20% CP-ECR, cooled at ≈10°C/s to 800°C, and water quenched. Measured ECR values are 20.3% for Zry-4 and 21.1% for ZIRLO. ....	85
57.	Comparison between weight gain data for ZIRLO and Zry-4 and CP-predicted weight gain for samples oxidized (two-sided) in steam at 1200°C and quenched at 800°C. ....	88
58a.	Offset strain vs. CP-ECR for 17×17 ZIRLO oxidized at 1200°C, cooled at ≈13°C/s to 800°C, quenched, and ring-compressed at RT and 135°C. ....	88
58b.	Permanent strain vs. CP-ECR for 17×17 ZIRLO oxidized at 1200°C, cooled at ≈13°C/s to 800°C, quenched, and ring-compressed at RT and 135°C. ....	89

59.	Offset strain vs. CP-ECR for 17×17 ZIRLO and Zry-4 oxidized at 1200°C, cooled at ≈13°C/s to 800°C, quenched, and ring-compressed at 135°C. ....	89
60.	Metallography of etched Zry-4 (a) and ZIRLO (b) oxidized in steam at 1200°C for ≈400 s and ≈440 s, respectively, cooled at ≈13°C/s to 800°C, and quenched. Measured ECR values are 20.8% for Zry-4 and 22.3% for ZIRLO. ....	91
61.	Metallography and microhardness indents across the radius of 17×17 Zry-4 (a) and ZIRLO (b) oxidized at 1200°C to 13% ECR, cooled at ≈13°C/s to 800°C, and quenched. The measured ECR values are 12.6% for Zry-4 and 13.4% for ZIRLO. ....	92
62.	Surface appearance and oxide layers of ZIRLO oxidized at 985°C for 3600 s with 270±165 wppm hydrogen pickup in a ring including the yellow area: (a) outer surface with yellow area (440 wppm H under this layer) in black matrix; (b) outer- and inner-surface oxide layers (no breakaway) under black area; (c) outer-surface (breakaway) and inner-surface (no breakaway) oxide layers under yellow area; and (d) outer- and inner-surface oxide layers under yellow, both in breakaway. ....	93
62e.	Offset strain at 135°C vs. hydrogen pickup for 17×17 ZIRLO and 15×15 Zry-4 breakaway oxidation samples oxidized at 970-1000°C and cooled without quench. ....	95
63.	Thermal benchmark results for 17×17 M5 oxidation tests at 1000°C. The cladding OD is 9.50 mm, and the wall thickness is 0.61 mm. Quench at 800°C is not shown in this figure. ....	97
64.	Thermal benchmark results for 17×17 M5 oxidation tests at 1100°C. The cladding OD is 9.50 mm, and the wall thickness is 0.61 mm. Quench at 800°C is not shown in this figure. ....	98
65.	Comparison between weight gain data for M5 and Zry-4 and weight gain predicted by the Cathcart-Pawel (CP) correlation for samples oxidized (two-sided) in steam at 1000°C (a) and 1100°C (b). Test times correspond to CP-ECR values of ≈5-20%. ....	100
66.	Post-quench ductility vs. measured (a) and CP-predicted (b) ECR for 17×17 M5 and Zry-4 oxidized in steam at 1000°C, cooled at ≈10°C/s to 800°C, and quenched. Offset strain was determined from results of ring-compression tests conducted at RT and 0.0333-mm/s displacement rate. ....	102
67.	Post-quench ductility vs. CP-predicted ECR for 17×17 M5 and Zry-4 oxidized in steam at 1100°C, cooled at ≈10°C/s to 800°C, and quenched. Offset strain was determined from results of ring-compression tests conducted at RT and 0.0333-mm/s displacement rate. ....	103
68.	Post-test appearance of M5 ring-compression samples tested at room temperature and 0.0333 mm/s: (a) samples oxidized at 1000°C and (b) samples oxidized at 1100°C. ECR values are calculated using the Cathcart-Pawel weight gain correlation and 0.57-mm wall. For 0.61-mm-wall M5, these values should be reduced to 4.7%, 9.3%, 14.1%, 16.0%, and 18.8%. ....	103
69.	Metallography of as-polished Zry-4 (a) and M5 (b) oxidized in steam at 1000°C for ≈3360 s, cooled at ≈10°C/s to 800°C, and water quenched. Measured ECR values are 22.4% for Zry-4 and 13.3% for M5. ....	105

70.	High-magnification image of etched M5 outer-surface oxide and alpha layers following oxidation at 1000°C for 3360 s. The outer-surface oxide layer is tetragonal, but the wavy oxide-metal interface is a precursor to breakaway oxidation.....	106
71.	Metallography of etched M5 (a) and Zry-4 (b) oxidized in steam at 1100°C for ≈1070 s, cooled at ≈10°C/s to 800°C, and water quenched. Measured ECR values are 19.1% for M5 and 20.3% for Zry-4.....	106
72.	Thermal benchmark results for first test train for 17×17 M5 oxidation tests at 1203±8°C. The cladding OD is 9.50 mm, and the wall thickness is 0.61 mm. Quench at 800°C is not shown in this figure.....	108
73.	Comparison between weight gain data for M5 and Zry-4 and CP-predicted weight gain for samples oxidized (two-sided) in steam at 1200°C and quenched at 800°C.....	110
74a.	Offset strain vs. CP-ECR for 17×17 M5 oxidized at 1200°C, cooled at ≈13°C/s to 800°C, quenched, and ring-compressed at 135°C.....	110
74b.	Permanent strain vs. CP-ECR for 17×17 M5 oxidized at 1200°C, cooled at ≈13°C/s to 800°C, quenched, and ring-compressed at 135°C.....	111
75.	Offset strain vs. CP-ECR for 17×17 M5 and Zry-4 oxidized at 1200°C, cooled at ≈13°C/s to 800°C, quenched, and ring-compressed at 135°C.....	111
76.	Metallography of etched Zry-4 (a) and M5 (b) oxidized in steam at 1200°C for ≈400 s, cooled at ≈13°C/s to 800°C, and water quenched. Measured ECR values are 20.8% for Zry-4 and 18.8% for M5.....	113
77.	Metallography and microhardness indents across the radius of 17×17 Zry-4 (a) and M5 (b) oxidized at 1200°C to 12-13% CP-ECR. The measured ECR values are 12.6% for Zry-4 and 13.1% for M5. Samples were quenched at 800°C following cooling at ≈13°C/s.....	114
78.	Outer surface of belt-polished 15×15 Zry-4: (a) smooth exterior and (b) local region of surface abrasions.....	116
79.	Metallographic images in the scratched region of an HBR-type 15×15 Zry-4 sample (HBRU#96) following oxidation at 985±12°C for 3600 s. The top and bottom sectors are in breakaway oxidation, while the left and right sectors are not. The sample was prepared from a region of the cladding with scratches observed during pre-test and post-test characterization.....	117
80.	Cross section of ZIRLO cladding with machined scratch ≈20-μm deep into outer surface.....	118
81.	Outer surface of scratched ZIRLO sample following oxidation at 985°C for 3400 s. The local hydrogen pickup under the yellow surface is 440 wppm.....	118
82.	Outer surface of scratched ZIRLO sample following oxidation at 970°C for 2600 s. The local hydrogen pickup under the yellow surface is 120 wppm.....	118

83a. Outer surface of E110 tubing in the as-received condition (0.35- $\mu\text{m}$ surface roughness). Axial direction is left to right. ....	122
83b. Outer surface of E110 tubing in the polished condition (0.14- $\mu\text{m}$ outer-surface roughness). Axial direction is left to right. ....	122
83c. Outer surface of E110 tubing following etching in HF-containing pickling solution. Axial direction is left to right. ....	122
84. Thermal benchmark results for as-received E110 tubing and cladding oxidized in steam at 1000°C. Ramp time is 75 s. ....	124
85. As-fabricated E110 tubing oxidized in steam for a 75-s ramp from 300°C to 1000°C, followed by a 5-s hold at 1000°C and slow cooling: (a) low magnification of lustrous black outer surface oxide and (b) higher magnification of outer surface oxide showing white spots and streaks believed to be monoclinic oxide and oxide-instability initiation sites. ....	126
86. As-fabricated E110 thermal-benchmark (EU#9) sample showing excessive monoclinic oxide formation around the welded thermocouple after 290-s hold time at 1000°C. ....	126
87. As-fabricated E110 sample oxidized in steam for a hold time of 290 s at 1000°C: (a) low magnification image of breakaway oxidation on the outer surface oxide of EU#12 sample and (b) higher magnification image of delaminated outer-surface oxide layer on EU#13 sample. ....	127
88. EU#11 sample oxidized for a hold time of 290 s at 950°C. Breakaway oxidation is as extensive as for the EU#12 sample oxidized for the same hold time at 1000°C. ....	128
89. Hydrogen content distribution in E110 after oxidation Test EU#38 with as-fabricated E110 exposed to steam at 1000°C for a hold time of 625 s ( $\approx 7\%$ CP-ECR). ....	128
90. EU#8 sample oxidized for a hold time of 1350 s at 1000°C. Breakaway oxidation, delamination, and spallation are evident. The hydrogen pickup was $\approx 4200$ wppm. ....	128
91. Room-temperature offset strain vs. CP-ECR of as-fabricated E110 tubing oxidized (two-sided) in steam at 1000°C for hold times of 0-825 s. Sample length is 8 mm, and displacement rate is 0.0333 mm/s. Embrittlement is due to excessive hydrogen pickup ( $>200$ wppm). ....	130
92. The effects of pickling (etching) E110 tubing prior to oxidation at 1000°C for 290 s: (a) etched (180-s exposure to 3.5% HF + 45% HNO <sub>3</sub> + 51.5% H <sub>2</sub> O) tubing sample; (b) polished-and-etched E110 sample; and (c) etched-and-polished E110 sample. ....	131
93. Hybrid E110 sample (EU#13) following oxidation at 1000°C for 290 s. Machined-and-polished section is lustrous black, while as-fabricated E110 section is in breakaway oxidation. ....	132

94.	Effects of polishing vs. machining-and-polishing on E110 oxidation at 1000°C for 290 s. ....	132
95.	High magnification (200X) image of outer-surface oxide layers following oxidation at 1000°C for 290 s: (a) as-fabricated E110, (b) machined-and-polished E110, and (c) polished E110. ....	133
96.	Machined-and-polished E110 sample (EU#16) after 1025-s hold time in steam at 1000°C: (a) lustrous black oxide surface on the other side of the sample and (b) extensive monoclinic oxide formation, delamination, and spallation evident on one side of the sample.....	134
97.	Hydrogen pickup vs. total test time for as-fabricated E110 tubing and ANL-modified machined-and-polished E110. The ramp time from 300°C to 1000°C is 75 s for the as-fabricated tubing (0.70-mm wall) and 90 s for the machined-and-polished samples (0.6-mm wall). ....	135
98.	Post-oxidation RT ductility vs. CP-ECR for ANL machined-and-polished (M-P) E110 samples and Bochvar-TVEL (BT) pickled E110 cladding following two-sided steam oxidation at 1100°C.....	137
99.	Thermal benchmark test results for slow-cooled 17×17 Zry-4, ZIRLO, and M5 samples oxidized at 1200°C. ....	139
100.	Effects of quench vs. slow cooling on the post-oxidation ductility of 17×17 Zry-4 (0.57-mm wall) oxidized at 1200°C, cooled at ≈13°C/s to 800°C, and either quenched at 800°C or slow cooled from 800°C to RT. Ring-compression tests were performed at 135°C and 0.0333-mm/s displacement rate. ....	140
101.	Effects of quench vs. slow cooling on the post-oxidation ductility of 17×17 ZIRLO (0.57-mm wall) oxidized at 1200°C, cooled at ≈13°C/s to 800°C, and either quenched at 800°C or slow cooled from 800°C to RT. Ring-compression tests were performed at 135°C and 0.0333-mm/s displacement rate.....	141
102.	Effects of quench vs. slow cooling on the post-oxidation ductility of 17×17 M5 (0.61-mm wall) oxidized at 1200°C, cooled at ≈13°C/s to 800°C, and either quenched at 800°C or slow cooled from 800°C to RT. Ring-compression tests were performed at 135°C and 0.0333-mm/s displacement rate.....	142
103.	Uniform distribution of circumferential hydrides across the wall of HBR-type 15×15 Zry-4 prehydrided to 400 wppm H. ....	147
104.	Hydrogen concentration in a prehydrided HBR-type 15×15 Zry-4 sample before and after oxidation at 1200°C to 5% CP-ECR. Hydrogen contents after oxidation were corrected for sample weight gain to allow direct comparison with pre-test hydrogen contents.....	148
105.	Hydride morphology for prehydrided (435±50 wppm) HBR-type 15×15 Zry-4 showing the dense hydride rim (≈46 μm) at the cladding inner surface.....	149

106. Variation of post-quench ductility with pre-test hydrogen content for modern 17×17 Zry-4 oxidized at 1200°C to 7.5% and 10% CP-ECR (see 20 for temperature history), cooled at ≈13°C/s, quenched at 800°C, and ring-compressed at 135°C and 0.0333 mm/s. ....	152
107. March 2006 thermal benchmark results for HBR-type 15×15 Zry-4 with a target oxidation temperature of 1200°C. ....	153
108. June 2006 thermal benchmark results for HBR-type 15×15 Zry-4 with a target oxidation temperature of 1200°C. ....	154
109. Variation of post-quench ductility with pre-test hydrogen content for HBR-type 15×15 Zry-4 oxidized to 5% CP-ECR with an end-of-heating temperature of 1180-1190°C (see Figures 10 and 107), cooled at ≈11°C/s, quenched at 800°C, and ring-compressed at 135°C. ....	157
110. Variation of post-quench ductility with pre-test hydrogen content for HBR-type 15×15 Zry-4 oxidized at 1204°C to 7.5% CP-ECR (see Figures 10, 107, and 108), cooled at ≈11°C/s, quenched at 800°C, and ring-compressed at 135°C. ....	157
111. Post-quench ductility vs. pre-test hydrogen content for modern 17×17 and HBR-type 15×15 Zry-4 oxidized at 1200°C to 7.5% CP-ECR, cooled at ≈11-13°C/s, quenched at 800°C, and ring-compressed at 135°C. ....	158
112. Metallographic images of HBR-type 15×15 Zry-4 following oxidation at ≈1200°C to 7.5% CP-ECR, cooling at ≈11°C/s to 800°C, and quench at 800°C: (a) as-received and (b) 600-wppm hydrogen. ....	159
113. RT microhardness profiles across the prior-beta layer of two samples oxidized at ≈1200°C to 7.5% CP-ECR, cooled at ≈11°C/s to 800°C, and quenched at 800°C: as-received and 600-wppm-hydrogen HBR-type 15×15 Zry-4. ....	160
114. RT microhardness and oxygen-concentration profiles across the beta layers of HBR-type 15×15 Zry-4 oxidized at ≈1200°C to 7.5% CP-ECR, cooled at ≈11°C/s to 800°C, and quenched at 800°C: (a) as-received and (b) 600-wppm hydrogen. ....	161
115. Effects of slow cooling vs. quench at 800°C on the post-test ductility at 135°C for HBR-type 15×15 Zry-4 oxidized to 5% CP-ECR at a peak temperature of 1180-1190°C prior to cooling. Plot includes data shown in 109. ....	164
116. Effects of slow cooling vs. quench at 700°C and 800°C on ductility at 135°C for HBR-type 15×15 Zry-4 oxidized to 7.5% CP-ECR at 1204°C prior to cooling. Plot includes data shown in 110. ....	166
117. November 2006 thermal benchmark results for HBR-type 15×15 Zry-4 with a sample oxidation temperature of 1201±3°C. Vertical blue lines indicate different quench temperatures for tests with prehydrated Zry-4 samples. ....	167

118. March 2007 thermal benchmark results for HBR-type 15×15 Zry-4 with a sample oxidation temperature of 1201±3°C. Vertical blue lines indicate different quench temperatures for tests with prehydrated Zry-4 samples. ....	169
118a. Embrittlement oxidation level (CP-ECR) vs. hydrogen content for 17×17 Zry-4 and 15×15 HBR-type Zry-4 oxidized at ≤1200°C, cooled at 11-13°C/s to 800°C and quenched. Results for samples with large circumferential distributions in hydrogen content (±100 wppm) are not included in this figure. ....	171
119. Gamma scan profile for HBR rod F07, from which samples were sectioned for hydrogen-content analysis, oxygen-content analysis, metallography, and two-sided oxidation tests.....	177
120. Gamma scan profile for HBR rod G10, from which samples were sectioned for hydrogen-content analysis, oxygen-content analysis, metallography, and one-sided oxidation tests. ....	177
121. Sectioning diagram for characterization samples and two-sided-oxidation test samples. Eight 1.5-mm-long hydrogen-content samples were cut from 7H. One 13-mm-long sample (7D) was prepared for metallography, one 25-mm-long sample was cut for hydrogen and oxygen analyses (7E), and four 25-mm-long samples (7B, 7C, 7F, and 7G) were sectioned from near the core midplane for oxidation tests. C2 and C6 were used as metallography samples, and C3 and C5 were used as oxidation test samples. ....	178
122. Sectioning diagram for characterization samples and one-sided-oxidation test samples. Sample 7E was used for hydrogen and oxygen analysis. Sample 7D was used for metallographic analysis. Four 32-mm-long samples (7B, 7C, 7F, and 7G) were sectioned from near the core midplane for oxidation tests. ....	179
123. High-burnup HBR fuel morphology for the fuel midplane cross section of rod F07 showing indications of asymmetric power and temperature distributions relative to the center of the pellet. ....	181
124. Fuel (dark region), cladding (light region), and fuel-cladding bond layer (gray) at the midplane of HBR rod F07. The image is a magnification of a small region from the fuel cross section shown in 123. ....	182
125. High-magnification image of fuel-cladding bond layer at the fuel midplane of HBR rod A02. ....	182
126. Images of high-burnup Limerick BWR fuel-cladding bond at fuel-midplane location: (a) prior to defueling in nitric acid and (b) after defueling in nitric acid. ....	183
127. Outer-surface corrosion layer for two-sided-oxidation test samples from HBR rod F07: (a) fuel midplane (71 μm); (b) 320 mm above midplane (74 μm); and (c) 650 mm above midplane (95 μm). ....	184
128. Hydride distribution and morphology in HBR rod F07 cladding near locations used to section two-sided-oxidation test samples: a) fuel midplane (550-wppm H); b) 320 mm above midplane (550-wppm H); and c) 650 mm above midplane (740-wppm H). ....	185

129. Hydride distribution and morphology in HBR rod G10 cladding at the core midplane: (a) typical hydride distribution across cladding wall and (b) atypical hydride distribution with a very dense hydride band near the outer surface and smaller dense hydrides across the wall. ..	186
130. Out-of-cell thermal benchmark results for as-fabricated cladding in the test train used to conduct in-cell two-sided oxidation tests with high-burnup HBR cladding. The results were used to plan oxidation times for two-sided tests with high-burnup HBR cladding samples.....	188
131. Results of thermal benchmark test conducted after the in-cell oxidation tests with another test train and with TCs welded onto the outer surface of as-fabricated HBR-type Zry-4 cladding. Controller parameters were the same as those used to generate 130 results. ....	190
132. Thermal benchmark results for pre-oxidized HBR-type Zry-4 with TCs welded onto bare-cladding outer surface and with steam-induced oxide layers of 37 $\mu\text{m}$ grown on the inner and outer surface of the cladding sample prior to the temperature ramp. Controller parameters were the same as those used to generate results in Figures 130 and 131. ....	191
133. Temperature history used to calculate CP-ECR values and to interpret results for the in-cell two-sided oxidation tests conducted with high-burnup HBR Zry-4 cladding samples. ....	192
134. Measured average $([\text{OD}+\text{ID}]/2)$ alpha-layer thickness vs. CP-predicted value for high-burnup $(550\pm 100 \text{ wppm})$ HBR samples oxidized (two-sided) at 1100-1200°C and prehydrided (600 wppm) HBR-type Zry-4 sample oxidized at $\approx 1200^\circ\text{C}$ to 7.5% CP-ECR. ....	195
135. High-magnification images of the outer surface of high-burnup HBR Zry-4 sample following oxidation (two-sided) at 1200°C to 7.4% CP-ECR and slow cooling to RT: (a) OM and (b) SEM. ....	197
136. High-magnification images of the inner surface of high-burnup HBR Zry-4 sample following oxidation (two-sided) at 1200°C to 7.4% CP-ECR and slow cooling to RT: (a) OM and (b) SEM. ....	198
137. Optical microscopy images of the outer (a) and inner (b) surfaces of the high-burnup HBR Zry-4 sample oxidized (two-sided) at $\approx 1200^\circ\text{C}$ to 9.3% CP-ECR followed by slow cooling to RT. The sample is in the as-polished condition. ....	200
138. Optical microscopy images of the outer (a) and inner (b) surfaces of the high-burnup HBR Zry-4 sample oxidized (two-sided) at 1200°C to 9.3% CP-ECR followed by slow cooling to RT. The sample is in the etched condition. ....	200
139. Load-displacement curve for high-burnup HBR Zry-4 sample $(550\pm 100 \text{ wppm H})$ oxidized (two-sided) at $T \leq 1110^\circ\text{C}$ to 2.7% CP-ECR and slow cooled to RT. The ring-compression test was conducted at 135°C and 0.0333-mm/s displacement rate. The ring was intact after the test, indicating that ductility was $> 45\%$ . ....	202

140a. Load-displacement curve for high-burnup HBR Zry-4 Ring #1 (550±100 wppm H) cut from sample oxidized (two-sided) at $T \leq 1169^{\circ}\text{C}$ to 4.3% CP-ECR and slow cooled to RT. The ring-compression test was conducted at $135^{\circ}\text{C}$ and 0.0333-mm/s displacement rate. The ring had a partial-wall crack after the first load drop, indicating that ductility was $> 12\%$ . .....	203
140b. Load-displacement curve for high-burnup HBR Zry-4 Ring #2 (550±100 wppm H) cut from sample oxidized (two-sided) at $T \leq 1169^{\circ}\text{C}$ to 4.3% CP-ECR and slow cooled to RT. The ring-compression test was conducted at $135^{\circ}\text{C}$ and 0.0333-mm/s displacement rate. The ring had a single through-wall crack after 53% offset strain. Because it is not clear at what strain this crack occurred, the offset strain (37%) corresponding to a 40% load drop is used to represent the ductility of the sample. ....	204
141. Load-displacement curve for high-burnup HBR Zry-4 (550±100 wppm H) sample oxidized (two-sided) at $T \leq 1196^{\circ}\text{C}$ to 6.4% CP-ECR and slow cooled to RT. The ring-compression test was conducted at $135^{\circ}\text{C}$ and 0.0333-mm/s displacement rate. The ring had a single through-wall crack along the length of the sample at 4.0% offset strain, corresponding to the sharp load drop.....	206
142. Load-displacement curve for high-burnup HBR Zry-4 (550±100 wppm H) sample oxidized (two-sided) at $1197^{\circ}\text{C}$ to 7.4% CP-ECR and slow cooled to RT. The ring-compression test was conducted at $135^{\circ}\text{C}$ and 0.0333-mm/s displacement rate. The ring had a single through-wall crack along the length of the sample at 4.0% offset strain, corresponding to the sharp load drop. ....	207
143. Load-displacement curve for high-burnup HBR Zry-4 (740±110 wppm H) sample oxidized (two-sided) at $1198^{\circ}\text{C}$ to 7.5% CP-ECR and quenched at $800^{\circ}\text{C}$ . The ring-compression test was conducted at $135^{\circ}\text{C}$ and 0.0333-mm/s displacement rate. The sharp load drop occurred essentially in the elastic deformation region and corresponded to a single through-wall crack along the length of the sample and no ductility. ....	208
144. Load-displacement curve for high-burnup HBR Zry-4 (550±100 wppm H) sample oxidized (two-sided) at $1198^{\circ}\text{C}$ to 9.3% CP-ECR and slow cooled to RT. The ring-compression test was conducted at $135^{\circ}\text{C}$ and 0.0333-mm/s displacement rate. The ring had a single through-wall crack along the length of the sample at very low offset strain (brittle), corresponding to the sharp load drop.....	209
145. Ductility at $135^{\circ}\text{C}$ vs. CP-ECR for high-burnup HBR Zry-4 cladding following oxidation (two-sided) at $\leq 1200^{\circ}\text{C}$ and either slow cooling to room temperature or quench at $800^{\circ}\text{C}$ . For the slow-cooled samples, the ductile-to-brittle transition CP-ECR is $\approx 8\%$ . ....	210
146. Permanent strain data from two-sided oxidation tests at $1200^{\circ}\text{C}$ followed by slow cooling to RT for high-burnup and prehydrided (unirradiated) Zry-4 cladding samples.....	211
147. Thermal-benchmark results for unirradiated, HBR-type Zry-4 exposed to one-sided (outer-surface) oxidation: as-fabricated, pre-oxidized to 42- $\mu\text{m}$ outer-surface oxide layer; and pre-oxidized to 62- $\mu\text{m}$ outer-surface oxide layer. The temperature history for the 42- $\mu\text{m}$ oxide layer benchmark was used to plan and interpret the results from the one-sided oxidation tests with corroded (68- $\mu\text{m}$ ), high-burnup HBR Zry-4. ....	213

148. Temperature histories for the one-sided and two-sided steam oxidation tests using high-burnup HBR Zry-4 cladding samples.....	214
149. Sectioning diagram for high-burnup HBR Zry-4 samples after one-sided oxidation. Points of triangles indicate surfaces designated for metallographic characterization. ....	215
150. Comparison of measured and CP-predicted values for steam-induced outer-surface oxide layer thicknesses for high-burnup HBR Zry-4 samples oxidized at 1200°C to one-sided CP-ECR values of 4.9-9.7%. Samples had a 68- $\mu$ m pre-test corrosion layer. ....	216
151. Outer surface of high-burnup HBR Zry-4 sample one-side oxidized at 1200°C for 174-s test time to 4.9% CP-ECR: (a) contrast for viewing the oxide layer and (b) contrast for viewing the alpha layer. ....	218
152. Inner surface of high-burnup HBR Zry-4 sample one-side oxidized at 1200°C for 174-s test time to 4.9% CP-ECR: (a) normal contrast and (b) contrast and brightness adjusted for viewing the alpha layer in the central part of the micrograph.....	219
153. High-burnup HBR Zry-4 sample one-side oxidized at 1200°C to 7.3% CP-ECR: (a) outer surface and (b) inner surface. ....	220
154. High-burnup HBR Zry-4 sample one-side oxidized at 1200°C to 8.5% CP-ECR: (a) outer surface and (b) inner surface. ....	221
155. Comparison of Zry-4 samples oxidized (one-sided) in steam at 1200°C to 5% CP-ECR: (a) as-fabricated HBR-type Zry-4 at 4 mm from sample midplane and (b) high-burnup HBR Zry-4 at 4 mm from sample midplane.....	223
156. Load-displacement curve for HBRI#11 sample one-side oxidized to 4.8% CP-ECR at 1200°C and ring-compressed at 135°C and 0.0333 mm/s displacement rate. The sample developed a tight through-wall crack along the 8-mm length at the support position, with the crack initiating from the inner surface. Offset displacement was 0.39 mm, and permanent displacement in the loading direction was 0.27 mm. ....	224
157. Load-displacement curve for HBRI#12 sample one-side oxidized to 7.1% CP-ECR at 1200°C and ring-compressed at 135°C and 0.0333 mm/s displacement rate. The sample developed a tight through-wall crack along the 8-mm length at the support position, with the crack initiating from the inner surface. Offset displacement was 0.1 mm, and permanent displacement in the loading direction was 0.1 mm. ....	225
158. Offset strain data at 135°C for high-burnup HBR Zry-4 samples with $\approx$ 550-wppm hydrogen oxidized to a maximum temperature of 1200°C and slow cooled. Data are from two-sided and one-sided oxidation tests. Trend curve is based on two-sided-oxidation test results. ....	227
159. Temperature and pressure histories for full LOCA integral test sequence, including quench from 800°C to 100°C.....	230

160. Images of the OCL#8 test sample after heating in argon to burst at $\approx 770^{\circ}\text{C}$ (due to a maximum internal pressure of 8.62 MPa [gauge] and an estimated pressure of $\approx 7.7$ MPa just prior to burst) and slow cooling: (a) low magnification of side view of sample, (b) higher magnification of side view of ballooned-and-burst region, and (c) higher magnification of frontal view of burst opening. Top of the sample, from which the thermocouples were inserted prior to welding, is to the left in these photographs. ....	233
161. Axial profile of the diametral ballooning strain at $0^{\circ}$ and $90^{\circ}$ relative to the burst opening for test sample OCL#8 heated under internal pressure in argon up to burst at $\approx 770^{\circ}\text{C}$ and slow cooled to RT. ....	234
162. Cladding cross section at burst midplane for OCL#8 sample (see 161). ....	234
163. Ballooning strain profile for OCL#22 test sample held for 1 s at $1204^{\circ}\text{C}$ , cooled to $800^{\circ}\text{C}$ , and quenched. ....	235
164. Ballooning strain profile for OCL#17 test sample held for 120 s at $1204^{\circ}\text{C}$ , cooled to $800^{\circ}\text{C}$ , and quenched. ....	236
165. Ballooning strain profile for OCL#13 test sample held for 300 s at $1204^{\circ}\text{C}$ , cooled to $800^{\circ}\text{C}$ , and quenched. ....	236
166. LECO oxygen and hydrogen content for OCL#22 sample ramped in steam from $300^{\circ}\text{C}$ to $1204^{\circ}\text{C}$ at $5^{\circ}\text{C/s}$ , held at $1204^{\circ}\text{C}$ for 1 s, cooled at $3^{\circ}\text{C/s}$ to $800^{\circ}\text{C}$ , and quenched. ....	238
167. LECO oxygen and hydrogen content for OCL#17 sample ramped in steam from $300^{\circ}\text{C}$ to $1204^{\circ}\text{C}$ at $5^{\circ}\text{C/s}$ , held at $1204^{\circ}\text{C}$ for 120 s, cooled at $3^{\circ}\text{C/s}$ to $800^{\circ}\text{C}$ , and quenched. ....	238
168. Data for OCL#11 sample ramped in steam from $300^{\circ}\text{C}$ to $1204^{\circ}\text{C}$ at $5^{\circ}\text{C/s}$ , held at $1204^{\circ}\text{C}$ for 300 s, cooled at $3^{\circ}\text{C/s}$ to $800^{\circ}\text{C}$ , and slow cooled from $800^{\circ}\text{C}$ to RT: (a) LECO oxygen and hydrogen content and (b) ECR derived from LECO and metallography data and hydrogen pickup derived from LECO data. ....	239
169. Metallographic images at nine locations around the cross section of the midplane of the burst region of the OCL#11 test sample (300 s at $1204^{\circ}\text{C}$ ). The cross-section-averaged ECR is 18.5%. Locally, the oxidation level varies from $>36\%$ to 13%. ....	240
170. Bending test results for LOCA integral test sample OCL#22: (a) pretest appearance with burst area on bottom, (b) post-test appearance with burst area on bottom, and (c) bending load vs. displacement (flexure extension) at the loading points. ....	242
171. Bending test results for LOCA integral test sample OCL#17: (a) pretest appearance with burst area on bottom, (b) post-test appearance with burst area on bottom, and (c) bending load vs. displacement (flexure extension) at the loading points. ....	243

172. Gamma scan profile for high-burnup Limerick rod F9 showing locations of LOCA integral samples ICL#1 (labeled Phase A) and ICL#2 (labeled Phase B). Fuel and cladding characterization were performed at the fuel midplane, at 0.7 m above the midplane, and at $\approx 1.1$ m above fuel midplane.....	245
173. Gamma scan profile for high-burnup Limerick rod J4 showing axial locations of LOCA integral samples ICL#3 and ICL#4.....	246
174. Comparison of burst openings for (a) in-cell LOCA integral test ICL#1 specimen from high-burnup Limerick rod F9 and (b) out-of-cell companion test OCL#5 specimen from unirradiated Zry-2 cladding. Burst lengths are both $\approx 13$ -mm long for these ramp-to-burst test samples.....	248
175. Comparison of burst openings for (a) high-burnup Limerick ICL#2 specimen and (b) unirradiated OCL#11 Zry-2 specimen after 300-s exposure to steam at 1204°C, followed by slow cooling to RT.....	249
176a. Outer-diameter strain for in-cell test ICL#1 sample (high-burnup Limerick fueled Zry-2) and companion out-of-cell test OCL#5 sample (unirradiated Zry-2 filled with zirconia pellets). Both tests were ramp-to-burst tests in argon, followed by slow cooling to RT.....	250
176b. Outer-diameter strain for in-cell test ICL#2 sample (high-burnup Limerick fueled Zry-2) and companion out-of-cell test OCL#5 sample (unirradiated Zry-2 filled with zirconia pellets). Both samples were ramped to 1204°C in steam, held at 1204°C for 300 s, and slow cooled to RT.....	250
177. Comparison of ballooned-and-burst regions of four in-cell LOCA integral test samples.....	251
178. Sectioning diagram for ICL#2 (300 s at 1204°C, slow cooling to RT) sample. Locations A, B, and C are metallography locations. H <sub>1</sub> and H <sub>2</sub> are locations for LECO hydrogen and oxygen measurements.....	253
179. Sectioning diagram for ICL#3 (300 s at 1204°C, quench from 800°C to 460°C, slow cooling to RT) sample. The sample fractured at locations A, B, and C during handling prior to the sectioning at D. LECO hydrogen and oxygen samples not shown.....	254
180. LECO oxygen-and hydrogen content for ICL#2 and ICL#3 test samples, both oxidized for 300 s at 1204°C. Concentrations are referenced to the weight of the oxidized samples.....	255
181. Axial distribution of ECR (based on LECO oxygen and metallographic data) and hydrogen pickup (based on LECO data in 180) for ICL#2 and ICL#3 test samples.....	255
182. SEM fractography for ICL#3 samples at axial location C in 179 ( $\approx 20$ mm above the burst midplane): (a) cladding cross section, (b) oxide layer, (c) oxygen-stabilized alpha layer, and (d) prior-beta layer. Interpolating from the results in 181, the estimated hydrogen pickup is $\approx 3000$ wppm, and the estimated measured ECR is $\approx 10\%$ .....	256

183. High-burnup Limerick oxidation sample following one-sided oxidation in steam at 1200°C for a 300-s hold time. ....	257
184. Metallographic results for a circumferential location at the burst midplane of the ICL#3 sample, oxidized for 300 s at 1204°C. Fuel particles adherent to the cladding inner surface are shown in (c). ....	258
185. Fuel morphology for ICL#2 LOCA sample: (a) as-irradiated, pre-test condition; (b) post-test condition 180 mm below burst midplane; and (c) post-test condition at 50 mm above the burst midplane. ....	259
186. Evidence of local area on cladding inner surface of oxygen-stabilized alpha (B) for ICL#2 sample at 50 mm above the burst midplane. The inner-surface region indicated by "A" does not have such an alpha layer and is more typical of what is observed for most of the inner surface at this axial location. ....	260
187. Offset strains for high-burnup Zry-4 (71-74 μm corrosion-layer thickness) and as-fabricated (fresh) HBR-type 15×15 Zry-4. Cladding samples were two-side oxidized at ≈1200°C and cooled at ≈11°C/s to 800°C. As-fabricated samples were quenched at 800°C, while the high-burnup samples were slow cooled from 800°C to RT. ....	265
188. Embrittlement oxidation level (CP-ECR) vs. hydrogen content for 17×17 Zry-4 and 15×15 HBR-type Zry-4 oxidized at ≤1200°C, cooled at 11-13°C/s to 800°C and quenched. Results for samples with large circumferential distributions in hydrogen content (±100 wppm) are not included in this figure. ....	267
189. Embrittlement oxidation level (CP-ECR) vs. pre-test hydrogen content for high-burnup 15×15 Zry-4, 17×17 ZIRLO and 17×17 M5 oxidized at ≤1200°C, cooled at 11-13°C/s to 800°C and either quenched or cooled without quench. ....	269
190. Embrittlement oxidation level (CP-ECR) vs. post-test hydrogen content for high-burnup 15×15 Zry-4, 17×17 ZIRLO and 17×17 M5 oxidized at ≤1200°C, cooled at 11-13°C/s to 800°C and either quenched or cooled without quench. ....	270
191. Embrittlement oxidation level (CP-ECR) vs. hydrogen content for high-burnup HBR-Zry-4 and prehydrided 17×17 Zry-4 and 15×15 HBR-type Zry-4 oxidized at ≤1200°C, cooled at 11-13°C/s to 800°C and either quenched or cooled without quench. ....	270

---

DRAFT

This page is intentionally left blank.

## Tables

---

1	Nominal Composition of Commercial Cladding Alloys.....	2
2	Typical Dimensions of Commercial Fuel Rods [10,11].....	4
3	Dimensions and Chemistry of Zr-lined Zry-2 Used in the ANL Test Program (the "<" sign means below the detection limit). .....	10
4	Dimensions and Chemistry of Zry-4 Used in the ANL Test Program (the "<" sign means below the detection limit).....	11
5	Dimensions and Chemistry of ZIRLO and M5 Used in the ANL Test Program (the "<" sign means below the detection limit).....	12
6	Dimensions and Chemistry of E110 Tubing and Cladding Used in the ANL Test Program (the "<" sign means below the detection limit). .....	13
7	Characteristics of High-burnup Fuel Rod Segments and Defueled High-burnup Cladding for the ANL LOCA Test Program.....	14
8	Weight Gain (Wg in mg/cm <sup>2</sup> ) and Measured ECR (%) Values for 17×17 Zry-4 Oxidized in Steam at 1000°C and 1100°C. ECR = 1.538 Wg for 0.57-mm-wall cladding. Multiply weight gain results by a factor of 10 to convert to g/m <sup>2</sup> . CP = Cathcart-Pawel.....	34
9	Ring Compression Test Results for 17×17 Zry-4 Samples Oxidized at 1000° C and 1100° C, Cooled at ≈10° C/s to 800°C, and Quenched. ECR = 1.538 Wg for 0.57-mm-wall cladding. Tests were performed on 8-mm-long samples at RT and at 0.0333 mm/s displacement rate. Displacements in the loading direction were normalized to the as-fabricated outer diameter (9.50 mm) to calculate offset strain. A complete set of tests was performed with a Model 4505 Instron. A limited number of confirmation tests were performed with a Model 5566 Instron on rings cut from the same oxidation samples. ....	35
10	Summary of Characterization Results for Highly Oxidized 17×17 Zry-4 Samples after Exposure to Steam at 1000°C and 1100°C, Cooling at ≈10°C/s to 800°C, and Quench. CP-predicted ECR is 20%.....	36
11	Ring Compression Test (RCT) Results for 17×17 Zry-4 Cladding Oxidized at 1200±5°C, Cooled at ≈13°C/s to 800°C, and Quenched. ECR = 1.538 Wg for 0.57-mm-wall cladding. Tests were performed on ≈8-mm-long samples at RT and 135°C and at 0.0333-mm/s displacement rate. Displacements in the loading direction were normalized to the as-fabricated outer diameter (9.50 mm) to calculate offset and permanent strains.....	40
12	Summary of Characterization Results for 17×17 Zry-4 Samples after Exposure to Steam at 1200°C to 13% and 20% CP-ECR, Cooling at ≈13°C/s to 800°C, and Quench.....	42

13	Ring Compression Test (RCT) Results for HBR-type 15×15 Low-tin Zry-4 Samples Oxidized at 1200±17°C, Cooled at ≈11°C/s to 800°C, and Quenched. ECR = 1.1535 Wg for 0.76-mm-wall cladding. Tests were performed on ≈8-mm-long samples at RT and 135°C and at 0.0333-mm/s displacement rate. Displacements in the loading direction were normalized to the as-fabricated outer diameter (10.77 mm) to calculate offset and permanent strains. ....	45
14	Oxide, Alpha, and Prior-Beta Layer Thicknesses at Four CP-ECR Values for HBR-type 15×15 Low-tin Zry-4 Oxidized at 1200±17°C, Cooled at ≈11°C/s to 800°C, and Quenched. ....	46
15	Ring Compression Test Results for HBR-type 15×15 Low-tin Zry-4 Cladding Oxidized at 1204±10°C, Cooled at ≈11°C/s to 800°C, and Quenched. ECR = 1.1535 Wg for 0.76-mm-wall cladding. Tests were performed on ≈8-mm-long samples at RT, 100°C, and 135°C and at 0.0333-mm/s displacement rate. Samples from two lots were used to generate these data: 10.77-mm OD and 0.76-mm wall; and 10.76-mm OD and 0.77-mm wall. Displacements in the loading direction were normalized to the as-fabricated outer diameter to calculate offset and permanent strains.....	47
16	Ring Compression Test (RCT) Results for Belt-polished 15×15 Zry-4 Cladding Oxidized at 1200°C, Cooled at ≈11°C/s to 800°C, and Quenched. ECR = 1.308 Wg for 0.67-mm wall cladding. RCTs were performed on ≈8-mm-long samples at 135°C and 0.0333-mm/s displacement rate.....	50
17	Breakaway Oxidation Time vs. Temperature for Zry-4 in Terms of Increase in Weight Gain Rate and Hydrogen-content Increase (200 wppm). References are: L-S = Leistikow and Schanz [19,20] and M = Mardon et al. [21]. ....	51
18	Results of Breakaway Oxidation Tests at 984±10°C for HBR-type 15×15 low-tin Zry-4. The hydrogen content ( $C_{Hi}$ ) of the as-fabricated cladding is 22 wppm. The hydrogen content of the oxidized sample ( $L_H$ ) was measured with the LECO Hydrogen Determinator. Breakaway-oxidation time based on 200-wppm hydrogen pickup is ≈3800 s.....	58
19	First Set of Results for Breakaway Oxidation at 986±12°C (Figure 31) for Belt-polished 15×15 Low-tin Zry-4. The hydrogen content ( $C_{Hi}$ ) of the as-fabricated cladding is 26 wppm. The hydrogen content of the oxidized sample ( $L_H$ ) was measured with the LECO Hydrogen Determinator. Breakaway-oxidation time based on 200-wppm hydrogen pickup is ≈5000 s. ....	60
20	Second Set of Results for Breakaway Oxidation of Belt-polished 15×15 Low-tin Zry-4 at Long-time Test Temperatures of 986°C (see Figure 32), 1000°C, and 1014°C. Hydrogen content ( $C_{Hi}$ ) of as-fabricated cladding is 26 wppm; hydrogen content of the oxidized sample ( $L_H$ ) was measured with the LECO Hydrogen Determinator; breakaway-oxidation time based on 200-wppm hydrogen pickup is >5400 s. ....	61

21	Ring Compression Test (RCT) Results for 10×10 Zry-2 Cladding Oxidized at 1000°C, Cooled at ≈10°C/s to 800°C, and Quenched. ECR = 1.328 Wg for 0.66-mm-wall cladding. Tests were performed on ≈8-mm-long samples at RT and 0.0333-mm/s displacement rate. Displacements in the loading direction were normalized to the as-fabricated outer diameter (10.29 mm) to calculate strains. ....	67
22	Ring Compression Test (RCT) Results for 10×10 Zry-2 Cladding Oxidized at 1200°C, Cooled at ≈13°C/s to 800°C, and Quenched. ECR = 1.328 Wg for 0.66-mm wall cladding. Tests were performed on ≈8-mm-long samples at 135°C and 0.0333-mm/s displacement rate. Displacements in the loading direction were normalized to the as-fabricated outer diameter (10.29 mm) to calculate strains. ....	71
23	Results for Breakaway Oxidation Studies of 10x10 Zry-2 Cladding. Test times are given from the beginning of the ramp from 300°C to the end of the hold time at temperature. ....	75
24	Weight Gain (Wg in mg/cm <sup>2</sup> ) and Measured ECR (%) Values for 17×17 ZIRLO Oxidized in Steam at 1000°C and 1100°C and Quenched at 800°C. ECR = 1.538 Wg for the 0.57-mm- wall thickness. Multiply weight gain results by a factor of 10 to convert to g/m <sup>2</sup> .....	78
25	Ring Compression Test Results for 17×17 ZIRLO Samples Oxidized at 1000°C and 1100°C, Cooled at ≈10°C/s to 800°C, and Quenched. ECR = 1.538 Wg for 0.57-mm-wall cladding. Tests were performed on 8-mm-long samples at RT and 0.0333-mm/s displacement rate. Displacements in the loading direction were normalized to the as-fabricated outer diameter (9.50 mm) to calculate offset strain. A complete set of tests was performed with the Model 4505 Instron. A limited number of confirmation tests were performed with the Model 5566 Instron on rings cut from the same oxidation samples.....	79
26	Characterization of Highly Oxidized (20% CP-ECR) 17×17 Zry-4 and ZIRLO Samples after Exposure to Steam at 1000°C and 1100°C, Cooling at ≈10°C/s to 800°C, and Quench. ....	82
27	Ring Compression Test (RCT) Results for 17×17 ZIRLO Cladding Oxidized at 1200°C, Cooled at ≈13°C/s to 800°C, and Quenched. ECR = 1.538 Wg for 0.57-mm-wall thickness. Tests were performed on ≈8-mm-long samples at RT and 135°C and at 0.0333-mm/s displacement rate. Displacements in the loading direction were normalized to the as-fabricated outer diameter (9.50 mm) to calculate offset and permanent strains.....	87
28	Characterization of 17×17 Zry-4 and ZIRLO Samples after Exposure to Steam at 1200°C to 13% and 20% CP-ECR, Cooling at ≈13°C/s to 800°C, and Quenching .....	90
29	Data Summary for ZIRLO Breakaway Oxidation Tests at 950-1015°C and 800°C. ZIRLO-2003 samples were quenched at 800°C; ZIRLO-2006 samples were slow cooled from the hold temperature to RT.....	94
30	Post-oxidation Ductility of ZIRLO with Significant Hydrogen Pickup during Breakaway Oxidation. ZIRLO-2006 samples summarized in Table 29 were oxidized at 985°C and 970°C, then cooled without quench to RT and ring-compressed at 135°C; average hydrogen values are reported for the 8-mm-long rings compressed at 0.0333 mm/s. ....	95

31	Weight Gain (Wg in mg/cm <sup>2</sup> ) and Measured ECR (%) Values for 17×17 M5 Oxidized in Steam at 1000°C and 1100°C and Quenched at 800°C, ECR = 1.437 Wg for the 0.61-mm-wall thickness; multiply weight gain results by a factor of 10 to convert to g/m <sup>2</sup> . ....	99
32	Ring Compression Test Results for 17×17 M5 Samples Oxidized at 1000°C and 1100°C, Cooled at ≈10°C/s to 800°C, and Quenched. ECR = 1.437 Wg for 0.61-mm-wall cladding. Displacements in the loading direction were normalized to the as-fabricated outer diameter (9.50 mm) to calculate offset strain. Tests were performed on 8-mm-long samples at RT and 0.0333-mm/s displacement rate in the Model 4505 Instron. Some confirmation tests were conducted in the new Model 5566 Instron on rings from the same oxidation samples. ....	101
33	Characterization of Highly Oxidized 17×17 Zry-4 and M5 Samples after Exposure to Steam at 1000°C and 1100°C, Cooling at ≈10°C/s to 800°C, and Water Quench.....	104
34	Ring Compression Test (RCT) Results for 17×17 M5 Cladding Oxidized at 1200°C, Cooled at ≈13°C/s to 800°C, and Quenched. ECR = 1.437 Wg for 0.61-mm-wall thickness. Tests were performed on ≈8-mm-long samples at RT and 135°C and at 0.0333-mm/s displacement rate. Displacements in the loading direction were normalized to the as-fabricated outer diameter (9.50 mm) to calculate offset and permanent strains.....	109
35	Characterization of 17×17 Zry-4 and M5 Samples after Exposure to Steam at 1200°C for Durations of 166 and 400 s, Cooling at ≈13°C/s to 800°C, and Water Quench.....	112
36	Data Summary for ANL M5 Breakaway Oxidation Tests at 1000°C; test times are from beginning of ramp at 300°C to the end of the hold time. ....	115
37	Effects of Pre-filming on the Breakaway Oxidation Time for ZIRLO. Hydrogen pickup values for as-fabricated (bare) ZIRLO samples are also listed. Samples were slow cooled from the hold temperature to RT and ring-compressed at 135°C and 0.0333 mm/s. ....	119
38	Two-Sided Steam Oxidation Tests Conducted at 1000°C with As-received E110 Tubing. Cladding dimensions are 9.17-mm OD; 0.71-mm wall thickness; CP-ECR = 1.235 CP-Wg; outer-surface roughness = 0.35 μm; sample length = ≈25-mm. Hydrogen samples were cut from center (C) and off-center (OC) sample locations. Note that Test EU#11 was conducted at 950°C. ....	125
39	Ring-Compression Test Results for E110 Samples Oxidized at 1000°C and Slow Cooled. Tests were performed on 8-mm-long samples at RT and 0.0333-mm/s displacement rate.....	130
40	Two-Sided Oxidation Tests Conducted on Modified E110 Cladding at 1000°C. Samples had polished cladding outer diameter (9.17 mm), machined and polished inner diameter (7.98 mm), and 0.6-mm wall thickness. ....	134
41	Comparison of E110 Post-Oxidation RT Ductility between ANL Machined-and-Polished (M-P) Cladding Samples and Bochvar-TVEL (BT) Lots 2-4 Pickled Cladding Samples [25] Following Two-sided Steam Oxidation at 1100°C. ....	136

42	Post-oxidation Ductility at 135°C for ANL Machined-and-Polished E110 Samples following Oxidation at 1200°C and Slow Cooling. Samples were fabricated from E110 cladding (etched and anodized): polished outer diameter (9.07 mm), machined-and-polished inner surface, and 0.6-mm wall thickness.....	137
43	Ring Compression Test Results at 135°C and 0.0333 mm/s for 17×17 Zry-4 Cladding Oxidized at 1200°C and Slow Cooled (SC). ECR = 1.538 Wg for 0.57-mm-wall cladding.....	138
44	Ring Compression Test Results at 135°C and 0.0333 mm/s for 17×17 ZIRLO Cladding Oxidized at 1200°C and Slow Cooled (SC). ECR = 1.538 Wg for 0.57-mm-wall cladding.....	141
45	Ring-Compression Test Results at 135°C and 0.0333 mm/s for 17×17 M5 Cladding Oxidized at 1200°C and Slow Cooled (SC). ECR = 1.437 Wg for 0.61-mm-wall cladding.....	142
46	Ring Compression Test Results for Prehydrided 17×17 Zry-4 Cladding Oxidized at 1200°C, Cooled at ≈13°C/s to 800°C, and Quenched. ECR = 1.538 Wg for 0.57-mm-wall cladding. Tests were performed on ≈8-mm-long samples at 135°C and 0.0333-mm/s displacement rate.....	151
47	Post-quench Ductility of Prehydrided HBR-type 15×15 Zry-4 Cladding Oxidized to 5% CP-ECR with T = 1180-1190°C at End of Heating Ramp, Cooled at ≈11°C/s to 800°C, and Quenched (Q). Ring-compression tests were performed on ≈8-mm-long samples at 135°C and 0.0333-mm/s displacement rate; ECR = 1.1535 Wg for 0.76-mm-wall and 1.1385 Wg for 0.77-mm wall; displacements were normalized to 10.77-mm OD for 0.76-mm-wall and 10.76-mm OD for 0.77-mm wall.....	155
48	Post-quench Ductility of Prehydrided HBR-type 15×15 Zry-4 Cladding Oxidized at 1200°C to 7.5% CP-ECR, Cooled at ≈11°C/s to 800°C, and Quenched (Q). Ring-compression tests were performed on ≈8-mm-long samples at 135°C and 0.0333-mm/s displacement rate. ECR = 1.1535 Wg for 0.76-mm wall and 1.1385 Wg for 0.77-mm wall; displacements were normalized to 10.77-mm OD for 0.76-mm wall and 10.76-mm OD for 0.77-mm wall.....	156
49	Comparison of Results for As-received and 600-wppm-prehydrided HBR-type 15×15 Zry-4 Samples after Exposure to Steam at ≈1200°C to 7.5% CP-ECR, Cooling at ≈11°C/s to 800°C, and Quench at 800°C.....	159
50	Post-quench Ductility of Prehydrided HBR-type 15×15 Zry-4 Cladding Oxidized to 5% CP-ECR with T = 1180°C at End of Heating Ramp, Cooled at ≈11°C/s to 800°C, and either Quenched (Q) at 800°C or Slow Cooled to RT. ECR = 1.1385 Wg; ring-compression tests performed on ≈8-mm-long samples at 135°C and 0.0333 mm/s displacement rate.....	163
51	Post-quench Ductility of Prehydrided HBR-type 15×15 Zry-4 Cladding Oxidized to 7.5% CP-ECR at 1204°C, Cooled at ≈11°C/s to 800°C, and Quenched (Q) at 800°C, or Quenched at 700°C, or Slow Cooled to RT, ECR = 1.1385 Wg; ring-compression tests performed on ≈8-mm-long samples at 135°C and 0.0333-mm/s displacement rate.....	165

52	Post-quench Ductility of Prehydrided HBR-type 15×15 Zry-4 Cladding Oxidized to 6% CP-ECR at 1200°C, Cooled at ≈11°C/s to 800°C and Quenched (Q) at 800°C, Cooled from 800°C to 700°C at 3°C/s and Quenched at 700°C, Cooled from 700°C to 600°C at 2°C/s and Quenched at 600°C, or Slow Cooled from 600°C to RT at <2°C/s. Thermal history is shown in Figure 117; CP-ECR is calculated from beginning of ramp to end of hold time; ring-compression tests performed on ≈8-mm-long samples at 135°C and 0.0333-mm/s displacement rate.....	168
53	Comparison between ANL and CEA Test Samples, Test Conditions, and Results for Post-quench Ductility of Prehydrided Zry-4 as a Function of Quench Temperature .....	173
54	Corrosion Layer Thickness and Hydrogen Content Results for H. B. Robinson Rods F07 and G10 and for Rods A02 and R01. Axial locations are relative to the midplane of the 3658-mm-long fuel column.....	180
55	Summary of Cladding Characterization for HBR Fuel Rod Segments Used for Pre- and Post-test Analysis of Two-sided and One-sided Oxidation Tests .....	187
56	Thermal Benchmark Results for Test HBRU#44 with As-fabricated Zry-4 (Figure 130), for Test HBRU#73A with As-fabricated Zry-4 (Figure 131), and for Test HBRU#73B with Pre-oxidized Zry-4 (Figure 133). Estimated temperatures for high-burnup test samples (HBRI) are given in column 3.....	189
57	Sample Characterization and Test Conditions for Two-sided Oxidation Tests Conducted with High-burnup HBR Zry-4 Cladding. SC is slow cooling, and Q is quench at 800°C. ....	193
58	Results of Quantitative Metallography for Two-sided-oxidized, High-burnup HBR Zry-4 following Steam Oxidation. Includes oxide layer thickness ( $\delta_{ox}$ ) and measured ECR; data are from optical microscopy (OM) images at eight circumferential locations around sample cross section (see Figures 135-137 for images from one-of-eight locations for HBRI#4 and #5 samples). ....	194
59	Results of Quantitative Metallography for Two-sided-oxidized, High-burnup HBR Zry-4 following Steam Oxidation. Includes oxygen-stabilized alpha layer thickness ( $\delta_{\alpha}$ ); data are from images at eight circumferential locations around sample cross section (see Figures 135 and 136 for OM images from one-of-eight locations for sample HBRI#5). ....	195
60	Results of Ring-compression Tests for High-burnup HBR Zry-4 Cladding Samples Oxidized (Two-sided) at 1110-1198°C to 2.7-9.3% CP-ECR and Slow Cooled (SC) to RT or Quenched (Q) at 800°C. Tests were conducted on ≈8-mm-long rings at 135°C and 0.0333-mm/s displacement rate; offset and permanent displacements were normalized to the cladding metal outer diameter (10.6 mm) to calculate strains.....	201
61	Ductility Data from Two-sided Oxidation Tests at 1200°C with High-burnup and Prehydrided (Unirradiated) Zry-4. Q = quench and SC= slow cooling .....	205
62	Ductility Data from Two-sided Oxidation Tests at 1200°C followed by Slow Cooling for High-burnup and Prehydrided (Unirradiated) Zry-4 Cladding Samples. ....	211

63	Sample Characterization and Test Conditions for One-sided Steam Oxidation Tests (HBRI) Conducted with High-burnup HBR Zry-4 Cladding. SC is slow cooling.....	215
64	Post-test Results for High-temperature Oxide Layer Thickness and Hydrogen Content for High-burnup HBR Zry-4 Samples (HBRI) Oxidized in Steam (One-sided) at 1200°C.....	216
65	Post-test Results for Outer- and Inner-surface Alpha Layers Stabilized at 1200°C for High-burnup HBR Zry-4 Samples (HBRI) Oxidized in Steam (One-sided). ....	217
66	Ring-Compression Test Results for the Ductility at 135°C of High-burnup HBR Zry-4 Samples Oxidized (One-sided) in Steam at 1200°C and Slow Cooled to RT. CP-ECR values are based on outer-surface oxidation. ....	222
67	Post-oxidation Ductility Values for High-burnup HBR Zry-4 Cladding Samples Oxidized at $\leq 1200^{\circ}\text{C}$ and Slow Cooled to RT. Test type is indicated by 2-S for two-sided oxidation and 1-S for one-sided oxidation; tests were conducted on $\approx 8$ -mm-long rings at 135°C and 0.0333-mm/s displacement rate; offset and permanent displacements were normalized to the cladding metal outer diameter (10.6 mm) to calculate strains.....	226
68	Summary of LOCA Integral Test Results for Out-of-cell Tests with Near-archival As-fabricated (Unirradiated) 9×9 Zry-2 Samples Filled with Zirconia Pellets. Outer diameter and wall thickness of as-fabricated cladding are 11.18 mm and 0.71 mm, respectively. ....	232
69	Summary of In-cell LOCA Integral Tests (ICL) with High-burnup Fueled Cladding Specimens from Limerick BWR. Also shown are the results of companion out-of-cell tests OCL#5 and OCL#11 with non-irradiated Zry-2 cladding. ....	247
70	Embrittlement Threshold (CP-ECR) for As-fabricated Cladding Alloys Oxidized at 1200°C, Cooled at 11-13°C/s to 800 °C, Quenched at 800°C and Ring-compressed at 135°C. For CP-ECR values 1% higher than the embrittlement threshold, the alloys are classified as brittle. Results are rounded off to the nearest whole-number percent. ....	263
71	Embrittlement Threshold (CP-ECR) for High-burnup Cladding Alloys Oxidized at $\leq 1200^{\circ}\text{C}$ , Cooled at 11-13°C/s to 800°C, and either Quenched (Q) at 800°C or cooled without quench. Ring-compression tests were performed at 135°C. For CP-ECR values 1% higher than the embrittlement threshold, the alloys are brittle. Results are rounded off to the nearest whole-number percent. SC = slow cooling without quench. ....	268

## Executive Summary

---

Text to be provided.

DRAFT

DRAFT

This page is intentionally left blank.

## Acknowledgments

---

Text to be provided.

DRAFT

DRAFT

This page is intentionally left blank.

## Acronyms and Abbreviations

---

Text to be provided.

DRAFT

DRAFT

This page is intentionally left blank.

## Symbols

---

Text to be provided.

DRAFT

DRAFT

This page is intentionally left blank.

# 1 Introduction

---

By the mid 1990s, it was well known that significant cladding oxidation (corrosion) takes place during extended periods of normal operation, and that some of the liberated hydrogen from the interaction with water is absorbed in the zirconium alloy cladding material. It thus seemed likely that an oxide layer on the surface and hydrogen in the metal would affect the cladding's behavior under conditions of a loss-of-coolant accident (LOCA). Because cladding behavior under those conditions is important in reactor safety analyses, research was begun in 1997 to investigate any such burnup-related effects.

Several aspects of cladding behavior under LOCA conditions are involved in safety analyses: ballooning strains, flow area reduction, rupture conditions, axial distribution of heat sources, and cladding embrittlement. All are being investigated in a broad research program at Argonne National Laboratory (ANL), but only cladding embrittlement will be addressed in this report. The conditions under which cladding on high-burnup fuel loses its ductility and becomes embrittled are needed to assess, and perhaps revise, the embrittlement criteria in 10 CFR 50.46(b) of the NRC's regulations. These criteria are given as limits on cladding temperature and on oxidation level calculated as a percentage of cladding oxidized (equivalent cladding reacted [ECR]).

The current embrittlement criteria were based on tests with unirradiated Zircaloy cladding material and were adopted in 1973. The history of the development of these criteria is summarized in a paper by Hache and Chung [1]. The ductility tests themselves were of the ring-compression type, and the test results were evaluated at 135°C, the saturation temperature during reflood. The ECR was calculated for these tests using the Baker-Just oxidation kinetics equations.

Although significantly improved testing techniques and oxidation kinetics equations are employed in the present study, the basis for the embrittlement criteria has remained the same. Most importantly, the materials tested in the current work include cladding from high-burnup fuel rods, which were taken from commercial reactors, and a variety of unirradiated cladding alloys, so that both burnup and alloy effects can be determined.

## 1.1 Cladding materials

Table 1 lists the nominal compositions of commercial cladding alloys that have been tested in this program. Zircaloy-2 cladding is used in boiling water reactors (BWRs). Zircaloy-4, ZIRLO, and M5 are used in pressurized water reactors (PWRs). The Russian E110 cladding is used in VVERs (Russian version of PWR) and was included in the study because it has a similar composition to M5 yet behaves very differently under LOCA conditions [2]. Specific dimensions and alloy compositions for the materials tested in this program are described in Section 2.1.

The traditional zirconium-based alloys used in the U.S. were variations of Zircaloy, which has tin as the major alloying element. In Russia, niobium was used as the major alloying element. Zirconium-niobium alloys tend to corrode less during normal operation than zirconium-tin alloys, so niobium has been added in recent years to alloys used in the U.S.

Niobium exhibits several differences compared with tin that affect the behavior of cladding under LOCA conditions. One is that the niobium solubility in zirconium is limited to about 0.5% at moderate temperatures such that about half of the niobium in the niobium-bearing alloys exists as precipitates or

Table 1 Nominal Composition of Commercial Cladding Alloys.

Element	Zircaloy-2 <sup>a</sup>	Zircaloy-4 <sup>a</sup>	ZIRLO <sup>b,c</sup>	M5 <sup>d</sup>	E110 <sup>e</sup>
Sn (wt%)	1.45	1.45	1.1	--	--
Nb (wt%)	--	--	1.1	1.0	1.0
Fe (wt%)	0.14	0.21	0.1	0.038	0.009
Cr (wt%)	0.10	0.10	--	--	--
Ni (wt%)	0.06	--	--	--	--
O (wt%) <sup>f</sup>	0.125	0.125	0.120	0.135	0.06
Zr	Balance	Balance	Balance	Balance	Balance

<sup>a</sup>ASTM B811 [3].

<sup>b</sup>R. Comstock et al. [4].

<sup>c</sup>W. Leech [5].

<sup>d</sup>J-P. Mardon et al. [6].

<sup>e</sup>P. V. Shebaldov et al [7].

<sup>f</sup>Oxygen is considered an alloying element in these alloys.

second-phase particles. This is in contrast to tin, which goes into complete solution with zirconium in Zircaloy. The niobium precipitates affect phase changes during a LOCA (see Section 1.2). These changes are observable in metallography and may account for some of the differences in the behavior of these alloys.

Another difference is that niobium, like zirconium, has a strong affinity for oxygen – unlike tin. This can be seen in Figure 1, which shows the free energy of formation of oxides of alloy constituents and some impurities [8,9]. Additionally, the prevalent form of niobium oxide is Nb<sub>2</sub>O<sub>5</sub>. That is, niobium has a valence of +5 in the oxide, whereas zirconium has a valence of +4. Taken together, these characteristics lead to the inclusion of niobium in the oxide layer, and it is present there as an aliovalent impurity, which can affect the behavior of the oxide.

Because many of the results described in the following depend on cladding thickness and diameter, typical dimensions of commercial fuel rods are given in Table 2 [10,11].

## 1.2 Transient phase transformations

During a LOCA transient, much of the coolant inventory would be lost during the blowdown, and the fuel cladding would begin to heat up. Around 800°C on the temperature rise, the pressurized cladding would reach its ultimate tensile strength, and a local instability would produce a large ballooning strain and a rupture in fuel rods with sufficient pressure and temperature increase. A modest temperature reduction would accompany this deformation in the vicinity of the balloon because of

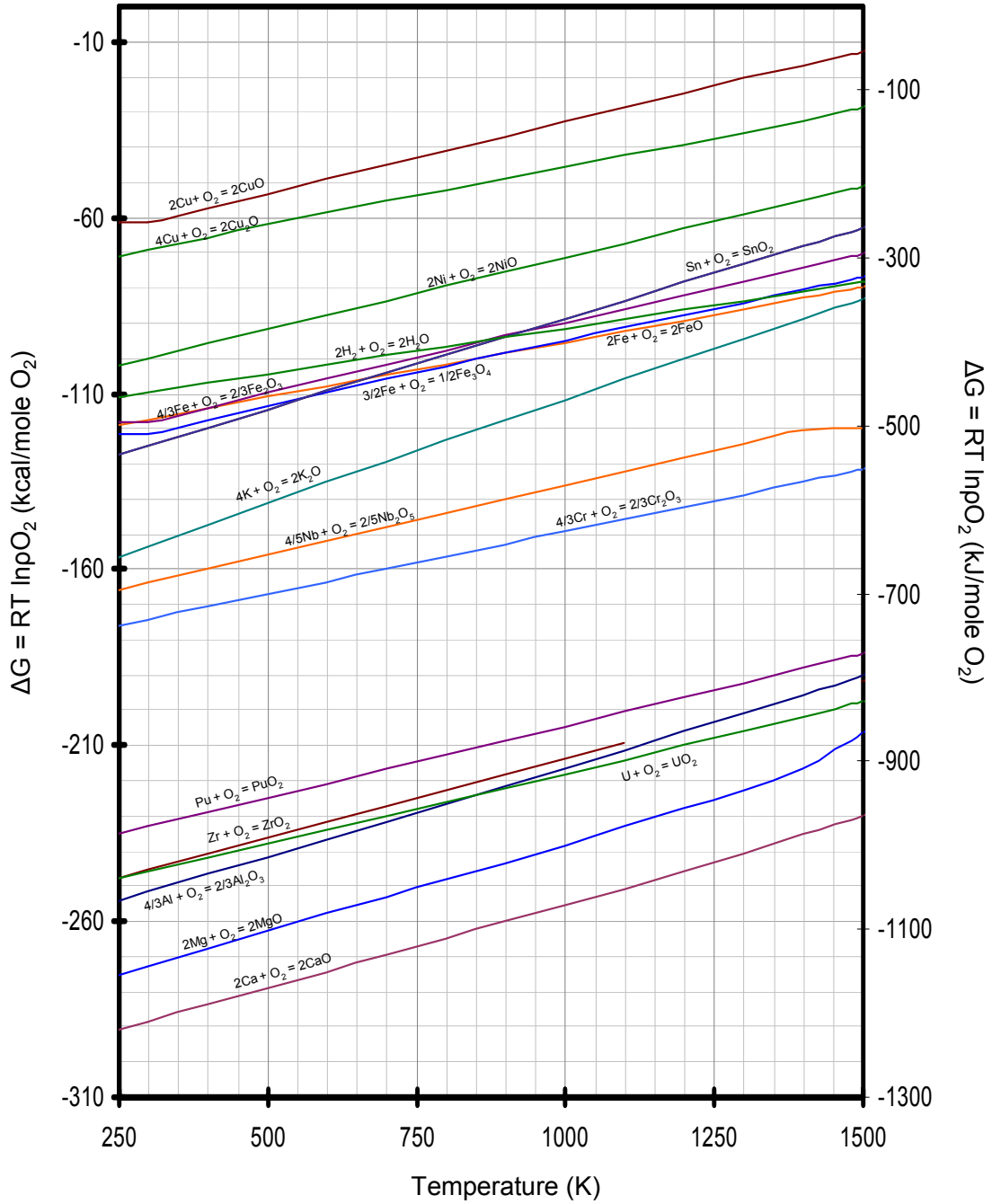


Figure 1. Free energy of formation of oxides of alloy constituents and some impurities [8,9].

Table 2 Typical Dimensions of Commercial Fuel Rods [10,11].

Cladding Type and Dimensions	BWR 8×8	BWR 9×9	BWR 10×10	PWR 14×14	PWR 15×15	PWR 16×16	PWR 17×17	VVER Hex.
Outside Diam. (mm)	12.3	10.8	10.0	11.2	10.7	9.7	9.4	9.1
Thickness (mm)	0.813	0.711	0.660	0.737	0.711	0.635	0.610	0.705

enhanced cooling, but the temperature would then continue to rise. Eventually, the emergency cooling water would stop the temperature rise and begin to cool the cladding. When the temperature decreases to 400-800°C, wetting of the cladding occurs and rapid cooling, or quenching, would take place. Such a temperature transient is shown schematically in Figure 2.

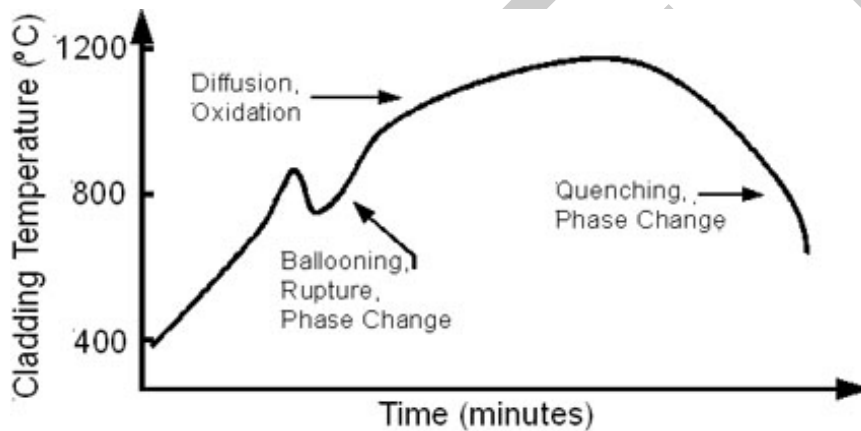


Figure 2. Schematic of cladding temperature during a LOCA.

From room temperature up to about 650-800°C, the zirconium-based cladding alloys of interest have a hexagonal crystal structure, which is called the alpha phase. Above this temperature, which varies with alloy composition, there is a mixed-phase regime in which the crystal structure begins to change to a face-centered cubic geometry or beta phase. For Zry-4 with initial oxygen concentration of 0.11 wt. %, the alpha to the mixed alpha-beta phase change temperature is 810°C, and the alpha-beta to beta phase change temperature is about 980°C. These values increase as the oxygen content increases, and they decrease with increasing hydrogen. They also decrease with the substitution of Nb for Sn because Nb stabilizes the beta phase at a lower temperature. The terms commonly used to describe these effects are: oxygen is an alpha-stabilizer and both hydrogen and Nb are beta-stabilizers.

Oxygen diffusion in Zr metal and in ZrO<sub>2</sub> oxide becomes rapid enough above 800°C that measurable changes occur during a LOCA transient. Diffusion controls the oxidation process and other processes involved in cladding embrittlement. Thus, after the zirconium alloy changes from the alpha to the alpha + beta to the beta phase, the temperature becomes high enough that oxygen diffuses from the surface into the metal, quickly exceeding its solubility limit in the outer region of the cladding. Rather than precipitating some other phase or gas bubbles, this oxygen-rich metal transforms back to the alpha phase, where the oxygen solubility limit is much higher than in the beta phase. Upon cooling, the beta

phase also converts back to the alpha phase, but the prior-beta region and the oxygen-stabilized alpha layer are easily distinguished at room temperature in metallographic sections. Figure 3 is a qualitative diagram of this situation for an oxidation temperature greater than the alpha-plus-beta to beta-phase temperature and for a location away from the balloon, where steam is not able to get inside the cladding.

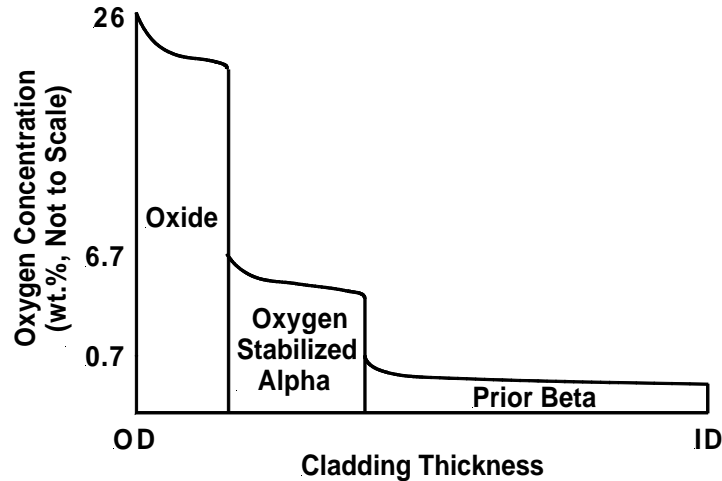


Figure 3. Qualitative diagram of oxygen concentration in Zircaloy cladding exposed at high temperature (>980°C) to steam on the outside surface and cooled to room temperature. OD and ID are outer and inner diameters, respectively.

Figure 4 shows what these phases look like in a micrograph of an etched section of unirradiated Zircaloy-2 cladding after being oxidized (outside surface only) in steam for 600 seconds at 1200°C.

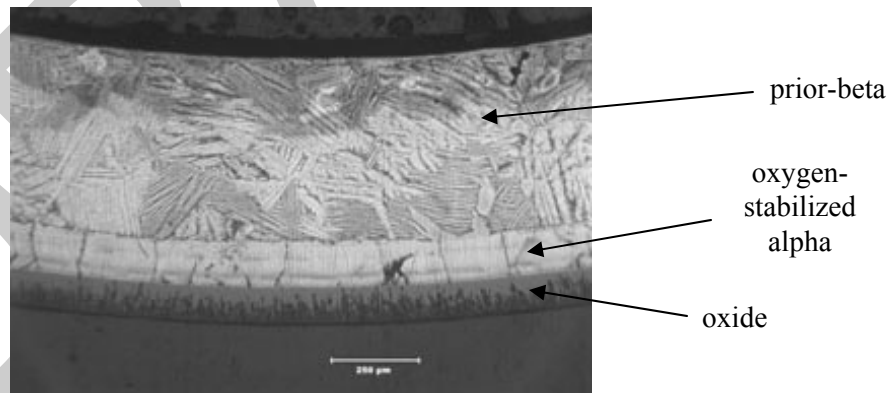


Figure 4. Unirradiated Zircaloy-2 after oxidation in steam at 1200°C for 600 seconds. Scale marker indicates for 200-μm length.

The presence of niobium in zirconium alloys alters this picture somewhat, with a more uneven boundary between the alpha and prior-beta layers, but the principle is the same. Within a ruptured balloon, steam will also enter through the rupture and produce a similar oxygen profile on the inside surface of the cladding.

### 1.3 Oxidation equations

Although the Baker-Just equations [12] have been used in many LOCA analyses, the Cathcart-Pawel (CP) equations are more accurate for Zircaloys and will be used throughout this report. In their

report [13], Cathcart et al. gave four related rate equations, one for each of the following: (a) the oxide layer thickness; (b) the alpha layer thickness; (c) the sum of the oxide-plus-alpha layer thickness; and (d) the total oxygen consumed, which was given as weight gain in grams per square centimeter of surface area. All of these obeyed parabolic kinetics. The rate equation for weight gain, Wg (Cathcart et al. called it  $\tau$ ), is:

$$d(Wg)/dt = (k^2/2)/Wg, \quad (1)$$

where k is a temperature-dependent coefficient (Cathcart et al. labeled it  $\delta_\tau$ ). Under isothermal oxidation conditions, the integration of Equation 1 is simply

$$(Wg)^2/2 = (k^2/2) t, \quad (2)$$

or

$$Wg = k t^{1/2}, \quad (2a)$$

which plots as a parabola.

The coefficient, k, is an Arrhenius-type function of temperature:

$$k = a \exp(-Q/[RT]), \quad (3)$$

where R is the universal gas constant, and the parameters a and Q are given by Cathcart et al. for each of the four rate equations reported. Using the Cathcart et al. (CP) values for "a" and "Q" for weight gain determined from metallographic results and the assumption of stoichiometric oxide, the isothermal CP equation becomes

$$Wg = 0.602 \exp(-1.005 \times 10^4/T) t^{1/2}, \quad (4)$$

where Wg is given by Cathcart et al. in  $g/cm^2$ , T is temperature in K, and t is time in s. Thus, the weight gain increases as the square root of time at a given temperature, and the rate increases exponentially with temperature. The results of Equation 4 should be multiplied by a factor of 10 to convert to the SI units of  $kg/m^2$ . For convenience in the current work, the measured weight gain is expressed as  $mg/cm^2$ . In comparing the measured weight gain per unit surface area to the CP-predicted weight gain, the results of Equation 4 are multiplied by  $10^3$  to give units of  $mg/cm^2$ .

A related parameter that is often used is ECR, or equivalent cladding reacted. ECR is defined as the percentage of the cladding thickness that would be oxidized if all the oxygen pickup stayed in the oxide layer as  $ZrO_2$ . This is an artificial parameter because some of the oxygen diffuses into the metal, but it is useful and is directly related to weight gain by simple geometric factors, along with factors based on the density of Zr ( $6500 \text{ kg/m}^3 = 6.5 \text{ g/cm}^3$ ), the atomic mass of Zr ( $91.2 \text{ kg/kg-mole}$ ), and the atomic mass of diatomic oxygen ( $32.0 \text{ kg/kg-mole}$ ). The conversion is given in Equation 5 for one-sided oxidation and Equation 6 for two-sided oxidation.

$$\text{One-sided oxidation} \quad ECR = 43.9 [(Wg/h)/(1 - h/Do)], \quad (5)$$

$$\text{Two-sided oxidation} \quad ECR = 87.8 Wg/h, \quad (6)$$

where ECR is in %, Wg is in  $g/cm^2$ , h is cladding thickness in cm, and Do is cladding OD in cm.

## 1.4 Embrittlement mechanisms

Six embrittlement mechanisms are described below. Three of them were known before this research was initiated and three were not. Data relating to all of these mechanisms are presented in subsequent sections of this report.

### 1.4.1 Beta-layer embrittlement by oxygen

As temperature increases during a LOCA transient, the amount of oxygen that the beta phase can hold also increases. Above about 1200°C, oxygen solubility in the beta phase becomes high enough in these cladding alloys that, after cooling, the prior-beta region will embrittle for relatively short oxidation times. This mechanism was understood in 1973, and the 1204°C (2200°F) temperature limit in NRC's regulation precluded such embrittlement in unirradiated Zircaloy [1].

### 1.4.2 Beta-layer thinning

With increasing time, diffusion of oxygen into the metal will convert more and more of the beta phase to the oxygen-stabilized alpha phase – the alpha layer grows and the beta region shrinks. For long times at temperature, the ductile prior-beta region becomes so thin that the macroscopic specimen exhibits brittle behavior. This mechanism was also understood in 1973 and is accommodated by the 17% ECR limit in NRC's regulation, provided oxidation is calculated with the Baker-Just correlation that was used in deriving the limit [1].

### 1.4.3 Localized hydrogen-induced embrittlement in the balloon region

Steam that enters through a rupture in a balloon causes oxidation inside the cladding. Hydrogen that is freed during this reaction is not swept away as it is on the outside of the cladding, but is absorbed in the metal. This absorption results in enhanced embrittlement in the balloon region or just beyond the necks of the balloon. This effect, which is neither burnup nor alloy dependent, was discovered earlier [1] and has been confirmed in the present research program.

### 1.4.4 Hydrogen-enhanced beta-layer embrittlement by oxygen

During normal operation, some hydrogen from the corrosion process is absorbed in the cladding metal. When that cladding is exposed to high-temperature LOCA conditions, the elevated hydrogen levels increase the solubility of oxygen in the beta phase and the rate of diffusion of oxygen into the beta phase. Thus, even for LOCA temperatures below 1204°C, embrittlement can occur for times corresponding to less than 17% oxidation in corroded cladding with significant hydrogen pickup.

### 1.4.5 General hydrogen-induced embrittlement from breakaway oxidation

Zirconium dioxide ( $ZrO_2$ ) can exist in several crystallographic forms (allotropes). The normal tetragonal oxide that develops under LOCA conditions is dense, adherent, and protective with respect to hydrogen pickup. There are, however, conditions that promote a transformation to the monoclinic phase – the phase that is grown during normal operation – that is neither fully dense nor protective. The tetragonal-to-monoclinic transformation is an instability that initiates at local regions of the metal-oxide interface and grows rapidly throughout the oxide layer. As this transformation results in an increase in oxidation rate, it is referred to as breakaway oxidation. Along with this increase in oxidation rate due to cracks in the monoclinic oxide, there is significant hydrogen pickup. Hydrogen that enters in this manner during a LOCA transient has the same effect on embrittlement as hydrogen from the normal burnup

process. Although breakaway oxidation was known in 1973, a connection to embrittlement was not made at that time.

#### 1.4.6 Oxygen pickup from the cladding inner surface

Figure 3 illustrates a situation where there is an oxygen source only on the cladding outer surface. For unirradiated cladding this oxygen source is the steam followed by the zirconium dioxide layer that forms during high temperature oxidation in steam. As burnup increases, normal corrosion will contribute to the outer-surface oxygen source. There will also be oxygen sources on the inner surface of irradiated cladding due to gas-phase  $UO_3$  transport prior to gap closure, fuel-cladding-bond formation ( $UO_2$  in solid solution with  $ZrO_2$ ), the fuel bonded to this layer. Under LOCA conditions, oxygen can thus enter the cladding from the inner surface even away from the balloon location. The situation is like a multilayer diffusion couple as illustrated in Figure 5. The actual thicknesses of the OD and ID oxygen sources may be relatively unimportant at high burnup because they contain much more oxygen than will diffuse into the metal (see related tests by Hofmann and Politis [14]). If the inner-surface oxide layer or the oxide-bond-fuel layer is well developed, then two-sided oxidation would have to be accounted for in LOCA calculations away from the balloon region.

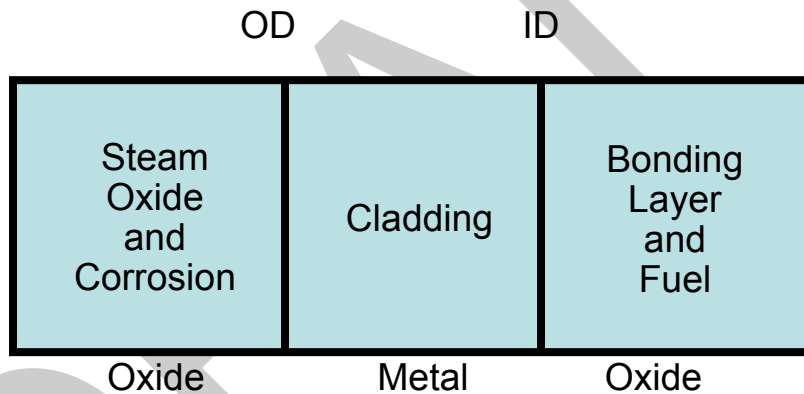


Figure 5. Diffusion couple character of oxygen sources and cladding metal.

## 2 Materials, Test Methods, and Procedures

---

The proper interpretation and use of LOCA-relevant data, require an understanding of cladding materials used for test samples, test methods, test procedures. These are described in this section.

### 2.1 Description of cladding alloys and high-burnup fuel segments

Unirradiated cladding alloys were provided by Global Nuclear Fuel (8×8, 9×9, and 10×10 Zry-2), Westinghouse (17×17 low-tin Zry-4 and ZIRLO), AREVA (1970s 15×15 Zry-4 tubing, 1980s 15×15 low-tin Zry-4, 15×15 low-tin Zry-4, 15×15 M5, and 17×17 M5), and Fortum (E110 tubing and cladding). Alloys, except for E110, that are listed without a decade are modern, belt-polished cladding alloys. The 8×8 Zry-2 was used for early thermal and metallurgical benchmark testing of the LOCA integral apparatus. The 9×9 Zry-2, although not archival cladding from the same lot, was fabricated by the same methods used to fabricate high-burnup Limerick fuel-rod cladding and has the same nominal composition and dimensions as the Limerick cladding. It has been used in this test program to generate baseline LOCA integral data and one-sided, high-temperature steam oxidation data. The 1970s 15×15 Zry-4 tubing is close to being archive material for the high-burnup H. B. Robinson (HBR) cladding tested in this program. However, this tubing has ≈0.05-mm larger outer diameter and ≈0.025-mm thicker wall than the HBR cladding. The final finishing step after fueling the HBR tubing to convert it to cladding was an outer-surface pickling to remove ≈0.05 mm from the outer diameter. Because this tubing was not in final form, it was not used to generate baseline data for the high-burnup HBR cladding. Rather, the 1980s 15×15 low-tin Zry-4 cladding, which has similar dimensions, oxygen content, and mechanical properties as the HBR cladding, is used in this work to determine baseline HBR oxidation and post-quench ductility properties.

Initial lengths of 15×15 and 17×17 M5 were provided by AREVA for benchmarking purposes but not for advanced-alloy data generation. This 17×17 M5 (0.57-mm wall) was characterized in terms of chemical composition and used to develop and benchmark the two-sided oxidation test train. At a later date, AREVA provided 17×17 M5 with 0.61-mm wall thickness for the purpose of data generation. The post-quench ductility of the 15×15 M5 and the 0.61-mm-wall 17×17 M5 was compared to confirm that post-quench ductility correlated with extent of oxidation (ECR) at a given temperature independent of cladding wall thickness and outer diameter.

For the advanced-alloy post-quench ductility program, the primary alloys of interest are 10×10 Zry-2, 17×17 low-tin Zry-4, 17×17 ZIRLO, and 17×17 M5 (0.61-mm wall). E110 was also added to the advanced-alloy testing program to try to determine why its steam-oxidation behavior is so poor as compared to M5, even though its alloy composition is similar. E110 tubing and cladding were provided by Fortum (Finland). The cladding was pickled (etched) and anodized to increase the outer-surface hardness. In addition to the supplied forms of E110, ANL-modified E110 had several variants, which included surface modification (polished, etched, etched-and-polished) and reduction in wall thickness to ≈61 mm (inner-surface machined and polished). Valuable lessons were learned from the E110 study regarding the destabilizing effects of surface roughness, surface scratches, and surface chemistry (e.g., F from etching) on oxidation at 950-1100°C. These experiences helped in planning the breakaway oxidation studies for all alloys.

For the breakaway-oxidation studies, it was planned to use the same alloys as for the post-quench-ductility studies. However, due to the very limited supply of 17×17 low-tin Zry-4, belt-polished 15×15 and HBR-type (rough surface) 15×15 low-tin Zry-4 were used instead. This choice allowed the effects of surface roughness to be included in these studies for Zry-4 samples with similar geometry, tin content,

and oxygen content. The other three alloys (10×10 Zry-2, 17×17 ZIRLO, and 17×17 M5) used in the post-quench-ductility tests were also used in the breakaway oxidation tests.

For most of the cladding alloys received by ANL, measurements were performed to determine the OD, wall thickness, surface roughness, oxygen content, and tin content. Some of the alloys were sent to an outside organization to determine chemical composition. For ZIRLO cladding, Westinghouse also performed chemical analysis on a sample of the cladding sent to ANL.

Table 3 summarizes the dimensions, surface conditions, and chemical composition of the Zr-lined Zry-2 used in the ANL test program. The Zr liner is on the cladding inner surface ( $\approx 10\%$  of the wall thickness). Chemical composition data listed in Table 3 refer to the final cladding product ( $\approx 90\%$  Zry-2 and  $\approx 10\%$  Zr liner). They should not be interpreted as the composition of standard Zry-2. The chemical composition listed in Table 1 for Zry-2 is closer to the composition of the Zry-2 alloys tested at ANL.

Table 3 Dimensions and Chemistry of Zr-lined Zry-2 Used in the ANL Test Program (the “<” sign means below the detection limit).

Parameter	8×8 Zry-2	9×9 Zry-2	10×10 Zry-2
OD, mm	12.27	11.18	10.29
Wall Thickness, mm	0.82	0.71	0.66
ID Liner Thickness, mm	$\approx 0.08$	$\approx 0.07$	$\approx 0.07$
OD Surface Roughness, $\mu\text{m}$	---	0.14	0.11
Sn, wt. %	---	1.18	---
Nb, wt. %	---	<0.01	---
O, wt. %	---	0.11	---
Fe, wt. %	---	0.20	---
Cr, wt. %	---	0.12	---
Ni, wppm	---	550	---
S, wppm	---	30	---
C, wppm	---	250	---
Hf, wppm	---	<100	---
Si, wppm	---	$\leq 100$	---
N, wppm	---	45	---
H, wppm	---	6	13

The dimensions and chemistry of the Zry-4 used in the ANL test program are listed in Table 4. Included in Table 4 are the dimensions and chemistry for near-archive HBR tubing, even though this tubing was not used in the post-quench-ductility or breakaway-oxidation studies. Pickling was used for the inner surfaces of both the near-archive HBR tubing and the HBR baseline cladding.

The dimensions and chemistry for 17×17 ZIRLO, 17×17 M5 (validation lot), 17×17 M5 (data lot), and 15×15 M5 (validation lot) used in the ANL test program are listed in Table 5.

Table 4 Dimensions and Chemistry of Zry-4 Used in the ANL Test Program (the "<" sign means below the detection limit).

Parameter	15×15 Zry-4 HBR Archive Tubing 1977 <sup>a</sup>	15×15 Zry-4 HBR Baseline Cladding ≈1980 <sup>b</sup>	15×15 Zry-4 Cladding Modern <sup>c</sup>	17×17 Zry-4 Cladding Modern <sup>d</sup>
OD, mm	10.84	10.77 (10.76)	10.91	9.50
Wall Thickness, mm	0.80	0.76 (0.77)	0.67	0.57
OD Surface Roughness, μm	0.36	0.32 (0.31)	0.10	0.14
Sn, wt.%	1.42	1.29	1.29±0.1	1.29±0.1
Nb, wt.%	---	---	---	---
O, wt.%	0.137	0.136	0.124	0.120
Fe, wt.%	0.21	---	---	---
Cr, wt.%	0.10	---	---	---
Ni, wppm	<35	---	---	---
S, wppm	---	---	---	---
C, wppm	140	---	---	---
Hf, wppm	<50	---	---	---
Si, wppm	92	---	---	---
N, wppm	54	---	---	---
H, wppm	12	22	26	5

<sup>a</sup>Sandvik Special Metals Corp Certificate of Quality; based on tubing (H, N, O) and ingot; 06-30-77.

<sup>b</sup>ANL data based on two AREVA lots received in April 2003 (0403) and November 2004 (1104).

<sup>c</sup>ANL data for AREVA cladding received in December 2004.

<sup>d</sup>ANL data for cladding provided by Westinghouse.

Fortum sent two types of E110 to ANL: tubing and cladding. The processing of tubing into cladding involves pickling (etching) and anodizing to grow a fine (<<1 μm) oxide layer on the outer surface of the tubing. The oxide layer enhances the surface hardness and protects the soft E110 cladding from scratching and abrading during handling and loading into fuel assemblies. The ANL test program modified some of this tubing and cladding to study the effects of surface roughness and chemistry. The modifications are listed in Table 6 under the categories of "polished" and "machined-and-polished".

Irradiated materials used in the ANL test program are summarized in Table 7. The Electric Power Research Institute (EPRI) provided ANL with two fueled TMI-1 PWR rods at 48-50 GWd/MTU for validation of characterization and test methodologies, seven fueled Limerick BWR rods at 54-57 GWd/MTU for LOCA data generation, and seven fueled H. B. Robinson PWR rods at 64-67 GWd/MTU.

Table 5 Dimensions and Chemistry of ZIRLO and M5 Used in the ANL Test Program (the "<" sign means below the detection limit).

Parameter	17×17 ZIRLO <sup>a</sup>	17×17 M5 <sup>b</sup> (Validation)	17×17 M5 <sup>c</sup> (Data)	15×15 M5 <sup>c</sup> (Validation)
OD, mm	9.50	9.50	9.50	10.91
Wall Thickness, mm	0.57	0.57	0.61	0.64
OD Surface Roughness, μm	0.11	0.12	0.12	0.11
Sn, wt.%	0.99	0.02	---	---
Nb, wt.%	0.98	1.02	---	---
O, wt.%	0.12	0.145	0.145	---
Fe, wt.%	0.11	0.05	---	---
Cr, wt.%	<0.01	<0.01	---	---
Ni, wppm	<100	<100	---	---
S, wppm	---	25±5	---	---
C, wppm	135	110	---	---
Hf, wppm	40	<100	---	---
Si, wppm	53	<100	---	---
N, wppm	46	55	---	---
H, wppm	5	6	5	---

<sup>a</sup>Chemical data provided by Westinghouse and CONAM Materials Analysis Group; H and O content confirmed by ANL.

<sup>b</sup>Chemical data provided by CONAM Materials Analysis Group; H and O content confirmed by ANL.

<sup>c</sup>ANL data for AREVA M5 cladding.

EPRI and AREVA provided two high-burnup fueled M5 rods at 63 and 70 GWd/MTU for LOCA integral testing of fueled-cladding samples. In addition, under agreements among NRC-Studsvik-AREVA and NRC-Studsvik-Westinghouse, high-burnup defueled M5 cladding from the European Ringhals PWR reactor and high-burnup defueled ZIRLO cladding from the North Anna PWR reactor, respectively, have been supplied to ANL for post-quench ductility testing. Cladding materials are characterized in sections relevant to the post-quench ductility and LOCA integral testing of these materials.

## 2.2 Oxidation and quench tests with short defueled cladding samples

The LOCA integral apparatus is designed to perform both LOCA integral tests using long (≈300 mm) fueled cladding samples and oxidation-quench tests using short (25 mm) defueled cladding samples. One out-of-cell unit is maintained for thermal-benchmarking purposes and for generating data for as-fabricated and prehydrided alloys. An in-cell unit is maintained for testing fueled and defueled cladding. Both units use the same control and data acquisition systems. The main difference between LOCA-integral and oxidation-quench tests is the test train holding the sample in position within the quad-elliptical, radiant furnace and the connections required. Both use the quartz-tube steam chamber.

Table 6 Dimensions and Chemistry of E110 Tubing and Cladding Used in the ANL Test Program (the "<" sign means below the detection limit).

Parameter	E110 Tubing <sup>a</sup>	E110 <sup>b</sup> Cladding	E110 <sup>c</sup> (Polished)	E110 <sup>d</sup> (Machined-and-Polished)
OD, mm	9.17	9.13	9.14	9.14
Wall Thickness, mm	0.71	0.70	0.69	0.58-0.69
OD Surface Roughness, $\mu\text{m}$	0.35	0.19	0.14	0.14
Sn, wt.%	0.02	---	0.02	0.02
Nb, wt.%	1.03	---	1.03	1.03
O, wt.%	0.05	---	0.05	0.05
Fe, wt.%	0.055 $\pm$ 0.015	---	0.055 $\pm$ 0.015	0.055 $\pm$ 0.015
Cr, wt.%	<0.01	---	<0.01	<0.01
Ni, wppm	<100	---	<100	<100
S, wppm	25 $\pm$ 15	---	25 $\pm$ 15	25 $\pm$ 15
C, wppm	135	---	135	135
Hf, wppm	100	---	100	100
Si, wppm	100	---	100	100
N, wppm	46	---	46	46
H, wppm	5	---	5	5

<sup>a</sup>Chemical data provided by CONAM Materials Analysis Group; H and O content confirmed by ANL.

<sup>b</sup>Pickled and anodized to harden the outer-surface layer.

<sup>c</sup>Polishing done for about 2 minutes with 9- $\mu\text{m}$  and 3- $\mu\text{m}$ -grit  $\text{Al}_2\text{O}_3$  paper.

<sup>d</sup>Machining of inner surface and polishing of both outer and inner surfaces; a few test samples were prepared by machining 25  $\mu\text{m}$  off the outer surface followed by polishing of both surfaces.

The furnace has a 250-mm-high uniform heating zone with radiant heating from four vertical bulbs and a reflecting inner surface. The LOCA integral tests are conducted with long samples initially under high internal pressure (7-15 MPa), which requires a connection to the high-pressure helium line, along with top and bottom pressure transducers. The oxidation-quench tests do not require the high-pressure connection or pressure transducers. Figure 6 shows the out-of-cell apparatus, with the essential components labeled. Figure 7 shows a schematic of the out-of-cell apparatus and the in-cell apparatus. The test chamber is first purged with high-purity argon gas to remove air (out-of-cell and beta-gamma in-cell) or nitrogen (alpha-gamma in-cell) test chamber. Steam, at near-atmospheric pressure, flows up through the test chamber at 0.32 $\pm$ 0.02 g/cm<sup>2</sup>/minute (5.3 g/minute) and exits the chamber into a condenser. The quartz test chamber is 686-mm long, 50-mm OD, and 1.5-mm wall thickness. Following oxidation and slow-cooling phases, steam flow is turned off, and quench water is introduced through bottom flooding to give very rapid sample cooling at the desired time and temperature during cooling.

Table 7 Characteristics of High-burnup Fuel Rod Segments and Defueled High-burnup Cladding for the ANL LOCA Test Program.

Parameter	TMI-1	Limerick	H. B. Robinson	North Anna M5	North Anna ZIRLO	Ringhals M5
Reactor	PWR	BWR	PWR	PWR	PWR	PWR
Enrichment, wt. %	4.00	3.95 (3.40-3.95)	2.90	4.20	≈4	≈4
Burnup, GWd/MTU	48-50	54-57	63-67	63-70	71	63
Discharge Date	1997	1998	1995	2004	2001	2003
Fast Fluence, $10^{25}$ n/m <sup>2</sup>	9	11	14	Not Provided	Not Provided	Not Provided
Cladding	15×15 Low-Sn Zry-4	9×9 Zr-lined Zry-2	15×15 Zry-4	17×17 M5	17×17 ZIRLO	17×17 M5
Initial Wall Thickness, mm	0.69	0.71	0.76	0.57	0.57	0.57
OD Oxide, μm	≤30	≈10 + ≈10 crud	≤100	<25	≈20-50	<25
Hydrogen Pickup, wppm	≤300	70	≤800	<120	<700	<100
Fueled	Yes	Yes	Yes	Yes	No	No

The apparatus shown in the Figure 7 schematic was initially used for oxidation-kinetics tests of near-archive Limerick 9×9 Zry-2, high-burnup Limerick 9×9 Zry-2, and intermediate-burnup TMI-1 15×15 Zry-4 [15]. These one-sided oxidation tests, which were conducted in-cell, were performed without quench. Also, a slow-flowing argon purge was maintained inside the cladding and test train to minimize steam and hydrogen build-up. The test train used to conduct these in-cell tests is shown in Figure 8. Three Type S thermocouples are welded 120° apart onto the Inconel sample holder just above the sample. One of these thermocouples is used to control the furnace power to achieve the desired hold temperature. The other two are for monitoring circumferential temperature distribution. For these tests, a fourth thermocouple is suspended within the sample to determine the circumferentially averaged temperature. Prior to conducting these in-cell tests, thermal and metallurgical benchmark tests were conducted out-of-cell with thermocouples welded directly onto the sample outer surface. The thermal results showed excellent agreement in the long-time hold temperatures among the thermocouples welded onto the sample, the three thermocouples welded onto the Inconel holder above the sample, and the thermocouple (TC) suspended inside the sample. Although not important for these long-time tests (≥300 s), the temperature rise of the suspended TC lagged the temperature rise of the holder TCs, which lagged the temperature rise of the TCs welded onto the sample.



Figure 6. Overview of the out-of-cell LOCA integral test apparatus. The in-cell unit is located at Workstation 6 of the Alpha-Gamma Hot Cell Facility (AGHCF) behind the hot-cell shield and seal windows. H. B. Robinson high-burnup Zry-4 oxidation/quench tests, as well as Limerick high-burnup integral tests, were conducted in the AGHCF. Following closure of the AGHCF to programmatic work on January 13, 2006, the in-cell apparatus was no longer available and the out-cell apparatus was moved to a different laboratory. A third apparatus was installed in Cell#4 of the Irradiated Materials Laboratory for performing oxidation-and-quench of high-burnup ZIRLO and M5 cladding samples.

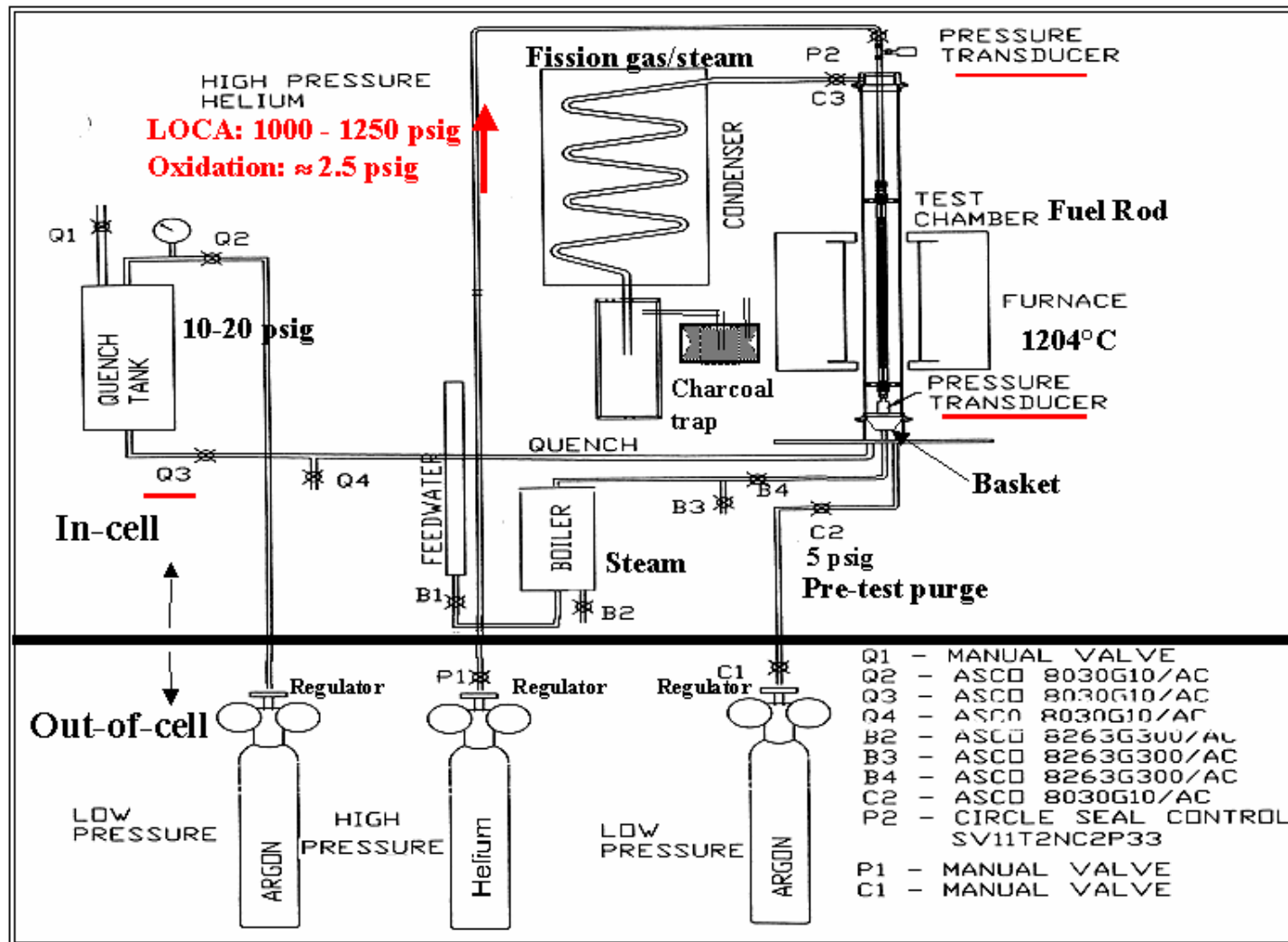


Figure 7. Schematic of oxidation kinetics, oxidation-quench, and LOCA integral test apparatus; test train and sample are shown for LOCA integral testing.

The test train in Figure 8 was modified for the advanced-alloy post-quench ductility tests in order to conduct two-sided steam oxidation tests. The two-sided tests offered many advantages over the one-sided tests: better temperature control, uniform inner-surface oxidation, no change in sample hydrogen content due to inner-surface hydrogen pickup or hydrogen desorption to the purge gas, and a reliable and cost-effective way to determine weight gain by simply weighing the sample before and after the test. Figure 9 shows the test train used for oxidizing and quenching the samples prior to conducted post-quench ductility tests. Holes were drilled into the hollow Inconel holder below and above the sample to allow adequate steam flow inside the cladding sample. Other changes were made to the Inconel holder wall thickness and outer-diameter to reduce the thermal mass and transient temperature lag of the holder.



Figure 8. Test train for conducting one-sided steam-oxidation kinetics tests in-cell using  $\approx 25$ -mm-long Zircaloy cladding samples: a) test train within quartz tube; and b) enlarged view of sample region along the test train showing alumina spacers to inhibit Zircaloy-Inconel interaction and zirconia washers to minimize steam leakage to the sample inner surface.

Temperature control and monitoring are extremely important in conducting oxidation-quench tests, followed by post-quench ductility tests. As discussed in Section 1, the time-at-temperature for the transition between ductile and brittle behavior is a strong function of temperature. The furnace power and sample temperature are controlled by feedback from the designated TC output through a proportional-integral-differential (PID) controller to the furnace power. Because the sample has such low thermal mass per unit length, it is important to ramp to the hold temperature at a relatively fast rate for these tests without temperature overshoot due to the initially rapid heat generation rate from cladding oxidation. In setting the controller parameters, the requirements are that the temperature overshoot during the ramp be  $< 20^\circ\text{C}$  relative to the target hold temperature for a short period of time (few seconds), and that the average hold temperature be within  $10^\circ\text{C}$  of the target temperature. The  $10^\circ\text{C}$  is reasonable given the uncertainty in the Type S thermocouples – a few degrees – at the maximum oxidation temperature ( $1204^\circ\text{C}$ ). Temperature overshoot is not much of an issue for long-time oxidation temperatures  $\leq 1100^\circ\text{C}$ , but it can have a significant embrittlement effect for higher oxidation temperatures. For tests conducted at  $1200^\circ\text{C}$ , temperature overshoot was minimized by slowing down the heating rate at ramp temperatures within  $50$ - $100^\circ\text{C}$  of the target temperature.



Figure 9. Test train design for two-sided oxidation tests with four holes drilled into the Inconel holder below the sample (left) for steam ingress and four holes drilled into the holder above the sample for steam egress. Also shown are the three thermocouples permanently welded to the Inconel holder just above the sample.

The following benchmarking procedure has been established for each test train:

- a) Calibrate all purchased TCs to ANL-owned, NIST-calibrated TC wire; this step was introduced in January 2006.
- b) Weld two calibrated Type S TCs to sample at same orientation as holder control TC and another holder TC  $\pm 120^\circ$  from the control TC.
- c) Use repeated testing with fresh samples and same orientation for TCs welded to sample to determine optimum controller parameters for desired temperature ramp and hold temperature.
- d) For larger-diameter cladding (e.g., BWR 9×9 and PWR 15×15) which exhibit higher circumferential temperature variation, repeat test with new sample, where one TC is welded on the sample at the same orientation as the holder control TC, and one TC is welded on sample at the same orientation as the third holder TC; this provides a good check of reproducibility of temperature results, as well as a better determination of circumferential variation.
- e) Perform metallographic examination to determine oxide-layer thickness at eight circumferential locations on the outer and inner surfaces; compare measured and predicted average values to the Cathcart-Pawel (CP)-predicted values to ensure  $<10\%$  difference; compared circumferential variation in measured oxide layer thickness to ANL criterion ( $\leq \pm 3 \mu\text{m}$ ).
- f) Conduct oxidation test without TCs welded on the sample and compare the measured sample weight gain at a time corresponding to  $\approx 10\%$  CP-ECR to the weight gain calculated with the CP-correlation; also perform metallographic examination to determine the average inner- and outer-surface oxide layer thicknesses, as well as the variation.
- g) If temperature requirements are satisfied, if measured weight gain is within 10% of predicted weight gain, if average oxide layer thickness on inner and outer surfaces is within 10% of the CP predicted thickness, and if the circumferential variation in oxide layer thickness is consistent with the circumferential temperature variation, then begin oxidation testing with this test train.
- h) Continue to run tests with the benchmarked test train and controller parameters for specific hold temperature until the measured weight gain and CP-predicted weight gain differ by  $\geq 10\%$ ; repeated

quench will cause some warping of the test train, which moves the sample away from the furnace focal point; generally, a test train will be good for  $\approx 15$  runs with quench and more without quench.

Figure 10 shows thermal benchmark results for as-fabricated HBR-type  $15 \times 15$  Zry-4 cladding. In order not to obscure the results, the three holder temperatures for each of the two tests are not shown. For the controller parameters chosen, the hold temperature is  $1204 \pm 10^\circ\text{C}$ , where the  $\pm 10^\circ\text{C}$  is the circumferential variation in temperature based on sample TC readings at  $0^\circ$ ,  $120^\circ$ , and  $240^\circ$ . On the average, there is no temperature overshoot. The highest reading of any one TC is  $1220^\circ\text{C}$  for a brief period of time. For this particular set of controller parameters, the temperature rise consists of a very fast ramp ( $\approx 75^\circ\text{C/s}$ ) from  $300^\circ\text{C}$  to  $\approx 1100^\circ\text{C}$  and a slow ramp ( $\approx 1.3^\circ\text{C/s}$ ) from  $1100^\circ\text{C}$  to  $1204^\circ\text{C}$ . At the end of the hold time, the furnace power is turned off, and the sample cools in steam at an average of  $\approx 11^\circ\text{C/s}$  to the desired quench temperature of  $800^\circ\text{C}$ . The actual cooling rate decreases exponentially with time, as would be expected for this zero-furnace-power phase of the transient. Part of the thermal benchmark testing is to determine the test time and temperature at which to stop the steam flow and initiate bottom-flooding quench-water flow to induce very rapid cooling at the specified temperature. Rapid cooling ( $\approx 150^\circ\text{C/s}$ ) from the quench temperature to  $100^\circ\text{C}$  is fast enough for these tests, but not as fast as in-reactor cooling rates following wetting. This lower rate is due to the limited quench water supply that can be used in-cell ( $< 3$  liters based on hot-cell criticality limitations). There is only enough quench water to fill the quartz tube chamber to an elevation just above the furnace.

As shown in Figure 10, the test is not an isothermal test. The significance of the weight gain during the initial heating ramp depends on the hold temperature and the hold time. For the temperature history shown in Figure 10, the CP-predicted weight gain is determined numerically by integrating Equation 1 over the time-dependent temperature profile  $T(t)$ :

$$(\text{Wg})^2 = 0.362 \int_0^t \exp(-20100/T) dt, \quad (7)$$

where  $\text{Wg}$  is in  $\text{g/cm}^2$ ,  $T$  is in K, and  $t$  is in s. Because of the parabolic nature of the weight gain correlation, the small weight gain during the cooling ramp can generally be ignored. Also, the CP set of correlations was validated for  $T \geq 1000^\circ\text{C}$  (1273 K). However, the weight gain correlation appears to give results consistent with ANL data for  $T \geq 950^\circ\text{C}$ . For the ANL work, the integral in Eq. 7 is converted to an integral with respect to temperature and the integration for the high-temperature oxidation tests (e.g., Figure 10) is generally performed for  $T \geq 1000^\circ\text{C}$ .

For oxidation and quench of as-fabricated and prehydrided samples used for post-quench ductility tests, the procedure is the same as the one used in the thermal and metallurgical benchmark tests:

- a) Stabilize the system at  $300^\circ\text{C}$  in flowing saturated steam for 500 s.
- b) Initiate temperature ramp with feedback between the holder TC and the furnace power.
- c) Hold at temperature for a predetermined time to achieve the desired CP weight gain and ECR.
- d) Turn furnace power off while maintaining steam flow at the end of the hold time.
- e) Stop steam flow and initiate bottom-flooding quench at a test time that will give rapid cooling at the desired cladding temperature.

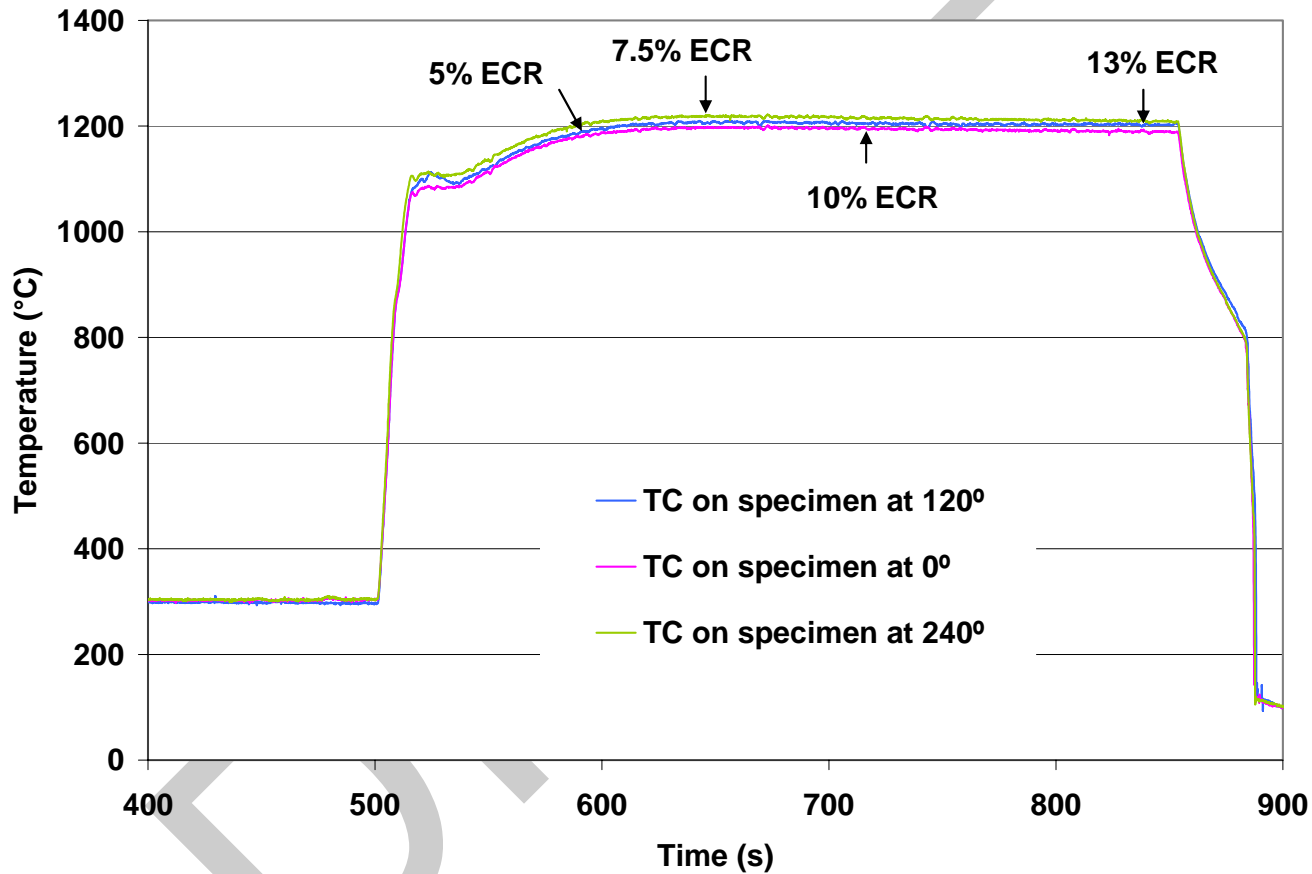


Figure 10. Thermal benchmark results from two tests, each with two TCs welded onto as-fabricated, HBR-type 15×15 Zry-4 cladding. Test HBRU#20 had TCs welded onto the sample at 0° and 120°, while test HBRU#29 had TCs welded onto a new sample at 0° and 240°. The sample hold temperature is  $1204 \pm 10^\circ\text{C}$ , where  $1204^\circ\text{C}$  is the average of the three TC readings and  $\pm 10^\circ\text{C}$  is the standard deviation.

The procedure for conducting in-cell oxidation-quench tests with high-burnup cladding samples is similar to the one described above for out-of-cell tests with unirradiated cladding samples. However, the corroded, irradiated samples were not directly thermally benchmarked because ANL does not have the in-cell capability to locally remove the corrosion layer and spot-weld TCs to the cladding metal surface. With respect to the temperature history shown in Figure 10 for bare, unirradiated cladding, it is expected that pretest cladding corrosion would slow down the initial oxidation rate and the heating rate associated with the exothermic oxidation reaction. The presence of the corrosion layer would basically affect the peak temperature reached during the very rapid heating ramp. This effect has been confirmed in out-of-cell tests using the following procedure to determine the temperature profile for high-burnup Zry-4 cladding with a 70- $\mu\text{m}$ -thick corrosion layer and an  $11\pm 4$ - $\mu\text{m}$ -thick fuel-cladding bond layer:

- a) With TCs welded onto bare as-fabricated cladding, conduct the thermal benchmark test for a hold time selected to grow 40- $\mu\text{m}$ -thick oxide layers on the inner and outer surfaces of the cladding.
- b) Cool to 300°C and repeat thermal benchmark test using the same controller parameters as were used in (a); compare the two sets of results with emphasis on the maximum temperature at the end of the rapid temperature rise (first peak), the time to reach the hold temperature, and the hold temperature.
- c) If necessary, increase the holder control temperature to achieve the desired hold temperature for cladding with pre-transient oxide layers.
- d) Install the calibrated test train in the in-cell furnace and conduct a metallurgical benchmark test with as-fabricated cladding without the TCs welded onto the cladding and with the hold time chosen to give a weight gain equivalent to 10% CP-ECR; if the out-of-cell and in-cell weight gains and converted ECRs are in good agreement, then the use of the test train in the in-cell furnace has been validated.
- e) Use the results of the thermal benchmark in (b) and (c) – the one with oxide layers grown on the inner and outer surfaces prior to initiating the temperature ramp – to choose test times to give the desired CP-ECR values and to interpret the experimental results for high-burnup cladding.

The results of benchmark tests (a) and (b) indicated the following for HBR-type 15×15 Zry-4: the peak temperature at the end of the rapid heating rate was 40°C less for pre-oxidized cladding as compared to bare cladding; the time to reach the hold temperature was about the same for both cases; and the hold temperature for the pre-oxidized cladding was  $\approx 8^\circ\text{C}$  less than the hold temperature for the bare cladding. Knowing these effects helps to choose the optimum controller parameters for in-cell tests with high-burnup cladding samples. For example, higher heating rates and desired hold temperatures for high-burnup ZIRLO and M5 cladding can be achieved by selecting controller parameters to give rapid heating to the hold temperature for bare cladding and repeating the test with the appropriate steam-grown oxide layer thicknesses chosen to match the sum of the corrosion layer thickness and the fuel-cladding bond thickness. For high-burnup M5 with a 20- $\mu\text{m}$ -thick corrosion layer and a 10- $\mu\text{m}$ -thick fuel-cladding bond layer, the test time for the first benchmark would be chosen to grow 15- $\mu\text{m}$ -thick oxide layers on the cladding inner and outer surfaces, and the hold temperature would be chosen to be slightly higher (e.g., 1205-1210°C) than the hold temperature targeted for the in-cell high-burnup cladding. Following cooling to 300°C, the same controller parameters would be used to conduct the thermal benchmark for the in-cell tests. A bare-cladding thermal history, which is a candidate for testing high-burnup ZIRLO and M5, is shown in Figure 11.

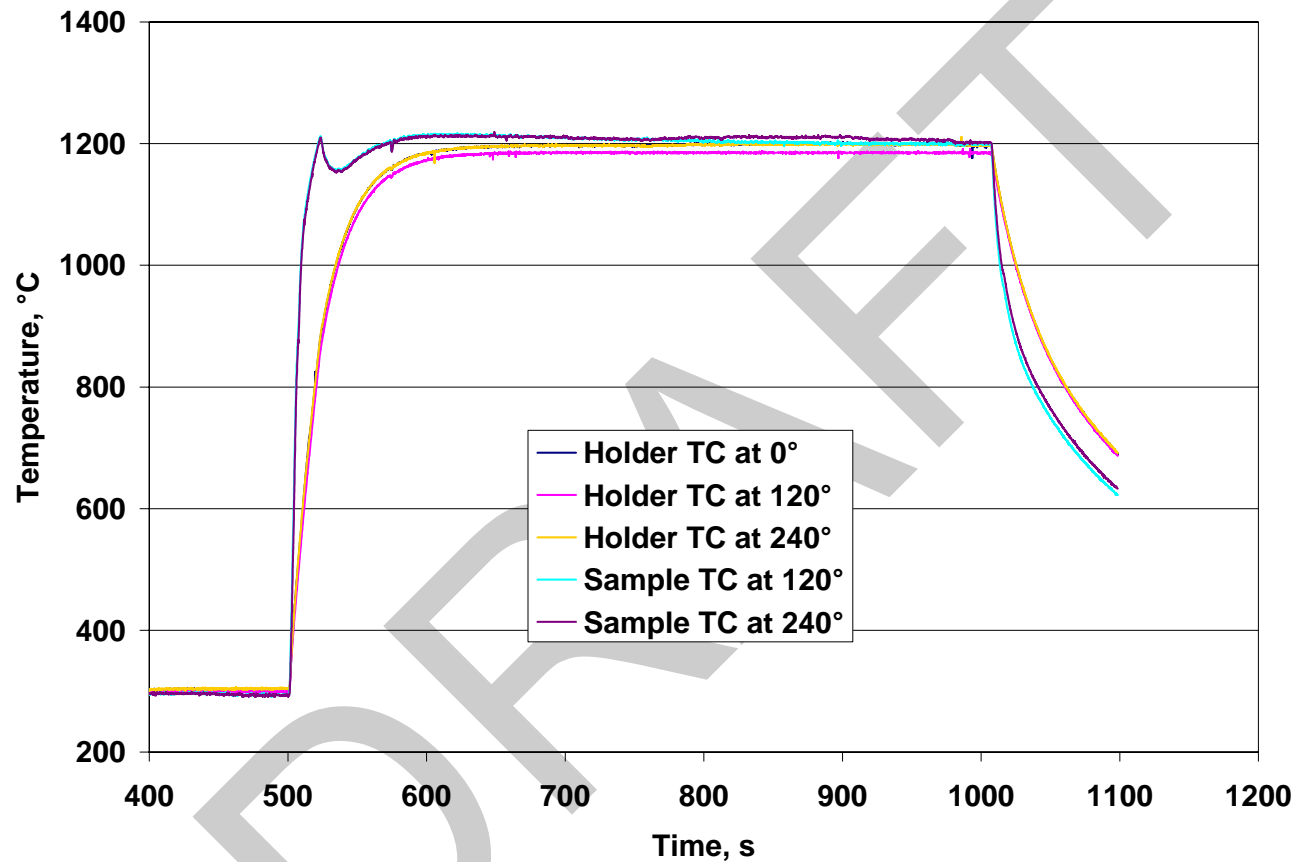


Figure 11. Thermal benchmark results with as-fabricated 17×17 ZIRLO sample. Repeating this test following the growth of inner- and outer-surface oxide layers decreased the first peak during the heating ramp to <1200°C and decreased the overshoot during the early part of the hold time to ≈1200°C; the controller parameters used to generate this thermal history can be used for in-cell tests with high-burnup ZIRLO and M5 cladding samples.

### 2.3 Ductility determination using ring-compression tests

Hobson [16] and Hobson and Rittenhouse [17] performed low- and high-strain-rate ring compression tests, respectively, using two-sided oxidized Zry-4 cladding samples over a wide range of temperatures. The results of the low-strain-rate tests at  $\approx 135^\circ\text{C}$  ( $275^\circ\text{F}$ ) were used to formulate the  $1204^\circ\text{C}$  ( $2200^\circ\text{F}$ ) peak cladding temperature and 17% maximum oxidation level (Baker-Just ECR [12]). The ring-compression test is a good ductility screening test that is often used for near-brittle to brittle materials. However, the methods used by Hobson to determine oxidation temperatures and levels leading to brittle behavior were crude. Rings were crushed to complete failure – often four cracks at the  $0^\circ$  (12 o'clock),  $90^\circ$  (3 o'clock),  $180^\circ$  (6 o'clock), and  $270^\circ$  (9 o'clock) positions relative to the loading platen. The pieces were reassembled. If the cracked pieces formed a circular shape vs. an oval shape, they were classified as brittle. Load-displacement curves for these tests were never published and apparently not used.

In the current work, 8-mm-long rings are compressed at a low-displacement rate ( $0.0333\text{ mm/s}$ ) in an Instron test machine. The load-displacement curves are analyzed in the standard way: linearize the initial loading curve (see blue line in Fig. 12), use the slope of the initial loading curve to mathematically unload the sample at the peak load before a significant load drop ( $\approx 30\text{-}50\%$ ) indicating a through-wall crack along the length of the sample (see green line in Fig. 12), and determine the offset displacement (distance along the displacement axis between loading and unloading lines). This offset displacement is normalized to the outer diameter of the pre-oxidation-test cladding to determine a relative plastic strain. The methodology is illustrated in Figure 12 for  $17\times 17$  Zry-4 oxidized at  $1100^\circ\text{C}$  to 20% CP-ECR (20.3% based on measured weight gain), quenched at  $800^\circ\text{C}$  and ring-compressed at room temperature (RT). The offset displacement for this sample is  $0.455\text{ mm}$ . Normalizing this to the outer diameter of  $9.50\text{ mm}$  for

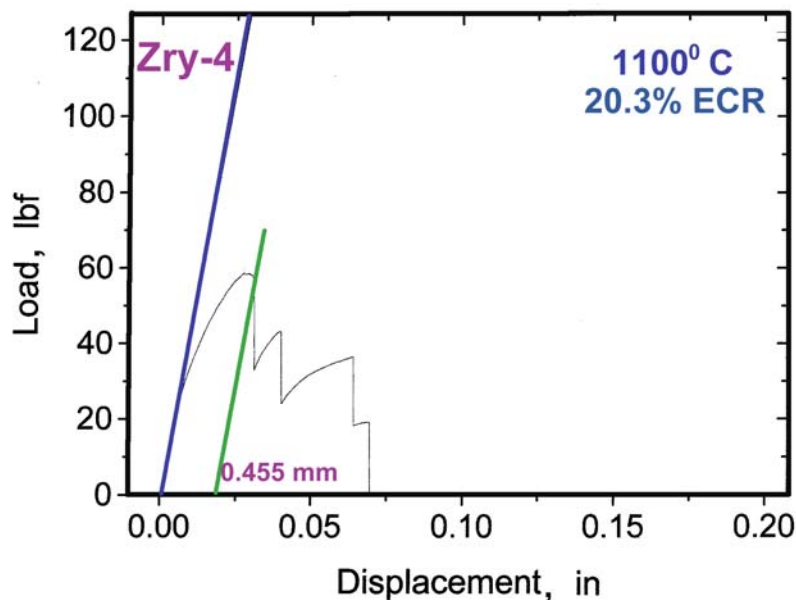


Figure 12. Ring-compression load-displacement data at room temperature for Zry-4 oxidized to 20% CP-ECR (20.3% ECR based on measured weight gain) at  $1100^\circ\text{C}$ . The sample fractured into four pieces. The offset strain ( $0.455\text{ mm}$ ) is the distance along the displacement axis between the loading slope (blue) and the unloading slope (green).

the pre-oxidation-test cladding gives an offset strain of 4.8%. Cladding alloys (Zry-4, ZIRLO, M5, and E110) oxidized at 1000°C and 1100°C were tested and analyzed with this procedure. However, a few questions arose during this work regarding the methodology: would the ring actually unload prior to failure at the initial loading slope; what is the uncertainty in determining offset strain; and, given this uncertainty, what minimum value of offset strain should be used as the criterion for nil ductility?

To answer these questions, most of the cladding alloys listed in Tables 3-6 were compressed at RT and 0.0333 mm/s in the as-fabricated condition to a total displacement of 2 mm. The samples were unloaded, and the post-test outer diameter for each ring was measured and compared to the pre-test outer diameter. The difference between these two diameters normalized to the initial diameter is a more direct measure of permanent strain and the ability of the material to deform plastically (i.e., exhibit ductility). It was found that the measured permanent displacement was  $\leq 0.18$  mm smaller than the offset displacement determined by the standard methodology shown in Figure 12. This converts to an over-prediction of  $\leq 2\%$  by using the offset-displacement method. The logical explanation for this difference is that the unloading slope must be less than the loading slope. When the sample is loaded, it starts out circular with zero internal stress and behaves like an elastic spring with spring constant  $k_s$ . For the 17×17, 15×15, and E110 samples tested, the calculated and measured spring constants were in good agreement, ranging from 0.9 to 2.0 kN/mm for 8-mm-long samples. The low value is for 17×17 Zry-4, ZIRLO and M5 with 0.57-mm wall thickness. The high value is for thick-wall/small-diameter E110. The HBR-type 15×15 Zry-4 has an intermediate value of 1.4 kN/mm. When the sample is unloaded, it is somewhat oval, has residual bending stresses from non-uniform plastic deformation, and has a lower unloading slope. This was confirmed both experimentally and analytically. The experimental confirmation is presented in the following.

The 8511 servo-hydraulic Instron was programmed for a compression displacement of 2 mm at 0.0333 mm/s, followed by unloading at a controlled rate of 0.0333 mm/s. The sample used was HBR-type 15×15 Zry-4. The results are shown in Figure 13. Clearly, the unloading slope is not as steep as the loading slope. The offset displacement (1.32 mm) based on mathematical unloading of the sample at the loading slope is larger than the true offset displacement (1.19 mm) based on the unloading curve. The difference (0.13 mm) is equivalent to 1.2% for this cladding. The permanent displacement determined directly by measuring the pre-test and post-test diameter in the loading direction is in excellent agreement with the 1.19 mm determined from the full load-displacement curve, including unloading.

For oxidized samples, controlled unloading is not possible just prior to failure because the displacement at which failure will occur is unknown. Therefore, the standard procedure shown Figure 12 is used to determine offset displacement and strain. To compensate for this over-estimation of offset strain, a limiting offset strain of 2% is set in the determination of the ductile-to-brittle transition. In other words, there is confidence in labeling samples with  $\geq 2\%$  offset strain as ductile. For samples with offset strains  $< 2\%$ , it is not clear if they are ductile or brittle.

The 17×17 Zry-4, ZIRLO, and M5 samples oxidized at 1000°C and 1100°C to 5-20% CP-ECR and quenched at 800°C were initially compressed at RT and 0.0333 mm/s to complete failure (three to four cracks) indicated by a load drop to zero. For samples that exhibited offset strains  $< 2\%$  (e.g., one M5 sample at 1.8%), the test was repeated with another 8-mm ring from the same oxidation-quench sample by stopping the test after the first significant load drop (30-50%). The sample was removed from the Instron and examined under a microscope to verify that a through-wall crack along the whole length of the sample had occurred. The post-test diameter was measured in the loading direction and compared to the pre-test diameter to determine permanent displacement and strain.

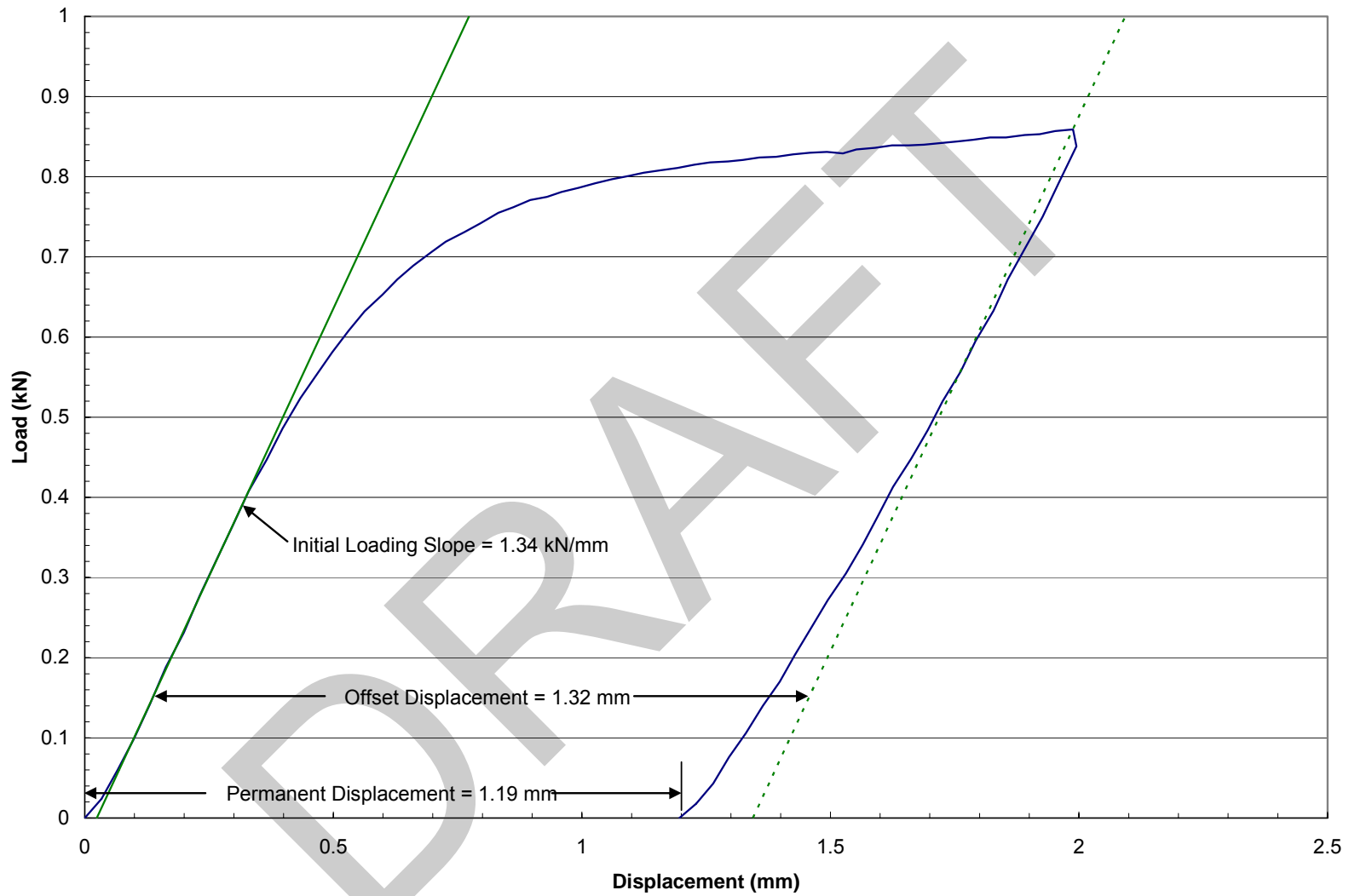


Figure 13. Load-displacement results from RT compression and unloading of an 8-mm-long ring of HBR-type 15×15 Zry-4 cladding.

If the measured permanent strain was  $\geq 1\%$ , the sample was classified as ductile. The 1% permanent strain criterion is based on uncertainties in measuring the post-test diameter of a cracked ring to infer the permanent strain for the sample if it had been unloaded just prior to cracking. If the permanent strain were  $< 1\%$  based on the RT test, a new sample with the same oxidation conditions would have been compressed at  $135^\circ\text{C}$ . However, such was not necessary for the samples oxidized at  $1000^\circ\text{C}$  and  $1100^\circ\text{C}$ .

The procedure of interrupting the test following the first load drop worked so well that it was adopted for all ring-compression tests of as-fabricated and prehydrided cladding oxidized at  $1200^\circ\text{C}$ . The effects of hydrogen and high-temperature oxidation cause the cladding to embrittle at  $< 17\%$  CP-ECR for RT tests. As samples under these conditions had to be retested at  $135^\circ\text{C}$  anyway, the RT tests were eventually eliminated for as-fabricated and prehydrided samples oxidized at  $1200^\circ\text{C}$ .

The procedure for determining ductility and conditions (temperature, CP-ECR, H content, etc.) under which ductile-to-brittle-transition occurs is summarized in the following:

- a) Section one or more 8-mm-long rings from the oxidation-quench sample; measure and record the precise length and outer diameter of the oxidized sample; and mark the circumferential location that will be contacted by the loading platen.
- b) Load ring into Instron 8511 (see Figure 14) with flat support and loading platens.
- c) Compress at RT ( $1000^\circ\text{C}$ - and  $1100^\circ\text{C}$ -oxidized samples) or at  $135^\circ\text{C}$  ( $1200^\circ\text{C}$ -oxidized samples) and  $0.0333$  mm/s.
- d) Interrupt test following first significant load drop ( $> 30\%$ ); this is relatively easy to do as concurrent with the load drop is a loud cracking noise. Determine the offset strain from load-displacement data.
- e) Remove the sample from the Instron, allow sample to cool to RT, and examine it under a microscope to determine if the sample failed with a single through-wall crack along the whole length of the sample or with multiple cracks; generally, load drops of 30-50% imply a single crack, while larger load drops (80-100%) imply two or three cracks.
- f) If a single, tight, through-wall crack is found, measure the post-test diameter in the loading direction and determine the permanent displacement; normalize this displacement to the pre-oxidation-test outer diameter to determine the permanent strain; if the permanent strain is  $< 1\%$ , classify sample as brittle; if multiple cracks are found, the post-test diameter measurement is meaningless and this step is eliminated.
- g) If multiple cracks are found, use the offset displacement and strain from the load-displacement curve; for samples with  $< 2\%$  offset strain, classify samples as brittle.
- h) Record both offset and permanent strains, along with pre-oxidation-test characterization (as-fabricated, prehydriding H content, irradiated with a measured H content), oxidation temperature, CP-ECR, ECR determined from measured weight gain (i.e., measured ECR), quench temperature, ring compression test temperature, and number and location of cracks.

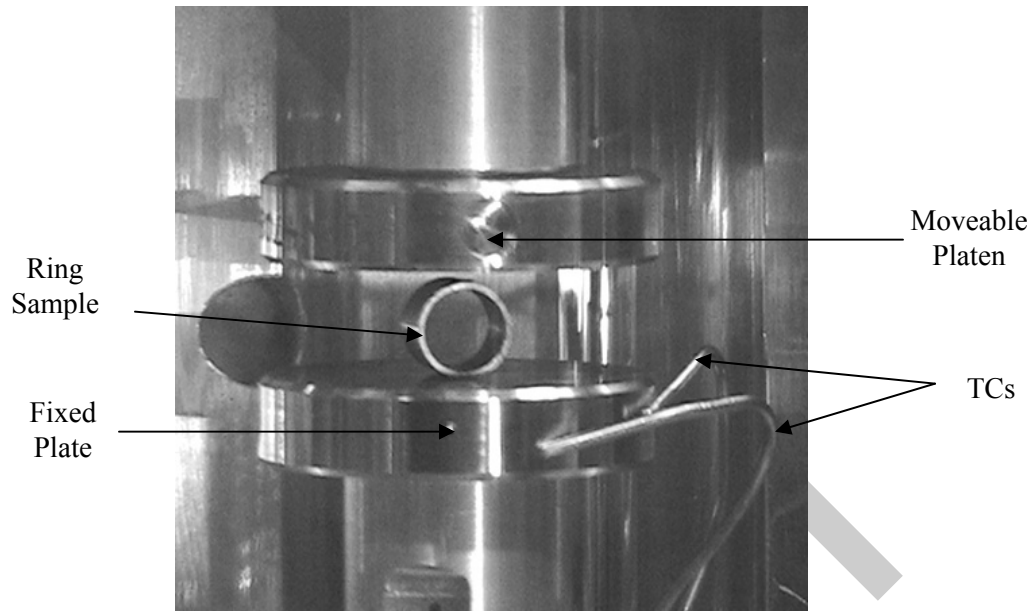


Figure 14. Photograph of ring compression sample supported by the fixed flat plate and loaded by the moveable, load-train platen for the Instron 8511. Not shown in the photograph is the control thermocouple which is located at the bottom inner surface of the ring. Also, thermocouples that rest against the side walls of the sample have been moved down to obtain a better image of the sample.

## 2.4 LOCA integral tests with fueled-and-pressurized samples

Out-of-cell LOCA integral tests with as-fabricated cladding are relatively straightforward with regard to sample preparation and test conduct. Figure 15 shows the LOCA test train with as-fabricated cladding. For these tests the cladding sample is filled with  $\approx 25$ -mm-long zirconia pellets to simulate the heat capacity of the fuel. The stack length of these pellets is  $\approx 270$ -mm long. There is a clearance of  $\approx 13$  mm between the top zirconia pellet and the top end fixture to prohibit contact during sample bending. The test train is supported at the top to minimize specimen bowing. The quartz tube encasing the test train provides an enclosed volume for steam flow and water quench, both of which are introduced through the bottom of the unit. The test train is centered within the quartz tube by means of two perforated spacer disks. Centering is very important as four vertical infrared lamps are focused within the furnace to heat the specimen. Swagelok fittings are used above the specimen to connect to the high-pressure gas line and top pressure gauge and below the specimen to connect to the bottom pressure-gauge line. The total gas volume above the fuel column is  $10 \text{ cm}^3$ , most of which is outside the heated zone. Four Type S thermocouple lead wires are fed in through the top. Two of the thermocouples are spot-welded at the specimen midplane,  $180^\circ$  apart. The other two are spot-welded 50 mm above and 50 mm below the midplane at the same angular orientation as one of the midplane thermocouples. These thermocouples are accurate to  $\pm 3^\circ\text{C}$  at  $1200^\circ\text{C}$ . The signal from the top thermocouple is used to control the furnace power to achieve the desired temperature ramp, hold temperature, and cooling rate prior to quench. Although the uniform heating zone of the furnace is 250-mm, the uniform temperature region of the undeformed sample is  $\approx 125$  mm, centered about the midplane of the sample. The system is designed to allow switching of the control thermocouple in case the top one fails. For the out-of-cell tests, hands-on assembly is used, and bare-wire thermocouple beads are welded directly onto unirradiated tubing.

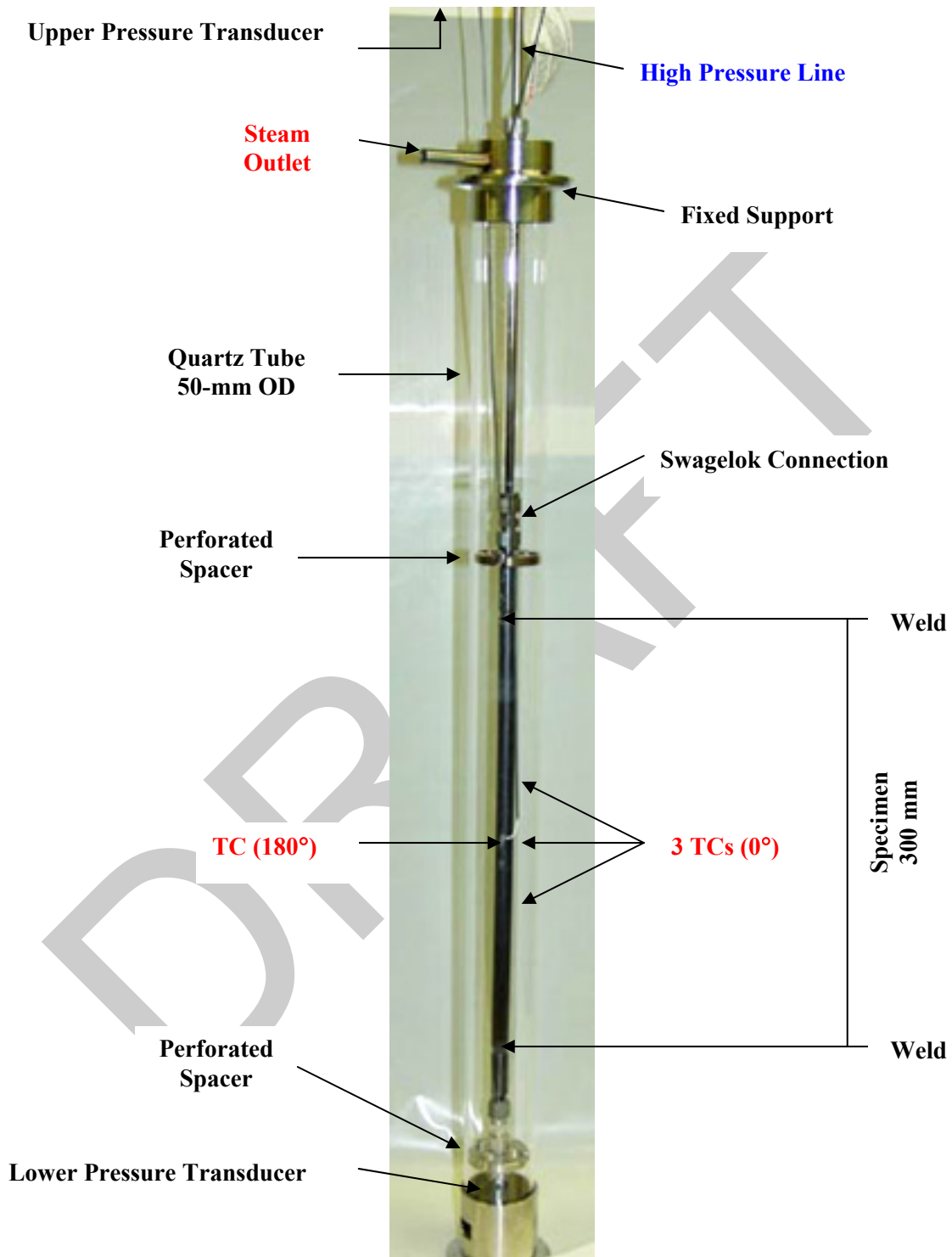


Figure 15. LOCA integral test train assembly and quartz tube. The 300-mm-long specimen is filled with zirconia pellets with a stack length of  $\approx 270$  mm. The quartz tube has an outer diameter of 50 mm, a wall thickness of 1.5 mm, and a length of 686 mm (27 inches).

Because of the high thermal mass of the sample, temperature control is much easier than for the short, defueled cladding oxidation samples. Figure 16 shows a schematic of the temperature history used for both out-of-cell and in-cell testing. The reference control parameters for BWR cladding are: 8.62-MPa (1250 psig) internal pressure with He at RT and 300°C, 5°C/s heating rate, 1200°C hold temperature, variable hold time, 3°C/s cooling rate from the hold temperature to 800°C, and rapid cooling from bottom-flooding quench at 800°C. As these parameters are controlled, they can be adjusted from test to test. The internal pressure of 8.62 MPa was chosen to ensure burst at  $\approx 750^\circ\text{C}$ , which is below the alpha-to-(alpha + beta) phase change temperature, for 9×9 Zry-2 cladding. This treatment also results in large ballooning strains. Although many such tests were conducted during the development of the LOCA integral apparatus, the most important ones are those that provided a baseline for the in-cell tests: a) ramp-to-burst followed by slow cooling; b) ramp to 1200°C, hold for 300 s at 1200°C followed by slow cooling; and c) the full LOCA sequence, including quench at 800°C.

For high-burnup test rod specimens, a drill with both rotary and cyclic horizontal motion is used to remove  $\approx 13$  mm of fuel from the bottom of the specimen (space for end-cap welding) and  $\approx 20$  mm of fuel from the top of the specimen ( $\approx 7$  mm for end-cap welding and 13 mm for clearance). Following end-cap welding, the specimen is inserted into a holder for attaching the Swagelok fittings and for strapping two thermocouples 180° apart to the specimen  $\approx 50$  mm above the midplane. Although a test train assembly device was designed and constructed to spot-weld TCs directly to the cladding metal following oxide removal, these operations were too challenging to perform remotely using manipulators. Comparisons between welded TCs and strapped TCs indicated less than a 10°C difference in readings. For the in-cell tests with high-burnup fueled cladding, internal axial gas flow rate is an important parameter. Prior to conducting the LOCA transient, the sample is pressurized rapidly at the top at RT and 300°C. The time response of the pressure transducer below the fuel column is used to evaluate the axial gas flow rate.

Online data of interest include the time response of the bottom pressure transducer at RT and 300°C, burst temperature, and burst pressure. Following the test, the sample is photographed (low quality) in-situ in the vertical position and moved to other workstations for non-destructive characterization in the horizontal position: photography (high quality), profilometry, and gamma scanning. Destructive examinations are performed on some of the samples to determine oxide and alpha layer thicknesses for inner- and outer-cladding surfaces (metallography), circumferential and axial distribution of oxygen (LECO), and circumferential and axial distribution of hydrogen (LECO). Prior to destructive examination, some of the samples are subjected to a four-point-bending test to determine failure bending moment and ductility. The four-point-bending fixture has been developed and tested with nonirradiated cladding in an out-of-cell Instron machine (Model 5566 table top Instron), for which sample heating is supplied by means of an oven. Most of the ductility tests with nonirradiated cladding oxidized at 1200°C and compressed at 135°C were conducted with the Model 5566 Instron. The control TC was located at the bottom inner surface for these tests.

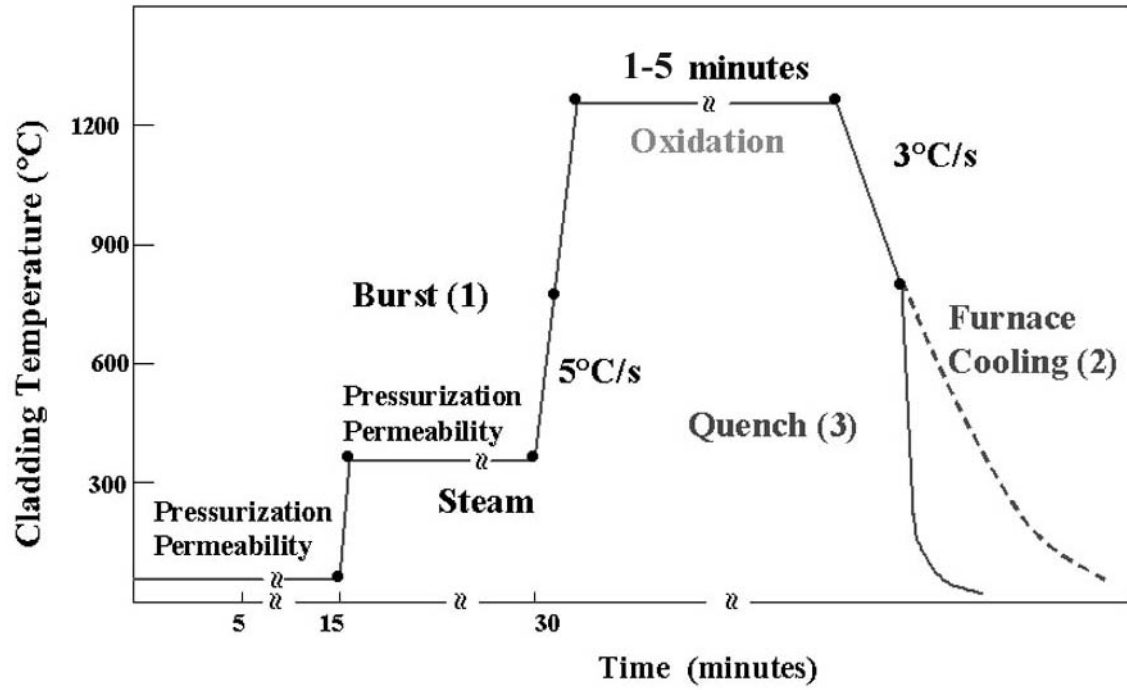


Figure 16. Schematic of the thermal history used for LOCA integral tests. Zirconia-filled, as-fabricated cladding samples are tested out-of-cell, and fueled high-burnup cladding samples are tested in-cell.

DRAFT

### 3 Results for As-fabricated Cladding Alloys

---

In this section, the performance of as-fabricated 17×17 ZIRLO and M5 is compared to the performance of modern 17×17 low-tin Zry-4. Modern Zr-lined 10×10 Zry-2 is also included in the test matrix. These materials are described in Tables 3-5. In parallel to these tests, considerable testing of HBR-type 15×15 Zry-4 (see Table 4) has been conducted to generate baseline data for the H. B. Robinson high-burnup cladding, as no high-burnup 17×17 low-tin Zry-4 was available to the program. Because the HBR-type 15×15 Zry-4 exhibited a lower post-quench-ductility transition ECR than 17×17 Zry-4, the post-quench ductility of modern (belt-polished) 15×15 Zry-4 (see Table 4) oxidized at 1200°C was also studied. Oxidation kinetics studies were also conducted with as-fabricated 9×9 Zry-2 to generate baseline data for high-burnup Limerick Zry-2. In addition, breakaway oxidation studies at 800-1000°C were conducted with HBR-type and belt-polished 15×15 Zry-4, 17×17 ZIRLO, and 17×17 M5. Furthermore, E110 (see Table 6) was included in the breakaway oxidation studies to develop some fundamental understanding as to why this Zr-1Nb alloy exhibits such low breakaway-oxidation time as compared to another Zr-1Nb alloy, M5.

#### 3.1 Zircaloy-4

##### 3.1.1 Post-quench ductility of 17×17 Zry-4 oxidized at 1000°C, 1100°C, and 1200°C

This work was divided into two campaigns: characterization and RT-ring-compression testing of samples exposed to two-sided oxidation at 1000°C and 1100°C and quenched at 800°C; and characterization and ring-compression testing (RT and 135°C) of samples exposed to two-sided oxidation at 1200°C and quenched at 800°C. Characterization included weight gain, oxide- and alpha-layer thickness (metallography), microhardness, and hydrogen pickup (LECO). All samples were oxidized in the same apparatus for test times corresponding to CP-predicted ECR values of 5, 10, 15, 17, and 20% for 0.57-mm-wall cladding. Additional tests were conducted at intermediate CP-ECR values for the 1200°C-oxidized samples to better determine the ductile-to-brittle transition CP-ECR.

##### 17×17 Zry-4 oxidized at 1000°C and 1100°C

Figures 17 and 18 show the thermal benchmark results for the 1000°C- and 1100°C- oxidation test trains, respectively. The ramp times to reach the hold temperature are short compared to the hold times at these temperatures. The average cooling rate to the 800°C quench temperature is  $\approx 10^\circ\text{C/s}$  ( $10^\circ\text{C/s}$  for 1100°C and  $11^\circ\text{C/s}$  for 1000°C). The temperature-time curves were used to calculate the CP-predicted weight gain and ECR values. Table 8 lists the weight gain results for the oxidation tests at these temperatures. They are in very good agreement with the CP-predicted weight gains.

Table 9 gives the results of the RT post-quench ductility tests. It is clear from the results that 17×17 Zry-4 retains post-quench ductility up to 20% CP-ECR – the limit of the test matrix – at these oxidation temperatures. For the 1000°C-oxidation tests, the offset strain levels off at  $\approx 3\%$ , while for the 1100°C-oxidation tests the offset strain levels off at  $\approx 5\%$ . These results suggest that Zry-4 will retain ductility at higher CP-ECR values and higher test times (e.g.,  $>3400$  s at 1000°C until breakaway oxidation occurs). For 1100°C-oxidized samples, breakaway oxidation does not occur, and the beta layer does not appear to embrittle due to the low oxygen solubility ( $\approx 0.4$  wt.%) in the beta phase at 1100°C. At much higher ECR values, beta-layer thinning would cause brittle behavior of compressed rings. Photographs of the ring-compressed samples are shown in Figure 19. The 5% CP-ECR samples were intact at the maximum Instron displacement for these samples.

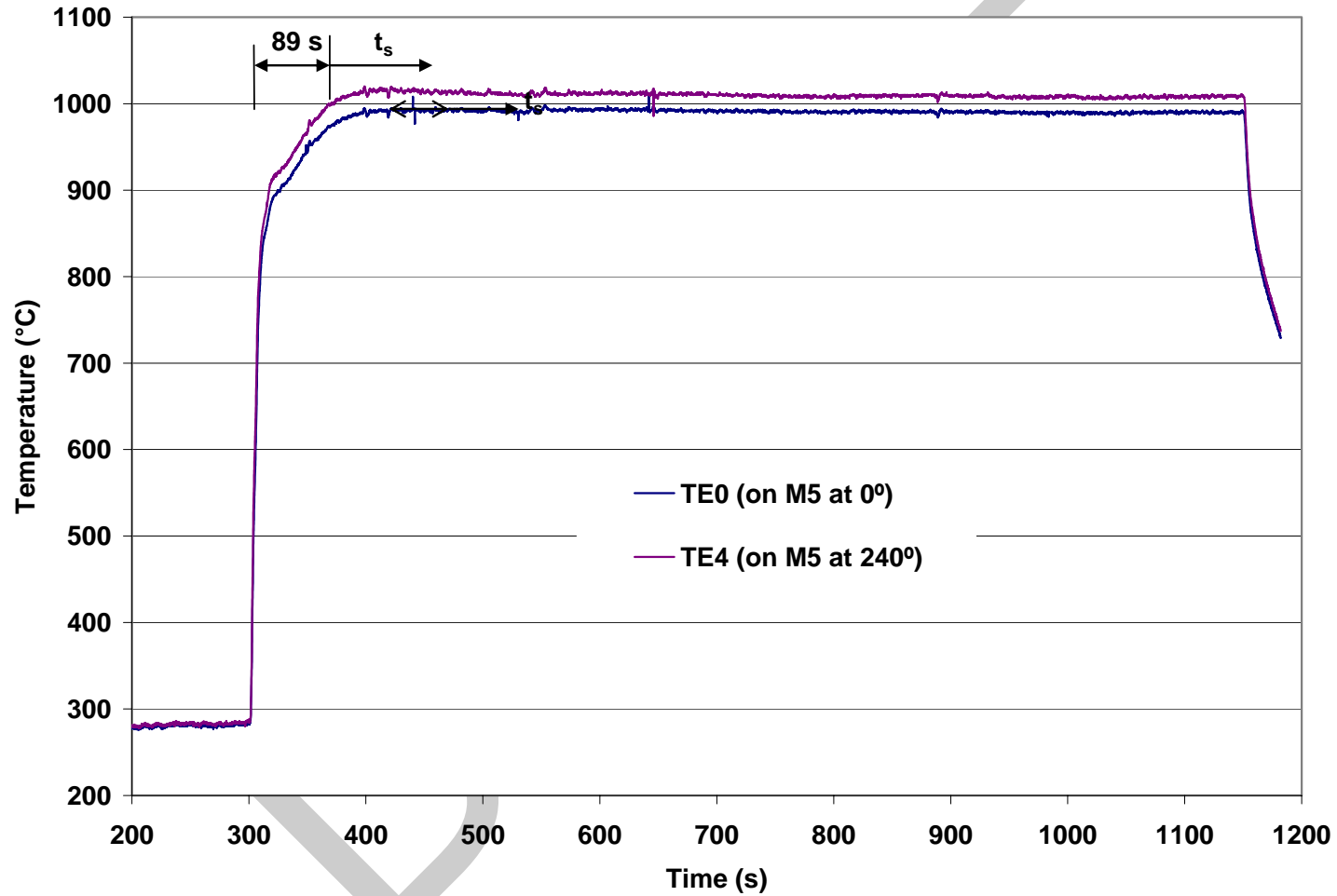


Figure 17. Thermal benchmark results for the  $1000 \pm 10^\circ\text{C}$  oxidation tests. The sample used was from the 0.57-mm-wall validation lot of M5, which has the same inner and outer diameter as 17 $\times$ 17 Zry-4 and ZIRLO. Quench at 800°C is not shown in this figure.

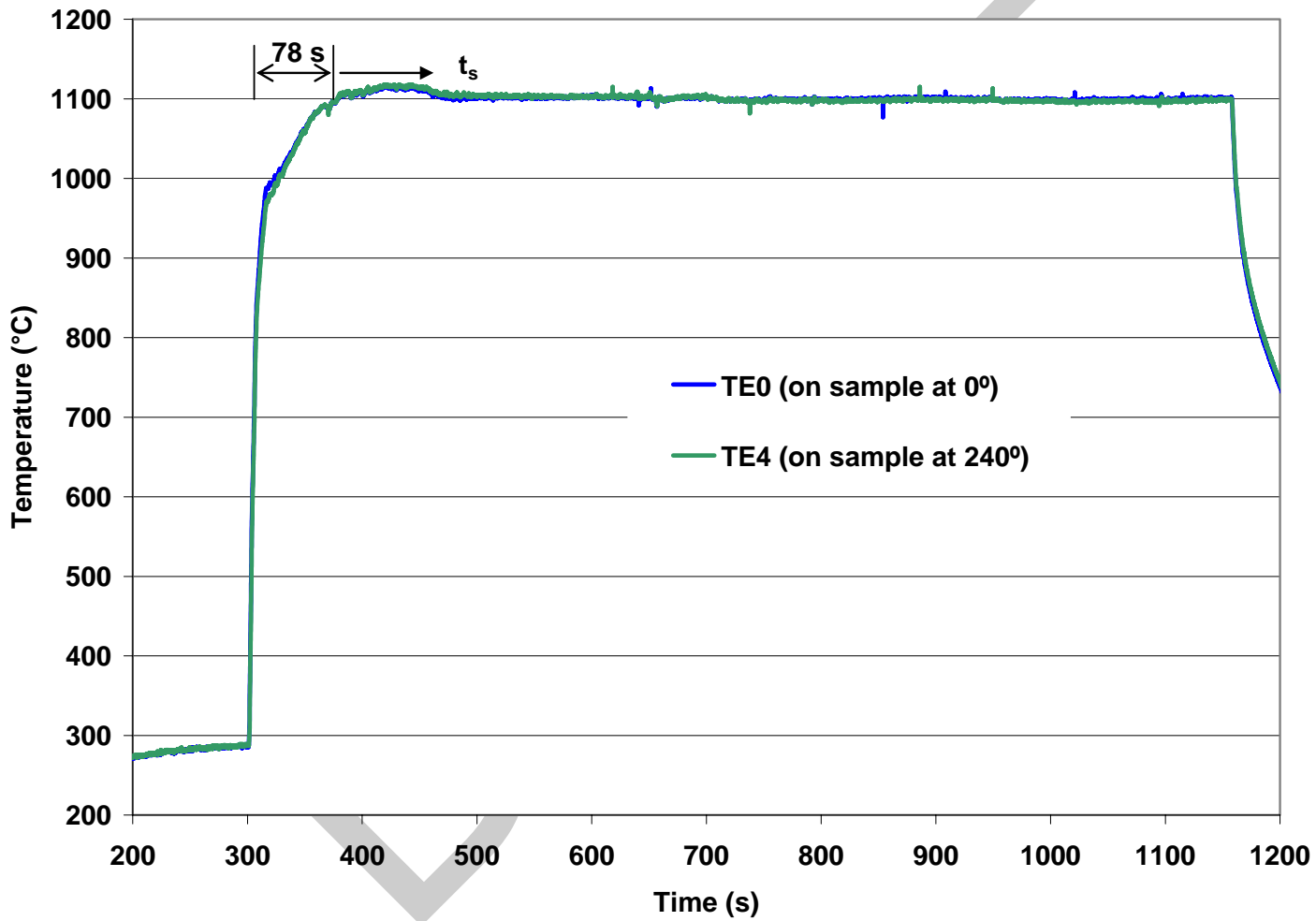


Figure 18. Thermal benchmark results for the  $1100\pm 2^\circ\text{C}$  oxidation tests. The sample used was from the 0.57-mm-wall validation lot of M5, which has the same inner and outer diameter as 17×17 Zry-4 and ZIRLO. Quench at 800°C is not shown in this figure.

Table 8 Weight Gain (Wg in mg/cm<sup>2</sup>) and Measured ECR (%) Values for 17×17Zry-4 Oxidized in Steam at 1000°C and 1100°C. ECR = 1.538 Wg for 0.57-mm-wall cladding. Multiply weight gain results by a factor of 10 to convert to g/m<sup>2</sup>. CP = Cathcart-Pawel.

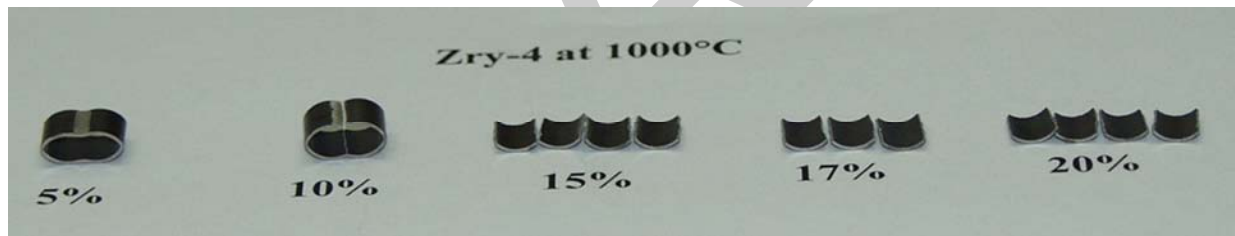
Oxidation Temperature, °C	CP-Predicted ECR, %	CP-Predicted Weight Gain, mg/cm <sup>2</sup>	Measured Weight Gain, mg/cm <sup>2</sup>	Measured ECR, %
1000	5	3.25	3.9	6.1
1000	10	6.50	7.2	11.0
1000	15	9.75	11.0	16.9
1000	17	11.05	12.5	19.3
1000	20	13.00	14.6	22.4
1100	5	3.25	4.0	6.2
1100	10	6.50	7.1	10.9
1100	15	9.75	10.6	16.3
1100	17	11.05	11.7	18.0
1100	20	13.00	13.2	20.3

Table 10 summarizes the results of the metallography, microhardness and hydrogen pickup measurements. The low hydrogen pickup indicates that no breakaway oxidation occurred for these test times. The results in Table 10 are consistent with the post-quench ductility results. Metallographic images and graphical results for 17×17 Zry-4 are presented in the ZIRLO (3.3.1) and M5 (3.4.1) sections for purposes of comparison.

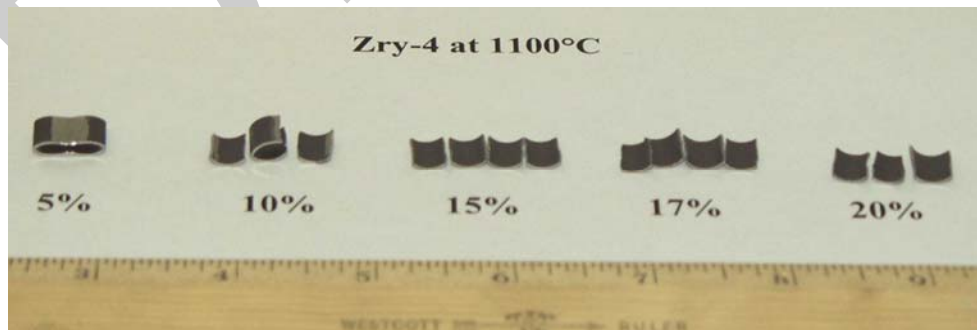
The post-quench ductility, as measured by offset strain, for Zry-4 oxidized at 1100°C decreased with ECR up to ≈15% and remained essentially constant at ≈5% offset strain from 15 to 20% ECR (see Table 10). As the ductility of the prior-beta layer decreases with increasing oxygen content, the results suggest that the oxygen content in the beta layer reaches the solubility limit (0.38 wt.% [18]) at ≈15% CP-ECR, which corresponds to an equivalent isothermal time of ≈600 s. From 15% ECR (600 s) to 20% ECR (1065 s), the beta layer-thickness decreases to ≈300 μm, while the oxygen content and post-quench ductility of the prior-beta layer remain constant. Thus, neither oxygen- nor beta-layer-thinning-induced embrittlement was observed under these test conditions. As hydrogen pickup was negligible, hydrogen-induced embrittlement was also not observed.

Table 9 Ring Compression Test Results for 17×17 Zry-4 Samples Oxidized at 1000°C and 1100°C, Cooled at ≈10°C/s to 800°C, and Quenched. ECR = 1.538 Wg for 0.57-mm-wall cladding. Tests were performed on 8-mm-long samples at RT and at 0.0333 mm/s displacement rate. Displacements in the loading direction were normalized to the as-fabricated outer diameter (9.50 mm) to calculate offset strain. A complete set of tests was performed with a Model 4505 Instron. A limited number of confirmation tests were performed with a Model 5566 Instron on rings cut from the same oxidation samples.

Oxidation Temperature, °C	Cathcart-Pawel ECR, %	Measured ECR, %	Offset Displacement, mm	Offset Strain, %	Confirmation Tests Model 5566 Instron
1000	5	6.1	>4.4	>46	---
1000	10	11.0	2.74	29	Yes
1000	15	16.9	0.71	7.5	Yes
1000	17	19.3	0.48	5.1	---
1000	20	22.4	0.31	3.2	---
1100	5	6.2	>5.5	>58	---
1100	10	10.9	1.9	20	---
1100	15	16.3	0.52	5.4	---
1100	17	18.0	0.47	4.9	---
1100	20	20.3	0.46	4.8	---



(a)



(b)

Figure 19. Post-test appearance of Zry-4 samples compressed at RT and 0.0333 mm/s: (a) samples oxidized at 1000°C and (b) samples oxidized at 1100°C. ECR values below each sample are calculated using the Cathcart-Pawel weight gain correlation.

Table 10 Summary of Characterization Results for Highly Oxidized 17×17 Zry-4 Samples after Exposure to Steam at 1000°C and 1100°C, Cooling at ≈10°C/s to 800°C, and Quench. CP-predicted ECR is 20%.

Oxidation Temperature, °C		17×17 Zry-4
1000	Effective Oxidation Time, s	3364
	Weight Gain, mg/cm <sup>2</sup>	14.6
	Measured ECR, %	22.4
	RT Offset Displacement, mm	0.31
	RT Offset Strain, %	3.2 <b>(ductile)</b>
	Hydrogen Content, wppm	19
	Hydrogen Pickup, wppm	15
	OD/ID Oxide Layer Thickness, μm	83/82
	Microhardness within Middle 0.2 mm of Prior-beta Layer, DPH <sup>a</sup>	290-420
	1100	Effective Oxidation Time, s
Weight Gain, mg/cm <sup>2</sup>		13.2
Measured ECR, %		20.3
RT Offset Displacement, mm		0.46
RT Offset Strain, %		4.8 <b>(ductile)</b>
Hydrogen Content, wppm		22
Hydrogen Pickup, wppm		19
OD/ID Oxide Layer Thickness, μm		70/68
Microhardness within Middle 0.2 mm of Prior-beta Layer, DPH		240-470

<sup>a</sup>DPH = diamond pyramid hardness.

The variation of post-quench ductility with CP-ECR for 1000°C-oxidized Zry-4 is similar to the variation for the 1100°C-oxidized samples. The primary difference is the slow decrease in offset strain with ECR from 7.5% at 15% CP-ECR to 5.1% at 17% CP-ECR to 3.2% at 20% CP-ECR. The beta-layer oxygen-solubility at 1000°C is less (0.24 wt.% [18]) than it is at 1100°C, so higher ductility would be expected. However, 1000°C is very close to the (alpha + beta) → beta phase transformation temperature. The oxidation temperature based on the thermal-benchmark history in Figure 17 is 1000±10°C, which suggests that what is referred to as the beta layer may have contained a small fraction of alpha at the experimental oxidation temperature. Although it is not clear why 1000°C-oxidized Zry-4 has lower post-quench ductility at 20% CP-ECR than 1100°C-oxidized Zry-4 at 20% CP-ECR (3% vs. 5%), the differences are rather small and ductility is retained at both oxidation temperatures.

## 17×17 Zry-4 oxidized at 1200°C

Many tests were conducted with 17×17 Zry-4 oxidized at 1200±5°C to determine the ductile-to-brittle transition CP-ECR at RT and 135°C. This required eight test trains and eight sets of thermal benchmark tests. Figures 20 and 21 show the thermal-benchmark results for the first test train and the most recent test train, respectively. Although the temperature ramps are different, these have little effect on the long-time tests used to determine the transition CP-ECR of ≈17% at 135°C. Prior to quench, the sample cools at an average rate of ≈13°C/s (1200°C to 1000°C in 6 s and 1000°C to 800°C in 23 s). Also, all ring-compression tests were stopped after the first significant load drop (>30%) to allow a measure of the permanent strain based on the diameter change in the loading direction.

The weight gain results (expressed in terms of measured ECR) and the post-quench ductility (PQD) results are summarized in Table 11. The PQD results are plotted in Figure 22. It is clear that 17×17 Zry-4 embrittles at room temperature after oxidation to ≈9% CP-ECR and quench. This behavior is confirmed by both the offset strain criterion (<2%) and the permanent-strain criterion (<1%) for embrittlement, shown as horizontal dashed lines in Figure 22. The enhancement of ductility with the increase in ring-compression test temperature is quite pronounced. Based on the average of the permanent strain readings, the ductile-to-brittle transition CP-ECR is ≈18% at 135°C. Based on the minimum values of permanent strain, 17% CP-ECR is a more conservative estimate. Based on ductility data for three rings oxidized at 1200°C and quenched at 800°C, the offset strain was determined to be 2.5±0.5%, and the permanent strain was measured to be 1.1±0.4%. The "±" values represent one standard deviation. Using the conservative approach (average minus one standard deviation), the minimum offset and permanent strains are 2% and 0.7%, respectively. Based on the ANL offset strain criterion, 17×17 Zry-4 would be assessed as borderline ductile following oxidation to 17% CP-ECR. Based on the ANL permanent strain criterion, the material would be classified as brittle. However, three data points are not sufficient for determining good statistics. Given the absence of data between 13% and 17% CP-ECR, engineering judgment is used to select 17% CP-ECR as the ductile-to-brittle transition for 1200°C-oxidized and 800°C-quenched 17×17 Zry-4. The variations of offset and permanent strains with CP-ECR are shown in Figures 22a and 22b, respectively, for the RT and 135°C test conditions.

It is interesting to note that the oxygen solubility of the Zry-4 beta phase at 1200°C is 0.57 wt.% [18]. The results in Table 11 suggest that oxygen saturation of the beta layer occurs at ≈17% CP-ECR for 1200°C-oxidized Zry-4, and that an average oxygen content of ≈0.6 wt.% is enough to embrittle the Zry-4 prior-beta layer following quench. As is shown in Section 3.3.1, the physical picture is more complicated than this because the post-quench prior-beta layer consists of alpha incursions (>0.6 wt.% oxygen) in an oxygen-depleted (<0.6 wt.%) matrix due to precipitation of oxygen-stabilized alpha during cooling from 1200°C to 800°C.

Table 12 summarizes the characterization results for 17×17 Zry-4 oxidized at 1200°C to 13% and 20% CP-ECR and quenched at 800°C. The hydrogen pickup is very low. Also, there is excellent agreement between the inner-surface and outer-surface oxide layer thickness, indicating adequate steam flow at the inner surface. The microhardness results support the post-quench ductility results. Based on the room-temperature microhardness values, one would expect ductility at 13% CP-ECR and embrittlement at 20% CP-ECR at 135°C. Metallographic images and additional graphical results are presented for comparison purposes in the sections on ZIRLO (3.3.1) and M5 (3.4.1).

Based on the results in Table 12, the embrittlement observed at 17% CP-ECR in Figure 22 is not hydrogen-induced or beta-layer-thinning-induced (>300-μm thickness at 17% CP-ECR).

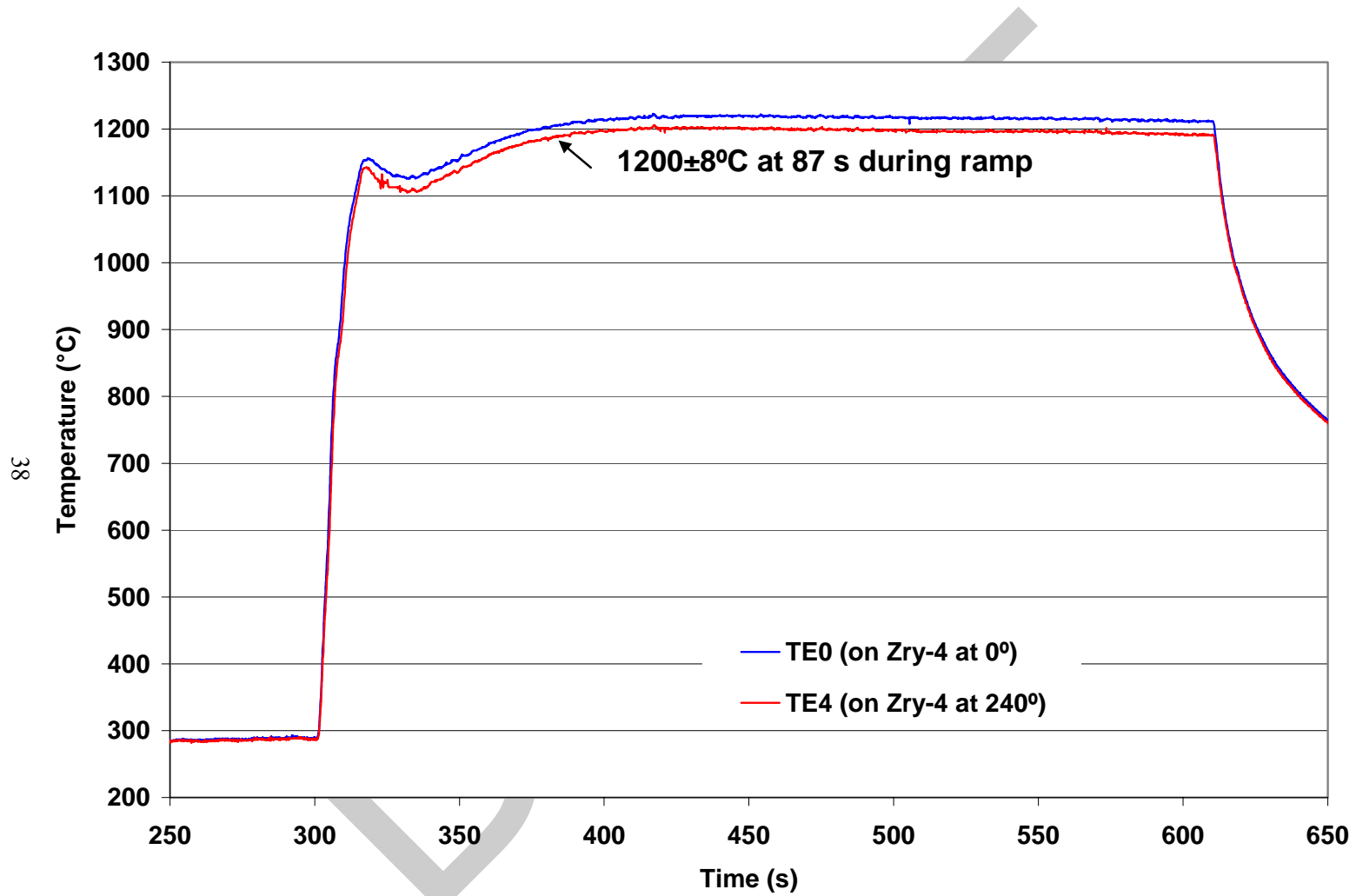


Figure 20. Thermal benchmark results (Test Train #1) for oxidation of 17×17 alloys at 1200±5°C. The sample used for this benchmark was 17×17 Zry-4 with a wall thickness of 0.57 mm. Quench is not shown in this figure.

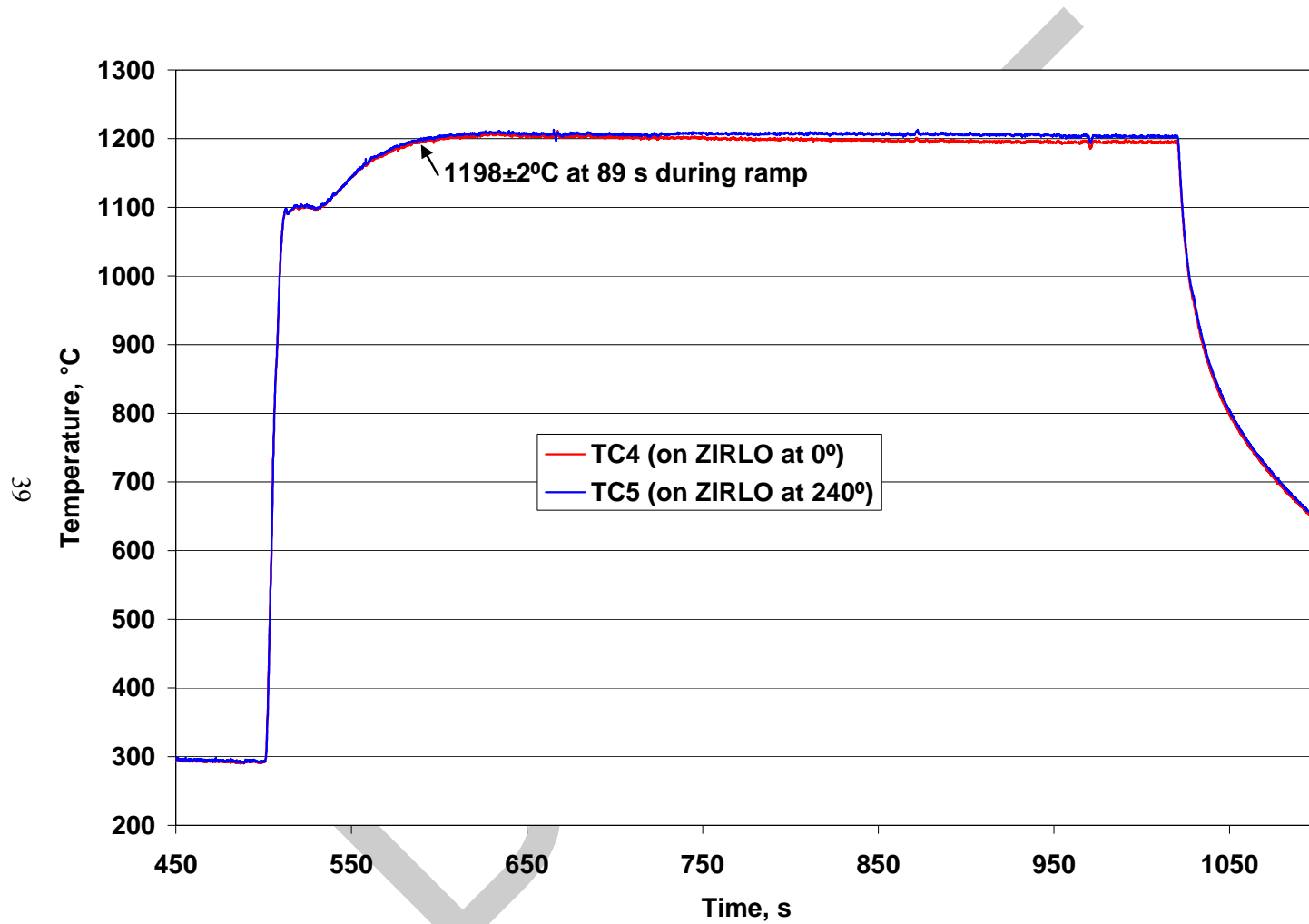


Figure 21. Thermal benchmark results (current test train) for oxidation of 17×17 alloys at 1200±5°C. The sample used for this benchmark was 17×17 ZIRLO with a wall thickness of 0.57 mm. Quench is not shown in this figure.

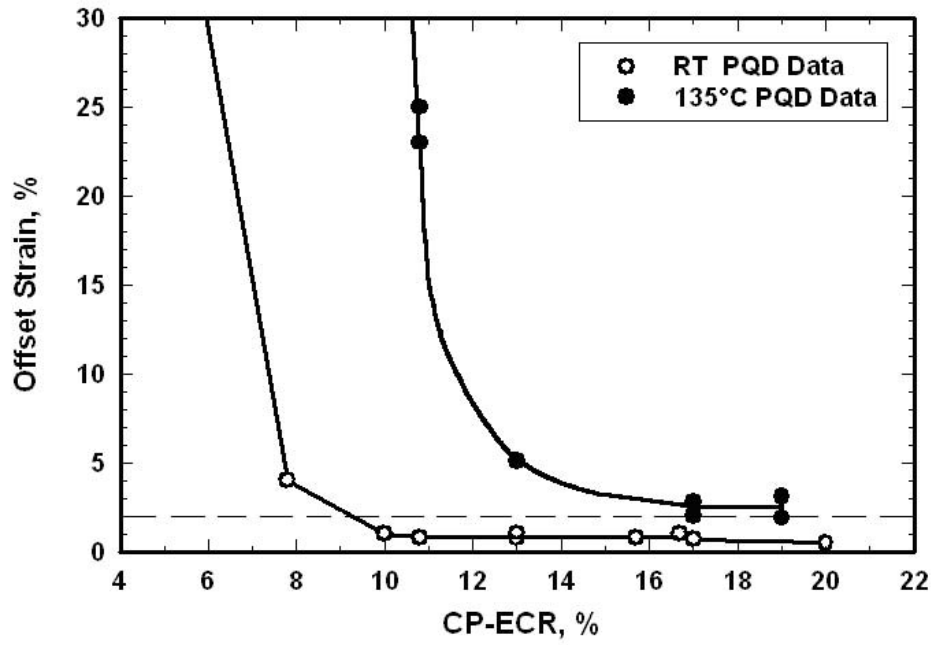
Table 11 Ring Compression Test (RCT) Results for 17×17 Zry-4 Cladding Oxidized at 1200±5°C, Cooled at ≈13°C/s to 800°C, and Quenched. ECR = 1.538 Wg for 0.57-mm-wall cladding. Tests were performed on ≈8-mm-long samples at RT and 135°C and at 0.0333-mm/s displacement rate. Displacements in the loading direction were normalized to the as-fabricated outer diameter (9.50 mm) to calculate offset and permanent strains.

Test Conditions		ECR, %		Plastic Displacement, mm		Plastic Strain, %	
RCT T, °C	Ox. Test Time, <sup>a</sup> s	CP	Meas.	Offset	Permanent	Offset	Permanent
RT	0	0	0	6.3	5.9	66	62
RT	60	4.9	5.5	>3.5	>3.23	>37	>34
RT	60	4.9	5.5	4.28	---	45	---
RT	100	7.8	8.2	0.38	0.21	4.0	2.2
RT	136	10.0	10.9	0.10	0.05	1.0	0.5
RT	151	10.8	11.9	0.08	0.05	0.8	0.5
135	151	10.8	11.9	2.14	---	23	---
135	151	10.8	11.9	>2.41	>1.92	>25	>20
RT	203	13.0	12.8	0.09	0.07	1.0	0.7
RT	203	13.0	14.6	0.08	0.06	0.8	0.6
135	203	13.0	14.6	0.49	0.29	5.1	3.1
RT	258	15.7	17.1	0.04-0.12	---	≈0.8	---
RT	310	16.7	18.0	0.10	0.06	1.0	0.6
RT	310	17.0	18.1	0.07	0.05	0.7	0.5
135	310	17.0	18.1	0.26	0.14	2.8	1.4
<b>135<sup>b</sup></b>	<b>318</b>	<b>17.0</b>	<b>18.5</b>	<b>0.26</b>	<b>0.12</b>	<b>2.8</b>	<b>1.3</b>
<b>135<sup>b</sup></b>	<b>318</b>	<b>17.0</b>	<b>18.5</b>	<b>0.19</b>	<b>0.07</b>	<b>2.0</b>	<b>0.7</b>
<b>135<sup>b</sup></b>	<b>390</b>	<b>19.0</b>	<b>20.3</b>	<b>0.29</b>	<b>0.10</b>	<b>3.1</b>	<b>1.1</b>
<b>135<sup>b</sup></b>	<b>390</b>	<b>19.0</b>	<b>20.3</b>	<b>0.18</b>	<b>0.08</b>	<b>1.9</b>	<b>0.8</b>
RT	428	20.0	20.7	0.05	0.04	0.5	0.4

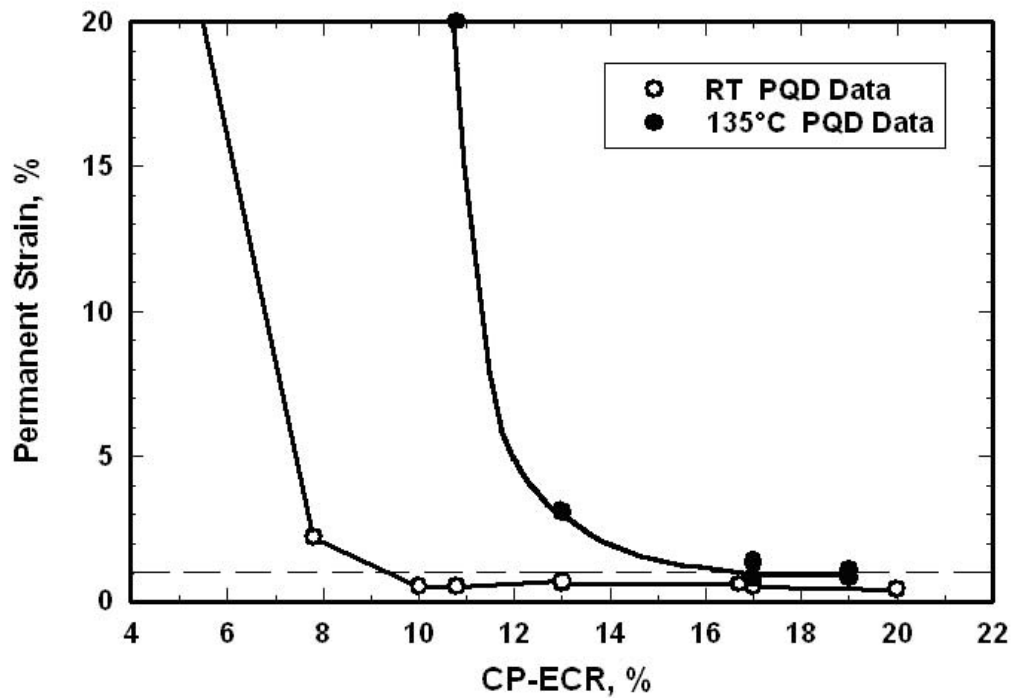
<sup>a</sup>Includes ramp from 300°C.

<sup>b</sup>Tests were conducted with current test train (see Figure 21 for thermal history).

Most other test results were conducted with the initial test train (see Figure 20 for thermal history).



(a)



(b)

Figure 22. Offset (a) and permanent (b) strains vs. CP-ECR for 17×17 Zry-4 oxidized at 1200°C, cooled at ≈13°C/s to 800°C, quenched, and ring-compressed at RT and 135°C.

Table 12 Summary of Characterization Results for 17×17 Zry-4 Samples after Exposure to Steam at 1200°C to 13% and 20% CP-ECR, Cooling at ≈13°C/s to 800°C, and Quench.

Parameter	17×17 Zry-4	
	20% CP-ECR	13% CP-ECR
Effective Oxidation Time, s	400	166
CP-Predicted Weight Gain, mg/cm <sup>2</sup>	13.5	8.35
Measured ECR, %	20.8	12.8
Offset Displacement, mm	0.049	0.090
RT Offset Strain, %	0.05	0.09
RT Measured Permanent Displacement, mm	0.04	0.07
RT Permanent Strain, %	0.4	0.7
RT Ductility, %	≤0.4 (brittle)	≤0.7 (brittle)
Hydrogen Content, wppm	17	low
Hydrogen Pickup, wppm	13	low
OD/ID Oxide Layer Thickness, μm	68/66	42/41
Prior-Beta-Layer Thickness, μm	266	419
Microhardness, DPH		
Oxide Layers	570-960	600-770
Alpha Layers	530-730	600-700
Prior-Beta Layer <sup>a</sup>	280-600	260-360

<sup>a</sup>Range includes microhardness values of oxygen-rich alpha incursions in this layer.

### 3.1.2 Post-quench ductility of 15×15 Zry-4 oxidized at 1200°C

Baseline data were generated for the post-quench ductility of HBR-type 15×15 low-tin Zry-4 oxidized at 1200°C and quenched at 800°C. A parallel study was conducted using belt-polished 15×15 low-tin Zry-4 to determine if modern Zry-4 has higher post-quench ductility than 1980s Zry-4. Data were also generated for both types of Zry-4 oxidized at 1000°C as part of the breakaway oxidation study. The breakaway oxidation results are reported in the Section 3.1.3.

The first 1200°C dataset was generated for a test train with the thermal benchmark shown in Figure 23. Based on two TCs welded to the sample 120° apart, the hold temperature was estimated to be 1200±17°C. The oxidation and post-quench ductility results for HBR-type 15×15 low-tin Zry-4 exposed to the thermal history in Figure 23 are summarized in Table 13. For the samples compressed at RT, marginal ductility is indicated in the offset and permanent strains at 7.5% CP-ECR. The RT ductile-to-brittle transition is estimated to be 8% CP-ECR. At 135°C, the samples are ductile at ≈10% CP-ECR and brittle at 13% CP-ECR. The ductile-to-brittle transition CP-ECR at 135°C is ≈12%. Additional samples were oxidized at ≈1188°C and ≈1176°C to 12-13% CP-ECR. These samples remained brittle at RT even

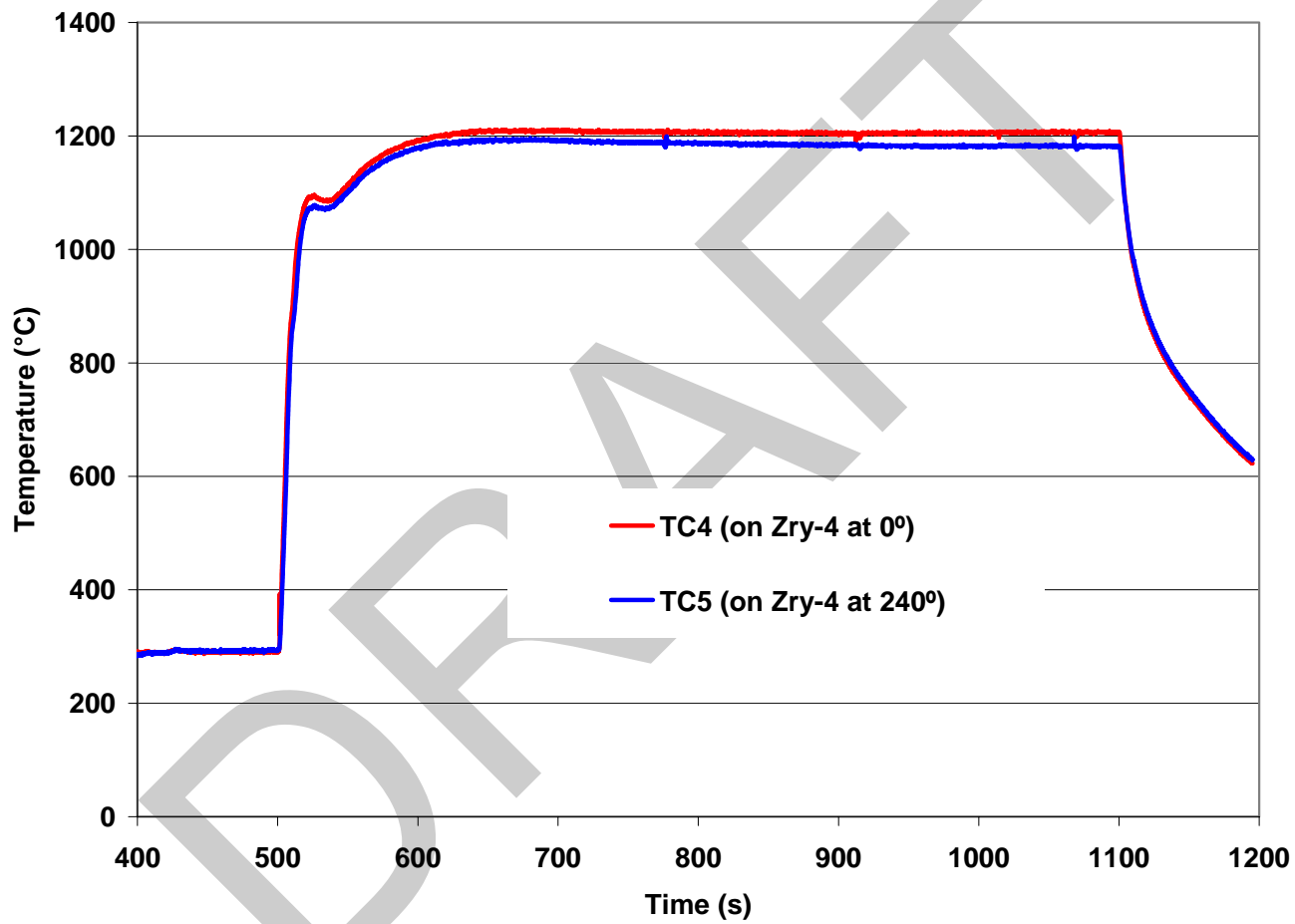


Figure 23. Thermal benchmark (HBRU#5A) results for first test train used to oxidize HBR-type 15×15 low-tin Zry-4. The hold temperature based on two sample-welded TCs is  $1200 \pm 17^\circ\text{C}$ .

with the reduction in oxidation temperature. Table 14 summarizes the results of the post-test characterization, while Figure 24 shows microhardness profiles across the prior-beta layer at three CP-ECR values. The microhardness values are consistent with the post-quench ductility results. The RT post-quench ductility results appear to be consistent with those shown in Figure 22a for 17×17 low-tin Zry-4, but the 135°C data are not consistent as they indicate a ductile-to-brittle transition of only ≈12% CP-ECR, as compared to 17% CP-ECR for 17×17 low-tin Zry-4.

At the time the results were generated, it was not clear whether the HBR-type 15×15 low-tin Zry-4 was inferior to the modern 17×17 low-tin Zry-4, or whether the large circumferential temperature gradient leading to local temperatures  $\geq 1217^\circ\text{C}$  was responsible for the low transition ECR. A new test train was built, and the thermal calibration was performed in two separate tests to give cladding temperatures at three circumferential locations: 0°, 120°, and 240°. During the calibration effort, the sample was rotated within the quartz tube to determine the sensitivity of temperature to angular orientation. Great care was exercised to center the larger-diameter cladding with respect to the test train, the quartz tube, and the furnace. The thermal benchmark results for the improved test train are shown in Figure 10. The hold temperature for this test train was  $1204 \pm 10^\circ\text{C}$ .

Extensive testing was performed using the thermal history in Figure 10 because of the higher degree of confidence in the average hold temperature and circumferential temperature variation:  $1204 \pm 10^\circ\text{C}$ . Each oxidized sample was sectioned into three ≈8-mm-long rings, which were then compressed at RT, 100°C, and 135°C. The 100°C temperature is reasonable to assess long-term, post-LOCA core coolability. Table 15 summarizes the oxidation results and the post-quench ductility results. Although samples from two lots were used in the testing, the agreement between these lots in terms of weight gain and post-quench ductility is excellent. Based on the data presented in Table 15 for permanent strains, the transition CP-ECR values are 7.5% at RT, 11.5% at 100°C, and 14% at 135°C.

Figure 25 shows a comparison between the measured weight gain and the CP-predicted weight gain for HBR-type 15×15 Zry-4 oxidized at 1200°C. The agreement is excellent. Figure 26 shows the decrease in post-quench ductility (offset strain) with increasing CP-ECR and decreasing ring-compression temperature. The lines in the figure represent trend curves rather than "best fits" to the data.

Although the post-quench-ductility results with the new test train (Figure 10) are better than the ones with the old test train, the ductile-to-brittle transition CP-ECR (14%) is still lower for the older rough-surface HBR-type 15×15 Zry-4 than for the modern belt-polished 17×17 low-tin Zry-4 (17%, Table 11). Several hypotheses were formulated and tested in an attempt to narrow down the reasons for these differences. The two alloys differ in surface roughness and possibly in surface chemistry, in OD and wall thickness, in as-fabricated oxygen content, and in test time to reach a given ECR. Modern belt-polished (BP) 15×15 low-tin Zry-4 was provided by AREVA (see Table 4) to determine if this cladding had comparable post-quench ductility to modern 17×17 low-tin Zry-4. As can be seen in Table 4, the modern alloys have comparable surface roughness and oxygen content. A new test train was constructed and benchmarked for the oxidation phase of the testing. The thermal benchmark results for this test train with TCs welded to the modern 15×15 Zry-4 are shown in Figure 27. The post-quench ductility results at 135°C are given in Table 16. The offset strains are compared in Figure 28 for the belt-polished 17×17 and 15×15 Zry-4, as well as the rough-surface HBR-type 15×15 Zry-4. The belt-polished 15×15 Zry-4 has a higher ductile-to-brittle transition CP-ECR (19%) than the belt-polished 17×17 Zry-4 (17%) and the rough-surface HBR-type 15×15 Zry-4 (14%). As the hydrogen pickup was insignificant for all three alloys and the as-fabricated oxygen content is comparable (see Table 4), there appears to be Zry-4 alloy-to-alloy differences, which may result in different oxygen solubility levels or oxygen diffusion rates.

Table 13 Ring Compression Test (RCT) Results for HBR-type 15×15 Low-tin Zry-4 Samples Oxidized at 1200±17°C, Cooled at ≈11°C/s to 800°C, and Quenched. ECR = 1.1535 Wg for 0.76-mm-wall cladding. Tests were performed on ≈8-mm-long samples at RT and 135°C and at 0.0333-mm/s displacement rate. Displacements in the loading direction were normalized to the as-fabricated outer diameter (10.77 mm) to calculate offset and permanent strains.

RCT Test Temperature, °C	ECR, %		Displacement, mm		Offset Strain, %	Permanent Strain, %
	CP	Meas.	Offset	Permanent		
RT	0	0	7.0	6.8	65	63
RT	4.9	6.1	1.77	1.22	16	11
RT	4.9	6.1	1.33	0.67	12	6
--- <sup>a</sup>	4.9	5.8	---	---	---	---
RT	7.5	8.0	0.22	0.01	2.0	0.9
RT	7.5	8.0	0.22	0.11	2.0	1.0
RT	9.8	10.6	0.06	0.05	0.6	0.5
135	9.8	10.6	0.31	0.19	2.9	1.8
RT	12.8	13.9	0.05	0.03	0.5	0.3
135	12.8	13.9	0.16	0.07	1.5	0.7
RT	16.7	17.8	0.06	0.05	0.6	0.5
135	16.7	17.8	0.14	0.05	1.3	0.5

<sup>a</sup>Additional test performed for metallographic and microhardness measurements.

Note that the prior-beta layer thickness of HBR-type 15×15 Zry-4 is ≈420 μm at the embrittlement CP-ECR of 14%, while the prior-beta layer thickness of modern 17×17 Zry-4 is ≈320 μm at the embrittlement CP-ECR of 17%. Thus, the ductile-to-brittle transition appears to be controlled by the average oxygen content in the beta layer and is relatively insensitive to beta-layer thickness for thicknesses > 300 μm.

The selection of 14% transition CP-ECR for HBR-type 15×15 Zry-4 is primarily due to a single ring-compression data point at 15% CP-ECR, which exhibited brittle behavior. As shown in Appendix A, multiple oxidation-quench tests were conducted in the narrow CP-ECR range of 13-16% using both HBR-archive tubing and HBR-type 15×15 Zry-4. Six ductility data points were generated at 135°C following oxidation at 1200°C to 15.2% and 16.0% CP-ECR and quench at 800°C. The results for permanent strain were 1.5±0.4% for 15.2% CP-ECR and 1.1±0.3% at 16% CP-ECR. By interpolation, the ductile-to-brittle transition CP-ECR would be 15.6%, which rounds off to 16% CP-ECR.

Table 14 Oxide, Alpha, and Prior-Beta Layer Thicknesses at Four CP-ECR Values for HBR-type 15×15 Low-tin Zry-4 Oxidized at 1200±17°C, Cooled at ≈11°C/s to 800°C, and Quenched.

Parameter	CP-ECR, %			
	≈5	7.5	9.8	12.8
Outer Oxide Layer Thickness, μm	26	35	61	80
Outer Alpha Layer Thickness, μm	24	41	113	102
Prior-Beta Layer Thickness, μm	690	636	513	453
Inner Alpha Layer Thickness, μm	23	40	113	108
Inner Oxide Layer Thickness, μm	24	36	62	79
Measured Weight Gain, mg/cm <sup>2</sup>	5.0	7.0	9.2	12.1
Measured ECR, %	5.8	8.0	10.6	13.9
RT Offset Strain, %	≈10%	≈1.0	0.3	0.5
135°C Offset Strain, %	---	---	2.9	1.5

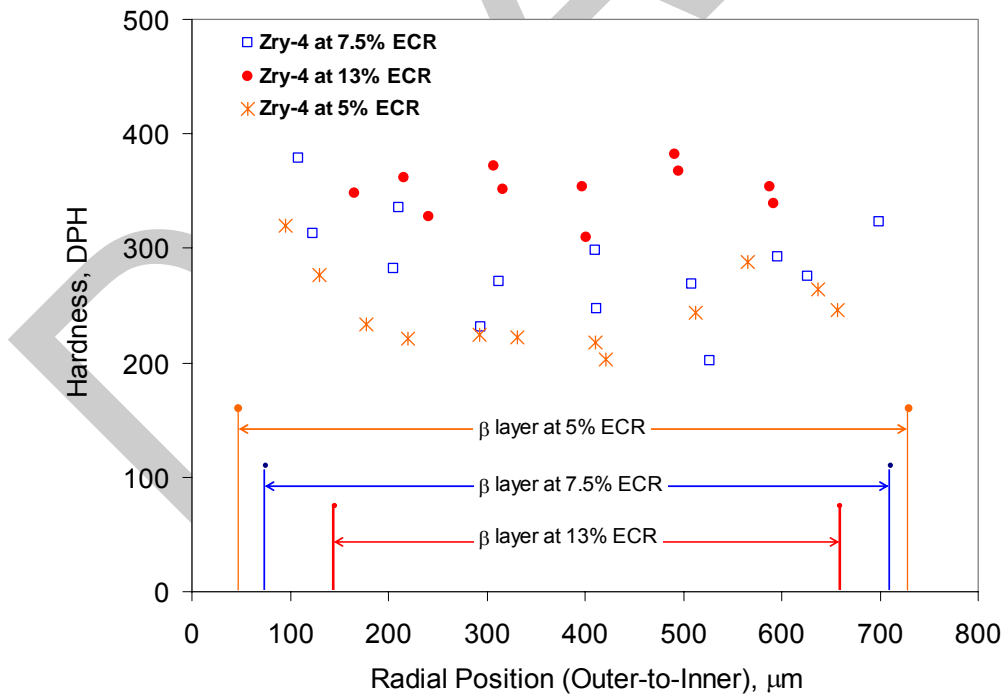


Figure 24. RT microhardness across prior-beta layer for 1200°C-oxidized HBR-type 15×15 Zry-4.

Table 15 Ring Compression Test Results for HBR-type 15×15 Low-tin Zry-4 Cladding Oxidized at 1204±10°C, Cooled at ≈11°C/s to 800°C, and Quenched. ECR = 1.1535 Wg for 0.76-mm-wall cladding. Tests were performed on ≈8-mm-long samples at RT, 100°C, and 135°C and at 0.0333-mm/s displacement rate. Samples from two lots were used to generate these data: 10.77-mm OD and 0.76-mm wall; and 10.76-mm OD and 0.77-mm wall. Displacements in the loading direction were normalized to the as-fabricated outer diameter to calculate offset and permanent strains.

Test Conditions		ECR, %		Plastic Displacement, mm		Plastic Strain, %	
T, °C	Test Time, <sup>a</sup> s	CP	Meas.	Offset	Permanent	Offset	Permanent
RT	0	0	0	7.0	6.8	65	63
RT	96	5.0	5.5	1.98	---	18	---
RT	93	5.0	5.1	2.34	---	20	---
RT	96	5.0	5.5	>5.5	>4.9	>51	>45
100	93	5.0	5.1	>5.6	>5.0	>52	>46
100	96	5.0	5.5	>5.6	>5.1	>52	>47
135	93	5.0	5.1	>6.0	>5.5	>56	>51
RT	154	7.5	8.1	0.25	0.11	2.3	1.0
RT	145	7.4	7.6	0.23	0.14	2.1	1.3
100	154	7.5	8.1	>3.9	>3.4	>36	>32
100	145	7.4	7.6	>2.2	>2.0	>20	>18
135	154	7.5	8.1	>4.7	>4.3	>43	>40
135	145	7.4	7.6	5.53	---	51	---
RT	230	10.0	10.4	0.08	0.04	0.7	0.4
RT	230	10.3	10.7	0.06	0.05	0.6	0.5
100	230	10.0	10.4	0.34	0.21	3.2	1.9
100	230	10.3	10.7	0.26	0.16	2.4	1.5
135	230	10.0	10.4	1.60	1.32	14.9	12.3
135	230	10.3	10.7	1.45	1.10	13.5	10.2
100	278	11.7	11.8	0.16	0.09	1.4	0.9
135	278	11.7	11.8	0.31	0.19	2.9	1.7
RT	353	13.0	13.2	0.04	0.03	0.4	0.3
RT	353	12.8	13.2	0.07	0.05	0.6	0.5
100	353	13.0	13.2	0.12	0.07	1.1	0.6
100	353	12.8	13.2	0.10	0.05	0.9	0.5
135	353	13.0	13.2	0.37	0.16	3.4	1.5
135	353	12.8	13.2	0.22	0.13	3.1	1.2
135	432	15.0	14.8	0.17	0.09	1.6	0.8

<sup>a</sup>Includes time for ramp from 300°C and hold time prior to cooling.

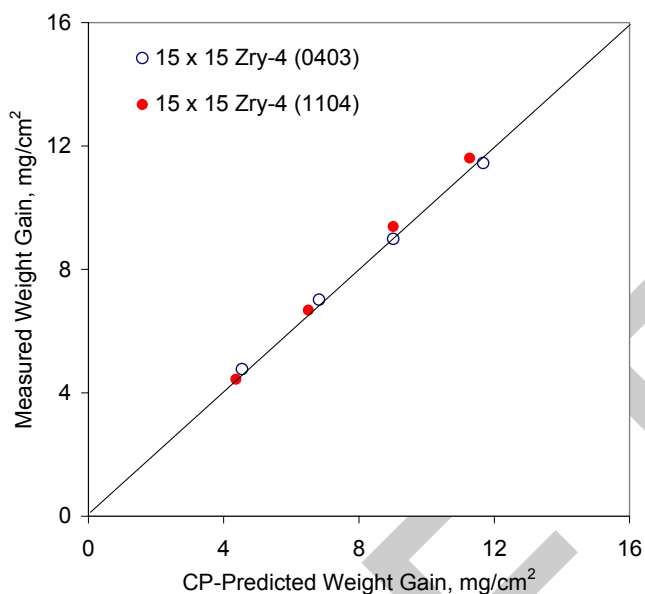


Figure 25. Measured vs. predicted weight gain for two lots of HBR-type 15×15 low-tin Zry-4 oxidized at 1204±10°C and quenched at 800°C.

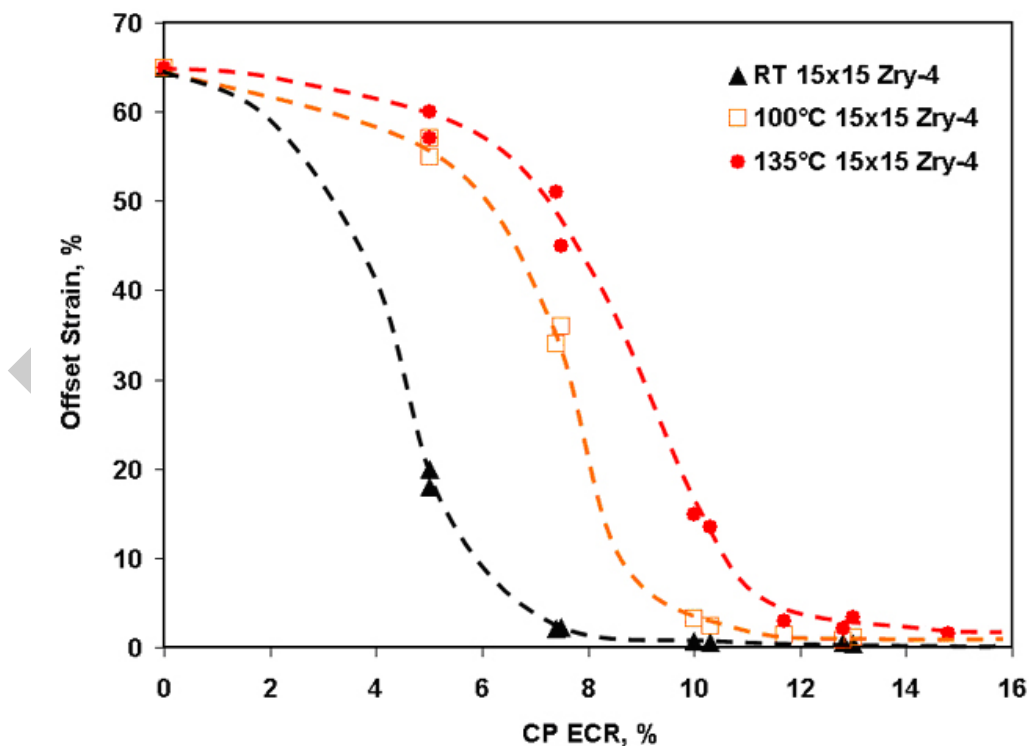


Figure 26. Offset strain vs. CP-ECR and ring-compression test temperature for two lots of HBR-type 15×15 low-tin Zry-4 oxidized at 1204±10°C, cooled at ≈11°C/s to 800°C, and quenched.

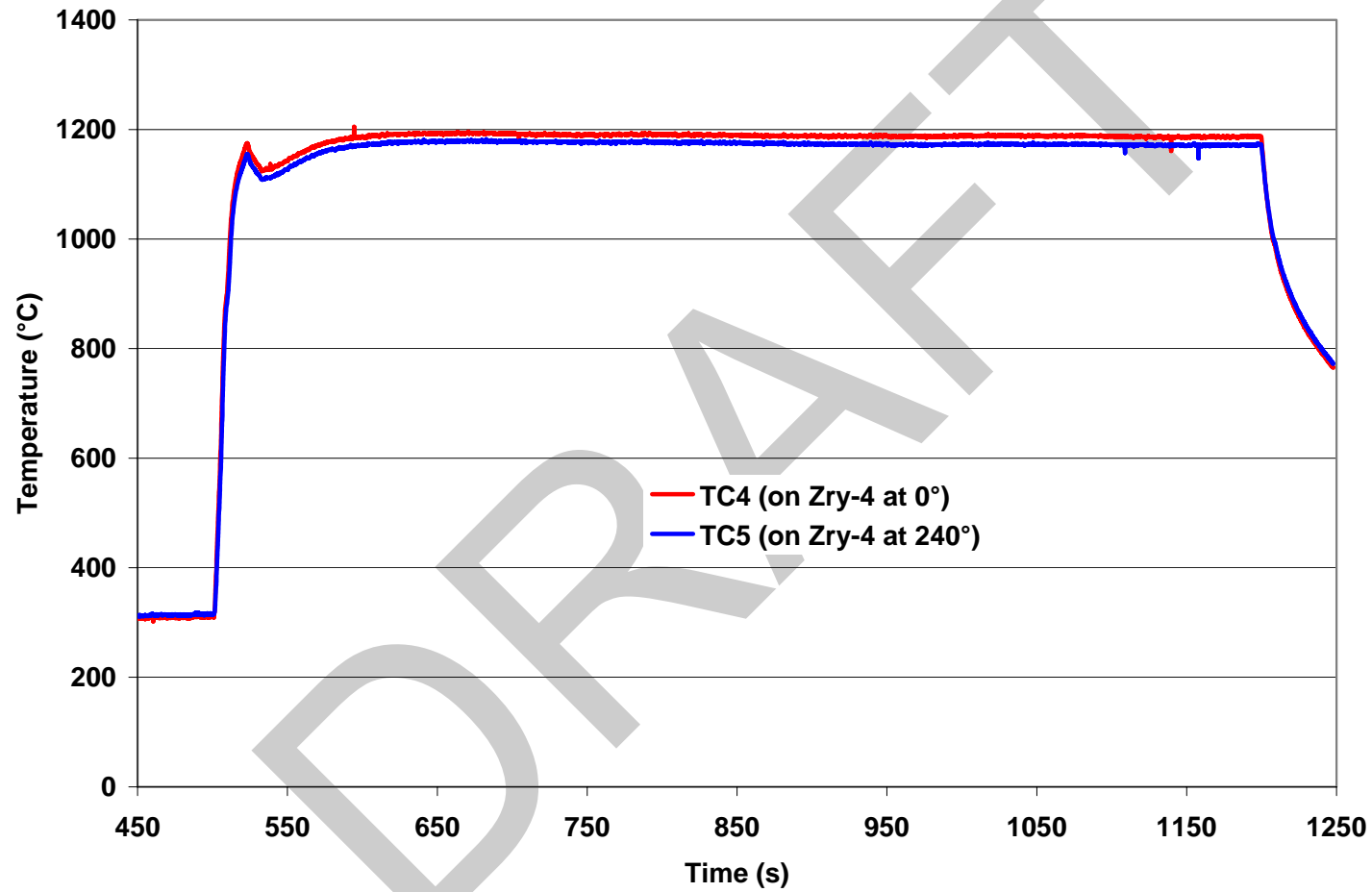


Figure 27. Thermal benchmark results for belt-polished 15x15 low-tin Zry-4 with a hold temperature of  $\approx 1190^{\circ}\text{C}$ . Data-generating tests were conducted by increasing the holder control TC setting by  $10^{\circ}\text{C}$  to give a hold temperature of  $1200^{\circ}\text{C}$ .

Table 16 Ring Compression Test (RCT) Results for Belt-polished 15×15 Zry-4 Cladding Oxidized at 1200°C, Cooled at ≈11°C/s to 800°C, and Quenched. ECR = 1.308 Wg for 0.67-mm wall cladding. RCTs were performed on ≈8-mm-long samples at 135°C and 0.0333-mm/s displacement rate.

Test Conditions		ECR, %		Plastic Displacement, mm		Plastic Strain, %	
RCT T, °C	Ox. Test Time, <sup>a</sup> s	CP	Meas.	Offset	Permanent	Offset	Permanent
135	210	11.0	11.5	>3.6	>3.2	>33	>29
135	210	11.0	11.5	>3.5	>3.1	>32	>28
135	280	13.0	12.7	4.15	3.58	38	33
135	280	13.0	12.7	2.60	2.35	24	22
135	360	15.0	15.0	0.50	0.24	4.6	2.2
135	360	15.0	15.0	0.35	0.17	3.2	1.6
135	495	17.0	17.2	0.42	0.22	3.8	2.0
135	495	17.0	17.2	0.30	0.16	2.7	1.5
135	620	20.0	19.8	0.28	0.15	2.6	1.4
135	620	20.0	19.8	0.23	0.09	2.1	0.8

<sup>a</sup>Includes ramp from 300°C.

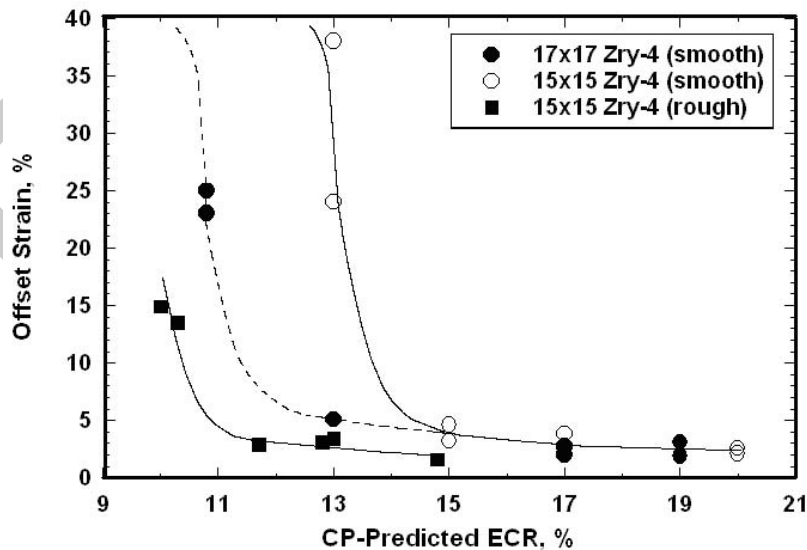


Figure 28. Offset strain vs. CP-ECR for 15×15 and 17×17 Zry-4 samples oxidized at 1200°C, cooled at ≈11°C/s to 800°C, and quenched. Ring compression tests were conducted at 135°C and 0.0333-mm/s displacement rate. Nominal offset strain for ductile-to-brittle transition ECR is 2%.

### 3.1.3 Breakaway oxidation time for 15×15 Zry-4 samples oxidized at 800-1015°C

Breakaway oxidation at  $T \leq 1000^\circ\text{C}$  has been studied by Leistikow and Schanz [19,20] for Zry-4 and Mardon et al. [21] for Zry-4 and M5. Although the breakaway oxidation time is generally defined as the time corresponding to an increase in oxidation rate (i.e., weight gain rate), it is the associated hydrogen pickup that causes embrittlement. Leistikow and Schanz presented trend curves (see Figure 6 in Ref. 20) for weight gain vs. time at temperature and a data plot (see Figure 8 in Ref. 20) for hydrogen content vs. time at temperature for 650-1000°C. They used an older vintage of standard Zry-4 with 1.6 wt.% Sn, 0.12 wt.% O, and 0.725-mm wall thickness. Typically the Zry-4 cladding of that vintage had  $\approx 0.3\text{-}\mu\text{m}$  outer-surface roughness. Sample preparation included degreasing, pickling in a nitric-fluoric acid mixture, and cleaning in boiling water. Such treatment may leave a fine surface layer containing fluorine impurities. Both surface roughness and surface fluorine impurities can destabilize the oxide layer growth through early transformation from the tight tetragonal phase to the weaker monoclinic phase. Two-sided oxidation tests were performed in their study. Thus, the condition of the cladding inner surface may influence the breakaway oxidation times reported by Leistikow and Schanz.

Mardon et al. [21] presented hydrogen-concentration results vs. time at 1000°C for belt-polished 17×17 low-tin Zry-4 (1.29 wt.% Sn, 0.12 wt.% O, and  $\approx 0.1\text{-}\mu\text{m}$  surface roughness). The oxidation was one-sided – outer-surface only. Thus, the condition of the cladding ID surface had no influence on the results.

The results of these two studies are compared in Table 17 in terms of breakaway time for weight-gain rate increase and hydrogen content increase to 200 wppm. It is clear that the belt-polished Zry-4 has a longer breakaway time at 1000°C than the pickled-and-cleaned, rough-surfaced Zry-4.

Table 17 Breakaway Oxidation Time vs. Temperature for Zry-4 in Terms of Increase in Weight Gain Rate and Hydrogen-content Increase (200 wppm). References are: L-S = Leistikow and Schanz [19,20] and M = Mardon et al. [21].

T, °C	Outer-Surface Treatment	Oxidation	Breakaway Time, s		Ref.
			Weight Gain Rate Increase <sup>a</sup>	200-wppm H Content	
1050	Pickled/Cleaned	2-sided	$\approx 5700$	---	L-S
1000	Pickled/Cleaned	2-sided	$\approx 1560$	1800	L-S
	Belt Polished	1-sided	---	5400	M
950	Pickled/Cleaned	2-sided	$\approx 3500$	---	L-S
900	Pickled/Cleaned	2-sided	$\approx 21,600$	50,400	L-S
850	Pickled/Cleaned	2-sided	$\approx 6300$	---	L-S
800	Pickled/Cleaned	2-sided	$\approx 1980$	3600	L-S
750	Pickled/Cleaned	2-sided	$\approx 2100$	---	L-S
700	Pickled/Cleaned	2-sided	$\approx 2640$	---	L-S
650	Pickled/Cleaned	2-sided	$\approx 11,400$	50,000	L-S

<sup>a</sup>For the L-S results, the hydrogen vs. time curve was used as a guide in determining breakaway oxidation time based on weight-gain-rate increase for curves with very gradual increase in slope.

The results in Table 17 indicate that breakaway oxidation time is not a monotonic function of decreasing or increasing oxidation temperature. To illustrate this point, a trend curve is plotted in Figure 29 based on the Leistikow and Schanz results for breakaway-oxidation weight gain. Comparing the results for older cladding (pickled-and-cleaned, high surface roughness) to modern cladding (belt polished) indicated significant differences in breakaway oxidation time for Zry-4 at the same oxidation temperature. There may also be a difference in results for one-sided (OD surface) vs. two-sided oxidation tests because the inner surface may have different surface conditions than the outer surface.

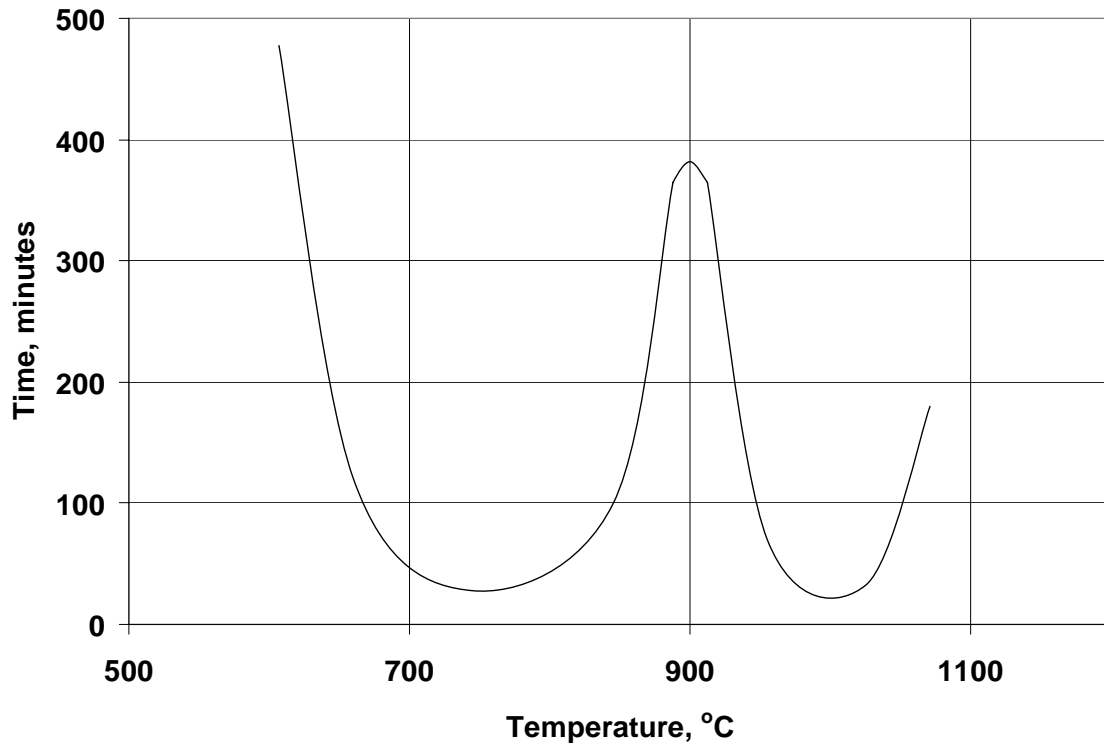


Figure 29. Breakaway-oxidation time vs. oxidation temperature determined from the trend curves presented by Leistikow and Schanz [19,20] for Zry-4 weight gain vs. time.

From the Leistikow and Schanz work, the minimum times for breakaway oxidation in Zry-4 appear to occur at oxidation temperatures of 800°C and 1000°C. In terms of hydrogen pickup, 1000°C-oxidation gives the minimum breakaway time. However, no studies were found that explored the sensitivity of breakaway-oxidation time to temperatures within the range of 975-1025°C. In the ANL tests, breakaway oxidation time was determined within this temperature range by targeting average temperatures of 985°C, 1000°C, and 1015°C for the two-sided oxidation tests. With the anticipated circumferential temperature variation of 10-15°C for large-diameter 15×15 cladding, these average temperatures include local temperatures of ≈975-1025°C. As the alpha + beta → beta phase transition temperature for Zry-4 is within this range, the results may shed some light on the effects of this transition temperature on breakaway oxidation. The alpha → alpha + beta phase transition temperature is ≈810°C for as-fabricated Zry-4. Breakaway oxidation tests were also conducted at 800°C oxidation temperature.

The ANL criterion for breakaway-oxidation time is a hydrogen pickup of 200 wppm. Post-quench ductility results at RT for ZIRLO oxidized at 1000°C showed ductility after a CP-equivalent oxidation

time of  $\approx 3360$  s at  $1000^\circ\text{C}$  with a hydrogen pickup of  $\approx 100$  wppm (see 3.3.1). Post-quench ductility results for E110 at RT after an oxidation time of  $\approx 300$  s at  $1000^\circ\text{C}$  showed ductility with a hydrogen pickup of  $\approx 150$  wppm (see 3.5.2). Ductility tests at  $135^\circ\text{C}$  were conducted on Zry-4 samples with  $\geq 200$  wppm hydrogen to confirm that ductility is retained with  $\leq 200$ -wppm H.

The classical view of the progression leading to breakaway oxidation is given by Leistikow and Schanz:

- a) breakaway-oxidation instability initiates at the metal oxide interface with local formation of monoclinic oxide;
- b) the precursor to breakaway oxidation is the transition from a "flat" oxide-metal interface to a wavy interface (i.e., referred to as "rugosity");
- c) the wavy surface creates alternating regions of tensile and compressive stresses in the near-surface oxide;
- d) local regions under tensile stress transform first from tetragonal to monoclinic oxide;
- e) the tetragonal-to-monoclinic oxide transition spreads from the inner surface to the outer surface; and
- f) cracking of the weak monoclinic oxide increases the weight-gain rate and hydrogen pickup.

Applying this conceptual model to experimental procedures indicates that, by the time the outer surface is observed to turn from black (tetragonal) to gray (monoclinic), the weight-gain rate and hydrogen-pickup rate are such that the oxide is well into the breakaway regime, and the breakaway-oxidation time is exceeded. As the furnace used for the ANL tests has a window for viewing a portion of the outer surface of the sample, it is relatively straightforward to turn off the furnace power and cool the sample at the oxidation time at which gray spots are observed on the outer surface of the cladding.

The thermal benchmark results for HBR and belt-polished  $15 \times 15$  Zry-4 are shown in Figures 30 and 31, respectively, for a target hold temperature of  $985^\circ\text{C}$ . These tests were conducted for a total test time of 1500 s, including the ramp time from  $300^\circ\text{C}$  to  $\approx 1000^\circ\text{C}$  through the end of the hold time. Samples were cooled without quench, which is the standard test protocol for determining breakaway-oxidation time. Excellent agreement was achieved between the CP-calculated and measured weight gain under these test conditions. For HBR-type Zry-4, the cladding temperature was  $992 \pm 9^\circ\text{C}$  at 78 s from temperature-ramp initiation and coasted down to a long-time temperature of  $984 \pm 10^\circ\text{C}$ . Based on the flatness of the temperature profile, the cladding temperature is assumed to be  $984 \pm 10^\circ\text{C}$  for test times beyond 1500 s. The breakaway-oxidation times reported in this work are referenced to zero time at the initiation of the ramp from  $300^\circ\text{C}$ . As the ramp time is short (78 s) relative to the breakaway-oxidation time and shorter than the expected data scatter in this time, the ramp time has no significant effect on the breakaway time.

For the belt-polished (BP) Zry-4 thermal history shown in Figure 31, the cladding temperature at 95 s was  $1000 \pm 12^\circ\text{C}$  and the long-time temperature was  $986 \pm 10^\circ\text{C}$ . Thus, within experimental uncertainty, the long-time oxidation temperature for BP Zry-4 was essentially the same as the temperature for HBR-type Zry-4. Because of the large data scatter found for BP Zry-4 hydrogen pickup – due partly to scratches introduced during sample sectioning – the BP thermal benchmark was rerun

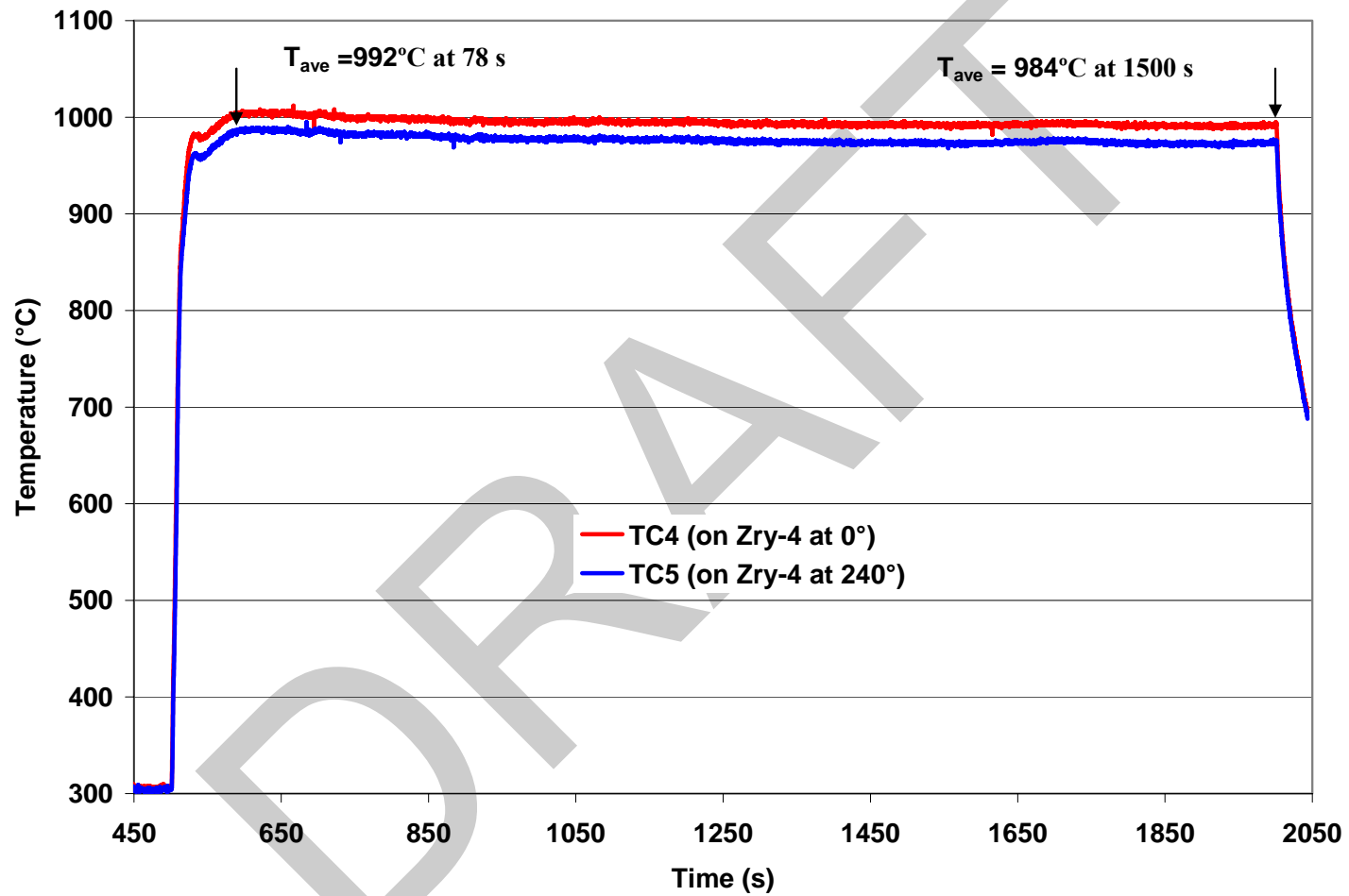


Figure 30. Results of thermal benchmark test with HBR-type 15×15 low-tin Zry-4. Measured weight gain is within 1% of the CP-predicted weight gain. Hold temperature is 992±9°C at 78 s and 984±10°C at 1500 s, beyond the temperature-ramp initiation.

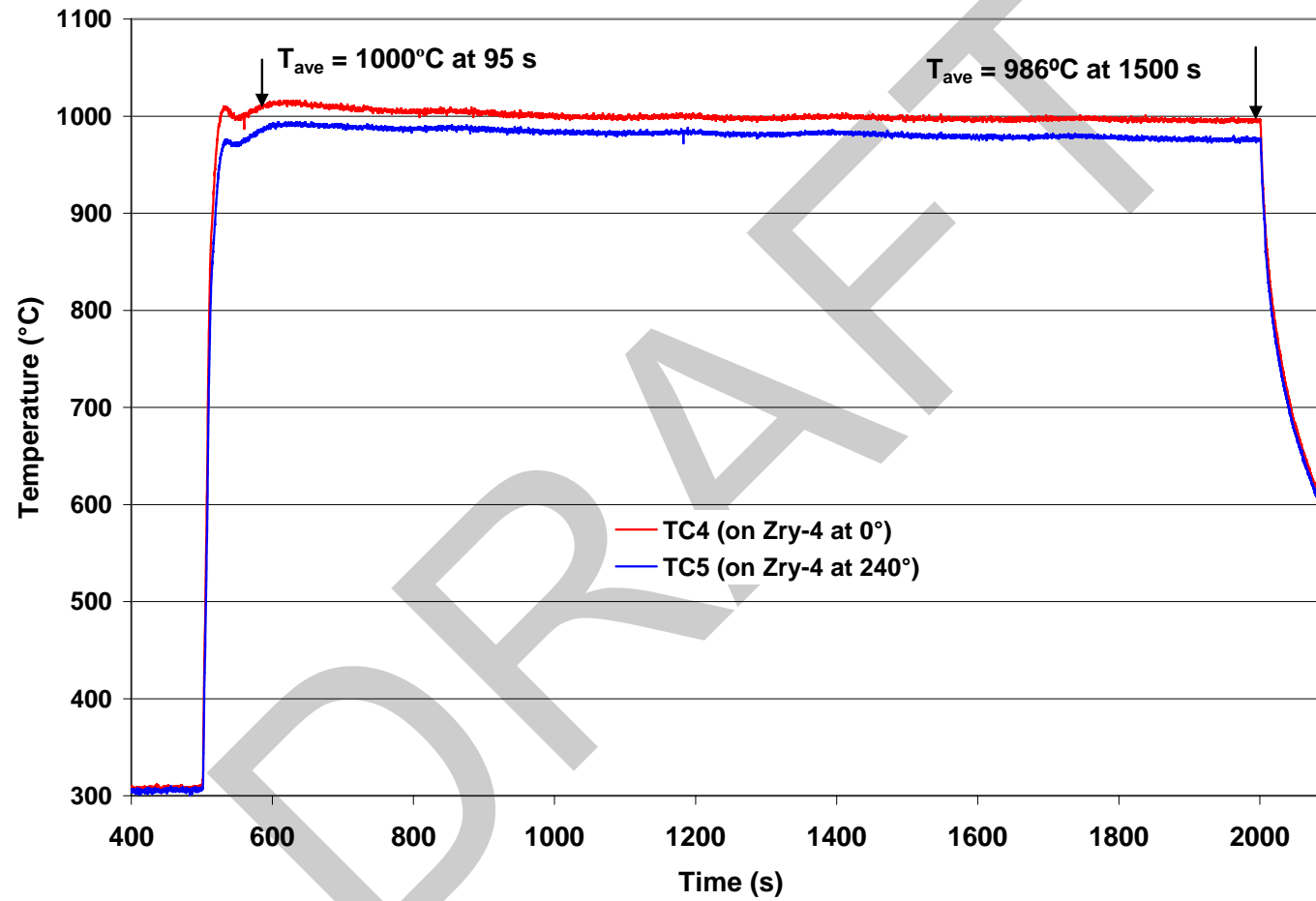


Figure 31. Results of first thermal benchmark test with belt-polished 15x15 low-tin Zry-4. Measured weight gain is within 6% of the CP-predicted weight gain. Hold temperature is  $1000 \pm 12^{\circ}\text{C}$  at 95 s and  $986 \pm 10^{\circ}\text{C}$  at 1500 s, beyond the temperature-ramp initiation.

for a longer time and with a controller setting designed to minimize overshoot (Figure 32). In addition, the test train length was decreased to adapt it to in-cell testing. The long-time temperature for this benchmark was  $986\pm 12^\circ\text{C}$ . Tests were also conducted at long-time temperatures of  $1000\pm 12^\circ\text{C}$  and  $1014\pm 12^\circ\text{C}$ . Because the  $\pm 12^\circ\text{C}$  was determined from three TC readings, it is also used for tests conducted at the temperatures shown in Figure 31.

Table 18 lists the breakaway-oxidation results at  $984\pm 10^\circ\text{C}$  for HBR-type, low-tin  $15\times 15$  Zry-4. Based on two tests at 3800 s, the hydrogen pickup is  $< 200$  wppm, and the breakaway time is  $> 3800$  s. Based on the 4000-s test result (1810-wppm H pickup), it was expected that a test time of 3900 s would give  $\approx 200$ -400 wppm H pickup. However, the H pickup after 3900 s was 1320 wppm. Given that considerable data scatter is expected for breakaway-oxidation time, no further testing was conducted for test times within 3800-3900 s, and 3800 s was identified as the breakaway-oxidation time. One sample (HBRU#96) had pretest surface scratches introduced during sectioning. The sample was subjected to post-oxidation ductility testing because of the hydrogen pickup ( $170\pm 80$  wppm). The offset and permanent strains for this sample at  $135^\circ\text{C}$  were 5.2% and 2.5%, respectively. These results indicate that Zry-4 is ductile with  $\approx 200$ -wppm H pickup. However, because the sample was scratched prior to testing, the hydrogen-pickup results were not used to determine breakaway oxidation time (see 3.5.1).

Metallography was performed for HBR-type Zry-4 samples oxidized for 159 s, 3600 s, and 5400 s. Results for these times are shown in Figures 33-35 at two magnifications. The results support the Leistikow and Schanz description of breakaway oxidation evolution. In Figure 33, the oxide layers are clearly tetragonal with a black outer surface and smooth interface between the oxide layers and the metal. In Figure 34 – taken from the black non-scratched area of the HBRU#96 test sample – the inner-surface and outer-surface oxide layers exhibit a wavy boundary at the oxide-metal interface. This is the precursor to breakaway oxidation. Both inner and outer oxides exhibit the same transition morphology, which suggests no preference for the inner surface to experience breakaway prior to the outer surface. In Figure 35, the oxide layers are well beyond the breakaway transition. The outer and inner surfaces are gray, and significant cracking is observed on and within the oxide layers.

The results for belt-polished Zry-4 oxidized at  $986\pm 12^\circ\text{C}$  (see Figure 31) are summarized in Table 19, followed by metallographic results in Figures 36-37. As expected, the breakaway oxidation time ( $\approx 5000$  s) is longer for belt-polished Zry-4 as compared to the rough-surface Zry-4 ( $\approx 3800$  s). The BPZ4#18 test sample, which was oxidized for 5000 s, had a hydrogen pickup of  $280\pm 160$  wppm. Although this is higher than the ANL 200-wppm-H criterion, the sample did retain ductility ( $\approx 6\%$  offset and permanent strains) at  $135^\circ\text{C}$ . The ductility results support the use of the ANL 200-wppm criterion for Zry-4 breakaway-oxidation time. Test sample BPZ4#18 is particularly interesting because it experienced local breakaway at the outer surface. Figure 38a shows the sample discoloration along an axial strip, and Figure 38b and 38c show the corresponding outer-surface oxide layer in this region. Tetragonal-to-monoclinic transition was observed only in this region. Also, the hydrogen concentration (224, 123, 467, and 352 wppm) at this axial location was highly non-uniform in the circumferential direction, indicating little time for hydrogen diffusion following local breakaway.

Because the test train used to generate the Table 18-19 results was at the end of its useful life, a new test train was built and benchmarked (see Figure 32). This shorter test train was used to examine the sensitivity of breakaway time to oxidation temperatures of  $986$ - $1014^\circ\text{C}$  and to mild surface scratches (see 3.5.1). No breakaway oxidation was observed (Table 20) at 5400 s for  $986^\circ\text{C}$ ,  $1000^\circ\text{C}$ , and  $1014^\circ\text{C}$ . Although the second test train gives longer breakaway oxidation times ( $> 5400$  s), such variation is not surprising because breakaway oxidation is an instability phenomenon, which is sensitive to local surface conditions and temperature gradients, as well as other subtle differences in test conditions. Nevertheless,

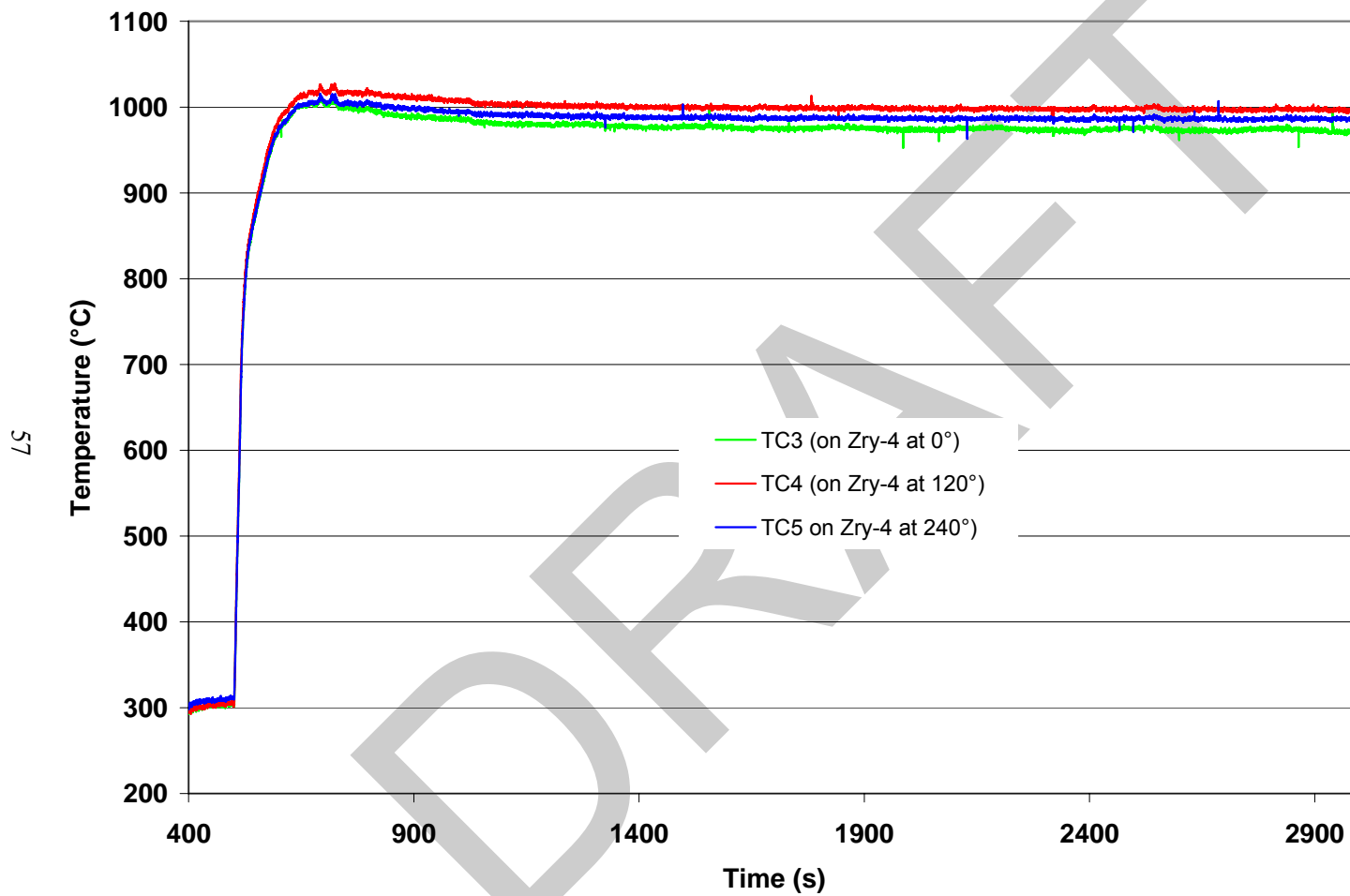


Figure 32. Results of second thermal benchmark test with belt-polished 15×15 low-tin Zry-4. Initial overshoot temperature is  $1012 \pm 7^\circ\text{C}$ , and long-time hold temperature is  $986 \pm 12^\circ\text{C}$ . Results are based on the readings of three TCs welded to the sample  $120^\circ$  apart.

Table 18 Results of Breakaway Oxidation Tests at  $984\pm 10^\circ\text{C}$  for HBR-type  $15\times 15$  low-tin Zry-4. The hydrogen content ( $C_{\text{Hi}}$ ) of the as-fabricated cladding is 22 wppm. The hydrogen content of the oxidized sample ( $L_{\text{H}}$ ) was measured with the LECO Hydrogen Determinator. Breakaway-oxidation time based on 200-wppm hydrogen pickup is  $\approx 3800$  s.

Test ID	Test Time, s	Weight Gain, $\text{mg}/\text{cm}^2$		H Content, wppm	H-pickup, <sup>a</sup> wppm	Offset Strain at $135^\circ\text{C}$ , %
		CP	Measured			
HBRU#93	159	2.45	2.82	Low	Low	---
HBRU#90	1500	7.89	7.85	Low	Low	---
HBRU#84	3600	12.2	10.7	57	40	---
<b>HBRU#96<sup>b</sup></b>	<b>3600</b>	<b>12.2</b>	<b>12.6</b>	<b>186</b>	<b>170</b>	<b>5.2</b>
HBRU#95	3800	12.5	10.6	61	40	---
HBRU#88	3800	12.5	10.7	42	20	---
HBRU#92	3900	12.7	16.4	1260	1320	0.9
HBRU#91	4000	12.9	16.2	1723	1810	---
HBRU#87	4500	13.6	16.4	1581	1650	---
HBRU#81	5400	14.9	22.2	2111	2300	---
HBRU#82	7200	17.4	28.8	2769	3170	---

<sup>a</sup>The hydrogen pickup ( $\Delta C_{\text{H}}$ ) is referenced to the as-fabricated weight of the sample and is calculated from  $\Delta C_{\text{H}} = (1 + 4 \times 10^{-3} \text{ Wg}) L_{\text{H}} - C_{\text{Hi}}$ , where Wg is the measured weight gain in  $\text{mg}/\text{cm}^2$ .

<sup>b</sup>Sample was scratched during pretest sectioning; see Section 3.5.1 for details.

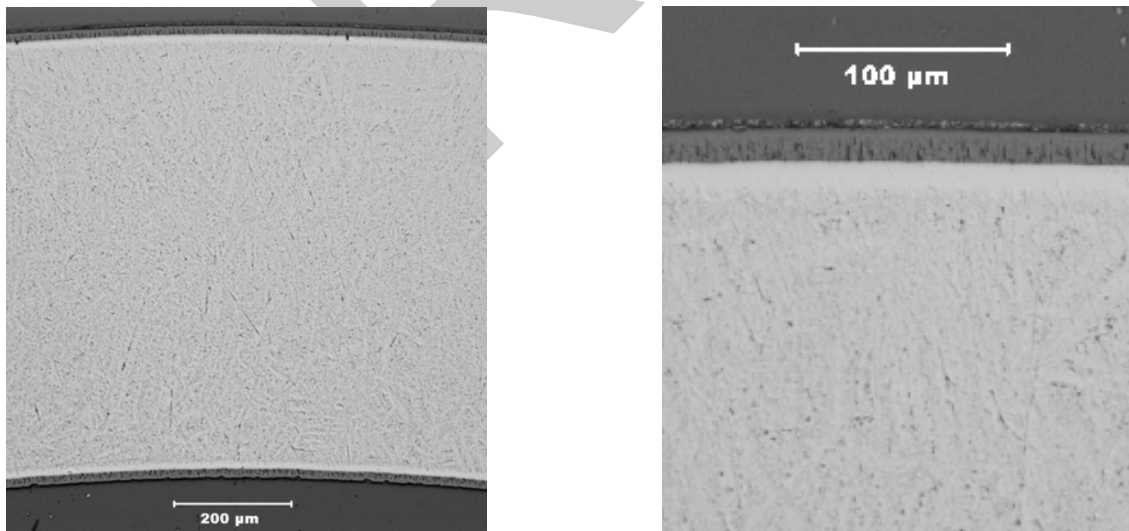


Figure 33. Low magnification (left) of inner- and outer-surface oxide layers for HBR-type  $15\times 15$  low-tin Zry-4 oxidized at  $\approx 1000^\circ\text{C}$  for 159 s; higher magnification (right) of the outer-surface oxide layer illustrating the smooth boundary between oxide and metal.

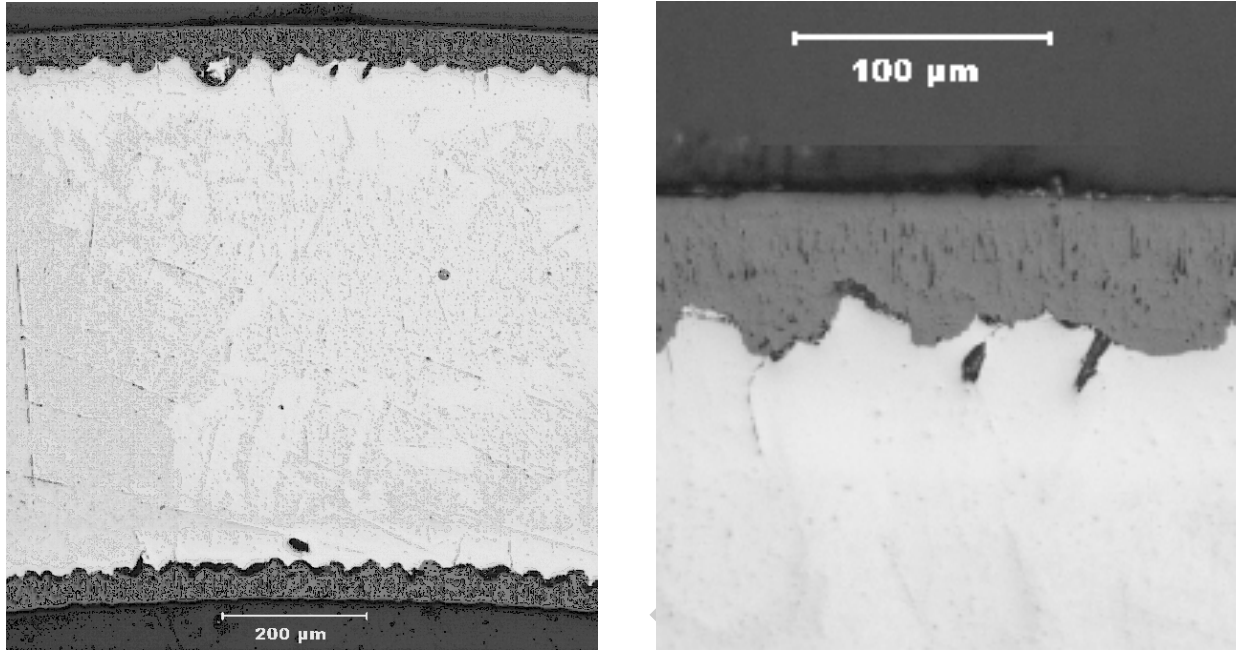


Figure 34. Low magnification (left) of inner- and outer-surface oxide layers for HBR-type 15×15 low-tin Zry-4 oxidized at 984±10°C for 3600 s; higher magnification (right) of the outer-surface oxide layer showing the wavy boundary between oxide and metal, which is a precursor to breakaway.

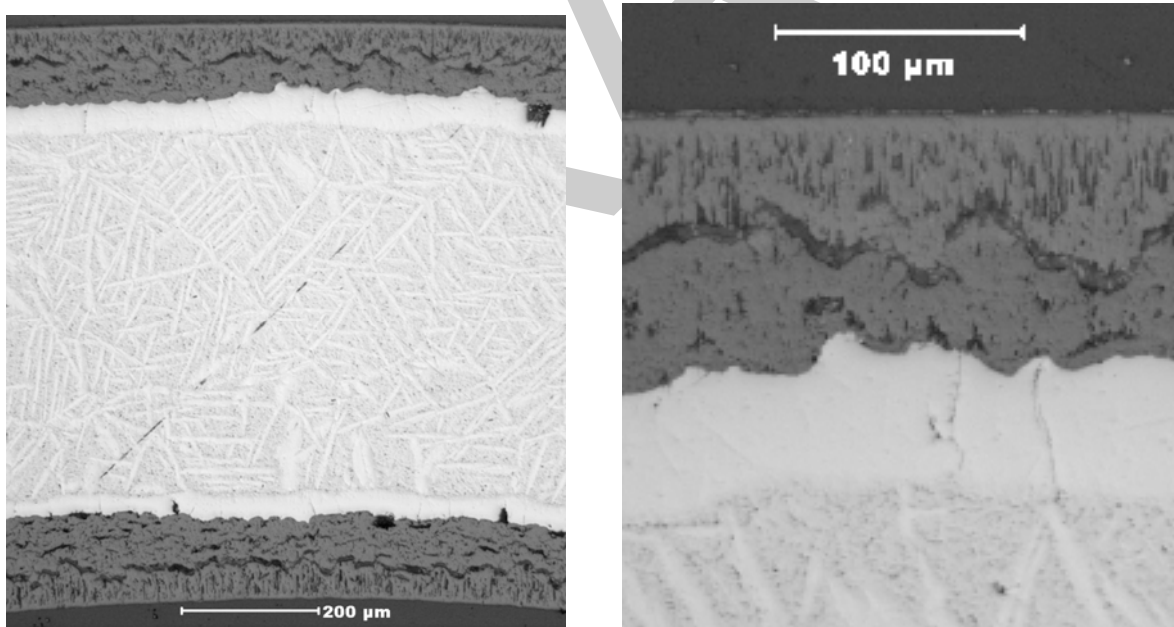


Figure 35. Low magnification (left) of inner- and outer-surface oxide layers for HBR-type 15×15 low-tin Zry-4 oxidized at 984±10°C for 5400 s; higher magnification (right) of outer-surface oxide layer showing cracks in monoclinic oxide layer formed during the transition to breakaway oxidation.

Table 19 First Set of Results for Breakaway Oxidation at  $986\pm 12^\circ\text{C}$  (Figure 31) for Belt-polished  $15\times 15$  Low-tin Zry-4. The hydrogen content ( $C_{\text{Hi}}$ ) of the as-fabricated cladding is 26 wppm. The hydrogen content of the oxidized sample ( $L_{\text{H}}$ ) was measured with the LECO Hydrogen Determinator. Breakaway-oxidation time based on 200-wppm hydrogen pickup is  $\approx 5000$  s.

Test ID	Test Time, s	Weight Gain, $\text{mg}/\text{cm}^2$		H Content, wppm	H Pickup, <sup>a</sup> wppm	Offset Strain at $135^\circ\text{C}$ , % ( $\Delta C_{\text{H}}$ , wppm)
		CP	Measured			
BPZ4#16	135	2.45	2.85	Low	Low	---
BPZ4#15	1500	8.58	8.07	Low	Low	---
BPZ4#10	3600	12.7	10.8	20	0	---
BPZ4#18	5000	14.9	12.6	286	280	6.0 (280)
BPZ4#13	5400	15.5	12.1	411	410	5.9 (260 $\pm$ 180)
BPZ4#12	7200	17.7	18.7	1798	1930	---

<sup>a</sup>The hydrogen pickup ( $\Delta C_{\text{H}}$ ) is referenced to the as-fabricated weight of the sample and is calculated from  $\Delta C_{\text{H}} = (1 + 4.6\times 10^{-3} \text{ Wg}) L_{\text{H}} - C_{\text{Hi}}$ , where Wg is the measured weight gain.

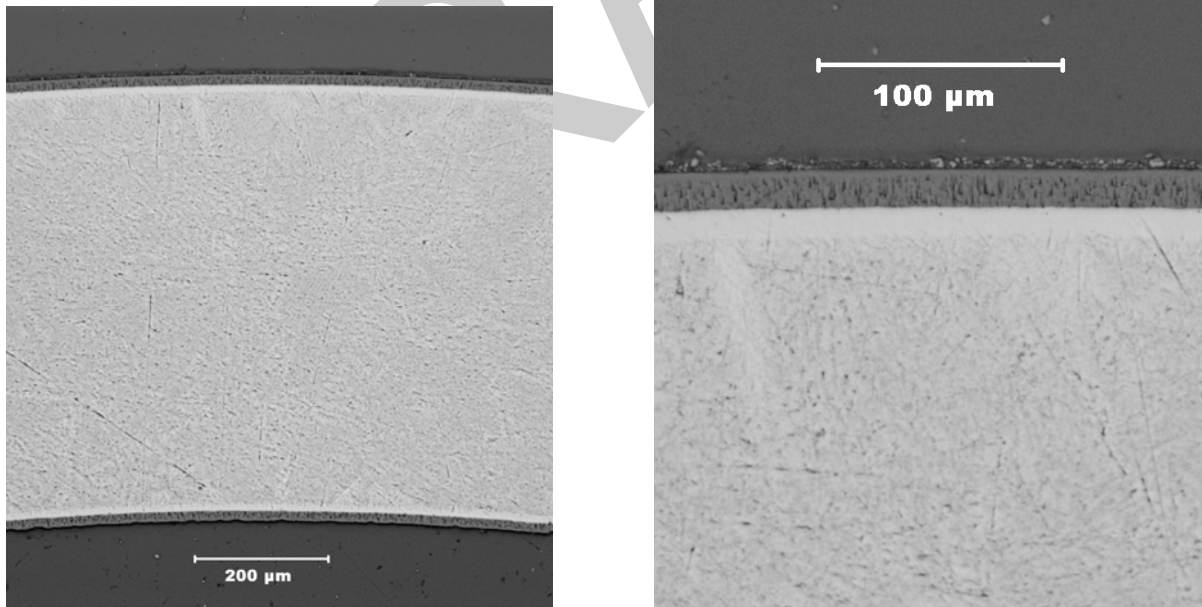


Figure 36. Low magnification (left) of inner- and outer-surface oxide layers for belt-polished  $15\times 15$  low-tin Zry-4 oxidized at  $\approx 1000^\circ\text{C}$  for 135 s; higher magnification (right) of outer-surface oxide layer showing the smooth boundary between oxide and metal.

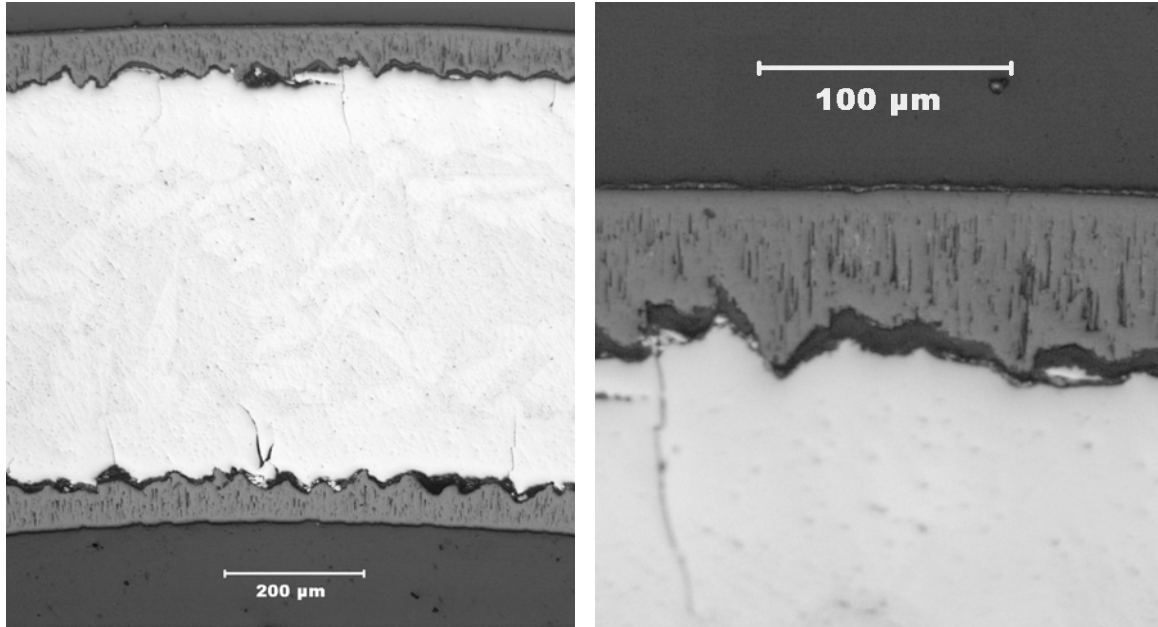
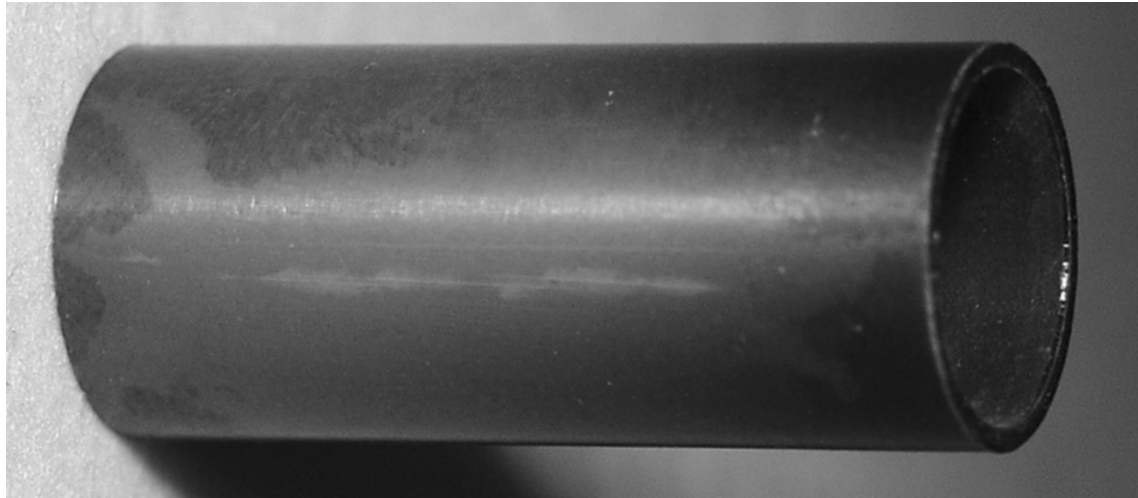


Figure 37. Low magnification (left) of inner- and outer-surface oxide layers for belt-polished 15×15 low-tin Zry-4 oxidized at 986±12°C for 5400 s (BPZ4#13); higher magnification (right) of outer-surface oxide layer showing wavy metal-oxide interface and initiation of breakaway oxidation.

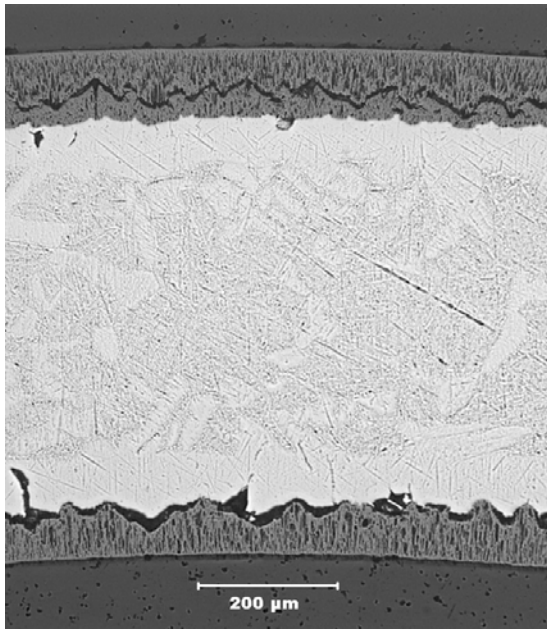
Table 20 Second Set of Results for Breakaway Oxidation of Belt-polished 15×15 Low-tin Zry-4 at Long-time Test Temperatures of 986°C (see Figure 32), 1000°C, and 1014°C. Hydrogen content ( $C_{Hi}$ ) of as-fabricated cladding is 26 wppm; hydrogen content of the oxidized sample ( $L_H$ ) was measured with the LECO Hydrogen Determinator; breakaway-oxidation time based on 200-wppm hydrogen pickup is >5400 s.

Test ID	Test T, °C	Test Time, s	Weight Gain, mg/cm <sup>2</sup>		H Content, wppm	H Pickup, <sup>a</sup> wppm
			CP	Measured		
BPZ4#30	986±12	4000	13.1	11.6	18	0
BPZ4#31	986±12	4500	13.9	12.8	18	0
BPZ4#33	986±12	5000	14.7	12.2	18	0
BPZ4#34	986±12	5400	15.2	11.7	19	0
BPZ4#38	1000±12	5400	16.6	14.6	18	0
BPZ4#41	1014±12	5400	18.1	15.3	19	0

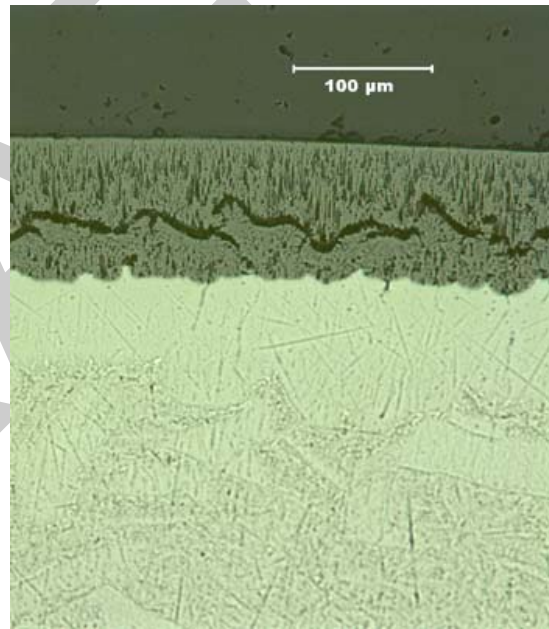
<sup>a</sup>The hydrogen pickup ( $\Delta C_H$ ) is referenced to the as-fabricated weight of the sample and is calculated from  $\Delta C_H = (1 + 4.6 \times 10^{-3} W_g) L_H - C_{Hi}$ , where  $W_g$  is the measured weight gain.



(a)



(b)



(c)

Figure 38. Images of belt-polished 15×15 sample BPZ4#18: (a) appearance of outer surface of sample showing local breakaway along a longitudinal strip; (b) inner and outer oxide layers showing pre-breakaway morphology of inner-surface oxide layer and post-breakaway morphology of outer-surface oxide layer; and (c) high magnification of outer-surface oxide layer.

for LOCA-criteria purposes it does not really matter whether the breakaway time for unscratched BP Zry-4 is 5000 s or >5400 s, as both times are very long.

The hydrogen pickup vs. oxidation time for rough-surface and belt-polished 15×15 Zry-4 is plotted in Figure 39 based on the data in Tables 18 and 19. Both sets of results were generated by the same

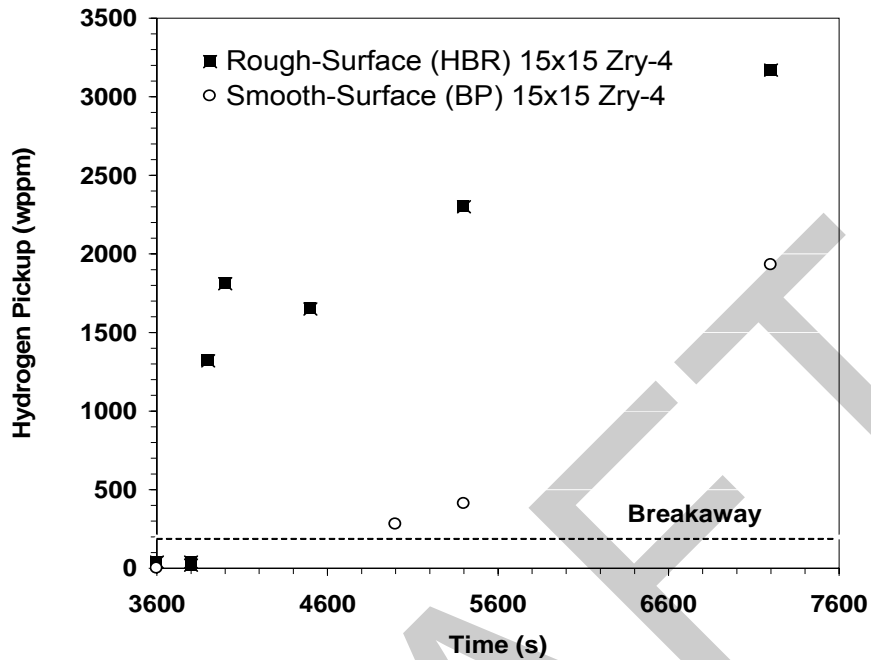


Figure 39. Breakaway-oxidation data for HBR-type (0.3- $\mu\text{m}$  surface roughness) and belt-polished (0.1- $\mu\text{m}$  surface roughness) 15 $\times$ 15 Zry-4 oxidized in the same apparatus at  $985\pm 12^\circ\text{C}$ . Based on the ANL 200-wppm-hydrogen-pickup criterion, breakaway oxidation time is  $\approx 3800$  s for HBR-type 15 $\times$ 15 Zry-4 and  $\approx 5000$  s for belt-polished (BP) 15 $\times$ 15 Zry-4.

oxidation test train. The lower breakaway-oxidation time for the rough-surface HBR-type Zry-4 appears to be due to its higher surface roughness. However, the surface and near-surface chemistry (i.e., impurities) and microstructure may be different for this cladding. Belt polishing removes surface impurities in the range of 0.1-0.3  $\mu\text{m}$  and may result in some additional cold working of the near-surface metal. In terms of hydrogen content or hydrogen pickup, the HBR-type Zry-4 (1980s) has a much higher breakaway-oxidation time ( $\approx 3800$  s) than the time ( $\approx 1800$  s) determined by Leistikow and Schanz [19,20] for 1970s Zry-4. The breakaway-oxidation time ( $\approx 5000$  s) for modern AREVA 15 $\times$ 15 Zry-4 tested by ANL is comparable to the breakaway-oxidation time ( $\approx 5400$  s) determined by Mardon et al. [21] for modern AREVA 17 $\times$ 17 Zry-4. Even though the Mardon et al. tests were one-sided with only outer-surface breakaway, the ANL two-sided oxidation test results are comparable because the outer-surface oxide layer experienced breakaway oxidation earlier than the inner surface.

### 3.2 Zircaloy-2

One-sided oxidation tests were conducted with as-fabricated and high-burnup 9×9 Zry-2 (see Tables 3 and 7 for material parameters) to determine the oxidation kinetics [15]. Tests were conducted at 1000°C (1200-6000 s), 1100°C (600-3000 s), and 1204°C (300-1200 s). Measured weight gain based on the increase in sample weight tended to be higher than CP-predictions due to some steam leakage causing inner-surface oxidation near the sample ends for all three oxidation temperatures. The weight-gain results based on metallographic images and analysis were in excellent agreement with the CP-predicted weight gains for the 1204°C-oxidized samples. The measured oxide layer thicknesses were also in excellent agreement with the CP-predicted oxide layer (see page 74 of Ref. 13). However, the measured thicknesses of the oxygen-stabilized alpha layer were as much as 40% higher than the CP-predicted values. This is important in evaluating the use of the CP-correlations in deducing beta-layer thickness vs. time at temperature. In the ANL tests, the argon purge flowing through the inside of the samples minimized hydrogen pickup (<50 wppm) from inner-surface oxidation and allowed desorption of hydrogen from the beta layer to the purge. According to Cathcart et al. (Ref. 3, Appendix B, Table B1, page 166), samples oxidized (one-sided) at 1203°C for only 236 s picked up 250-450 wppm hydrogen. Samples oxidized at lower temperatures for longer times picked up as much as 750-wppm hydrogen. Hydrogen is a beta-stabilizer, which results in a decrease in alpha layer thickness and an increase in beta-layer thickness. Figure 40 [22] shows the ANL measured (alpha + oxide)-layer thickness and the CP-predicted (alpha + oxide)-layer thickness. The higher measured values are due to the higher measured values for the alpha-layer thickness.

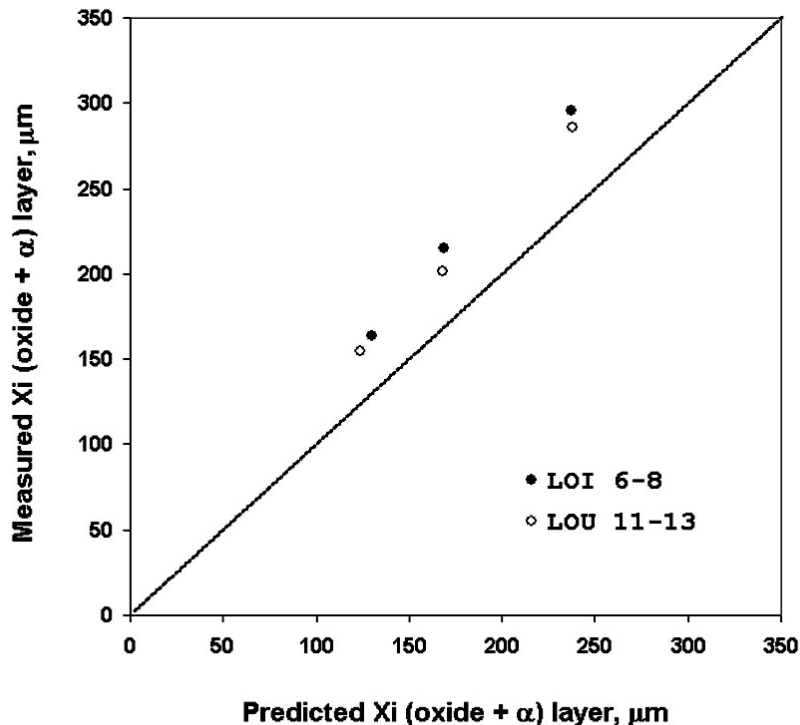


Figure 40. Measured vs. CP-model-predicted Xi (oxide + alpha) layers after steam-oxidation tests (300, 600, and 1200 s at ≈1204°C) with irradiated (LOI 6-8) and unirradiated (LOU 11-13) Zry-2.

### 3.2.1 Post-quench ductility of 10×10 Zry-2 oxidized at 1000°C and 1200°C

#### 10×10 Zry-2 Oxidized at 1000°C

10×10 Zry-2 cladding samples were oxidized (two-sided) at 1000°C to 10%, 13%, and 17% CP-ECR. Thermal benchmark results are shown in Figure 41. For the oxidation tests, the control TC was lowered by 5°C to give an average hold temperature of 1004±7°C up to 2000 s and a long-time (≥2000 s) hold temperature of 1000±8°C. Following the heating phase, samples were cooled from 1000°C to 800°C at ≈10°C/s, quenched, and ring-compressed at RT. An additional test at 20.7% CP-ECR was performed without quench for the breakaway oxidation studies (see 3.2.2). The weight gain and post-test ductility for this sample are included in this section.

As-fabricated Zry-2 rings were compressed to 2-mm displacement and to maximum displacement. The thin-ring analytical solution for loading stiffness of a homogeneous Zry-2 wall is 1.06 kN/mm. The stiffness determined from the load-displacement curve was 0.95 kN/mm. The measured value is thus ≈10% lower than the predicted value. This difference is reasonable because the Zr liner may have a lower elastic modulus than Zry-2; an isotropic approximation for the elastic modulus of Zry-4 was used; and machine compliance may cause a reduction in stiffness. The difference between offset (1.54 mm) and permanent (1.39 mm) displacements was 0.15 mm, which is consistent with other cladding alloys tested. The maximum offset strain that can be achieved with this cladding geometry is 60%.

The weight gains listed in Table 21 for the 1000°C-oxidized Zry-2 cladding are significantly lower than the CP-predicted weight gains and the measured weight gains for 17×17 Zry-4 (see Table 8 for Zry-4 results). Figure 42 shows the comparison. As indicated in Table 3, Zry-2 cladding has a Zr liner on the inner surface, which is about 10% of the wall thickness. Previous outer-surface oxidation tests conducted with 9×9 Zry-2 indicated excellent agreement between Zry-2 measured and predicted weight gains and oxide layer thicknesses. Quantitative metallography was performed for the Zry-2 sample used to generate the temperature history shown in Figure 41 (2000 s from ramp initiation to end of heating phase at 1000°C; ≈13% CP-ECR). The outer- and inner-surface oxide layers were 52±2 μm and 31±2 μm, respectively. The circumferential uniformity of the oxide layer thickness indicates little temperature variation. More significantly, the decrease of ≈40% in the inner-surface oxide layer relative to the outer-surface oxide layer and CP-predicted oxide layer thickness explains the lower-than-predicted weight gain. Figure 43 shows metallographic images of the sample oxidized to 10% CP-ECR: (a) one of eight cross-sectional arc lengths, (b) Zry-2 outer surface, and (c) the Zr-lined inner surface. The interface between the prior-beta-phase Zr-liner and Zry-2 is apparent in Figure 43c.

Ring-compression test results for the 1000°C-oxidized Zry-2 cladding are also summarized in Table 21. The post-quench ductility of 10×10 Zry-2 is higher than the ductility of 17×17 Zry-4 oxidized at 1000°C to 17% CP-ECR: 12±2% vs. 5.1% offset strain, respectively. Based on the 20.7% CP-ECR sample that was not quenched, Zry-2 oxidized at 1000°C retains RT post-quench ductility at >20% CP-ECR. Note that through-wall failure for two-sided-oxidized Zry-2 cladding rings appears as likely to initiate at the outer Zry-2 surface at ±90° from the loading direction as at the inner Zr surface along the loading direction. The 20.7% CP-ECR sample developed one through-wall crack at 90° from the loading direction (side wall) and a second nearly-through-wall crack along the loading direction at the bottom surface. The results suggest that the oxygen-stabilized alpha layer formed within the Zr liner may not be as brittle as the oxygen-stabilized alpha layer formed within the Zry-2 cladding.

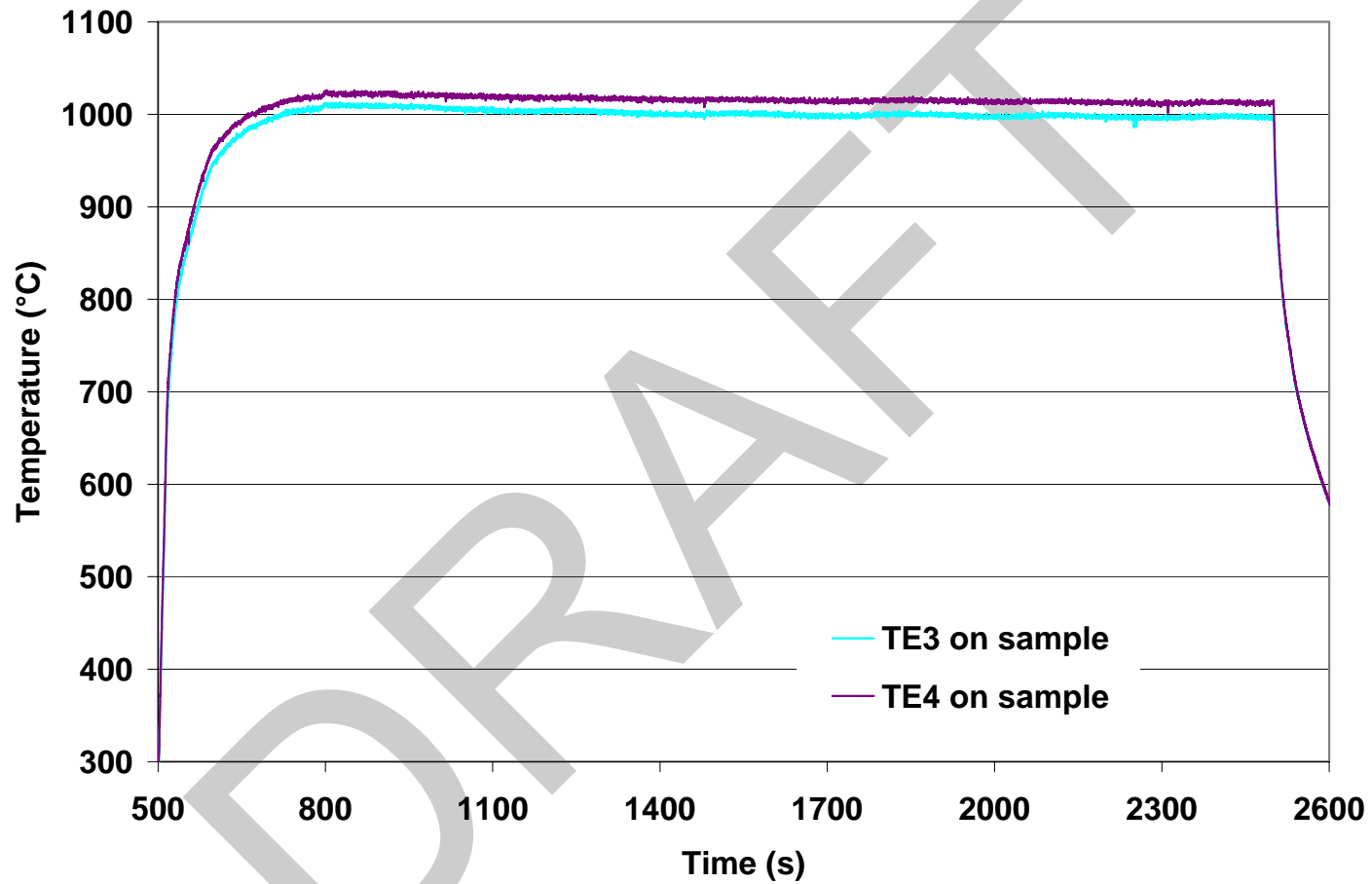


Figure 41. Thermal benchmark results for 10x10 Zry-2 at 1000°C target temperature. Average hold temperature is  $1009 \pm 7^\circ\text{C}$ . Hold temperature after 2000 s from ramp initiation is  $1005 \pm 8^\circ\text{C}$ . For oxidation tests, the control TC was lowered by  $\approx 5^\circ\text{C}$  to give a long-time hold temperature of  $1000 \pm 8^\circ\text{C}$ .

Table 21 Ring Compression Test (RCT) Results for 10×10 Zry-2 Cladding Oxidized at 1000°C, Cooled at ≈10°C/s to 800°C, and Quenched. ECR = 1.328 Wg for 0.66-mm-wall cladding. Tests were performed on ≈8-mm-long samples at RT and 0.0333-mm/s displacement rate. Displacements in the loading direction were normalized to the as-fabricated outer diameter (10.29 mm) to calculate strains.

Test Conditions			ECR, %		Plastic Displacement, mm		Plastic Strain, %	
T, °C		Test Time, <sup>a</sup> s	CP	Meas.	Offset	Permanent	Offset	Permanent
Ox.	RCT							
---	RT	--	0	0	6.0	---	60	---
1000	RT	1150	10.0	8.0	≥5.1 <6.6	≥5.1 ---	≥46 <64	≥40
1000	RT	1930	13.0	10.4	>1.16 4.81	>0.89 3.46	>11 47	>8.8 34
1000	RT	3420	17.0	13.6	1.48 0.95	1.28 0.55	14 9.2	12 5.3
1000 <sup>b</sup>	RT	5000	20.7	15.6	0.65	<0.5	6.3	<5

<sup>a</sup>Includes time for ramp from 300°C and hold time.

<sup>b</sup>Breakaway oxidation test conducted with cooling from 1000°C to RT without quench.

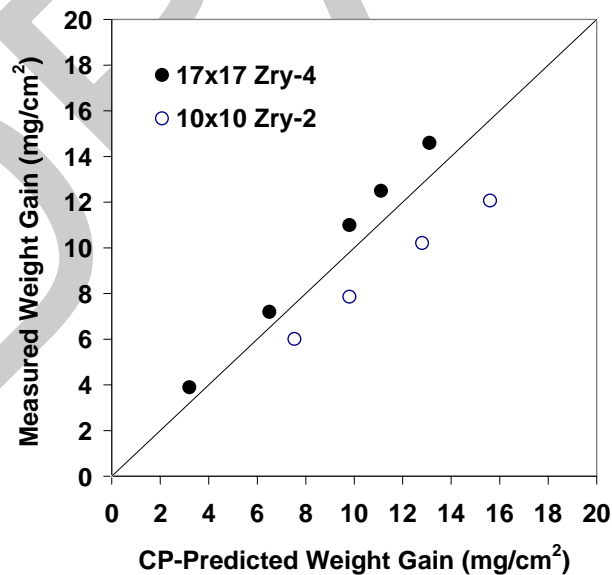
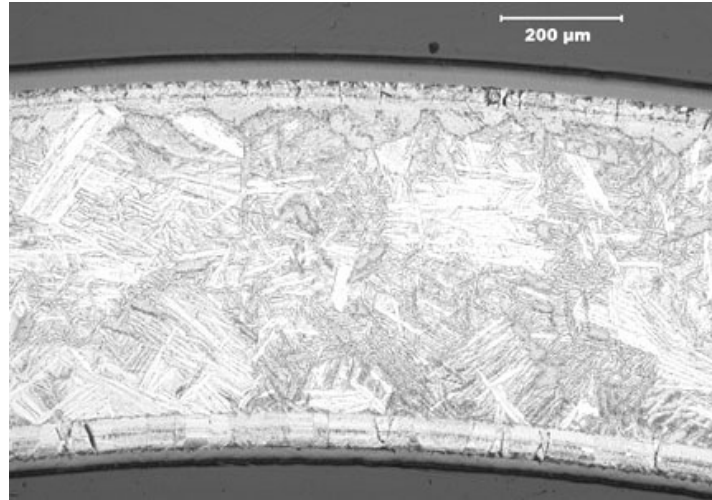
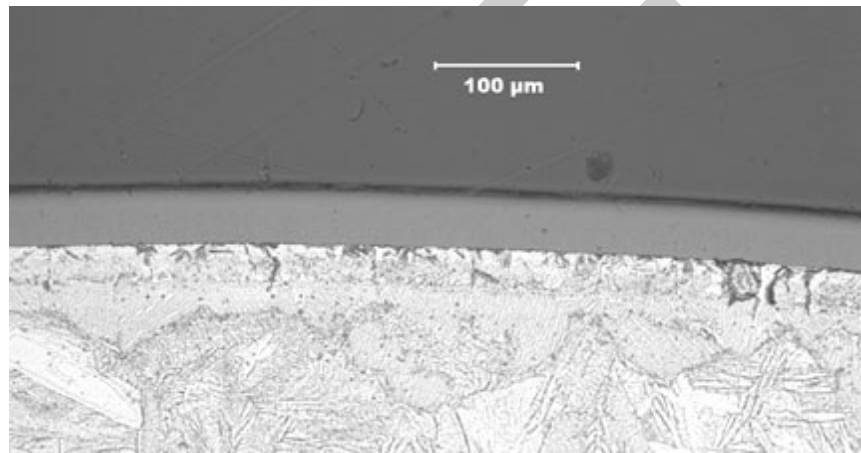


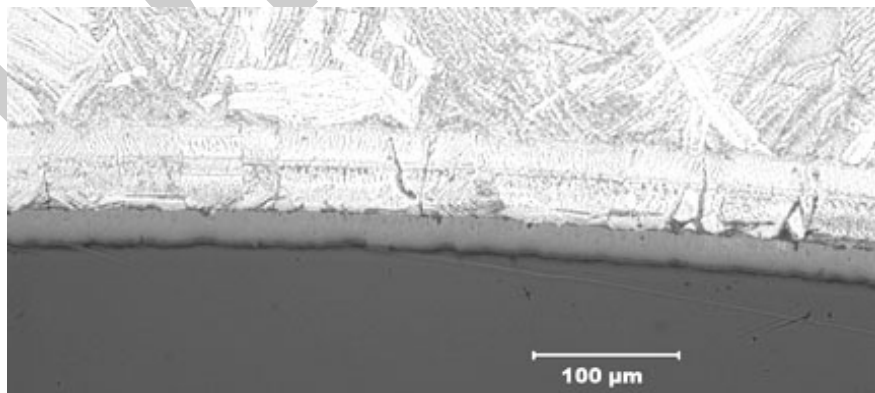
Figure 42. Comparison of measured and CP-predicted weight gains for Zr-lined 10x10 Zry-2 and 17x17 Zry-4 oxidized at 1000°C.



(a) Cross section



(b) Outer Zry-2 surface



(c) Inner Zr-lined surface

Figure 43. Micrographs of 10×10 Zry-2 sample oxidized at 1000°C to 10% CP-ECR: (a) one of eight cross-sectional arc lengths, (b) outer Zry-2 surface, and (c) inner Zr-liner surface.

### 10×10 Zry-2 Oxidized at 1200°C

10×10 Zry-2 cladding samples were oxidized (two-sided) at 1200°C to 10%, 13%, 17%, and 20% CP-ECR. Thermal benchmark results are shown in Figure 44. Following the heating phase, samples were cooled from 1200°C to 800°C at  $\approx 13^\circ\text{C/s}$ , quenched, and ring-compressed at 135°C.

As-fabricated Zry-2 rings were compressed at 135°C to 2 mm and to maximum displacement. The thin-ring analytical solution at 135°C for loading stiffness of a homogeneous Zry-2 wall is 0.98 kN/mm. The stiffness determined from the load-displacement curve was 0.81 kN/mm. The results suggest that the elastic modulus of the Zry-2/Zr composite may decrease more than the predicted 7.5% for Zry-4 from RT to 135°C. The difference between offset (1.65 mm) and permanent (1.52 mm) displacements was 0.13 mm, which is consistent with the RT results. The maximum offset strain that can be achieved with this cladding geometry and the thermocouple on the inner surface of the cladding is 50%.

The weight gains listed in Table 22 for the 1200°C-oxidized Zry-2 cladding are in good agreement with the CP-predicted weight gains and the measured weight gains for 17×17 Zry-4 (see Table 11 for Zry-4 results). Figure 45 shows the comparison. Although the measured weight gains are in good agreement, the oxide layer on the Zr liner is  $\approx 15\%$  thinner than the oxide layer on the Zry-2 outer surface. Quantitative metallography was performed on the Zry-2 cladding sample exposed to the temperature history shown in Figure 44 ( $\approx 17\%$  CP-ECR). The measured outer- and inner-surface oxide layers were  $62 \pm 2 \mu\text{m}$  and  $53 \pm 2 \mu\text{m}$ , respectively. As with the 1000°C-oxidized sample, the small circumferential variation in oxide thicknesses indicates good temperature uniformity. Micrographic images in Figures 46 (at 170 s and 10% CP-ECR) and 47 (at 423 s and 17% CP-ECR) show the differences in oxide layer thicknesses. Also, the oxygen-stabilized alpha layers, which are predicted to be about the same thickness as the oxide layers, are significantly thicker than predicted for both surfaces. Based on the results in Figures 46c and 47c, the Zr liner ( $\approx 66\text{-}\mu\text{m}$  thick) has been consumed by oxidation and transformation to oxygen-stabilized alpha for  $\geq 10\%$  CP-ECR ( $\geq 170\text{-s}$  test time) at 1200°C.

Ring-compression tests results for 1200°C-oxidized Zry-2 cladding rings are also summarized in Table 22. The transition CP-ECR is  $\approx 19\%$  based on interpolation. Although the transition value falls within the range measured for two types of Zry-4, the decrease in ductility with increasing CP-ECR for Zry-2 is clearly more gradual than the trend curves for Zry-4. Comparison of the Zry-2 and Zry-4 post-quench-ductility results is shown in Figure 48. This gradual decrease in ductility with CP-ECR may be due to the presence of the liner. For homogeneous Zry-4, the growth of the brittle oxide- and oxygen-stabilized-alpha layers is expected to be the same at the inner and outer surfaces. Also, the rate of oxygen diffusion into the beta layer is expected to be the same from the outer and inner surfaces of the beta layer. As such, through-wall failure of the compressed ring should initiate at the cladding inner surface under the loading plate or above the support plate. For 1200°C-oxidized Zry-2 cladding at 10% and 13% CP-ECR, through-wall failure was observed at the side of the sample, 90° from the loading direction. At the side locations, the maximum tensile bending stress is located at the cladding outer surface. The 17% CP-ECR samples failed with multiple through-wall cracks: top, 45°, and side for one sample; and bottom and 45° for the second sample. The 20% CP-ECR samples failed in the traditional manner with a single through-wall crack at either the top or bottom of the ring.

Chung and Kassner [18] measured the oxygen content (2.5 wt.%) needed to stabilize alpha in Zry-4 at 1200°C. They also reviewed previous studies of zirconium, for which 2.1-2.2 wt.% oxygen is sufficient to stabilize alpha in Zr at 1200°C. Based on these studies and on the ring compression results, the Zry-2 oxygen-stabilized alpha layer appears to be more brittle than the Zr-liner alpha layer, although both layers would be classified as brittle.

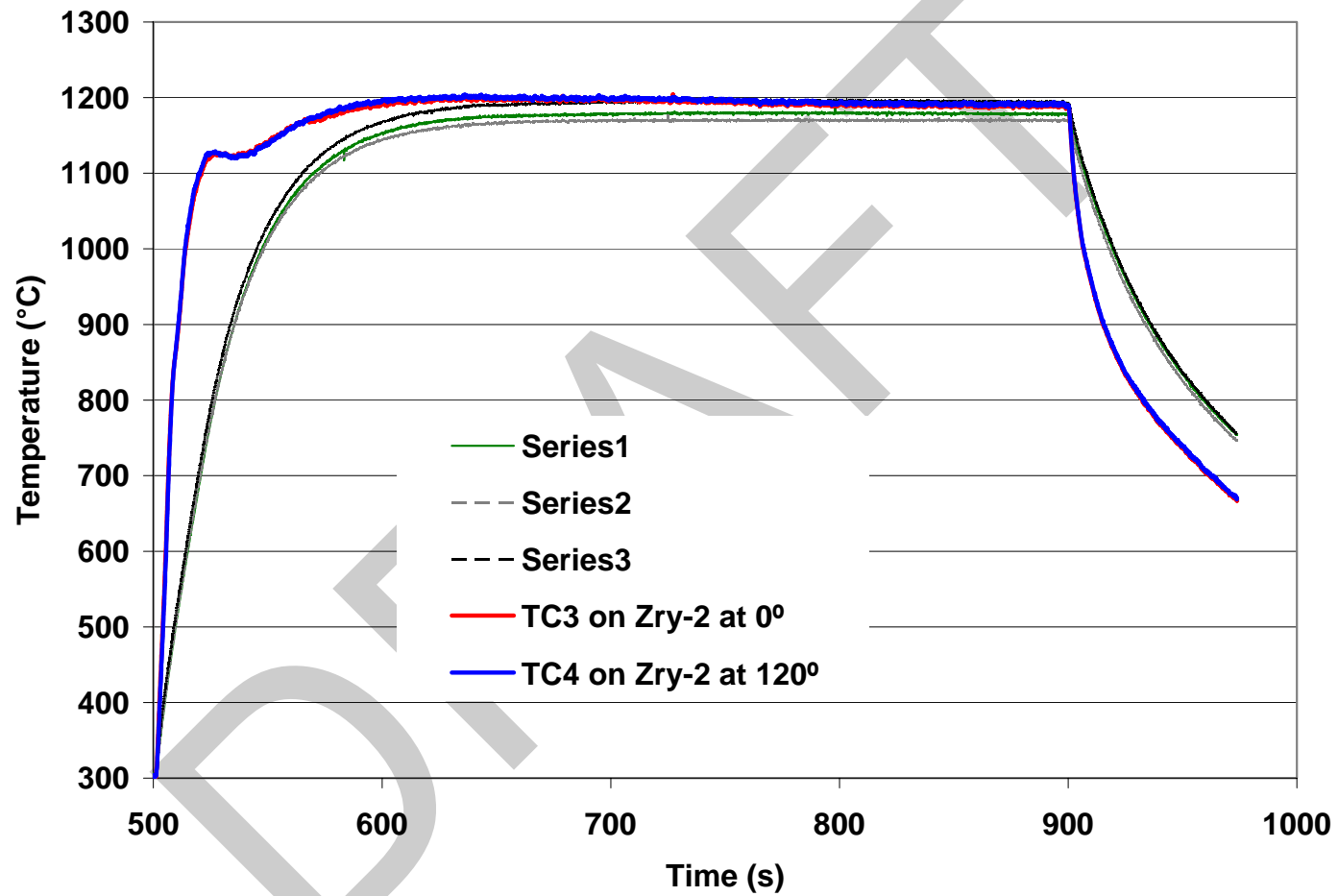


Figure 44. Thermal history for 10x10 Zry-2 oxidation tests at 1200±6°C. The raw data for the sample TC readings were corrected based on calibrating these TCs to an ANL NIST-calibrated TC. Also shown are the three TC readings for the holder TCs (Series 1-3).

Table 22 Ring Compression Test (RCT) Results for 10×10 Zry-2 Cladding Oxidized at 1200°C, Cooled at ≈13°C/s to 800°C, and Quenched. ECR = 1.328 Wg for 0.66-mm wall cladding. Tests were performed on ≈8-mm-long samples at 135°C and 0.0333-mm/s displacement rate. Displacements in the loading direction were normalized to the as-fabricated outer diameter (10.29 mm) to calculate strains.

Test Conditions		Test Time, <sup>a</sup> s	ECR, %		Plastic Displacement, mm		Plastic Strain, %	
Ox.	RCT		CP	Meas.	Offset	Permanent	Offset	Permanent
---	135	---	0	0	5.11	5.18	50	50
1200	135	170	10.0	10.8	2.48 2.60	2.12 2.27	24 25	21 22
1200	135	260	13.0	13.7	1.12 1.44	--- 1.34	11 14	--- 13
1200	135	423	17.0	17.1	0.75 0.56	--- 0.29	7.3 5.4	--- 2.8
1200	135	575	20.0	19.9	0.19 0.15	0.09 0.10	1.9 1.5	0.9 1.0

<sup>a</sup>Includes time for ramp from 300°C and hold time.

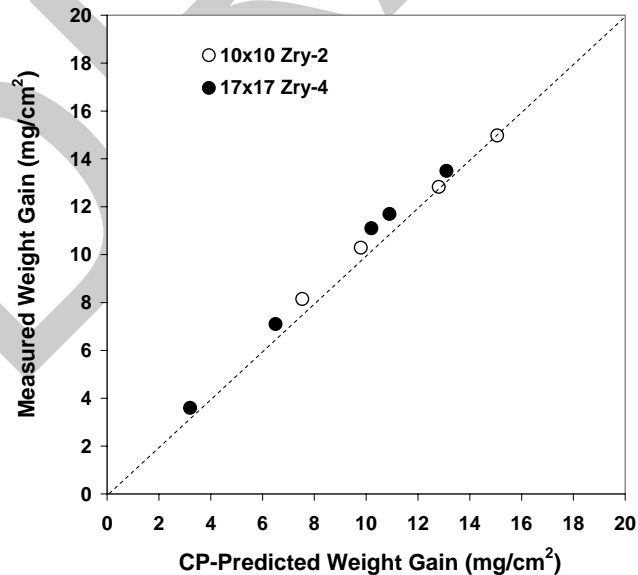
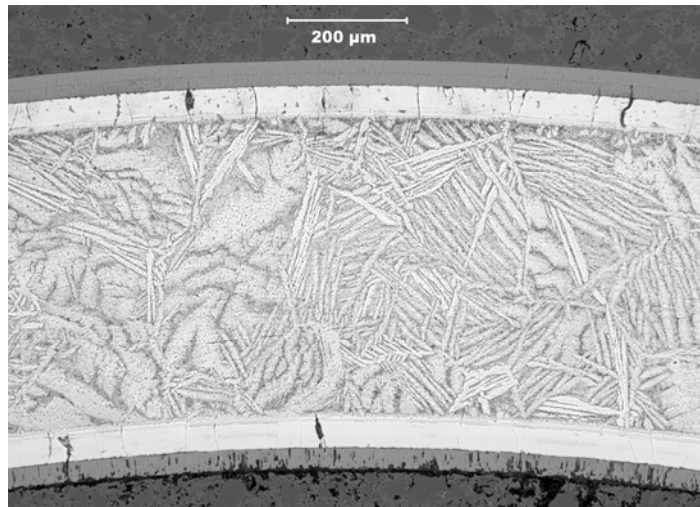
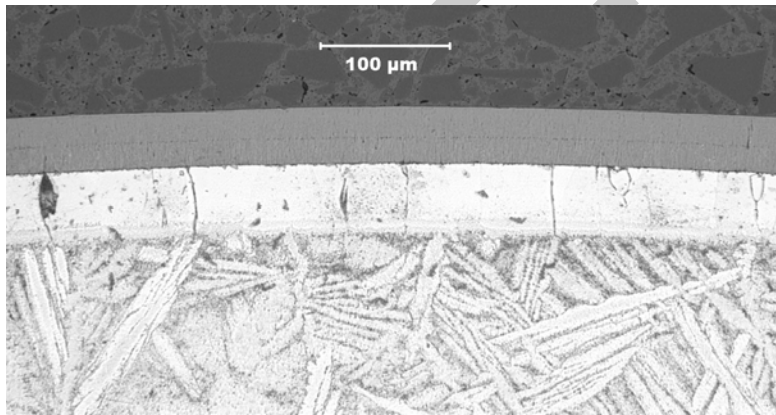


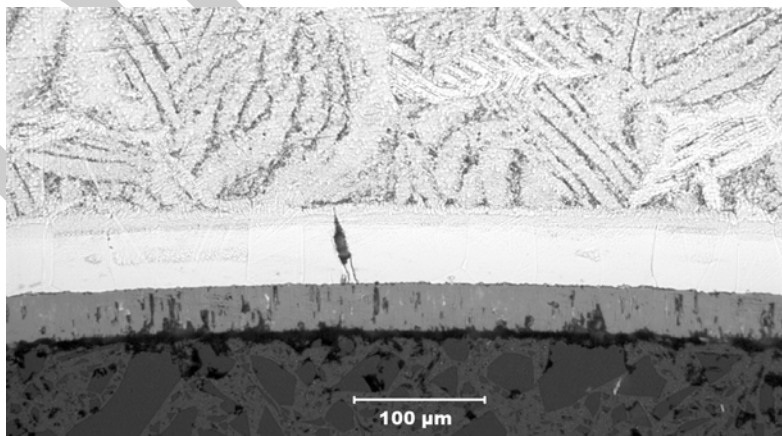
Figure 45. Comparison of measured and CP-predicted weight gains for 10x10 Zry-2 and 17x17 Zry-4 oxidized at 1200°C, cooled at ≈13°C/s to 800°C, and quenched at 800°C.



(a) Cross section

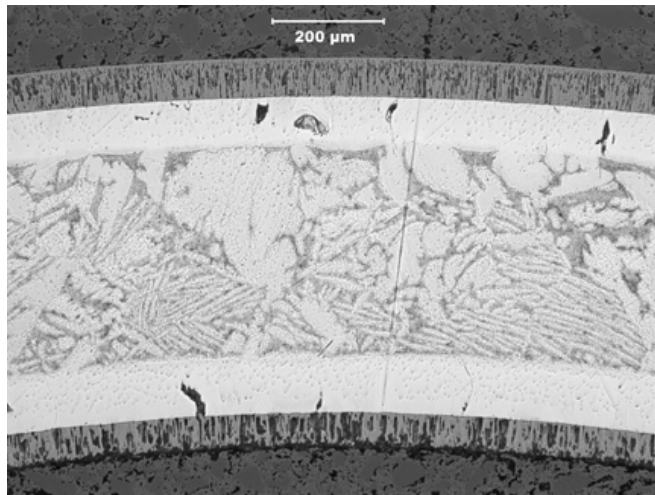


(b) Outer Zry-2 surface

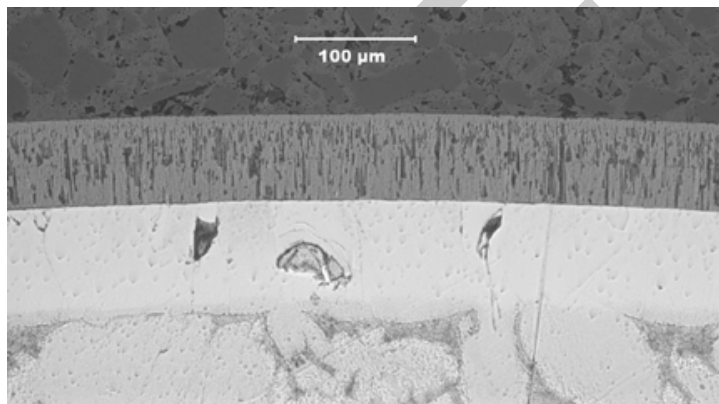


(c) Inner Zr-lined surface

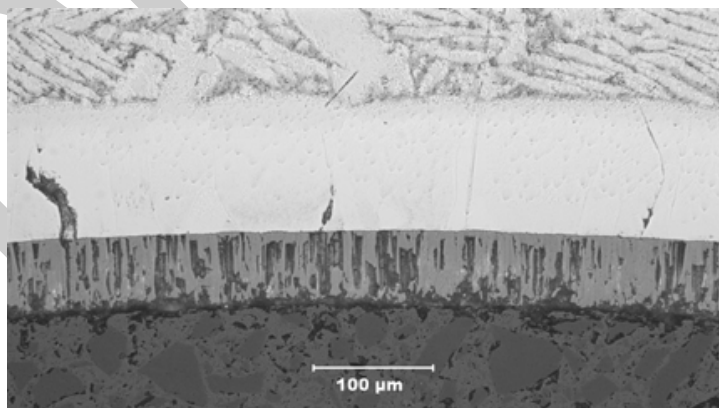
Figure 46. Metallographic images of 10×10 Zry-2 sample oxidized at 1200°C to 10% CP-ECR: (a) cross section (one of 8 orientations), (b) outer Zry-2 surface, and (c) inner Zr-lined surface.



(a)



(b) Outer Zry-2 surface



(c) Inner Zr-lined surface

Figure 47. Metallographic images of 10×10 Zry-2 sample oxidized at 1200°C to 17% CP-ECR: (a) cross section (one of 8 orientations), (b) outer Zry-2 surface, and (c) inner Zr-lined surface

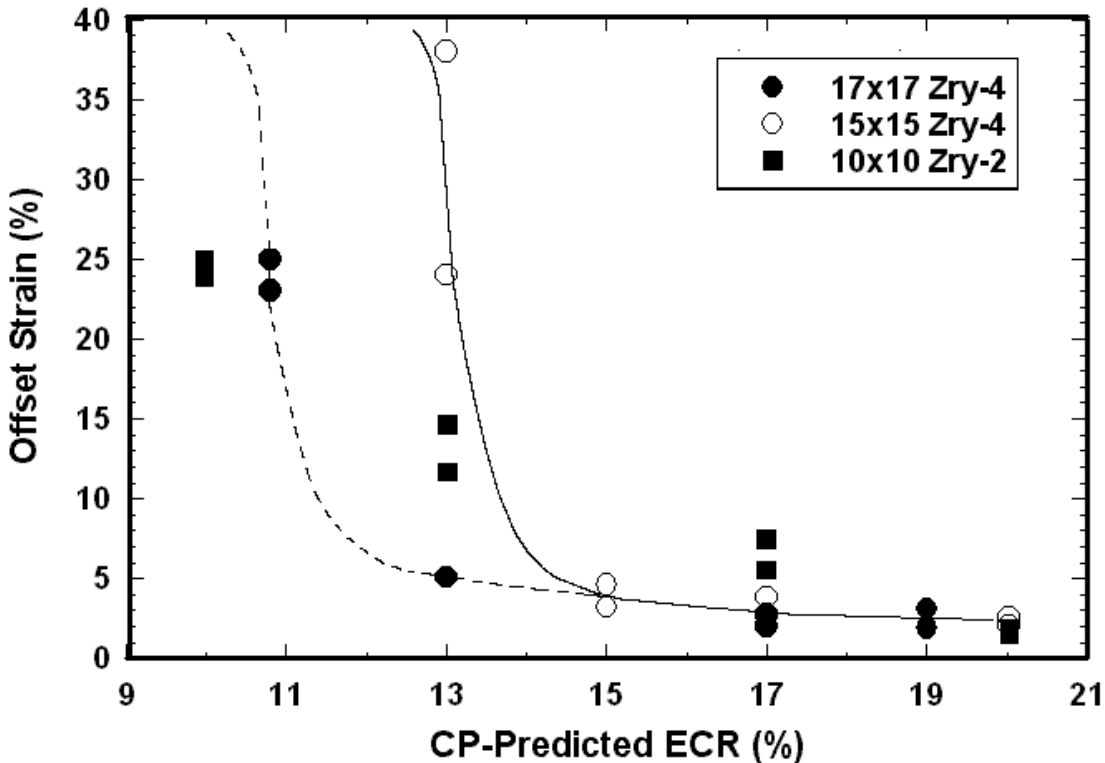


Figure 48. Post-quench ductility (offset strain) vs. CP-ECR for Westinghouse 17x17 Zry-4, AREVA 15x15 Zry-4, and 10x10 Zr-lined Zry-2, all oxidized at 1200°C, cooled at  $\approx 11-13^\circ\text{C/s}$  to 800°C, and quenched at 800°C. Ring-compression test temperature was 135°C.

### 3.2.2 Breakaway oxidation time for 10x10 Zry-2 samples oxidized at 970-1000°C

The breakaway oxidation time for 10x10 Zry-2 is expected to be about the same as the breakaway time for 9x9 Zry-2. One-sided oxidation tests using as-fabricated and high-burnup 9x9 Zry-2 were conducted at 1000°C for hold times of 1200 s, 3600 s, and 6000 s. Although metallographic analysis of these samples was not conducted, sample weight gains were measured for the high-burnup samples. The results from Yan et al. [22] are presented in Figure 49. Even with the artifact of some inner-surface oxidation contributing to the measured weight gain, the 3600-s sample showed no evidence of breakaway oxidation. The 6000-s sample had a weight gain 25% higher than the CP-predicted weight gain. At least 10% of this can be attributed to inner-surface oxidation near the ends of the sample. The remaining 15% may be a combination of breakaway oxidation and/or additional inner-surface oxidation for such a long test time. Based on the belt-polished 15x15 Zry-4 results, the breakaway oxidation time is expected to be  $\approx 5000$  s for belt-polished 10x10 and 9x9 Zry-2.

Two-sided breakaway oxidation tests were conducted with 10x10 Zry-2 cladding samples. Tests were run for 5000 s at long-time hold temperature of  $1000^\circ\pm 8^\circ\text{C}$  (see Figure 41). Samples were cooled to RT without quench. The tests were repeated by lowering the control temperature by 15°C, 30°C, and 200°C to give target temperatures of 985°C and 970°C. The test matrix is given in Table 23, along with the results for weight gain, hydrogen content, and calculated hydrogen pickup. Within the temperature range of  $\approx 960-1010^\circ\text{C}$ , the breakaway oxidation time for Zry-2 cladding is  $>5000$  s.

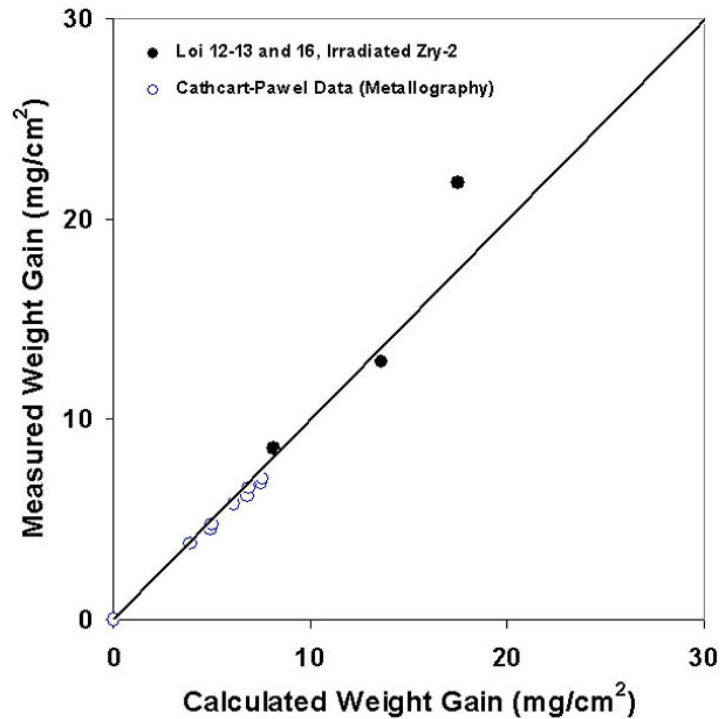


Figure 49. Comparison of Cathcart-Pawel model predictions to ANL sample weight gain data for irradiated (Limerick) Zry-2 after steam oxidation at  $\approx 1000^{\circ}\text{C}$  for test times of 1200 s, 3600 s, and 6000 s.

Table 23 Results for Breakaway Oxidation Studies of 10x10 Zry-2 Cladding. Test times are given from the beginning of the ramp from  $300^{\circ}\text{C}$  to the end of the hold time at temperature.

Oxidation T, $^{\circ}\text{C}$	Test Time, s	Weight Gain, $\text{mg}/\text{cm}^2$		H Content, wppm	H Pickup, <sup>a</sup> wppm	Outer Surface
		CP	Measured			
1000 $\pm$ 8	5000	15.6	12.1	16	4	Lustrous Black
<b>1000<math>\pm</math>8<sup>b</sup></b>	<b>5000</b>	<b>15.6</b>	<b>11.5</b>	<b>32</b>	<b>21</b>	<b>Lustrous Black</b>
985 $\pm$ 8	5000	14.4	9.8	27	15	Lustrous Black
970 $\pm$ 8	5000	13.1	8.7	15	3	Lustrous Black

<sup>a</sup>Hydrogen pickup ( $\Delta C_{\text{H}}$ ) is referenced to the as-fabricated weight of the sample and is calculated from  $\Delta C_{\text{H}} = (1 + 4.7 \times 10^{-3} \text{ Wg}) L_{\text{H}} - C_{\text{Hi}}$ , where Wg is the measured weight gain in  $\text{mg}/\text{cm}^2$ .  $C_{\text{Hi}}$  is 13 wppm.

<sup>b</sup>A 20- $\mu\text{m}$ -deep scratch was made along the length of the sample prior to testing.

### 3.3 ZIRLO

#### 3.3.1 Post-quench ductility of 17×17 ZIRLO oxidized at 1000°C, 1100°C, and 1200°C

This work was performed in sequence with the 17×17 Zry-4 testing and characterization. The same test trains, thermal-benchmark temperature histories (Figures 17, 18, 20 and 21), test times, and CP-ECR values were used, as the ZIRLO cladding has the same dimensions as the Zry-4 cladding. Results are also presented with the same subdivision as for Zry-4: characterization and RT-ring-compression testing of samples two-sided oxidized at 1000°C and 1100°C and quenched at 800°C; and characterization and ring-compression testing (RT and 135°C) of samples exposed to two-sided oxidation at 1200°C and quenched at 800°C. Characterization included weight gain, oxide- and alpha-layer thickness (metallography), microhardness, and hydrogen pickup (LECO). All samples were oxidized to CP-predicted ECR values of 5, 10, 15, 17, and 20%. Additional tests were conducted at intermediate CP-ECR values for the 1200°C-oxidized samples to better determine the ductile-to-brittle transition CP-ECR value for this oxidation temperature.

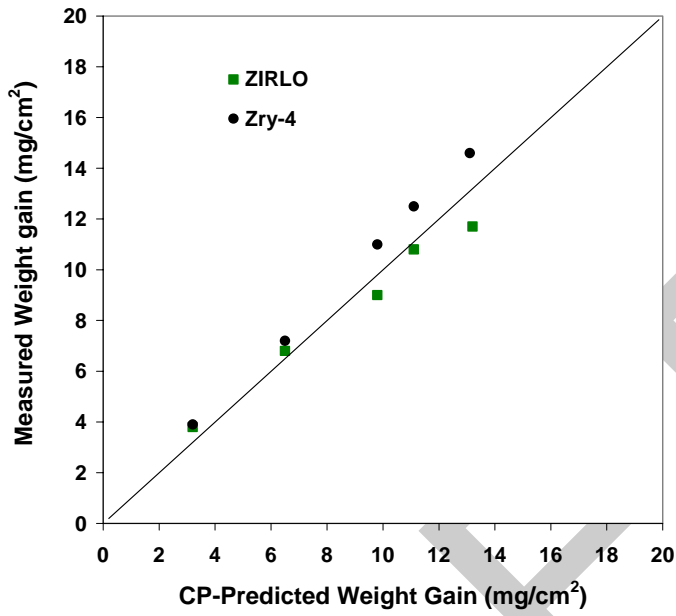
#### 17×17 ZIRLO oxidized at 1000°C and 1100°C

Table 24 shows the weight gain results for ZIRLO oxidized at 1000°C and 1100°C. They are in very good agreement with the CP-predicted weight gains at these oxidation temperatures, except for the lower measured values for the 1000°C-oxidation samples at  $\geq 15\%$  CP-ECR. Figures 50a and 50b show the measured weight gains for ZIRLO and Zry-4 oxidized at 1000°C and 1100°C, respectively, as compared to the CP-predicted weight gains.

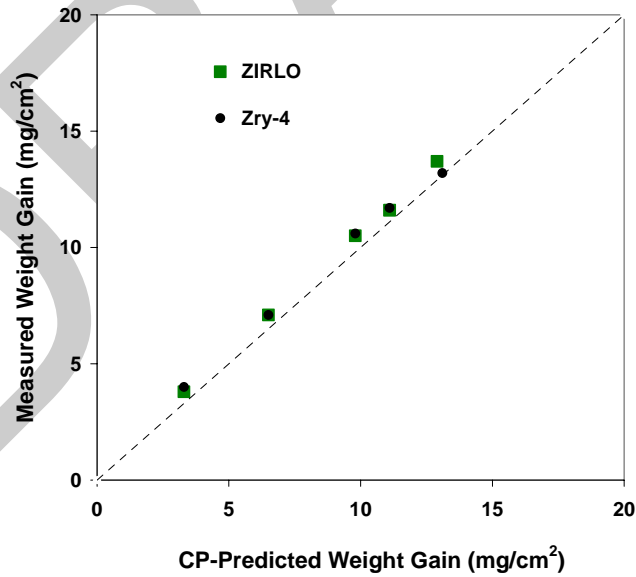
Table 25 lists the results of the RT post-quench ductility tests for the 1000°C- and 1100°C-oxidation samples. It is clear from the results that 17×17 ZIRLO retains post-quench ductility up to 20% CP-ECR – the limit of the test conditions – for these oxidation temperatures. The results are shown graphically in Figures 51 and 52 for 1000°C- and 1100°C-oxidized samples, respectively. Because of the differences in weight gain between ZIRLO and Zry-4 oxidized at 1000°C, offset strains are displayed as functions of measured ECR (51a) and CP-ECR (51b). For oxidation at 1100°C, both alloys exhibit essentially the same weight gain for the same test time, so post-quench ductility results are plotted in Figure 52 as a function of CP-ECR only. For the 1000°C- and 1100°C-oxidation tests, the offset strain leveled out at  $\approx 3\%$ . These results suggest that ZIRLO will retain ductility at higher CP-ECR values and higher test times ( $>3400$  s at 1000°C) until breakaway oxidation or beta-layer thinning occurs. For 1100°C-oxidation, breakaway oxidation should not occur, and the beta layer does not appear to embrittle due to the low saturation-level oxygen content. At much higher ECR values, the beta layer would thin enough to make the ring structure behave in a brittle manner. Photographs of the ring-compressed samples are shown in Figure 53a (1000°C) and 53b (1100°C). The 5% and 10% CP-ECR samples oxidized at 1000°C were intact at the maximum Instron displacement. The 5% CP-ECR sample oxidized at 1100°C was also intact.

Table 26 summarizes the results of the metallography, microhardness, and hydrogen pickup measurements for ZIRLO as compared to Zry-4. The hydrogen pickup is very low for 1100°C-oxidized ZIRLO samples. However, hydrogen pickup is  $\approx 100$  wppm for ZIRLO oxidized at 1000°C for 3364 s (20% CP-ECR). Metallographic images indicate that the inner-surface oxide is undergoing breakaway oxidation. Breakaway oxidation for ZIRLO oxidized at 800-1000°C is discussed in Section 3.3.2. The microhardness results in Table 26 are consistent with the post-quench ductility results.

Figure 54 shows metallographic images of ZIRLO and Zry-4 oxide layers following 1000°C oxidation to 20% CP-ECR. From these images, it is clear that the higher weight gain for Zry-4 oxidized



(a)



(b)

Figure 50. Comparison between weight gain data for ZIRLO and Zry-4 and weight gain predicted by the Cathcart-Pawel (CP) correlation for samples oxidized (two-sided) in steam at 1000°C (a) and 1100°C (b). Data correspond to CP-ECR values of 5, 10, 15, 17, and 20%.

Table 24 Weight Gain (Wg in mg/cm<sup>2</sup>) and Measured ECR (%) Values for 17×17 ZIRLO Oxidized in Steam at 1000°C and 1100°C and Quenched at 800°C. ECR = 1.538 Wg for the 0.57-mm-wall thickness. Multiply weight gain results by a factor of 10 to convert to g/m<sup>2</sup>.

Oxidation Temperature, °C	Cathcart-Pawel ECR, %	Measured Weight Gain (Wg), mg/cm <sup>2</sup>	Measured ECR, %
1000	5	3.8	5.9
1000	10	6.8	10.5
1000	15	9.0	13.8
1000	17	10.8	16.6
1000	20	11.7	18.0
1100	5	3.8	5.9
1100	10	7.1	10.9
1100	15	10.5	16.1
1100	17	11.6	17.9
1100	20	13.7	21.1

at this temperature is due to the thicker oxide layers grown on the Zry-4 surfaces. This is an alloy effect. Also, as is discussed in Section 3.3.2, the waviness of the ZIRLO oxide layers, particularly the inner-surface oxide layer, is a precursor to breakaway oxidation and hydrogen pickup. Table 26 lists the inner-surface oxide layer on ZIRLO as 9- $\mu$ m thicker than the outer-surface oxide. These results suggest that the inner-surface is transforming from the stable tetragonal phase to unstable monoclinic phase. Figure 55 shows higher magnification and better contrast for the outer- and inner-surface oxide layers grown on this ZIRLO sample. It is clear from Figure 55b that the inner-surface oxide layer is in transition from the tight tetragonal (dark) oxide phase to the cracked monoclinic (light) oxide phase. This supports the view that the ZIRLO hydrogen pickup is through the inner-surface oxide layer. Visual examination confirmed that the inner-surface oxide was gray, as compared to the black surface observed inside the Zry-4 sample oxidized under the same conditions.

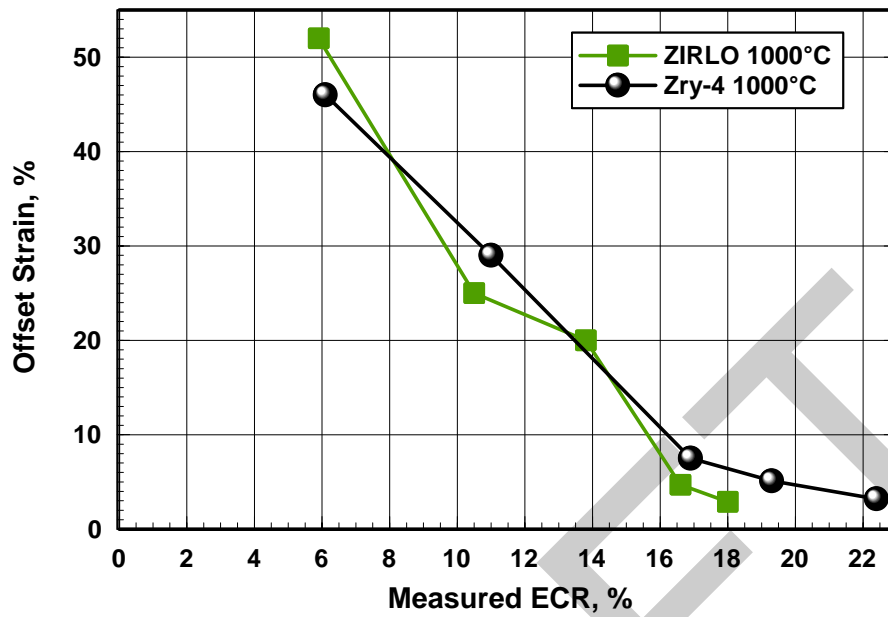
Figure 56 shows metallographic images for ZIRLO and Zry-4 oxidized to 20% CP-ECR at 1100°C. The Zry-4 prior-beta layer exhibits incursions of higher-oxygen alpha-phase material, which precipitated during cooling from 1100°C to 800°C prior to quench. The ZIRLO alpha and prior-beta layers are quite different in appearance from those of Zry-4. While oxygen is an alpha-stabilizer, Nb is a beta-stabilizer. The oxygen-stabilized alpha "layer" formed at high temperature in ZIRLO is not as uniform as the one formed in Zry-4, because Nb causes local regions of beta-stabilization even at higher oxygen contents. Precipitation of oxygen-stabilized alpha regions during cooling is also different in the ZIRLO prior-beta layer because of the presence of Nb. Yet, even with these differences in microstructure and phase distribution, the post-quench ductility of the two alloys oxidized at 1000°C and 1100°C is remarkably similar.

The comparison between ZIRLO and Zry-4 oxidized at 1000°C for up to  $\approx$ 3360 s (20% CP-ECR) indicates that the weight gain for ZIRLO is  $\approx$ 10% lower than predicted by the CP correlation, while the weight gain for Zry-4 is  $\approx$ 10% higher than the CP-predicted correlation; the 20% difference in weight gain has no influence on post-quench ductility, as it merely reflects the differences in oxide-layer thickness rather than the oxygen content in the prior-beta layer; both alloys have adequate post-quench

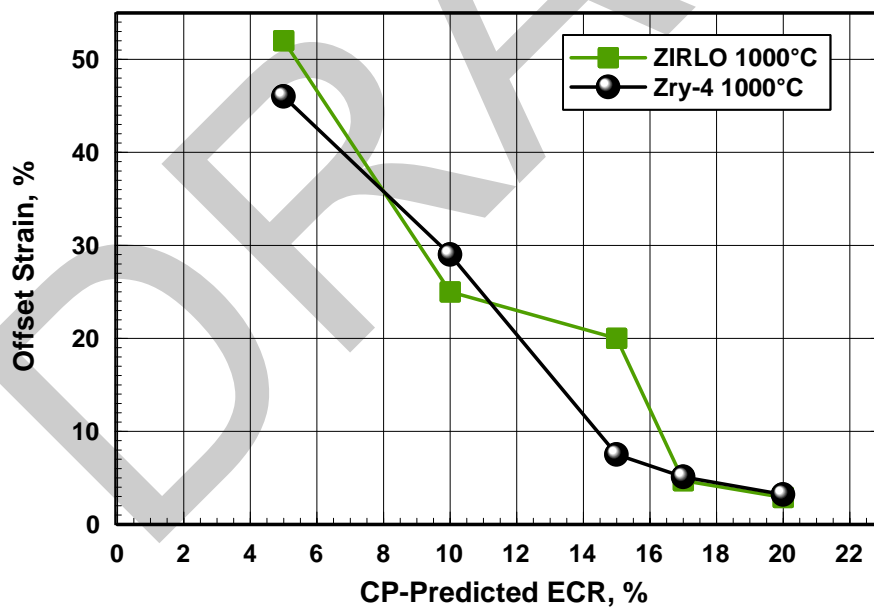
Table 25 Ring Compression Test Results for 17×17 ZIRLO Samples Oxidized at 1000°C and 1100°C, Cooled at ≈10°C/s to 800°C, and Quenched. ECR = 1.538 Wg for 0.57-mm-wall cladding. Tests were performed on 8-mm-long samples at RT and 0.0333-mm/s displacement rate. Displacements in the loading direction were normalized to the as-fabricated outer diameter (9.50 mm) to calculate offset strain. A complete set of tests was performed with the Model 4505 Instron. A limited number of confirmation tests were performed with the Model 5566 Instron on rings cut from the same oxidation samples.

Oxidation Temperature, °C	Cathcart-Pawel ECR, %	Measured ECR, %	Offset Displacement, mm	Offset Strain, %	Confirmation Tests Model 5566 Instron
1000	5	5.9	>4.9	>52	---
1000	10	10.5	>2.35	>25	Yes
1000	15	13.8	1.92	20	Yes
1000	17	16.6	0.45	4.7	---
1000	20	18.0	0.27	2.9	---
1100	5	5.9	>5.0	>52	---
1100	10	10.9	2.1	22	---
1100	15	16.1	0.48	5.1	Yes
1100	17	17.9	0.33	3.5	---
1100	20	21.1	0.32	3.3	---

ductility at 20% CP-ECR; and the ZIRLO inner-surface oxide layer is in breakaway-oxidation transition at 3360 s based on hydrogen pickup and metallographic imaging. The differences in weight gain are attributable to alloy effects, particularly the Nb in ZIRLO. Better agreement for the offset strains of these two alloys is observed at high oxidation times in Figure 51b, where the offset strain is plotted as a function of CP-ECR. The results in Figure 51b clearly show that Zry-4 and ZIRLO have essentially the same post-quench ductility for equivalent isothermal oxidation times of 2430-3365 s at 1000°C. The comparison between ZIRLO and Zry-4 oxidized at 1100°C for up to ≈1070 s (20% CP-ECR) indicates differences in microstructure and phase distribution but no significant differences in weight-gain kinetics and post-quench ductility.



(a)



(b)

Figure 51. Post-quench ductility vs. measured (a) and CP-predicted (b) ECR for ZIRLO and Zry-4 oxidized at 1000°C, cooled at  $\approx 10^\circ\text{C/s}$  to 800°C, and quenched. Ductility is based on offset strain determined from ring-compression data for tests conducted at RT and 0.0333-mm/s displacement rate.

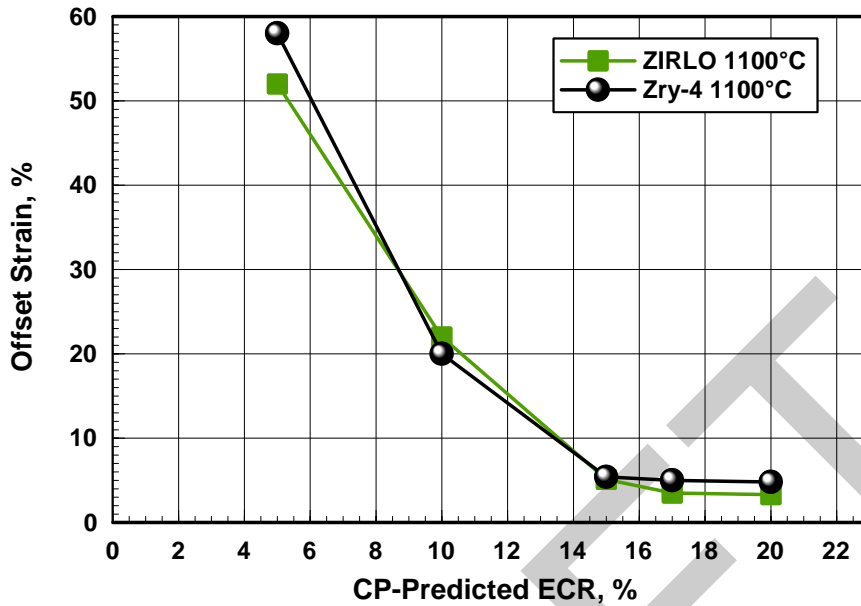
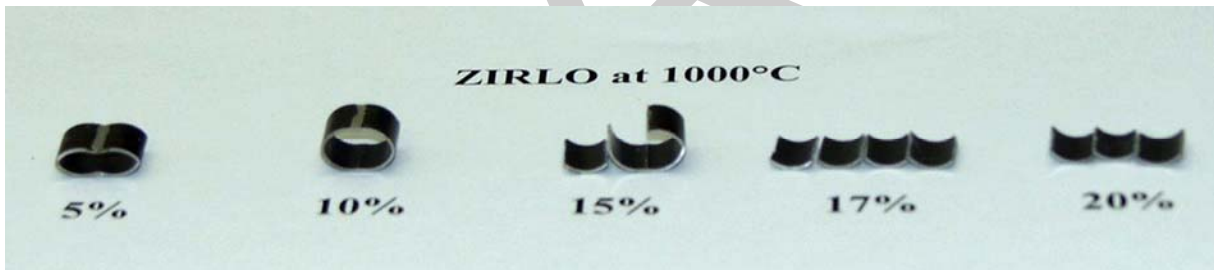
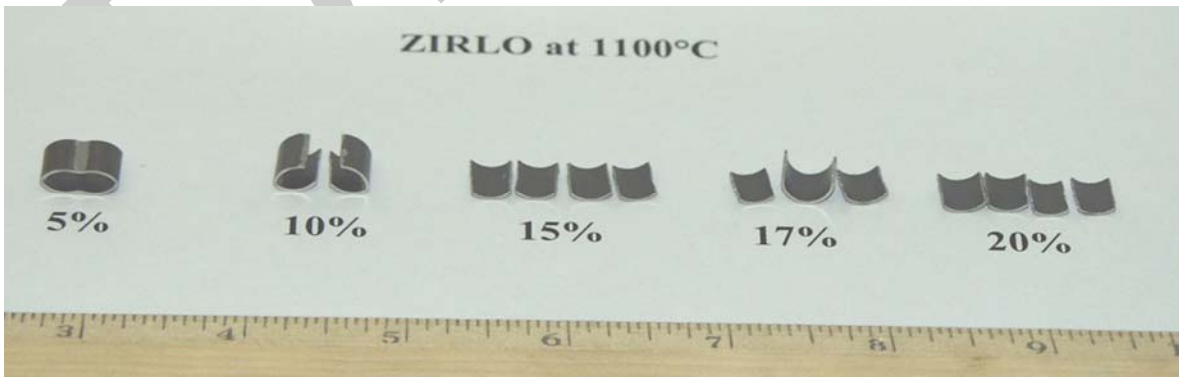


Figure 52. Post-quench ductility vs. CP-predicted ECR for ZIRLO and Zry-4 oxidized at 1100°C, cooled at  $\approx 10^\circ\text{C/s}$  to 800°C, and quenched. Ductility is based on offset strain determined from ring-compression data for tests conducted at RT and 0.0333-mm/s displacement rate.



(a)



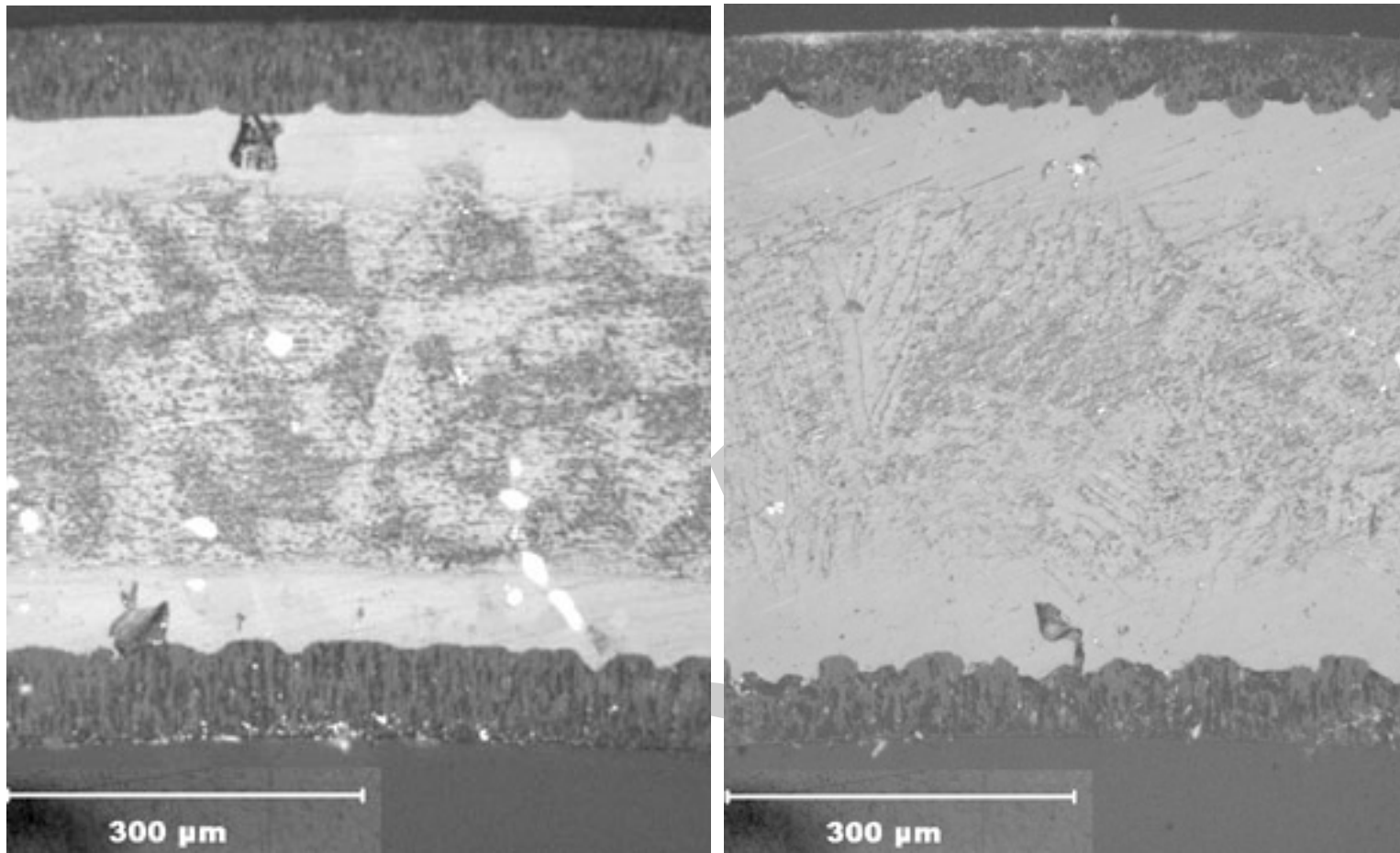
(b)

Figure 53. Post-test appearance of ZIRLO ring-compression samples tested at room temperature and 0.0333 mm/s: (a) samples oxidized at 1000°C and (b) samples oxidized at 1100°C. ECR values are calculated using the Cathcart-Pawel weight gain correlation.

Table 26 Characterization of Highly Oxidized (20% CP-ECR) 17×17 Zry-4 and ZIRLO Samples after Exposure to Steam at 1000°C and 1100°C, Cooling at ≈10°C/s to 800°C, and Quench.

Oxidation Temperature, °C	Parameter	Zry-4	ZIRLO
1000	Effective Oxidation Time, s	3364	3364
	Weight Gain, mg/cm <sup>2</sup>	14.6	11.7
	Measured ECR, %	22.4	18.0
	RT Offset Displacement, mm	0.31	0.27
	RT Offset Strain, %	3.2 (ductile)	2.9 (ductile)
	Hydrogen Content, wppm	19	102
	Hydrogen Pickup, wppm	15	103
	OD/ID Oxide Layer Thickness, μm	83/82	57/66
	Microhardness within Middle 0.2 mm, DPH	290-420	290-400
	1100	Effective Oxidation Time, s	1065
Weight Gain, mg/cm <sup>2</sup>		13.2	13.7
Measured ECR, %		20.3	21.1
RT Offset Displacement, mm		0.46	0.32
RT Offset Strain, %		4.8 (ductile)	3.3 (ductile)
Hydrogen Content, wppm		22	22
Hydrogen Pickup, wppm		19	18
OD/ID Oxide Layer Thickness, μm		70/68	72/69
Microhardness within Middle 0.2 mm, DPH <sup>a</sup>		240-470	330-460

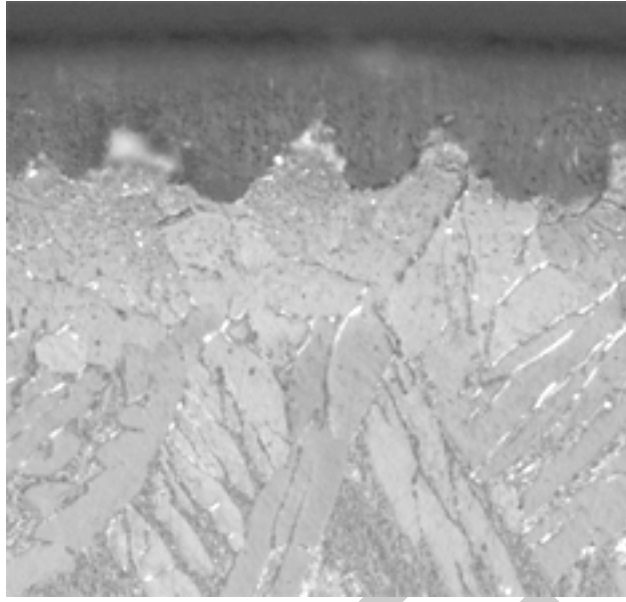
<sup>a</sup>Includes oxygen-stabilized alpha needles (ZIRLO) and alpha incursions (Zry-4) in prior-beta layer.



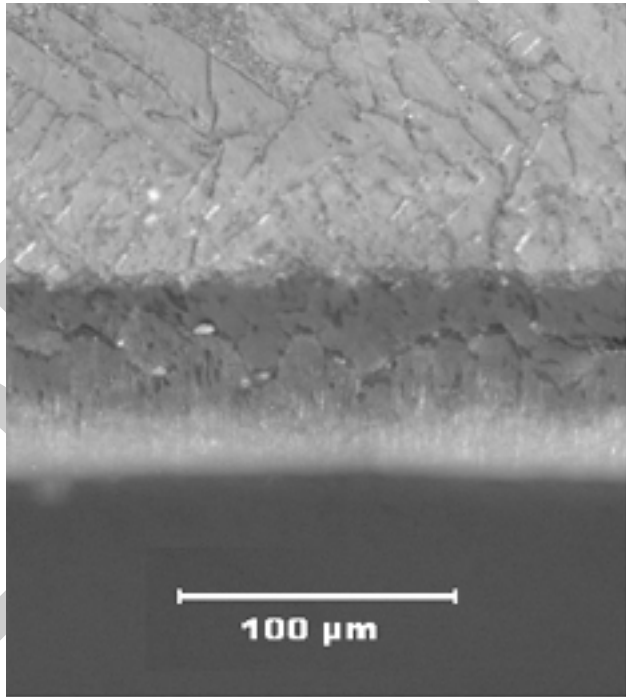
(a) Zry-4

(b) ZIRLO

Figure 54. Metallography of as-polished Zry-4 (a) and ZIRLO (b) oxidized in steam at 1000°C for  $\approx 3360$  s, cooled at  $\approx 10^\circ\text{C/s}$  to 800°C, and water quenched. Measured ECR values are 22.4% for Zry-4 and 18.0% for ZIRLO.



(a)

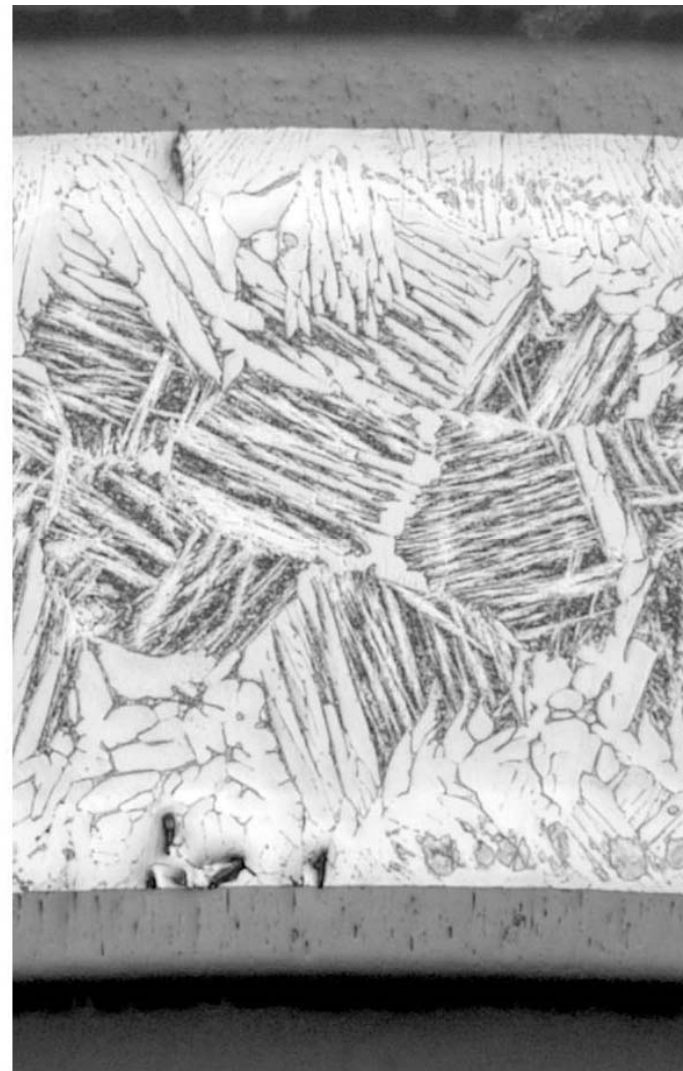


(b)

Figure 55. High-magnification images of etched ZIRLO sample following oxidation at 1000°C for 3360 s to 20% CP-ECR. The outer-surface oxide layer (a) is tetragonal, but the wavy oxide-metal interface indicates a precursor to breakaway oxidation. The inner-surface oxide layer (b) is thicker, has lateral cracks, appears to be monoclinic, and is in breakaway oxidation. The hydrogen pickup through the inner surface is  $\approx 100$  wppm.



(a) Zry-4



(b) ZIRLO

Figure 56. Metallography of etched Zry-4 (a) and ZIRLO (b) oxidized in steam at 1100°C for  $\approx 1070$  s to 20% CP-ECR, cooled at  $\approx 10^\circ\text{C/s}$  to 800°C, and water quenched. Measured ECR values are 20.3% for Zry-4 and 21.1% for ZIRLO.

## 17×17 ZIRLO oxidized at 1200°C

In parallel with the testing of Zry-4, numerous tests were conducted with 17×17 ZIRLO oxidized at 1200±5°C to determine the ductile-to-brittle transition CP-ECR at RT and 135°C. Figures 20 and 21 show the thermal-benchmark results for the first and most recent test trains. Although the temperature ramps are different, these have little effect on the long-time tests used to determine the high ductile-to-brittle transition CP-ECR for rings compressed at 135°C. Also, all tests were stopped after the first significant load drop to allow a measure of the permanent strain based on the diameter change in the loading direction.

The weight gain (expressed in terms of measured ECR) and the post-quench ductility results are summarized in Table 27. As noted in Table 27, initial ring-compression scoping tests were performed at 135°C with relatively short (≈5-mm long) end pieces of oxidized-and-quenched rings. These results provided valuable qualitative information, but they may not be as quantitatively accurate as the results listed in bold type for ≈8-mm-long sections from the center of the oxidation-quench samples or even rings sectioned from either side of the center sample. Figure 57 shows the ZIRLO and Zry-4 measured weight gains, as compared to the CP-predicted weight gains. The experimental results for both alloys are in excellent agreement with each other and with the predicted values.

ZIRLO appears to embrittle at room temperature after oxidation to ≈11% CP-ECR and quench. This observation is confirmed by both the offset (<2%) and the permanent-strain (<1%) criteria for embrittlement. The enhancement of ductility with the increase in test temperature is quite pronounced. Based on the offset and permanent strain data, the ductile-to-brittle transition CP-ECR is ≈19% at 135°C. The variations of offset strain and permanent strain with CP-ECR are shown in Figures 58a and 58b, respectively, for the RT and 135°C test conditions. Figure 59 is a comparison between the post-quench ductility (offset strain) at 135°C for ZIRLO and Zry-4 vs. CP-ECR following oxidation at 1200°C and quench at 800°C. At CP-ECR values <17%, ZIRLO has significantly higher post-quench ductility than Zry-4. However, both alloys show low ductility at ≥17% CP-ECR for ring-compression test at 135°C.

The higher ductile-to-brittle transition ECR for 17×17 ZIRLO (19%) as compared to 17×17 Zry-4 (17%) does not appear to be an alloy effect. Based on Figure 28, modern 15×15 Zry-4 has the same ductile-to-brittle transition ECR (19%) as modern 17×17 ZIRLO. It appears that fabrication differences from lot-to-lot of Zry-4 have more of an effect on the embrittlement threshold for 1200°C-oxidized cladding samples than alloy differences.

Table 27 Ring Compression Test (RCT) Results for 17×17 ZIRLO Cladding Oxidized at 1200°C, Cooled at ≈13°C/s to 800°C, and Quenched. ECR = 1.538 Wg for 0.57-mm-wall thickness. Tests were performed on ≈8-mm-long samples at RT and 135°C and at 0.0333-mm/s displacement rate. Displacements in the loading direction were normalized to the as-fabricated outer diameter (9.50 mm) to calculate offset and permanent strains.

Test Conditions		ECR, %		Plastic Displacement, mm		Plastic Strain, %	
RCT T, °C	Test Time, <sup>a</sup> s	CP	Meas.	Offset	Permanent	Offset	Permanent
RT	60	4.9	4.8	>5.55	>5.24	>58	>53
RT	136	10.0	10.3	0.26	0.13	2.7	1.4
135 <sup>b</sup>	136	10.0	10.3	>4.8	>4.8	>51	>51
RT	203	13.0	13.4	0.11	0.07	1.2	0.7
<b>135<sup>c</sup></b>	<b>203</b>	<b>13.0</b>	<b>14.3</b>	<b>1.96</b>	<b>1.47</b>	<b>20.7</b>	<b>15.5</b>
<b>135<sup>c</sup></b>	<b>203</b>	<b>13.0</b>	<b>14.3</b>	<b>3.12</b>	<b>&gt;2.46</b>	<b>33</b>	<b>&gt;26</b>
RT	248	15.1	15.4	0.18	0.11	1.8	1.2
135 <sup>b</sup>	248	15.1	15.4	1.73	1.28	18.2	13.4
RT	310	17.1	17.8	0.16	0.06	1.0	0.6
135 <sup>b</sup>	310	17.1	17.8	0.66	---	7.0	---
<b>135<sup>c</sup></b>	<b>318</b>	<b>17.0</b>	<b>18.4</b>	<b>0.59</b>	<b>0.27</b>	<b>6.2</b>	<b>2.8</b>
<b>135<sup>b</sup></b>	<b>318</b>	<b>17.0</b>	<b>18.4</b>	<b>0.36</b>	<b>0.17</b>	<b>3.8</b>	<b>1.8</b>
<b>135<sup>c</sup></b>	<b>390</b>	<b>19.0</b>	<b>21.2</b>	<b>0.29</b>	<b>0.11</b>	<b>3.1</b>	<b>1.2</b>
<b>135<sup>b</sup></b>	<b>390</b>	<b>19.0</b>	<b>21.2</b>	<b>0.19</b>	<b>0.11</b>	<b>2.0</b>	<b>0.9</b>
RT <sup>d</sup>	428	21.2	22.3	0.11	0.06	1.1	0.6
135 <sup>d</sup>	448	21.7	23.4	0.20	0.11	2.1	1.2
135 <sup>d</sup>	448	21.7	23.4	0.20	---	2.1	---

<sup>a</sup>Includes time for ramp from 300°C and hold time.

<sup>b</sup>Short (≈5-mm long) rings sectioned from end of oxidation-quench samples.

<sup>c</sup>Tests were conducted with current test train (see Figure 21 for thermal history). Most other test results were generated with the initial test train (see Figure 20 for thermal history).

<sup>d</sup>Control TC switched prior to runs; estimated cladding temperature is ≈1215°C.

Table 28 summarizes the characterization results for 17×17 Zry-4 and ZIRLO oxidized at 1200°C to 13% and 20% ECR and quenched at 800°C. As expected, hydrogen pickup is very low. Also, there is excellent agreement between the inner-surface and outer-surface oxide layer thickness, indicating adequate steam flow at the inner surface. The microhardness results support the post-quench ductility results. Based on the room-temperature microhardness values, one would expect ductility at 13% CP-ECR and embrittlement at 20% CP-ECR at the 135°C test temperature. The microstructures across the cladding wall are shown in Figure 60a for Zry-4 and Figure 60b for ZIRLO oxidized at 1200°C to ≈20% CP-ECR. As with the lower oxidation temperatures, Zry-4 has well-defined oxygen-stabilized alpha layers grown at 1200°C, while the presence of Nb in ZIRLO results in a less clear distinction of this layer. The microhardness indents for Zry-4 and ZIRLO oxidized to ≈13% CP-ECR are shown in Figures 61a and 61b, respectively.

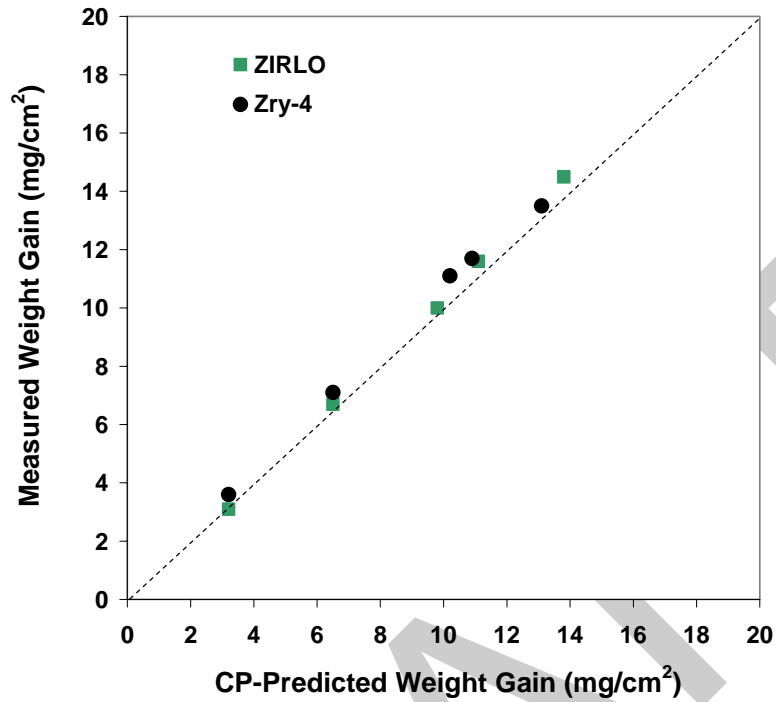


Figure 57. Comparison between weight gain data for ZIRLO and Zry-4 and CP-predicted weight gain for samples oxidized (two-sided) in steam at 1200°C and quenched at 800°C.

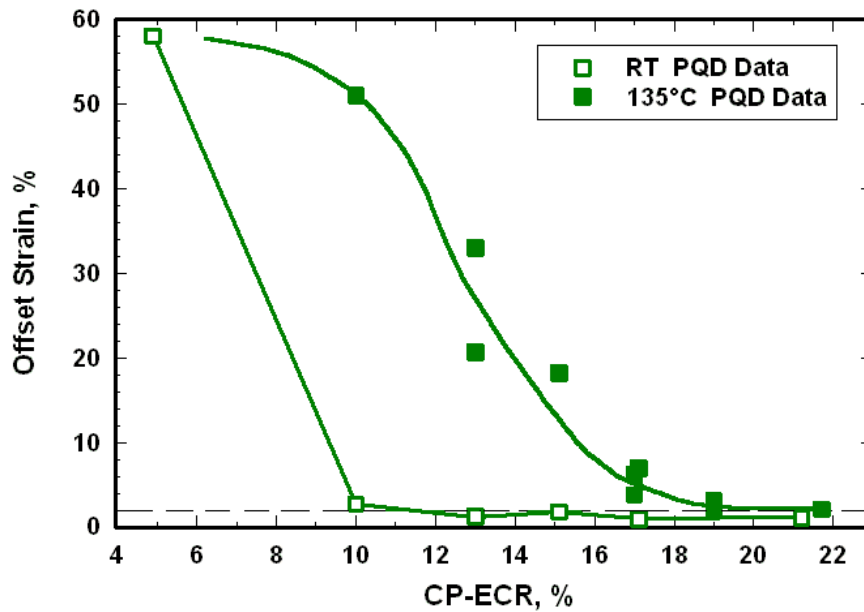


Figure 58a. Offset strain vs. CP-ECR for 17×17 ZIRLO oxidized at 1200°C, cooled at ≈13°C/s to 800°C, quenched, and ring-compressed at RT and 135°C.

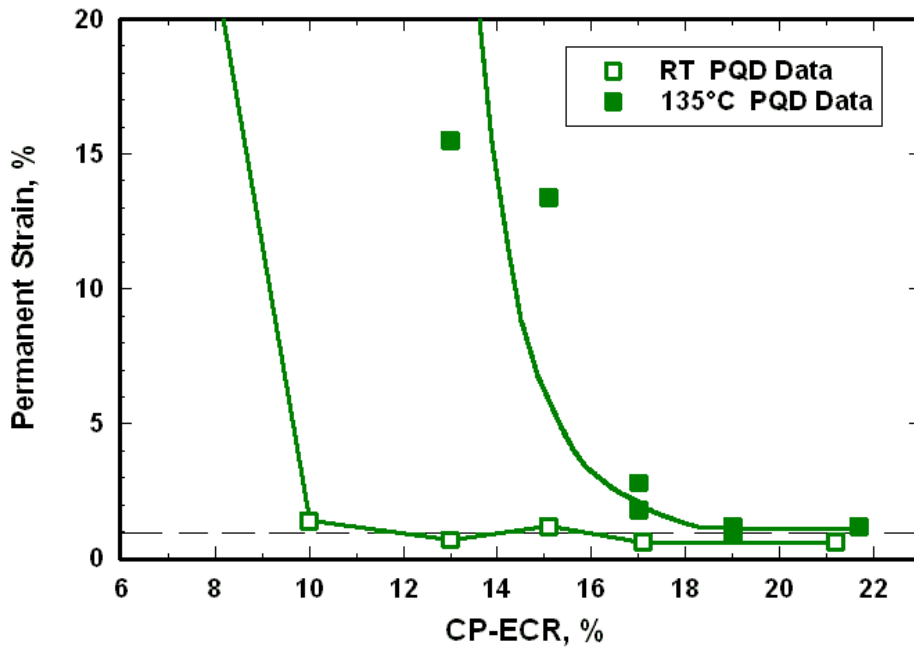


Figure 58b. Permanent strain vs. CP-ECR for 17×17 ZIRLO oxidized at 1200°C, cooled at ≈13°C/s to 800°C, quenched, and ring-compressed at RT and 135°C.

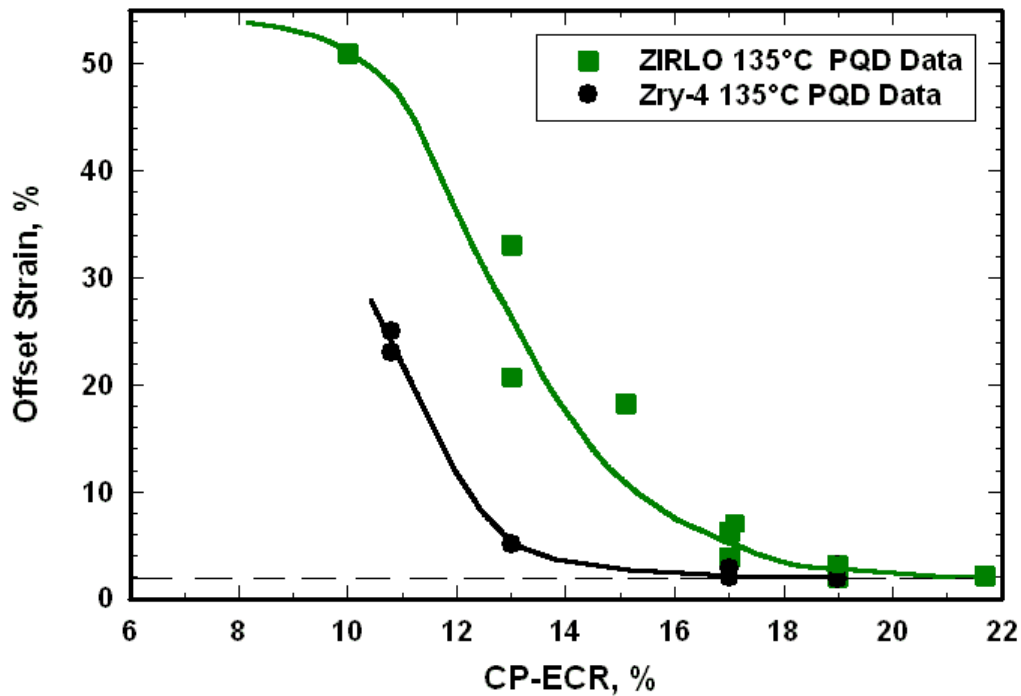
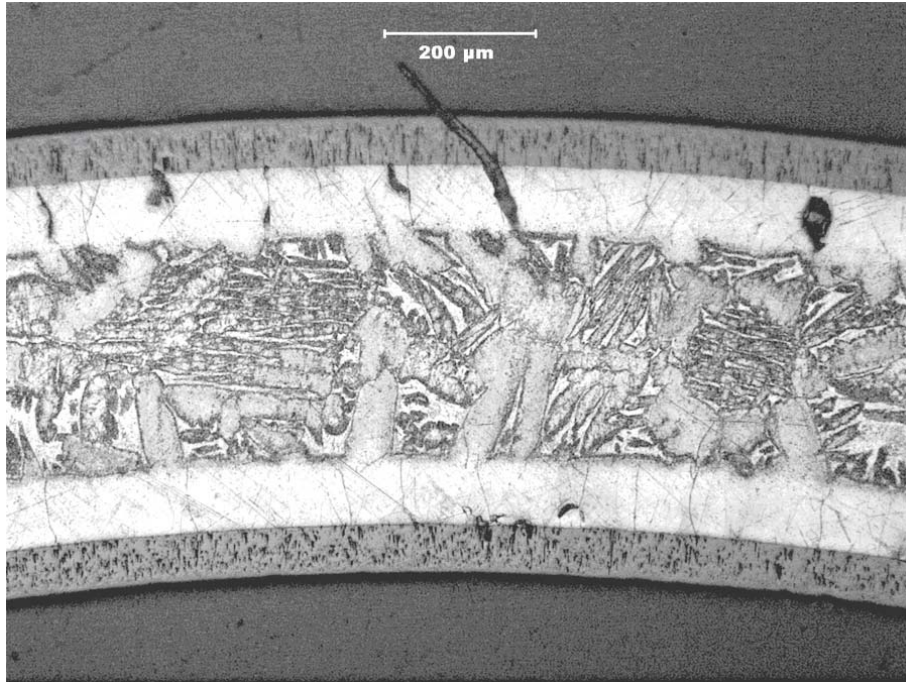


Figure 59. Offset strain vs. CP-ECR for 17×17 ZIRLO and Zry-4 oxidized at 1200°C, cooled at ≈13°C/s to 800°C, quenched, and ring-compressed at 135°C.

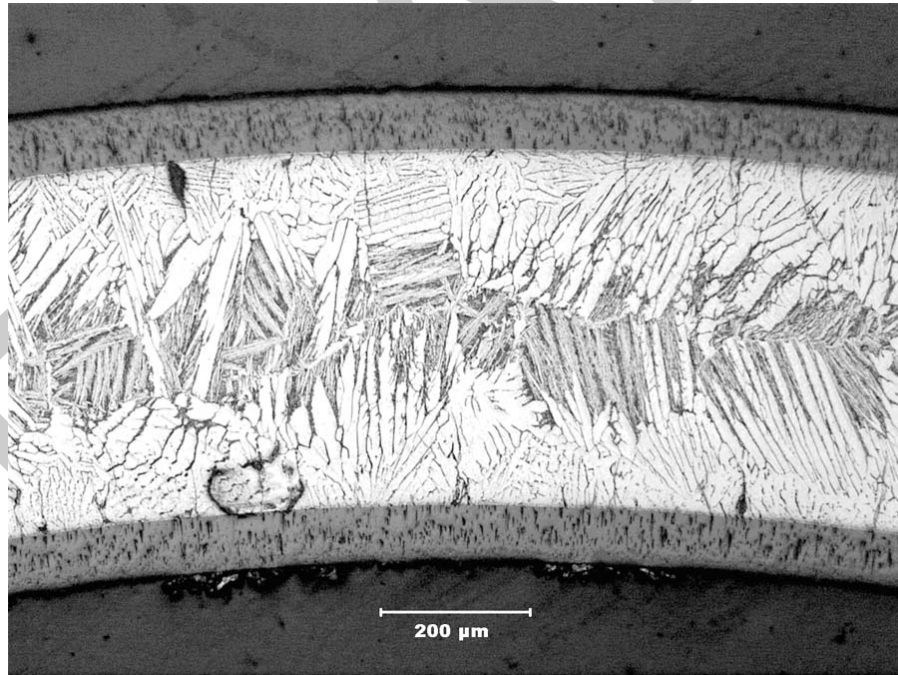
Table 28 Characterization of 17×17 Zry-4 and ZIRLO Samples after Exposure to Steam at 1200°C to 13% and 20% CP-ECR, Cooling at ≈13°C/s to 800°C, and Quenching

Parameter	Zry-4		ZIRLO	
	20% ECR	13% ECR	20% ECR	13% ECR
Effective Time, s	400	166	444	166
Weight Gain, mg/cm <sup>2</sup>	13.5	8.35	14.5	8.70
Measured ECR, %	20.8	12.8	22.3	13.4
RT Offset Displacement, mm	0.05	0.09	0.11	0.11
RT Offset Strain, %	0.5	0.9	1.2	1.2
RT Measured Permanent Displacement, mm	0.04	0.07	0.06	0.07
RT Permanent Strain, %	0.4	0.7	0.6	0.7
RT Ductility, %	≤0.4 (brittle)	≤0.7 (brittle)	≤0.6 (brittle)	≤0.7 (brittle)
Hydrogen Content, wppm	17	low	17	low
Hydrogen Pickup, wppm	13	low	14	low
OD/ID Oxide Thickness, μm	68/66	42/41	74/71	44/43
Prior-Beta-Layer Thickness, μm	266	419	≈150	≈370
Microhardness, DPH				
Oxide Layers	570-960	600-770	560-1160	610-770
Alpha Layers	530-730	600-700	600-800	650-860
Prior-Beta Layer <sup>a</sup>	280-600	260-360	350-530	350-450

<sup>a</sup>Range includes microhardness values of oxygen-rich alpha needles (ZIRLO) and alpha incursions (Zry-4) in this layer.

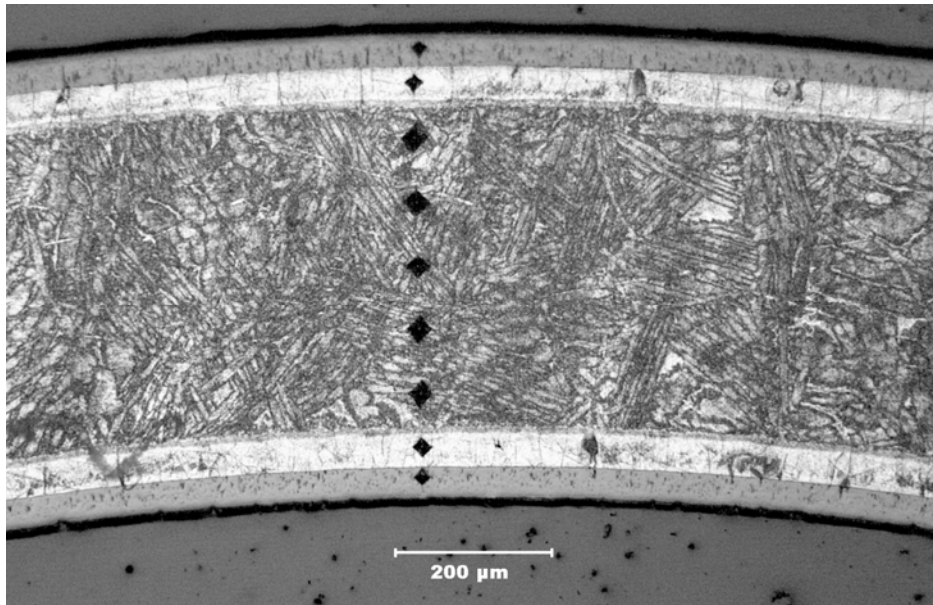


(a) Zry-4

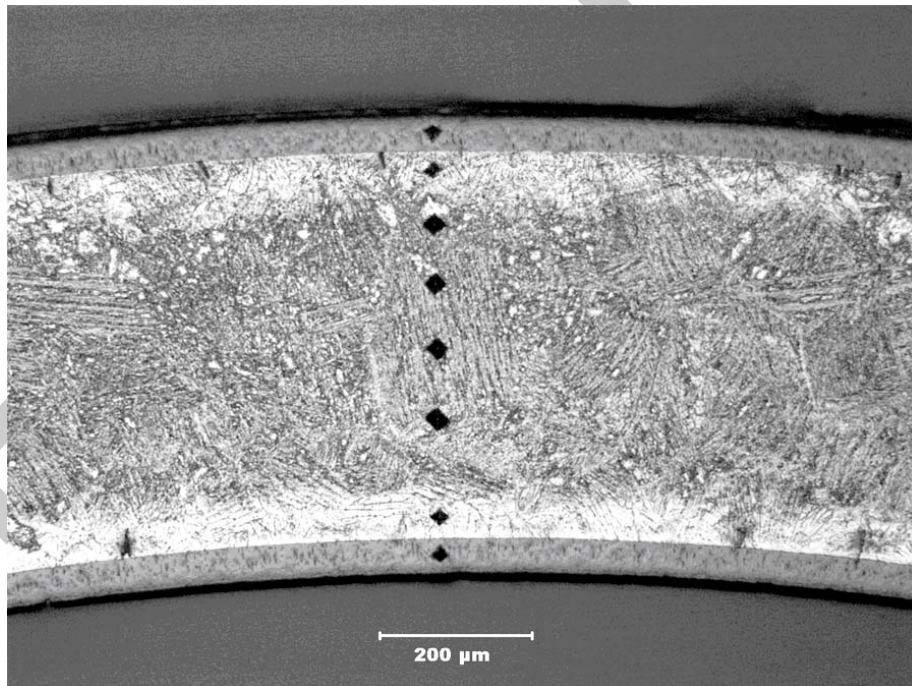


(b) ZIRLO

Figure 60. Metallography of etched Zry-4 (a) and ZIRLO (b) oxidized in steam at 1200°C for ≈400 s and ≈440 s, respectively, cooled at ≈13°C/s to 800°C, and quenched. Measured ECR values are 20.8% for Zry-4 and 22.3% for ZIRLO.



(a) Zry-4



(b) ZIRLO

Figure 61. Metallography and microhardness indents across the radius of 17×17 Zry-4 (a) and ZIRLO (b) oxidized at 1200°C to 13% ECR, cooled at  $\approx 13^\circ\text{C/s}$  to 800°C, and quenched. The measured ECR values are 12.6% for Zry-4 and 13.4% for ZIRLO.

### 3.3.2 Breakaway oxidation time for 17×17 ZIRLO samples oxidized at 800-1015°C

Unlike Zry-4, no published data were found for ZIRLO breakaway oxidation time vs. temperature. Thus, the approach adopted in this work was to explore breakaway oxidation times in the range of 950-1015°C to determine the minimum breakaway time. A test was also run at 800°C for a period greater than the minimum time for 950-1015°C to demonstrate that breakaway did not occur at earlier times at 800°C. Based on the results shown in Figure 55b for ZIRLO received and tested in 2003 (ZIRLO-2003), the inner-surface oxide layer is already in breakaway following oxidation at 1000°C for  $\approx 3400$  s. However, the breakaway oxidation time is most relevant to the cladding outer surface away from the balloon region. Given that ZIRLO may pick up hydrogen from the inner surface before the outer surface experiences breakaway oxidation, it was necessary to determine by visual inspection and metallography if the outer surface was in breakaway oxidation at the time corresponding to  $\approx 200$ -wppm hydrogen pickup. The outer-surface appearance and metallography are shown in Figure 62 for a sample oxidized for 3600 s at 985°C, which is beyond the breakaway transition with hydrogen pickup of  $270 \pm 165$  wppm.

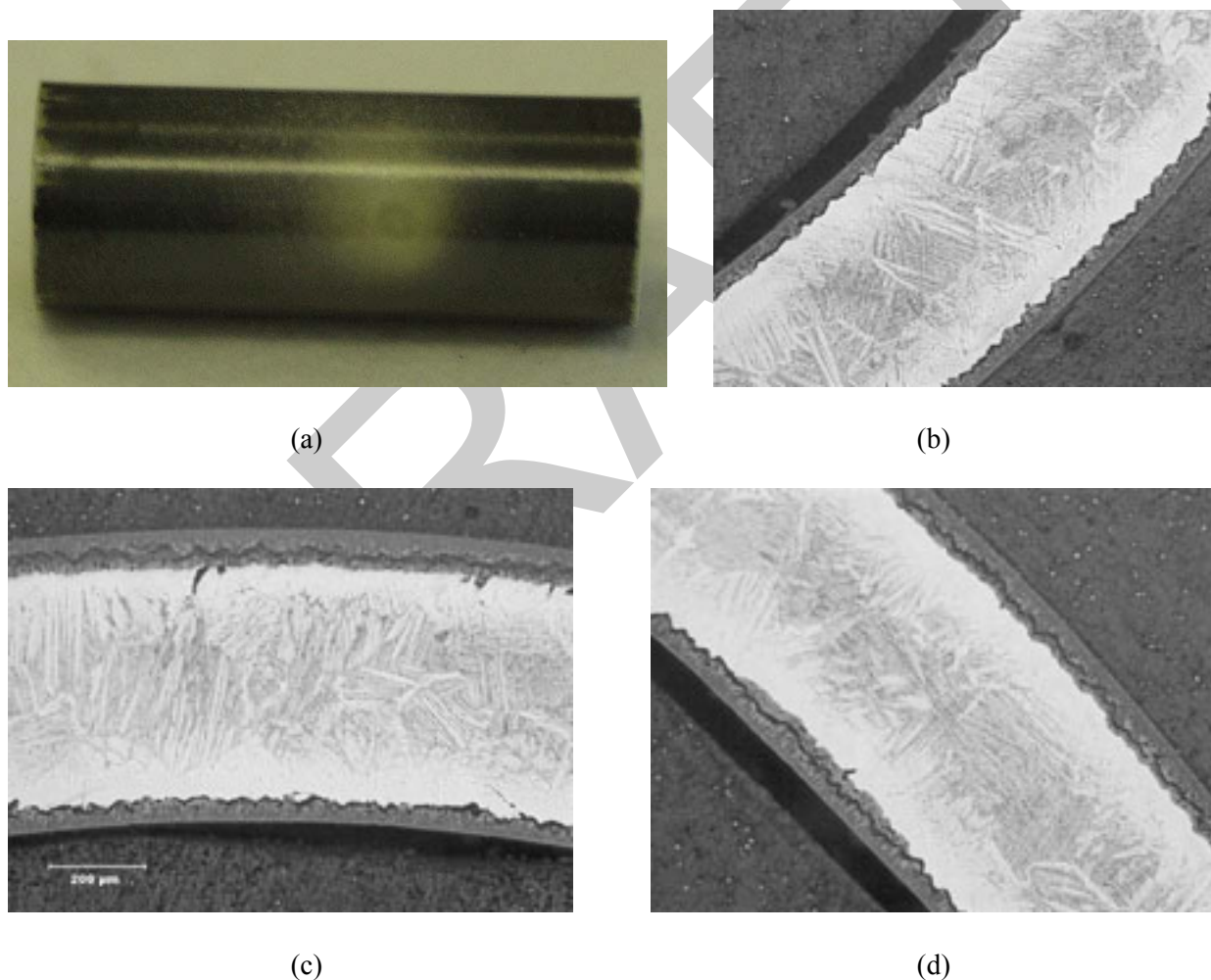


Figure 62. Surface appearance and oxide layers of ZIRLO oxidized at 985°C for 3600 s with  $270 \pm 165$  wppm hydrogen pickup in a ring including the yellow area: (a) outer surface with yellow area (440 wppm H under this layer) in black matrix; (b) outer- and inner-surface oxide layers (no breakaway) under black area; (c) outer-surface (breakaway) and inner-surface (no breakaway) oxide layers under yellow area; and (d) outer- and inner-surface oxide layers under yellow, both in breakaway.

ZIRLO tubing from a different lot was supplied to ANL by Westinghouse in 2006 for breakaway oxidation studies. Dimensions (9.49-mm OD, 0.57-mm wall), oxygen content (1164 wppm), and hydrogen content (11 wppm) are comparable to those for ZIRLO-2003. The outer surface roughness of ZIRLO-2006 is a little higher ( $0.17\pm 0.03\ \mu\text{m}$ ) than the roughness of ZIRLO-2003 ( $0.11\pm 0.01\ \mu\text{m}$ ). Table 29 summarizes the ZIRLO breakaway oxidation results. Based on the criterion of 200-wppm-hydrogen pickup, the minimum breakaway time is  $\approx 3000\ \text{s}$ , and it occurs at  $970^\circ\text{C}$ . The breakaway oxidation times for higher ( $985\text{-}1015^\circ\text{C}$ ) and lower ( $800^\circ\text{C}$  and  $950^\circ\text{C}$ ) oxidation temperatures were  $>3000\ \text{s}$ . The post-oxidation ductility at  $135^\circ\text{C}$  for samples with significant hydrogen pickup is summarized in Table 30. ZIRLO is ductile at  $135^\circ\text{C}$  with a hydrogen pickup  $\leq 440\ \text{wppm}$ , and it is brittle with a hydrogen pickup  $\geq 730\ \text{wppm}$  for oxidation temperatures in the range of  $970\text{-}985^\circ\text{C}$ . The hydrogen data in Table 30 represent the average hydrogen content of the 8-mm-long rings and not the maximum hydrogen content of the sample. The results are presented to demonstrate the ductility of ZIRLO at the breakaway-oxidation time criterion of 200-wppm-hydrogen pickup. Because breakaway oxidation is an instability phenomenon, it is not advisable to use a higher hydrogen pickup for this criterion even if the alloy has some ductility with  $>200\text{-wppm}$  hydrogen.

Table 29 Data Summary for ZIRLO Breakaway Oxidation Tests at  $950\text{-}1015^\circ\text{C}$  and  $800^\circ\text{C}$ . ZIRLO-2003 samples were quenched at  $800^\circ\text{C}$ ; ZIRLO-2006 samples were slow cooled to RT.

ZIRLO Lot	T, $^\circ\text{C}$	Test Time, <sup>a</sup> s	CP Wg, $\text{mg}/\text{cm}^2$	Measured Wg, $\text{mg}/\text{cm}^2$	Hydrogen Content ( $L_H$ ), wppm	Hydrogen Pickup ( $\Delta C_H$ ), <sup>b</sup> wppm
2006	1015	4000	15.6	15.1	30	21
2006	1000	1500	8.63	8.68	15	0
2003	1000	2440	11.1	10.8	36	33
2003	1000	3480	13.0	11.7	102	103
2006	1000	3600	13.5	11.4	68	60
2006	1000	4000	14.2	12.6	131 $\pm$ 12	130
2006	1000	4200	14.5	14.3	608 $\pm$ 366	630
2006	1000	5000	15.9	16.9	1246 $\pm$ 83	1350
2006	985	3400	11.9	9.6	46	37
<b>2006<sup>c</sup></b>	<b>985</b>	<b>3400</b>	<b>11.9</b>	<b>9.9</b>	<b>174<math>\pm</math>140</b>	<b>175<math>\pm</math>145</b>
2006	985	3600	12.3	10.0	267 $\pm$ 158	270
2006	985	4000	12.9	11.8	847 $\pm$ 143	890
<b>2006<sup>c</sup></b>	<b>970</b>	<b>2600</b>	<b>9.5</b>	<b>7.8</b>	<b>53</b>	<b>44</b>
2006	970	3000	10.2	8.1	199 $\pm$ 150	200
2006	970	3400	10.8	8.6	565 $\pm$ 85	580
2006	950	3000	8.9	6.8	31	20
2006	800	4000	---	2.62	14	3

<sup>a</sup>Includes time from beginning of ramp at  $300^\circ\text{C}$  to end of hold time at oxidation temperature.

<sup>b</sup>Hydrogen pickup ( $\Delta C_H$ ) is referenced to the as-fabricated sample weight:

$\Delta C_H = (1 + 5.4 \times 10^{-3} \text{ Wg}) L_H - C_{Hi}$ , where  $C_{Hi}$  is as-fabricated hydrogen content (11 wppm).

<sup>c</sup>Samples with machined scratch,  $\approx 20\text{-}\mu\text{m}$  deep into the outer surface (see Section 3.5.2).

Table 30 Post-oxidation Ductility of ZIRLO with Significant Hydrogen Pickup during Breakaway Oxidation. ZIRLO-2006 samples summarized in Table 29 were oxidized at 985°C and 970°C, then cooled without quench to RT and ring-compressed at 135°C; average hydrogen values are reported for the 8-mm-long rings compressed at 0.0333 mm/s.

Oxidation T, °C	Test Time, <sup>a</sup> s	H-Content L <sub>H</sub> , wppm	H-Pickup <sup>b</sup> ΔC <sub>H</sub> , wppm	Offset Strain, %	Permanent Strain, %
<b>985<sup>c</sup></b>	<b>3400</b>	<b>174±140</b>	<b>175±145</b>	<b>5.1</b>	<b>5.1</b>
985	3600	214±120	215±125	>1.7	---
985	4000	731±112 987±16	765±120 1040±20	0.8 0.8	0.2 0.7
970	3400	416±100	435±105	4.8	2.1

<sup>a</sup>Includes time from beginning of ramp at 300°C to end of hold time at oxidation temperature.

<sup>b</sup>Hydrogen pickup (ΔC<sub>H</sub>) is referenced to the as-fabricated sample weight:

ΔC<sub>H</sub> = (1 + 5.4×10<sup>-3</sup> Wg) L<sub>H</sub> - C<sub>Hi</sub>, where C<sub>Hi</sub> is as-fabricated hydrogen content.

<sup>c</sup>Samples with machined scratch, ≈20-μm deep into the outer surface (see Section 3.5.2 for details).

As shown in Figure 62e, both ZIRLO and Zry-4 maintain ductility for hydrogen pickup ≤440 wppm and embrittle for hydrogen pickup >700 wppm. Thus, ductility is retained for ≤200 wppm hydrogen pickup. The ductile-to-brittle transition hydrogen level for these oxidation temperatures is ≈500-700 wppm.

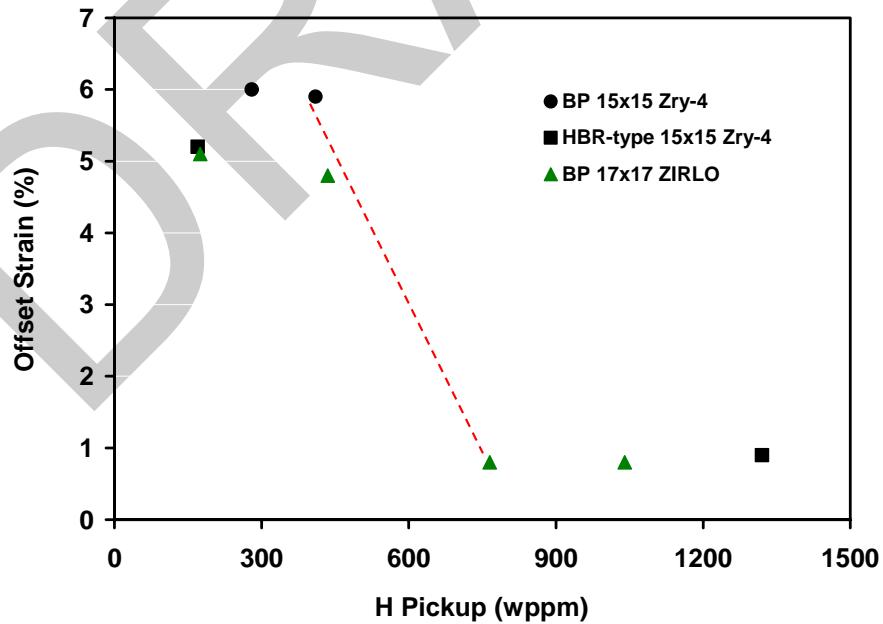


Figure 62e. Offset strain at 135°C vs. hydrogen pickup for 17×17 ZIRLO and 15×15 Zry-4 breakaway oxidation samples oxidized at 970-1000°C and cooled without quench.

### 3.4 M5

#### 3.4.1 Post-quench ductility of 17×17 M5 oxidized at 1000°C, 1100°C, and 1200°C

This work was performed in parallel with the 17×17 Zry-4 and ZIRLO testing and characterization. Although the same test times were used for M5 as for Zry-4 and ZIRLO, the thicker M5 wall (0.61 mm) required new thermal benchmarks for each oxidation temperature. Also, the CP-ECR was reduced by a factor of  $0.57/0.61 = 0.934$  for the M5 relative to Zry-4:  $ECR = 1.437 \text{ Wg}$ . The M5 results are presented with the same subdivision of topics as used for Zry-4: characterization and RT-ring-compression testing of samples that were two-sided oxidized at 1000°C and 1100°C and quenched at 800°C; and characterization and ring-compression testing (RT and 135°C) of samples exposed to two-sided oxidized at 1200°C and quenched at 800°C. Characterization included weight gain, oxide- and alpha-layer thickness measurements (metallography), microhardness, and hydrogen pickup (LECO). The M5 samples were oxidized to CP-predicted ECR values of 4.7, 9.3, 14.1, 16.0, and 18.8%. Additional M5 oxidation tests were conducted at 1000°C and 1100°C to 20-21% CP-ECR to allow a direct comparison with the Zry-4 results in terms of CP-ECR. As with the Zry-4 tests, additional M5 tests were conducted at intermediate CP-ECR values for the 1200°C-oxidized samples to better determine the ductile-to-brittle transition ECR value for this oxidation temperature.

#### 17×17 M5 oxidized at 1000°C and 1100°C

The thermal benchmarks used for the thicker M5 cladding are shown in Figure 63 for 1000°C tests and Figure 64 for 1100°C tests. Table 31 lists the weight gain results for M5 at 1000°C and 1100°C oxidation temperatures. The results at 1100°C are in good agreement with both the Zry-4 results and the CP-predicted weight gain. For 1000°C oxidation, M5 exhibits significantly lower weight gain than Zry-4 and the CP-predicted weight gain for the same oxidation time. The M5 and Zry-4 weight gains are plotted in Figure 65: 1000°C results in Figure 65a and 1100°C results in Figure 65b.

Table 32 lists the results of the RT post-quench ductility tests. It is clear that 17×17 M5 retains post-quench ductility up to 20% CP-ECR – the limit of the test conditions – at these oxidation temperatures. The results are shown graphically in Figures 66 and 67 for 1000°C and 1100°C oxidation temperatures, respectively. Because of differences in weight gain between M5 and Zry-4 oxidized at 1000°C, offset strains are plotted as functions of measured ECR (Figure 66a) and CP-ECR (Figure 66b). For oxidation at 1100°C, both alloys exhibit essentially the same weight gain for the same test time. Thus, post-quench ductility results are plotted in Figure 67 as a function of CP-ECR only. For the 1000°C- and 1100°C-oxidation tests, the M5 offset strain levels out at  $\approx 3\%$ . It appears that M5 will retain ductility at higher CP-ECR values and higher test times until breakaway oxidation ( $>4100 \text{ s}$  at 1000°C) or significant beta-layer thinning ( $>20\%$  CP-ECR at 1100°C) occurs. For 1100°C-oxidation, breakaway oxidation should not occur, and the beta layer does not appear to embrittle due to the low saturation-level oxygen content.

M5 post-quench ductility results for 1000°C-oxidized samples illustrate an important point. Post-quench ductility is determined by the oxygen concentration distribution in the beta phase. Even if the growth rate of the oxide layer is slower for M5 than for Zry-4 at 1000°C, sufficient oxygen is available in the oxide to transport oxygen from the oxide to the oxygen-stabilized alpha layer to the beta layer. The rate of diffusion into the beta layer is controlled by the alpha/beta boundary condition (i.e., solubility limit of oxygen in the M5 beta layer) and the oxygen concentration gradient in the beta layer. The excellent correlation between ductility loss and increasing CP-ECR is because both beta-layer oxygen pickup and CP-ECR are proportional to the square-root of time under isothermal conditions.

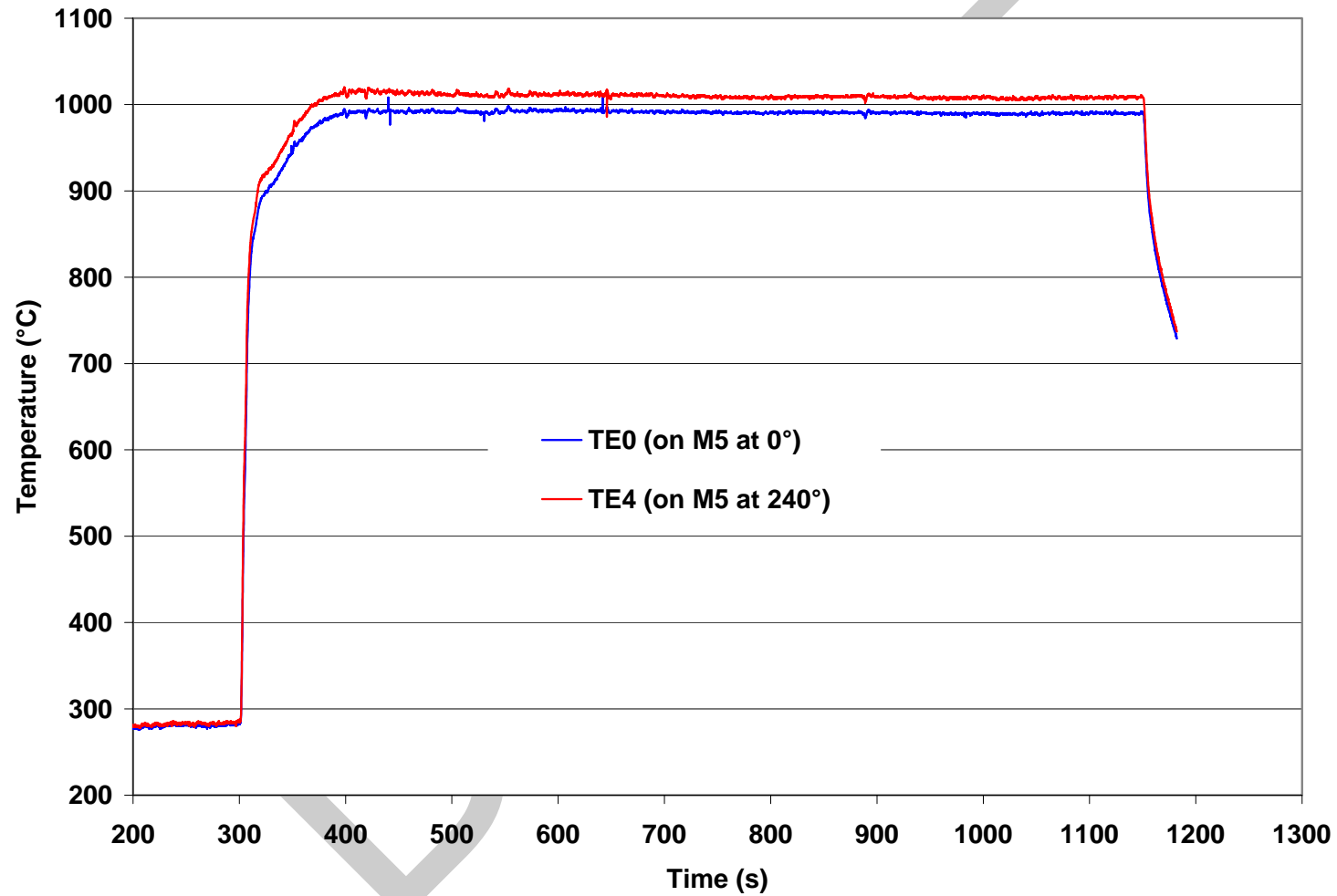


Figure 63. Thermal benchmark results for 17×17 M5 oxidation tests at 1000°C. The cladding OD is 9.50 mm, and the wall thickness is 0.61 mm. Quench at 800°C is not shown in this figure.

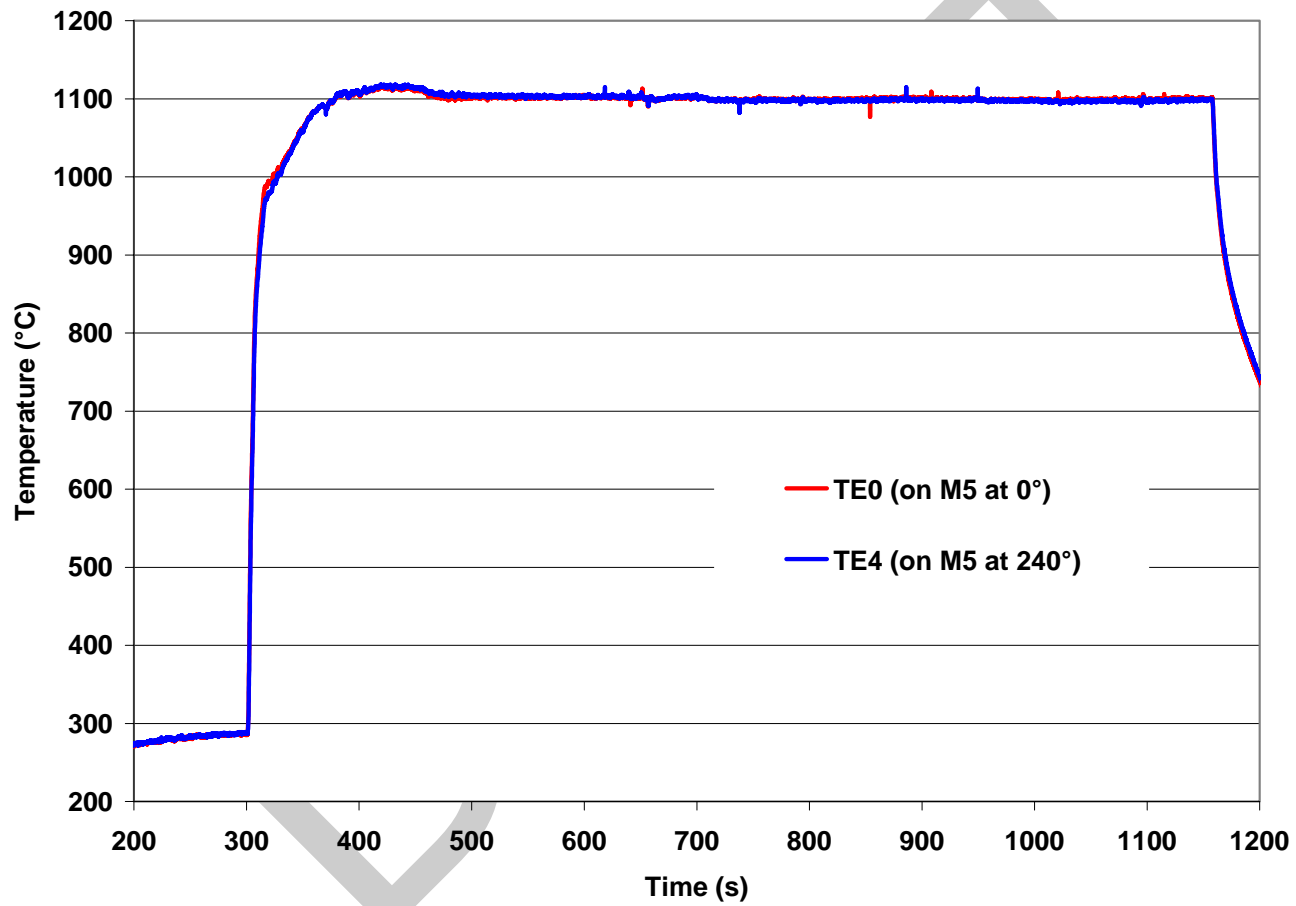


Figure 64. Thermal benchmark results for 17×17 M5 oxidation tests at 1100°C. The cladding OD is 9.50 mm, and the wall thickness is 0.61 mm. Quench at 800°C is not shown in this figure.

Table 31 Weight Gain (Wg in mg/cm<sup>2</sup>) and Measured ECR (%) Values for 17×17 M5 Oxidized in Steam at 1000°C and 1100°C and Quenched at 800°C, ECR = 1.437 Wg for the 0.61-mm-wall thickness; multiply weight gain results by a factor of 10 to convert to g/m<sup>2</sup>.

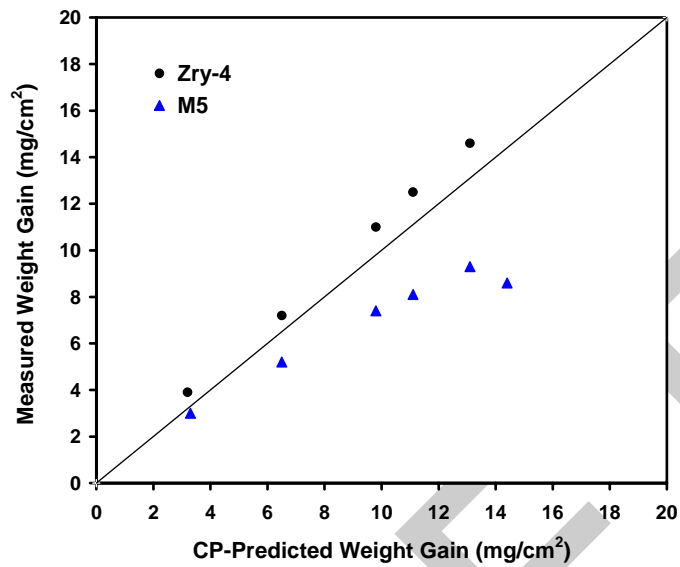
Oxidation Temperature, °C	Cathcart-Pawel ECR, %	Measured Weight Gain, mg/cm <sup>2</sup>	Measured ECR, %
1000	4.7	3.0	4.3
1000	9.3	5.3	7.6
1000	14.1	7.4	10.7
1000	16.0	8.0	11.6
1000	18.8	9.2	13.3
1000	20.7	8.6	12.4
1100	4.7	3.2	4.6
1100	9.3	6.4	9.2
1100	14.1	9.6	13.8
1100	16.0	11.3	16.2
1100	18.8	13.3	19.1
1100	20.4	14.3	20.6

Photographs of the ring-compressed samples are shown in Figure 68a for 1000°C-oxidized samples and Figure 68b for 1100°C-oxidized samples. The 5% (actually 4.3%) and 10% (actually 9.3%) CP-ECR samples oxidized at 1000°C were intact at the maximum test displacement. The 10% (actually 9.3%) CP-ECR sample oxidized at 1100°C was also intact.

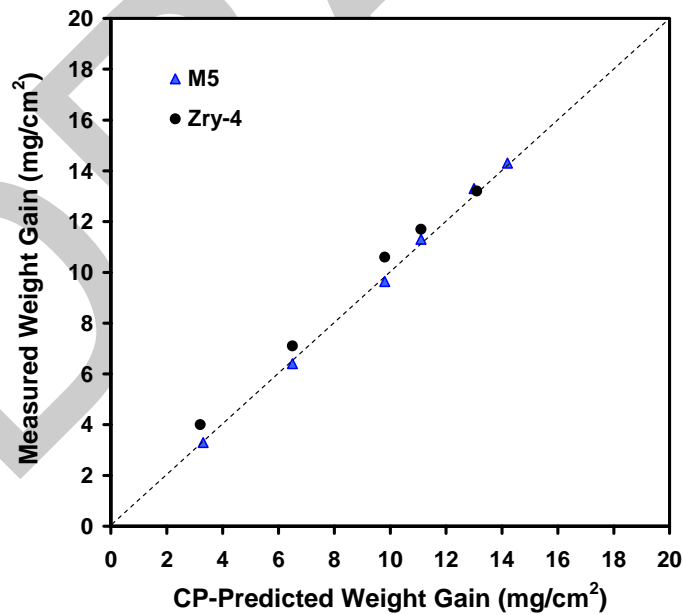
Table 33 summarizes the results of the metallography, microhardness, and hydrogen pickup measurements for M5 as compared to Zry-4. The hydrogen pickup is very low for the 1000°C- and 1100°C-oxidized samples. The results in Table 33 are consistent with the post-quench ductility results.

Figure 69 shows metallographic images of Zry-4 and M5 oxide layers following 1000°C oxidation for 3364 s. From these images, it is clear that the higher weight gain for Zry-4 oxidized at this temperature is due to the thicker oxide layers grown on the Zry-4 surfaces. This weight gain difference is clearly an alloy effect. Also, as will be discussed in Section 3.4.2, the mild waviness of the M5 oxide layers is an early precursor to breakaway oxidation and hydrogen pickup. Table 33 shows that the outer-surface oxide layer is only 4-µm thicker than the inner-surface oxide. These results, along with the results for the sample oxidized for 4100 s, suggest that the breakaway oxidation time for M5 oxidized at 1000°C may be significantly above 4100 s. Figure 70 shows higher magnification and better contrast for the outer-surface oxide layer grown on the M5 sample oxidized for ≈3400 s.

Figure 71 shows the metallography for M5 and Zry-4 oxidized at 1100°C for 1065 s. The Zry-4 prior-beta layer includes regions of higher-oxygen alpha-phase material – alpha incursions – which precipitated during cooling from 1100°C to 800°C prior to quench. The M5 alpha and prior-beta layers are quite different in appearance from those of Zry-4. While oxygen is an alpha-stabilizer,



(a)



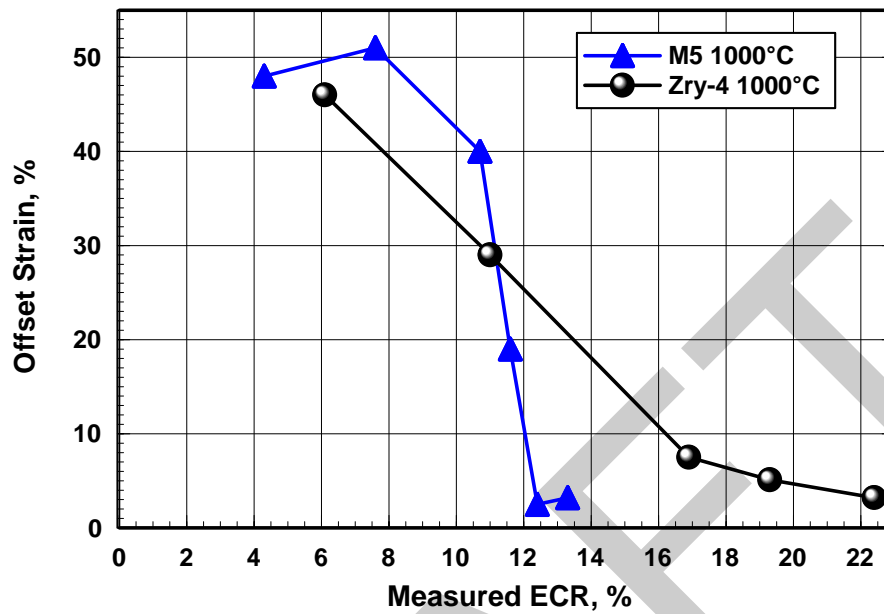
(b)

Figure 65. Comparison between weight gain data for M5 and Zry-4 and weight gain predicted by the Cathcart-Pawel (CP) correlation for samples oxidized (two-sided) in steam at 1000°C (a) and 1100°C (b). Test times correspond to CP-ECR values of  $\approx$ 5-20%.

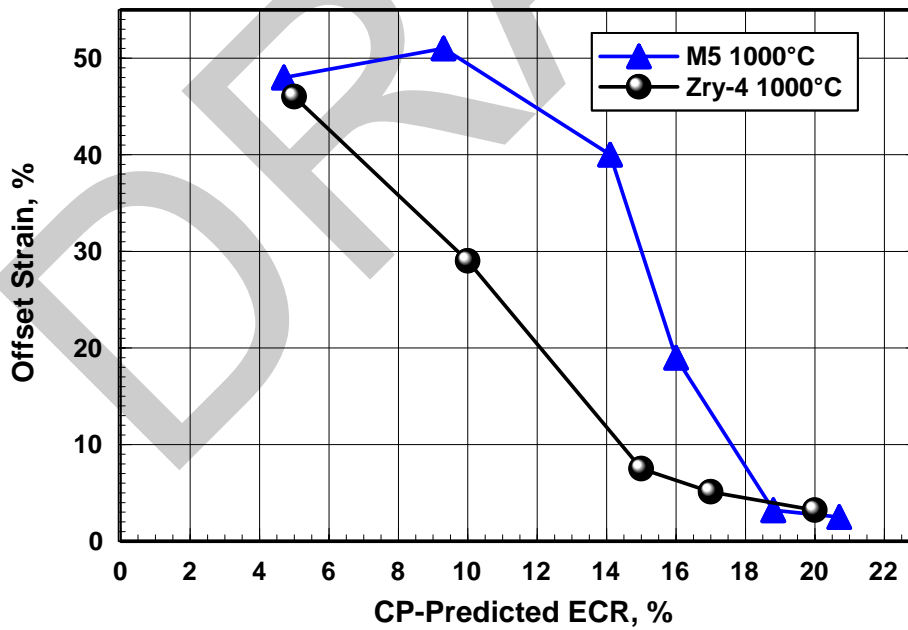
Table 32 Ring Compression Test Results for 17×17 M5 Samples Oxidized at 1000°C and 1100°C, Cooled at ≈10°C/s to 800°C, and Quenched. ECR = 1.437 Wg for 0.61-mm-wall cladding. Displacements in the loading direction were normalized to the as-fabricated outer diameter (9.50 mm) to calculate offset strain. Tests were performed on 8-mm-long samples at RT and 0.0333-mm/s displacement rate in the Model 4505 Instron. Some confirmation tests were conducted in the new Model 5566 Instron on rings from the same oxidation samples.

Oxidation Temperature, °C	Cathcart-Pawel ECR, %	Measured ECR, %	Offset Displacement, mm	Offset Strain, %	Confirmation Tests Model 5566 Instron
1000	4.7	4.3	>4.6	>48	---
1000	9.3	7.6	>4.9	>51	Yes
1000	14.1	10.7	3.76	40	Yes
1000	16.0	11.6	≤1.82	≤19	---
1000	18.8	13.3	0.302	3.2	---
1000	20.7	12.4	0.238	2.5	---
1100	4.7	4.6	5.4	57	---
1100	9.3	9.2	>3.7	>39	---
1100	14.1	13.8	0.71	7.5	Yes
1100	16.0	16.2	0.38	4.0	---
1100	18.7	19.1	0.17	1.8	---
1100	20.4	20.6	0.31	3.2	---

Nb is a beta-stabilizer. The oxygen-stabilized alpha "layer" formed at high temperature in M5 is not as uniform as the one formed in Zry-4 because Nb causes local regions of beta-stabilization even at higher oxygen contents. Precipitation of oxygen-stabilized alpha regions during cooling is also different in the M5 prior-beta layer because of the presence of Nb. Yet, even with these differences in microstructure and phase distribution, the post-quench ductility of the two alloys oxidized at 1000°C and 1100°C for the same duration is remarkably similar.



(a)



(b)

Figure 66. Post-quench ductility vs. measured (a) and CP-predicted (b) ECR for 17×17 M5 and Zry-4 oxidized in steam at 1000°C, cooled at ≈10°C/s to 800°C, and quenched. Offset strain was determined from results of ring-compression tests conducted at RT and 0.0333-mm/s displacement rate.

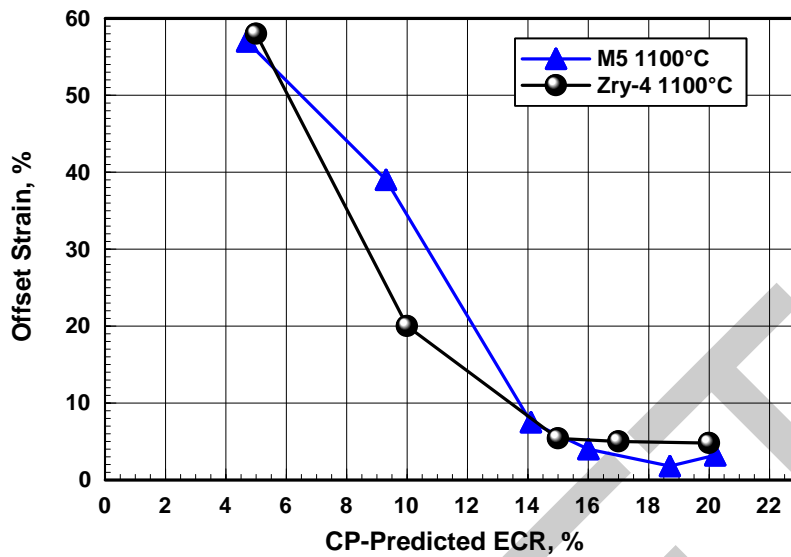
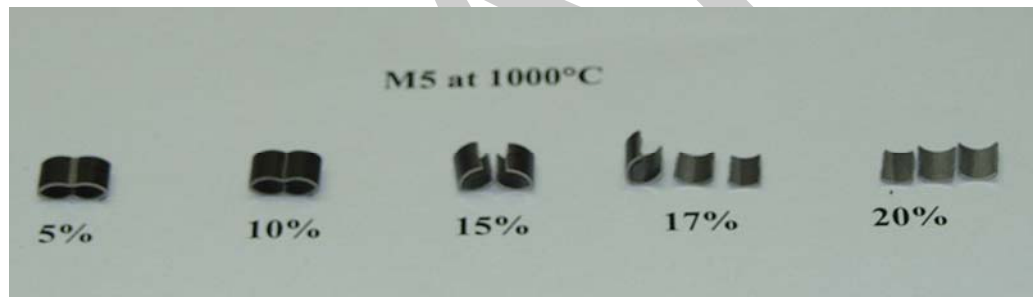
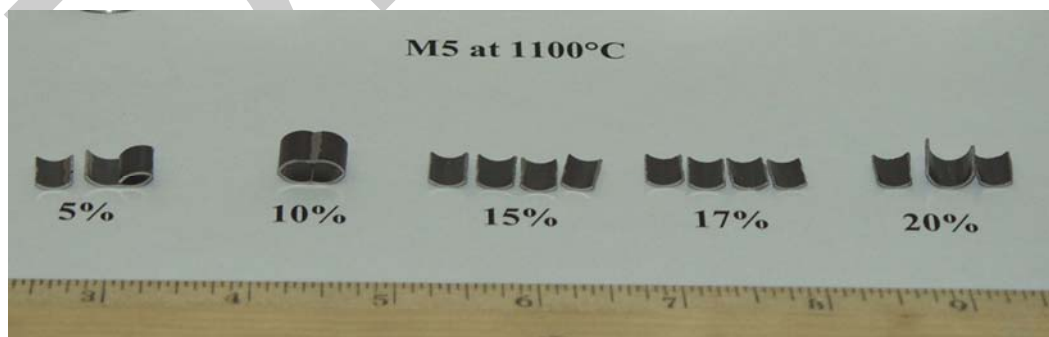


Figure 67. Post-quench ductility vs. CP-predicted ECR for 17×17 M5 and Zry-4 oxidized in steam at 1100°C, cooled at ≈10°C/s to 800°C, and quenched. Offset strain was determined from results of ring-compression tests conducted at RT and 0.0333-mm/s displacement rate.



(a)



(b)

Figure 68. Post-test appearance of M5 ring-compression samples tested at room temperature and 0.0333 mm/s: (a) samples oxidized at 1000°C and (b) samples oxidized at 1100°C. ECR values are calculated using the Cathcart-Pawel weight gain correlation and 0.57-mm wall. For 0.61-mm-wall M5, these values should be reduced to 4.7%, 9.3%, 14.1%, 16.0%, and 18.8%.

M5 exhibits very slow oxide-layer growth and weight-gain increase at 1000°C as compared to Zry-4. Also, above ≈10% CP-ECR (≈960 s equivalent isothermal time), weight gain does not increase in a consistent manner with oxidation time or the square root of time. For example, the ECR based on weight gain was determined to be 10.7% at 1890 s, 11.6% at 2430 s, 13.3% at 3365 s, and 12.2% at 4065 s. The offset strain decreases very steeply (40% to 3%) with a small increase in measured ECR (10.7% to 13.3%) corresponding to a large increase in oxidation time (1890 s to 4065 s). Based on fundamental considerations regarding oxygen increase in the beta layer, it appears more meaningful to express M5 post-quench ductility (offset strain) as a function of CP-ECR.

Table 33 Characterization of Highly Oxidized 17×17 Zry-4 and M5 Samples after Exposure to Steam at 1000°C and 1100°C, Cooling at ≈10°C/s to 800°C, and Water Quench

Oxidation Temperature, °C	Parameter	Zry-4 20% CP-ECR	M5 18.8% CP-ECR
1000	Effective Oxidation Time, s	3364	3364
	Weight Gain, mg/cm <sup>2</sup>	14.6	9.2
	Measured ECR, %	22.4	13.3
	RT Offset Displacement, mm	0.31	0.31
	RT Offset Strain, %	3.2 (ductile)	3.2 (ductile)
	Hydrogen Content, wppm	19	26
	Hydrogen Pickup, wppm	15	22
	OD/ID Oxide Thickness, μm	83/82	36/32
	Microhardness within Middle 0.2 mm, DPH	290-420	300-430
	1100	Effective Oxidation Time, s	1065
Weight Gain, mg/cm <sup>2</sup>		13.2	13.3
Measured ECR, %		20.3	19.1
Offset Displacement, mm		0.46	0.17
RT Offset Strain, %		4.8 (ductile)	1.8 (borderline <sup>a</sup> )
Hydrogen Content, wppm		22	17
Hydrogen Pickup, wppm		19	12
OD/ID Oxide Layer Thickness, μm		70/68	72/62
Microhardness within Middle 0.2 mm, DPH <sup>b</sup>		240-470	260-400

<sup>a</sup>New sample oxidized to higher EP-ECR (20.4%) was ductile (3.2% offset strain).

<sup>b</sup>Includes oxygen-stabilized alpha needles (M5) and alpha incursions (Zry-4) in prior-beta layer.

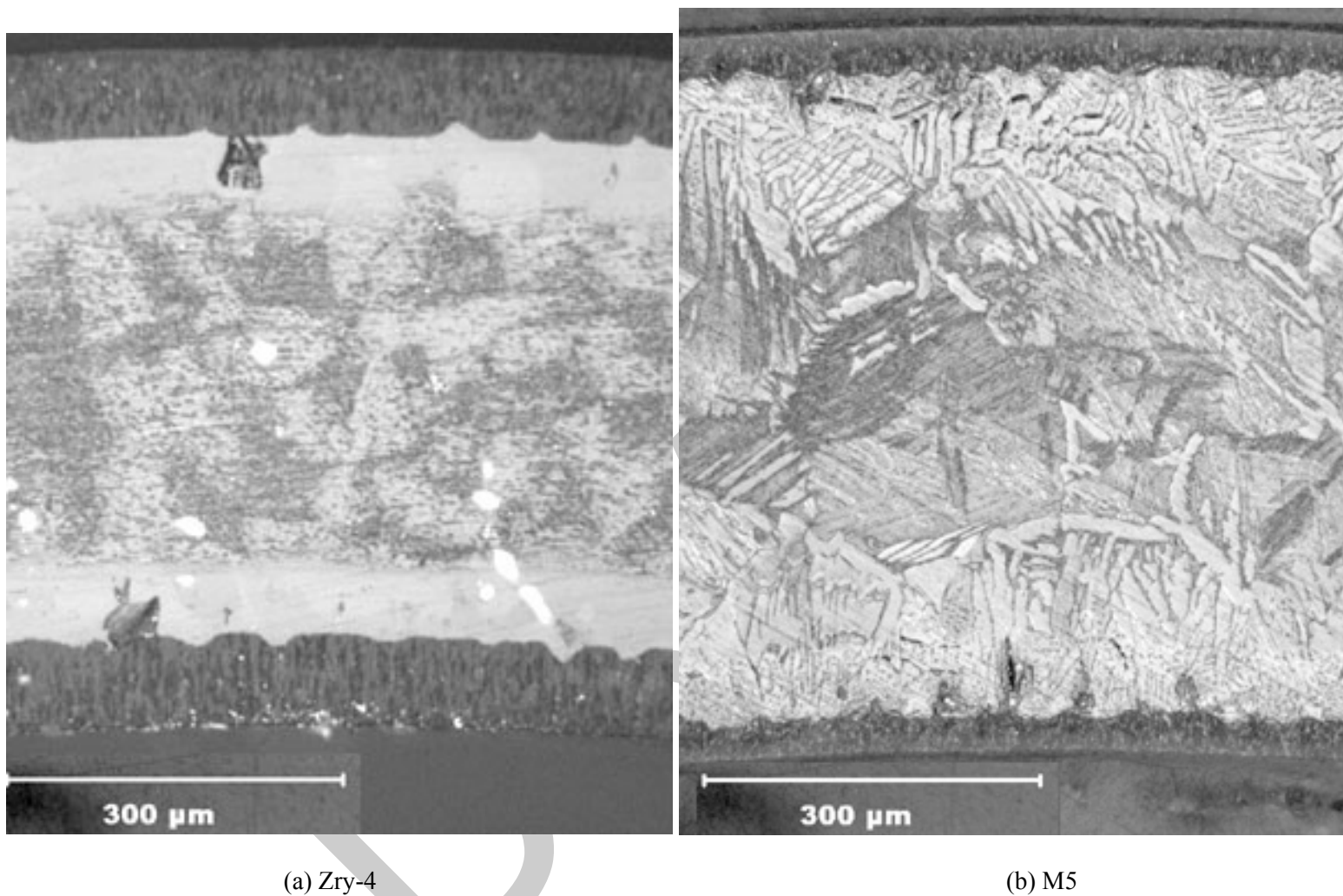


Figure 69. Metallography of as-polished Zry-4 (a) and M5 (b) oxidized in steam at 1000°C for ≈3360 s, cooled at ≈10°C/s to 800°C, and water quenched. Measured ECR values are 22.4% for Zry-4 and 13.3% for M5.

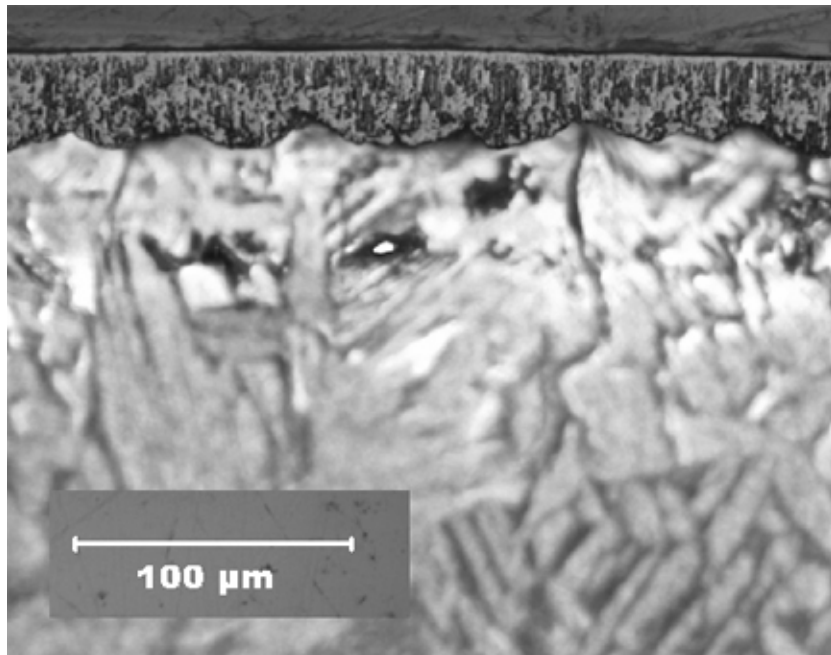
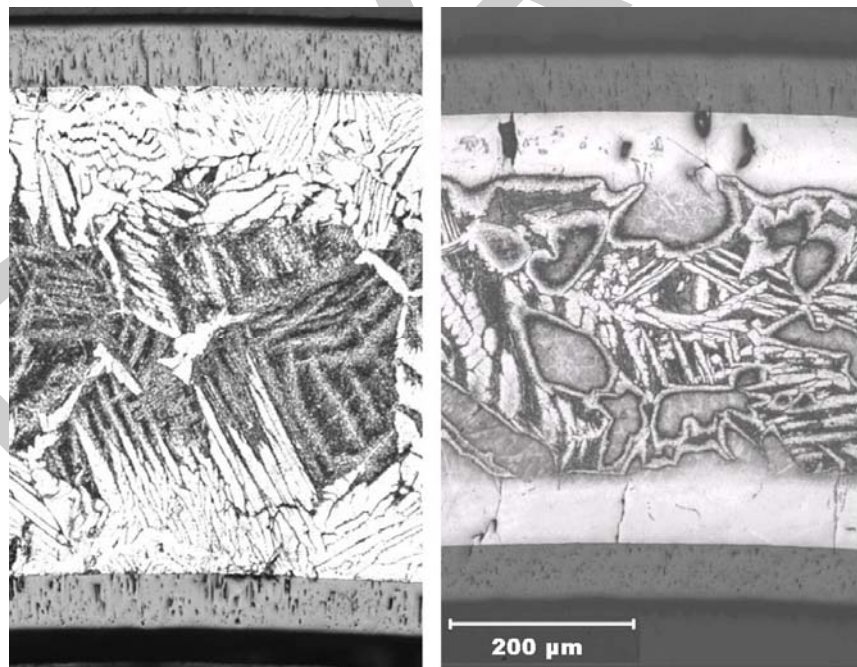


Figure 70. High-magnification image of etched M5 outer-surface oxide and alpha layers following oxidation at 1000°C for 3360 s. The outer-surface oxide layer is tetragonal, but the wavy oxide-metal interface is a precursor to breakaway oxidation.



(a) M5

(b) Zry-4

Figure 71. Metallography of etched M5 (a) and Zry-4 (b) oxidized in steam at 1100°C for  $\approx 1070$  s, cooled at  $\approx 10^\circ\text{C/s}$  to 800°C, and water quenched. Measured ECR values are 19.1% for M5 and 20.3% for Zry-4.

## 17×17 M5 oxidized at 1200°C

In parallel with the Zry-4 testing, numerous tests were conducted with 17×17 M5 oxidized at 1200±5°C to determine the ductile-to-brittle transition CP-ECR at RT and 135°C. Figure 72 shows the thermal-benchmark results for the first test train. Because the differences in ramp rates are small for the 0.61-mm M5 vs. the 0.57-mm Zry-4 and ZIRLO, the thermal benchmark results shown in Figure 21 were used for the more recent tests with M5. Although the temperature ramps are different, these have little effect on the long-time tests used to determine the high transition CP-ECR at a ring-compression temperature of 135°C. Also, all tests were stopped after the first significant load drop to allow a measure of the permanent strain based on the diameter change in the loading direction.

The weight gain results (expressed in terms of measured ECR) and the post-quench ductility results are summarized in Table 34. Figure 73 shows the measured M5 and Zry-4 weight gains, as compared to the CP-predicted weight gains. The experimental results for both alloys are in excellent agreement with each other and with the predicted values.

M5 appears to embrittle at room temperature after oxidation at 1200°C to ≈12% CP-ECR and quench. This observation is confirmed by both the offset strain-criterion (<2%) and the permanent-strain criterion (<1%) for embrittlement. The enhancement of ductility with the increase in test temperature is quite pronounced. Based on the offset and permanent strain data, the ductile-to-brittle transition CP-ECR is ≈20% at 135°C. The variations of offset and permanent strains with CP-ECR are shown in Figures 74a and 74b, respectively, for the RT and 135°C test conditions. Figure 75 is a comparison between the post-quench ductility (offset strain) at 135°C for M5 and Zry-4 vs. CP-ECR following oxidation at 1200°C and quench at 800°C. At <17% CP-ECR, M5 has significantly higher post-quench ductility than Zry-4.

Table 35 summarizes the characterization results for 17×17 Zry-4 and M5 oxidized at 1200°C for times equivalent to approximately 13% and 20% CP-ECR (based on 0.57-mm-wall cladding) and quenched at 800°C. As expected, the hydrogen pickup is very low. Also, there is excellent agreement between the inner-surface and outer-surface oxide layer thickness, indicating adequate steam flow at the inner surface. The microhardness results support the post-quench ductility results. Based on the room-temperature microhardness values, one would expect M5 to retain post-quench ductility at ≤20% CP-ECR at the elevated test temperature of 135°C. The microstructures across the cladding wall are shown in Figure 76 for Zry-4 and M5 oxidized at 1200°C to ≈20% CP-ECR. As with the lower oxidation temperatures, Zry-4 has well-defined oxygen-stabilized alpha layers grown at 1200°C, while the presence of Nb in M5 results in a less clear distinction of this layer. The microhardness indents for Zry-4 and M5 oxidized to ≈13% CP-ECR are shown in Figures 77a and 77b, respectively.

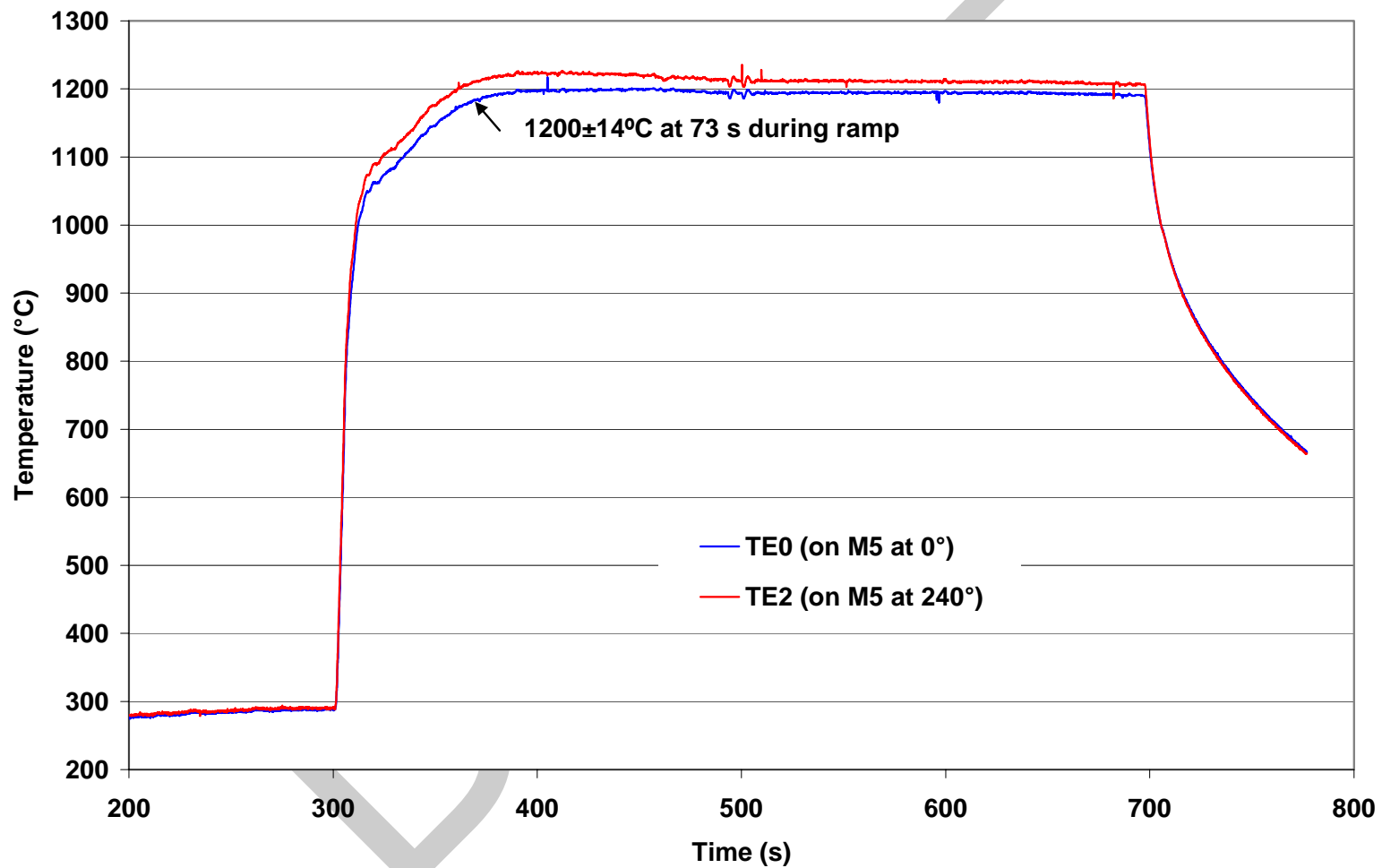


Figure 72. Thermal benchmark results for first test train for 17×17 M5 oxidation tests at 1203±8°C. The cladding OD is 9.50 mm, and the wall thickness is 0.61 mm. Quench at 800°C is not shown in this figure.

Table 34 Ring Compression Test (RCT) Results for 17×17 M5 Cladding Oxidized at 1200°C, Cooled at ≈13°C/s to 800°C, and Quenched. ECR = 1.437 Wg for 0.61-mm-wall thickness. Tests were performed on ≈8-mm-long samples at RT and 135°C and at 0.0333-mm/s displacement rate. Displacements in the loading direction were normalized to the as-fabricated outer diameter (9.50 mm) to calculate offset and permanent strains.

Test Conditions		ECR, %		Plastic Displacement, mm		Plastic Strain, %	
RCT T, °C	Test Time, <sup>a</sup> s	CP	Meas.	Offset	Permanent	Offset	Permanent
RT	58	4.5	4.0	>5.35	>5.0	>56	>53
RT	132	9.1	9.1	0.32	0.13	3.4	1.6
135	132	9.1	9.1	>4.8	>4.8	>51	>51
RT	203	12.1	13.1	0.17	0.09	1.8	0.9
<b>135<sup>b</sup></b>	<b>226</b>	<b>13.0</b>	<b>13.6</b>	<b>1.43</b>	<b>1.13</b>	<b>15.0</b>	<b>11.9</b>
<b>135<sup>b</sup></b>	<b>226</b>	<b>13.0</b>	<b>13.6</b>	<b>1.20</b>	<b>0.84</b>	<b>12.6</b>	<b>8.8</b>
RT	248	14.1	13.8	0.16	0.07	1.7	0.7
135	248	14.1	13.8	1.73	1.25	18.2	13
RT	308	16.0	15.7	0.13	0.06	1.4	0.6
135	308	16.0	15.7	1.02	---	10.7	---
<b>135<sup>b</sup></b>	<b>318</b>	<b>16.0</b>	<b>17.4</b>	<b>0.52</b>	<b>0.27</b>	<b>5.4</b>	<b>2.8</b>
<b>135<sup>b</sup></b>	<b>318</b>	<b>16.0</b>	<b>17.4</b>	<b>0.52</b>	---	<b>5.4</b>	---
RT	428	18.7	18.8	0.195	0.06	2.0	0.6
<b>135<sup>b</sup></b>	<b>480</b>	<b>19.9</b>	<b>21.4</b>	<b>0.36</b>	<b>0.10</b>	<b>3.8</b>	<b>1.0</b>
<b>135<sup>b</sup></b>	<b>480</b>	<b>19.9</b>	<b>21.4</b>	<b>0.29</b>	<b>0.10</b>	<b>3.1</b>	<b>1.0</b>

<sup>a</sup>Includes time for ramp from 300°C and hold time.

<sup>b</sup>Tests were conducted with current test train (see Figure 21 for thermal history). Most other test results were generated with the initial test train (see Figure 72 for thermal history).

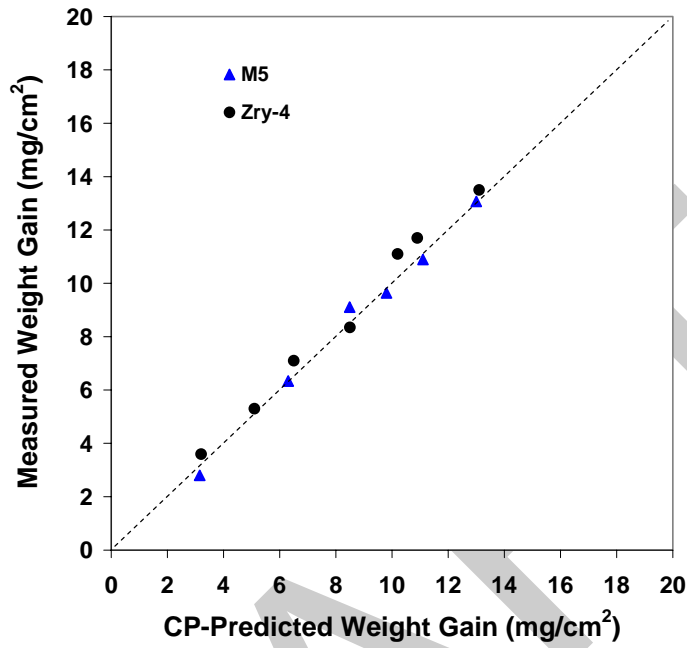


Figure 73. Comparison between weight gain data for M5 and Zry-4 and CP-predicted weight gain for samples oxidized (two-sided) in steam at 1200°C and quenched at 800°C.

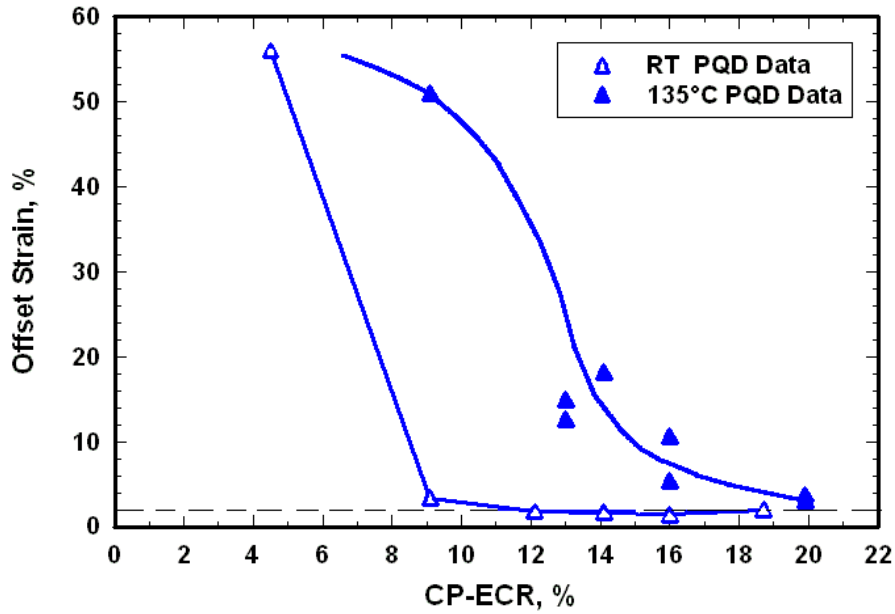


Figure 74a. Offset strain vs. CP-ECR for 17×17 M5 oxidized at 1200°C, cooled at ≈13°C/s to 800°C, quenched, and ring-compressed at 135°C.

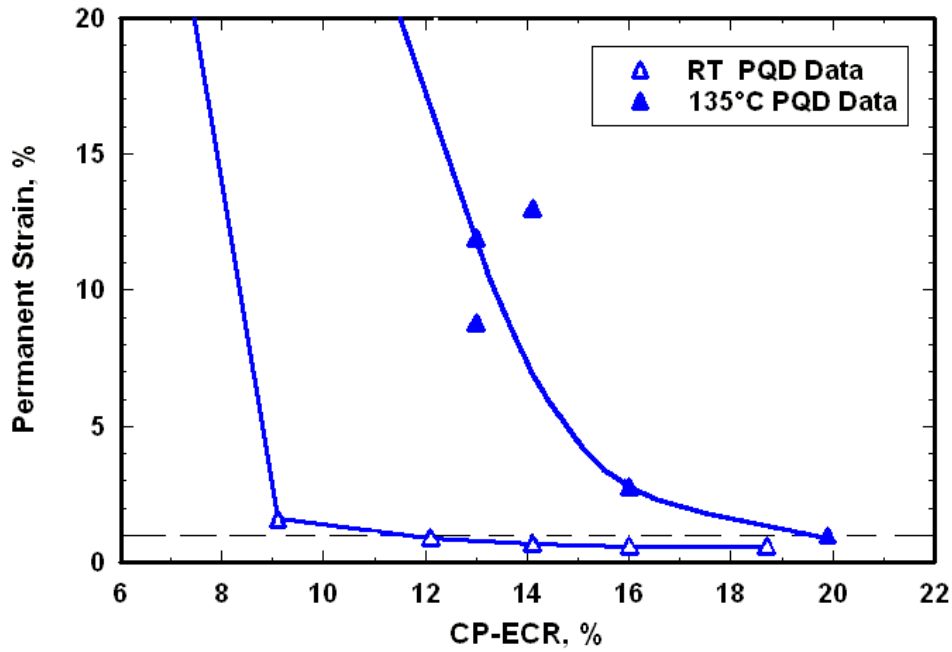


Figure 74b. Permanent strain vs. CP-ECR for 17×17 M5 oxidized at 1200°C, cooled at ≈13°C/s to 800°C, quenched, and ring-compressed at 135°C.

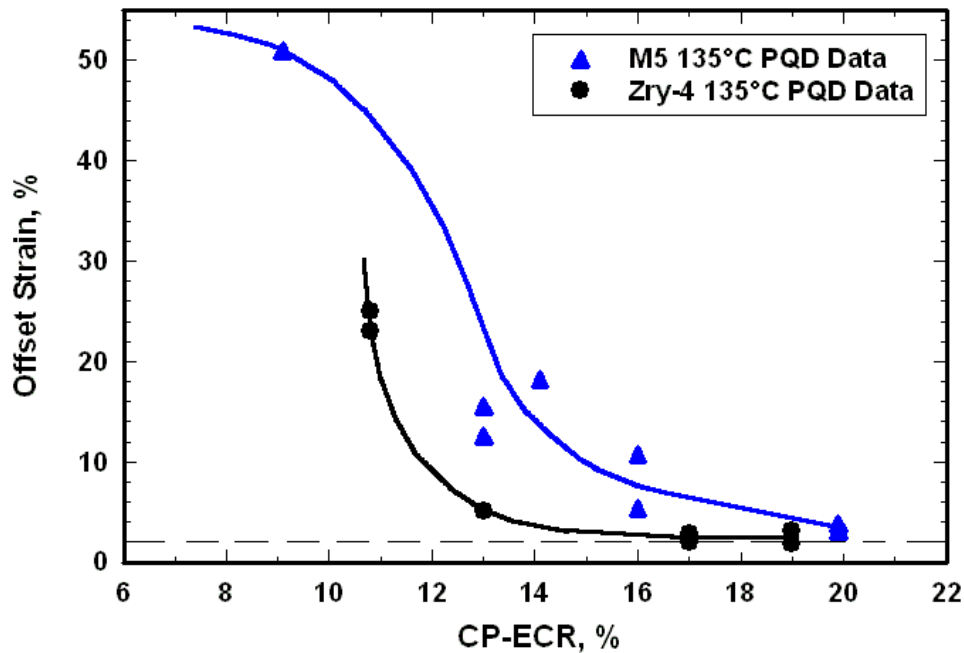
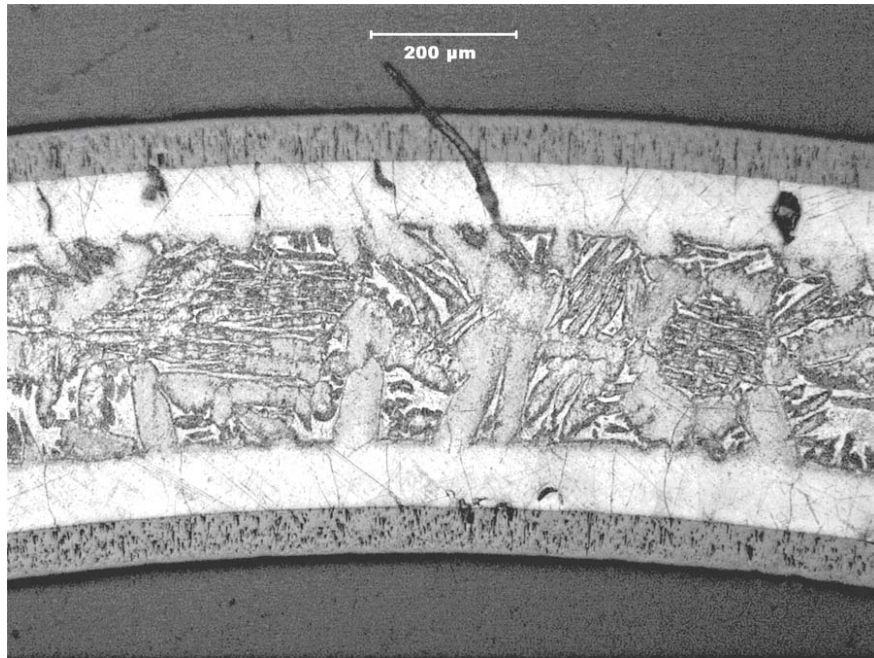


Figure 75. Offset strain vs. CP-ECR for 17×17 M5 and Zry-4 oxidized at 1200°C, cooled at ≈13°C/s to 800°C, quenched, and ring-compressed at 135°C.

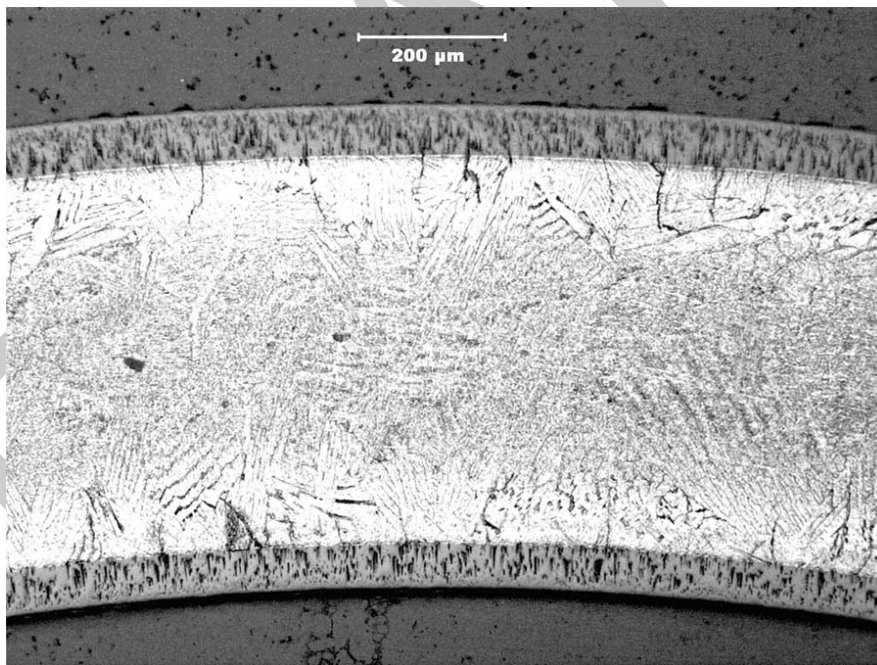
Table 35 Characterization of 17×17 Zry-4 and M5 Samples after Exposure to Steam at 1200°C for Durations of 166 and 400 s, Cooling at ≈13°C/s to 800°C, and Water Quench

Parameter	Zry-4		M5	
	20% ECR	13% ECR	18.7% ECR	12.1% ECR
Effective Time, s	400	166	400	166
Weight Gain, mg/cm <sup>2</sup>	13.5	8.35	13.1	9.11
Measured ECR, %	20.8	12.8	18.8	13.1
RT Offset Displacement, mm	0.05	0.09	0.20	0.11
RT Measured Permanent Displacement, mm	0.04	0.07	0.06	0.09
RT Permanent Strain, %	0.4	0.7	0.6	0.9
RT Ductility	≤0.4 (brittle)	≤0.7 (brittle)	≤0.6 (brittle)	≤0.9 (brittle)
Hydrogen Content, wppm	17	low	19	low
Hydrogen Pickup, wppm	13	low	14	low
OD/ID Oxide Thickness, μm	68/66	42/41	68/61	46/40
Prior-Beta-Layer Thickness, μm	266	419	≤360	≈442
Microhardness, DPH				
Oxide Layers	570-960	600-770	650-780	580-680
Alpha Layers	530-730	600-700	580-850	680-880
Prior-Beta Layer <sup>a</sup>	280-600	260-360	280-450	300-410

<sup>a</sup>Range includes microhardness values of oxygen-rich alpha needles (M5) and alpha incursions (Zry-4) in this layer.

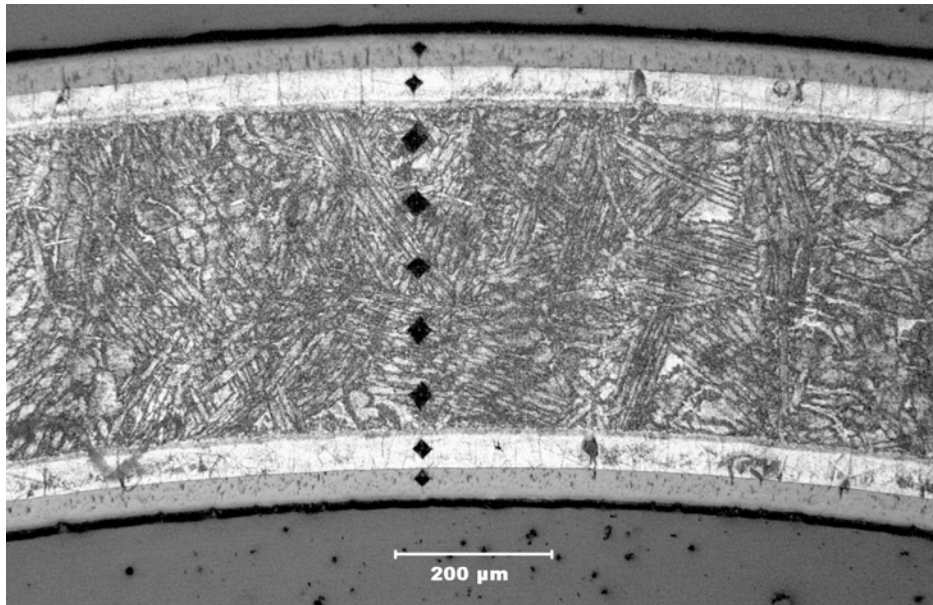


(a) Zry-4

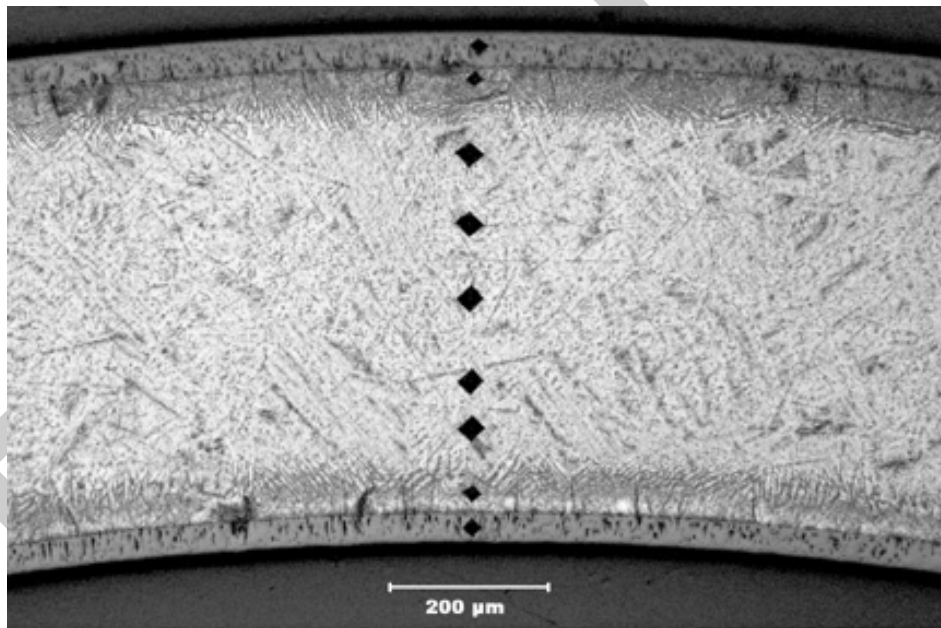


(b) M5

Figure 76. Metallography of etched Zry-4 (a) and M5 (b) oxidized in steam at 1200°C for ≈400 s, cooled at ≈13°C/s to 800°C, and water quenched. Measured ECR values are 20.8% for Zry-4 and 18.8% for M5.



(a) Zry-4



(b) M5

Figure 77. Metallography and microhardness indents across the radius of 17×17 Zry-4 (a) and M5 (b) oxidized at 1200°C to 12-13% CP-ECR. The measured ECR values are 12.6% for Zry-4 and 13.1% for M5. Samples were quenched at 800°C following cooling at  $\approx 13^\circ\text{C/s}$ .

### 3.4.2 Breakaway oxidation time for 17×17 M5 samples oxidized at 1000°C

Based on the work of Mardon et al. [21] the breakaway oxidation time for M5 corresponding to ≈200-wppm H pickup is ≈6400 s at 1000°C. However, M5 exhibits very slow growth rate of inner- and outer-surface oxide layers at 1000°C, which may prolong breakaway oxidation. Also, breakaway-oxidation times at 975-1025°C or at lower temperatures have not been reported in the open literature. Based on ANL data, M5 does not undergo breakaway oxidation at 1000°C for test times of 3450 and 4100 s

Table 36 Data Summary for ANL M5 Breakaway Oxidation Tests at 1000°C; test times are from beginning of ramp at 300°C to the end of the hold time.

Cooling	T, °C	Test Time, s	CP Wg, mg/cm <sup>2</sup>	Measured Wg, mg/cm <sup>2</sup>	Hydrogen Content (L <sub>H</sub> ), wppm	Hydrogen Pickup (ΔC <sub>H</sub> ), <sup>a</sup> wppm
Q at 800°C	1000	3450	13.1	9.2	26	22
Q at 800°C	1000	4100	11.1	10.8	13	8

<sup>a</sup>Hydrogen pickup (ΔC<sub>H</sub>) is referenced to the as-fabricated sample weight: ΔC<sub>H</sub> = (1 + 5.4×10<sup>-3</sup> Wg) L<sub>H</sub> - C<sub>Hi</sub>, where C<sub>Hi</sub> is as-fabricated hydrogen content.

### 3.5 Effects of surface conditions on cladding performance

Breakaway oxidation is an instability phenomenon that leads to transformation from the tight-tetragonal-oxide phase (black) to the cracked-monoclinic-oxide phase (gray or yellow). The time-at-temperature and temperature at which the breakaway occurs may be dependent on cladding surface conditions (roughness, scratches, and chemistry) and near-surface chemistry. The tetragonal oxide phase of ZrO<sub>2</sub> is not thermodynamically stable at temperatures below ≈1150°C. However, this black oxide phase is observed on cladding surfaces following steam oxidation at temperatures much less than 1150°C. It is even observed as part of the tight sub-micron corrosion layer adherent to the cladding surface grown at normal reactor operating temperatures. Compressive stress and hypostoichiometry [ZrO<sub>(2-x)</sub>] appear to stabilize the tetragonal phase at temperatures much lower than the phase-transition temperature. As the density of the oxide is lower than that of the cladding metal, the volume expansion during oxide formation leads to compressive stress in the oxide. Also, as oxidation progresses in steam at high temperature, oxygen continues to diffuse from the oxide to the oxygen-stabilized alpha layer, leaving an oxygen gradient in the oxide and hypostoichiometric oxide at the Zr-alloy surface. Conversely, irregularities in surface geometry can result in alternating regions of compressive and tensile stresses. According to Leistikow and Schanz [19,20], such irregularities along the metal-oxide surface are a precursor to tetragonal-to-monoclinic transformation and breakaway oxidation.

Surface and near-surface chemistry can play a significant role in the breakaway oxidation phenomenon. Cladding impurities and/or alloy constituents can induce early monoclinic-oxide formation. They can also delay the transformation. In general, impurities and alloy constituents in the oxide layer with valences less than +4 (e.g., Al<sup>+3</sup>, Cr<sup>+3</sup>, Ca<sup>+2</sup>, Mg<sup>+2</sup>) help preserve hypostoichiometry, while elements with valences greater than +4 (e.g., Nb<sup>+5</sup>) tend to drive the oxide toward ZrO<sub>2</sub> and the monoclinic phase. Also, fluorine surface impurities from pickling (i.e., etching) are known to induce early monoclinic oxide formation. Extensive studies have been performed by Cheng and Adamson [23] and Cheng et al. [24] on the effects of fluorine impurities on nodular corrosion in BWR cladding and early breakaway oxidation time.

In this section, the effects on breakaway oxidation of surface roughness, surface scratches, and surface chemistry are examined. HBR-type Zry-4 and modern Western cladding alloys are discussed in Section 3.5.1, while E110 is discussed in Section 3.5.2.

### 3.5.1 Effects of surface conditions on HBR-type Zry-4 and modern cladding alloys

#### Surface roughness and chemistry

The HBR-type 15×15 Zry-4 exhibited breakaway oxidation at  $\approx 3800$  s and 985°C, while the belt-polished (BP) 15×15 Zry-4 had a breakaway oxidation time of  $\approx 5000$  s at 985°C. Also, the hydrogen pickup rate was much higher for HBR-type Zry-4. HBR-type Zry-4 roughness (0.3  $\mu\text{m}$  for HBR vs. 0.1  $\mu\text{m}$  for BP) appears to have contributed to early breakaway time for the outer surface, and pickling (vs. grit-polishing) appears to have contributed to early inner-surface breakaway and rapid hydrogen pickup.

#### Surface scratches and abrasions

In the process of handling cladding during fueling, end-cap welding, insertion into the fuel assembly, and core loading, scratches and abrasions will occur on the cladding outer surface. Such scratches could reduce the breakaway oxidation time for fresh cladding in the reactor core. Vendors have a "design-basis" scratch depth, which is based on a stress criterion given that the scratch will locally thin the cladding wall and increase the hoop stress for a given pressure loading. For Western cladding alloys, the depth of the design-basis scratch is  $<10\%$  of the wall thickness, which is  $<57$   $\mu\text{m}$ . Generally, vendors use  $\approx 2$  mils ( $\approx 50$   $\mu\text{m}$ ) as the design-basis scratch depth.

The as-fabricated cladding segments received by Argonne did not have "normal" or "design-basis" scratches although they did have mild abrasions. Figure 78 shows images of the belt-polished 15×15 Zry-4 outer surface: (a) smooth and (b) local abrasions. This smooth exterior is characteristic of most of the belt-polished 15×15 Zry-4 cladding segments received by Argonne, as well as the belt-polished 17×17 PWR and 10×10 BWR alloys.

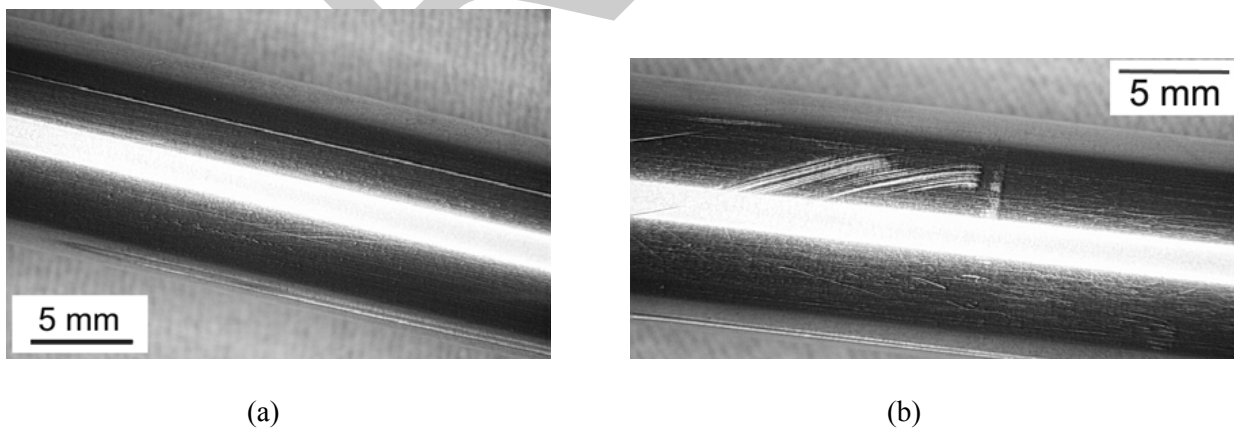


Figure 78. Outer surface of belt-polished 15×15 Zry-4: (a) smooth exterior and (b) local region of surface abrasions.

A sample was sectioned from the mildly abraded region and oxidized for 5000 s at  $986\pm 12^\circ\text{C}$ . The outer surface was lustrous black and the hydrogen pickup was negligible, indicating that mild abrasions do not have a significant effect on the breakaway oxidation time of Zry-4 within the range of times tested.

The HBR sample (HBRU#96) had visible outer-surface scratches prior to testing. Following oxidation at 985°C for 3600 s, the measured weight gain was only 3% higher than the CP-predicted weight gain and the outer surface was black. However, the hydrogen content and pickup were 186±75 wppm and 174±80 wppm, respectively. The oxidized sample was sectioned in the region of longitudinal scratches and examined by optical microscopy. The results at four circumferential locations of the cross section are shown in Figure 79. The 0° (top) and 180° (bottom) sectors are in breakaway oxidation, while the 90° and 270° are not. Based on the appearance of the outer surface and on the metallographic results, local breakaway oxidation and hydrogen pickup occurred in the scratched region. The results suggest that the breakaway oxidation time could be ≈200 s less at ≈1000°C for fuel rods clad in scratched HBR-type Zry-4 at the beginning of reactor operation.

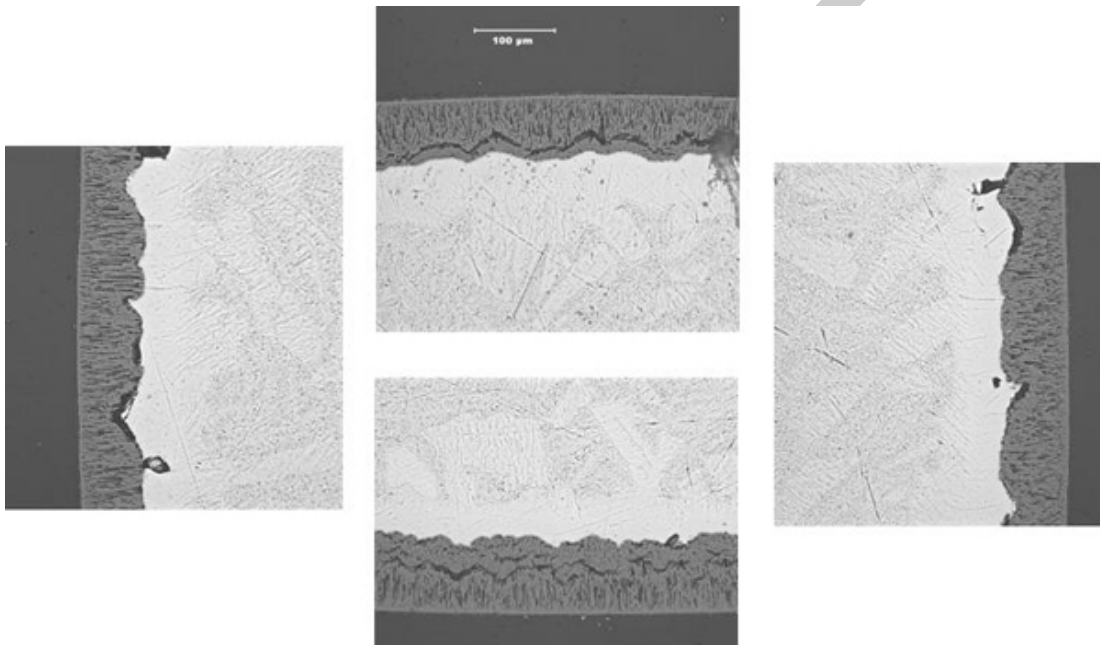


Figure 79. Metallographic images in the scratched region of an HBR-type 15×15 Zry-4 sample (HBRU#96) following oxidation at 985±12°C for 3600 s. The top and bottom sectors are in breakaway oxidation, while the left and right sectors are not. The sample was prepared from a region of the cladding with scratches observed during pre-test and post-test characterization.

A scratch depth of ≈20 μm was machined into the outer surface of belt-polished 17×17 ZIRLO along a length of about 2 inches. The scratch geometry is shown in Figure 80 for a cladding cross section. The scratched samples were oxidized for 985°C for 3400 s and at 970°C for 2600 s (see Table 29 for results). Breakaway oxidation did initiate along the scratched regions as shown in Figures 81 and 82. For the scratched sample oxidized at 985°C for 3400 s, the midplane hydrogen pickup was 175±145 wppm, as compared to only 37 wppm for the smooth sample oxidized under the same conditions. Underneath the yellow oxide shown in Figure 81, the hydrogen content was as high as 400 wppm. Given that the breakaway oxidation time is estimated to be 3500±100 s for smooth ZIRLO oxidized at 985°C, the 20-μm-deep scratch in the ZIRLO outer surface appears to reduce that time by only 100-200 s. For the scratched ZIRLO sample oxidized at 970°C for 2600 s, the average hydrogen pickup at the midplane was only 44 wppm, with a local hydrogen pickup under the yellow oxide of 120 wppm. Again, the scratch appears to reduce the breakaway oxidation time by ≈200 s relative to smooth cladding.

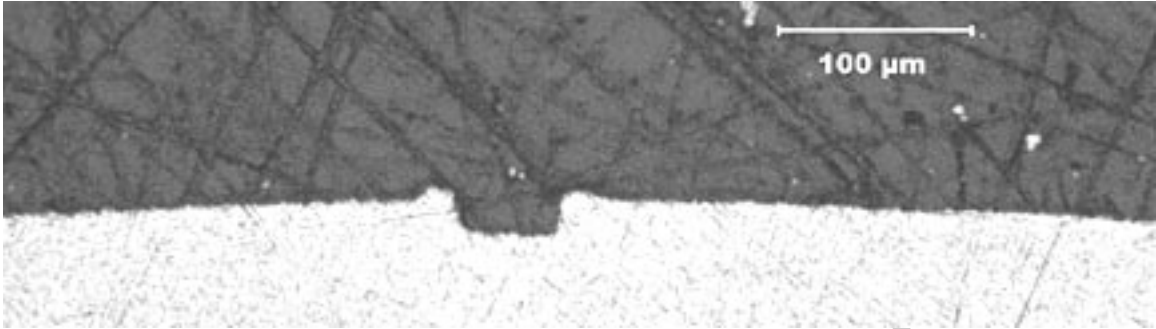


Figure 80. Cross section of ZIRLO cladding with machined scratch  $\approx 20\text{-}\mu\text{m}$  deep into outer surface.



Figure 81. Outer surface of scratched ZIRLO sample following oxidation at  $985^{\circ}\text{C}$  for 3400 s. The local hydrogen pickup under the yellow surface is 440 wppm.



Figure 82. Outer surface of scratched ZIRLO sample following oxidation at  $970^{\circ}\text{C}$  for 2600 s. The local hydrogen pickup under the yellow surface is 120 wppm.

## Surface oxide films

During reactor startup, water-side corrosion will initiate. By the time the fuel has enough decay heat for temperature elevation during a LOCA, the cladding outer surface will have an oxide film. For softer cladding alloys (e.g., E110 with 500 wppm oxygen), the cladding is pre-filmed (<1- $\mu\text{m}$  thick) through pickling-anodizing or autoclaving during fabrication to protect the cladding from excessive scratching during fuel loading. The effects of pre-filming or early in-reactor corrosion on breakaway oxidation time were studied for 17 $\times$ 17 ZIRLO. Westinghouse supplied ANL with pre-filmed (<1- $\mu\text{m}$  thick) ZIRLO that had been exposed to 360°C water for 36 hours in an autoclave. The samples were pre-oxidized on inner and outer surfaces prior to breakaway oxidation testing (see Table 37 for results).

Table 37 Effects of Pre-filming on the Breakaway Oxidation Time for ZIRLO. Hydrogen pickup values for as-fabricated (bare) ZIRLO samples are also listed. Samples were slow cooled from the hold temperature to RT and ring-compressed at 135°C and 0.0333 mm/s.

Surface Condition	T, °C	Test Time, <sup>a</sup> s	Measured Wg, mg/cm <sup>2</sup>	Hydrogen Content (L <sub>H</sub> ), wppm	Hydrogen Pickup ( $\Delta C_H$ ), <sup>b</sup> wppm	Comment
Bare	975	3000	9.01	39 $\pm$ 2	30 $\pm$ 2	Small yellow spot on OD
Bare	975	3500	8.65	108 $\pm$ 46	100 $\pm$ 50	Small yellow area on OD
Bare	980	3000	11.8	352 $\pm$ 118	370 $\pm$ 125	Post-breakaway
Bare	985	3000	9.10	104 $\pm$ 40	100 $\pm$ 40	Small yellow area on OD
Bare	985	3400	9.43	303 $\pm$ 164	310 $\pm$ 170	Post-breakaway
Pre-filmed	985	3000	9.00	59 $\pm$ 35	50 $\pm$ 40	Small yellow spot on OD
Pre-filmed	985	3400	9.28	259 $\pm$ 138	260 $\pm$ 145	Post-breakaway
Pre-filmed	985	4000	11.9	1070 $\pm$ 89	1130 $\pm$ 100	Post-breakaway
Pre-filmed	980	3200	8.67	125 $\pm$ 116	120 $\pm$ 120	Two yellow spots on OD
Pre-filmed	980	3200	8.84	101 $\pm$ 98	100 $\pm$ 100	Yellow spots on OD

<sup>a</sup>Includes time from beginning of ramp at 300°C to end of hold time at oxidation temperature.

<sup>b</sup>Hydrogen pickup ( $\Delta C_H$ ) is referenced to the as-fabricated sample weight:

$$\Delta C_H = (1 + 5.4 \times 10^{-3} \text{ Wg}) L_H - C_{Hi}, \text{ where } C_{Hi} \text{ is as-fabricated hydrogen content (11 wppm).}$$

As shown in Table 37, pre-filming with thin (<1  $\mu\text{m}$ ) oxide layers had only a small effect on breakaway oxidation time and temperature at which the minimum time occurred. The minimum

breakaway oxidation time for pre-filmed ZIRLO oxidized at 980-985°C is 3300±100 s. Combining the results in Table 29 for bare ZIRLO with and without machined scratches and the data in Table 37 for bare and pre-filmed ZIRLO, the minimum breakaway oxidation time at 970-985°C can be expressed as 3100±300 s for the range of ZIRLO surface conditions tested.

Westinghouse has generated an independent data set [Ref. to be provided] indicating that bare and pre-filmed ZIRLO samples do not experience breakaway oxidation for test times of 4400 s and 5400 s and oxidation temperatures in the range of 950-1000°C. Some samples exhibited regions of tan oxide near the sample ends, along with high hydrogen pickup. Excluding these end-effects, the Westinghouse results indicate a significantly higher breakaway oxidation time for ZIRLO, as compared to the ANL results. Differences in the results highlight the importance of establishing standardized methods for pretest surface cleaning, heating, temperature control, and steam flow rates for breakaway oxidation tests.

### *3.5.2 Effects of surface conditions on E110 tubing and cladding*

Although Russian E110 cladding is not used in the U.S., it was added to the ANL test program for the purposes of gaining some understanding as to why this particular Zr-1Nb alloy experiences such early breakaway oxidation time and ductility loss for steam-oxidation temperatures of 1000-1100°C. Breakaway oxidation times reported in the literature for E110 are as low as 500 s based on ductility loss, >200-wppm hydrogen pickup, weight-gain-rate increase, and/or visual appearance with correspondingly low CP-ECR values. However, in reviewing the literature for E110, we found it very difficult to compare data sets because oxidation test methods varied considerably (e.g., heating and cooling rates), as did E110 chemistry, thermomechanical treatment, and surface finish.

Concurrent with the ANL E110 study, an extensive study of E110 was conducted at the Russian Research Center "Kurchatov Institute" (RRC-KI) and the Research Institute of Atomic Reactors (RIAR). The RRC-KI/RIAR study was sponsored by NRC, Institute for Radiological Protection & Nuclear Safety (ISRN), and TVEL (E110 vendor). Close collaboration was maintained between the ANL program and the Russian program, particularly with regard to test-sample oxidation and methodologies for post-oxidation ductility determination methodologies. The Russian program results are well documented in NUREG/IA-0211 [2]. In some cases, efforts were duplicated to confirm results. For most of the research, ANL concentrated on the evolution of E110 breakaway oxidation at 1000°C – particularly the effects of surface roughness, surface scratches, and surface chemistry – while the Russian program, which had access to numerous heats of E110, concentrated on the effects of alloying elements and impurities in the bulk. In the Russian program, the following differences between Russian E110 and Western cladding alloys were considered and investigated: impurities in Zircon ore, electrolytic refinement vs. Kroll process for reducing the ore to produce Zr ingots, variations in alloying elements (e.g., oxygen), and fabrication processes for making tubing from the ingot. The most substantial improvement in E110 behavior came from fabricating E110 cladding from a Western Zr ingot. These results suggest that electrolytic refinement removes impurities that may help stabilize the oxide layer grown on the surface.

Argonne had access to only one heat of E110 – the tubing and cladding provided by Fortum in Finland. Because the ANL study was restricted to this one heat, the focus of the ANL program was on the effects of surface finish, which could be modified by machining, polishing, and etching.

### Characterization of E110 tubing and cladding

Dimensional, chemical, and microstructural analyses of E110 tubing were performed by ANL to verify that the E110 received from Fortum was within specifications and to try to ascertain any

differences that would explain the poor LOCA performance of E110 and the excellent performance of M5. The dimensional and chemical characterization results are listed in Table 6 for E110 and Table 5 for M5. For the alloying and impurity elements measured, the materials used in the ANL test program are within specifications for E110 [7] and M5 [6]. Three noticeable differences in materials are: thicker wall for E110 (0.71 mm vs. 0.57-0.61 mm for M5), higher surface roughness for E110 tubing (0.34  $\mu\text{m}$  vs. 0.12  $\mu\text{m}$  for M5), and lower oxygen content for E110 (0.05 wt.% vs. 0.145 wt.% for M5). As Zry-4 cladding with thicker walls (0.67-0.77 mm) showed no adverse effects due to wall thickness, it appeared highly unlikely that wall thickness alone would contribute to the poor LOCA performance of E110. The higher surface roughness could contribute directly or indirectly to early breakaway oxidation. However, the breakaway oxidation time ( $\approx 3800$  s at  $1000^\circ\text{C}$ ) determined by ANL for 0.32- $\mu\text{m}$ -rough HBR-type Zry-4 was significantly higher than what is reported for E110 in the Russian program [2] for  $1000^\circ\text{C}$  oxidation temperature. Also, E110 cladding (etched and anodized) had a lower surface roughness (0.19  $\mu\text{m}$ ) than the tubing, but the cladding exhibited early breakaway oxidation times comparable to the tubing in ANL tests for samples oxidized at  $1100^\circ\text{C}$  (one-sided). It seemed more likely that high surface roughness could result in earlier initiation of breakaway oxidation for an alloy that is inherently unstable. It is also likely that negative effects of surface impurities would be exaggerated for materials with higher surface roughness and higher local surface areas, which provide more sites for initiation of instability.

With regard to the lower oxygen content of E110 as compared to M5, the Russian program found that E110 heats with oxygen content as high as 0.11 wt.% exhibited early breakaway oxidation. In a study performed by the Bochvar Institute and TVEL [25], E110 heats with as much as 0.13 wt.% oxygen showed early breakaway oxidation and hydrogen pickup at oxidation temperatures as high as  $1100^\circ\text{C}$ .

Argonne performed scanning electron microscopy (SEM) and transmission electron microscopy (TEM) with E110 and M5 samples to determine if there were significant differences in grain size, in Zr(Nb, Fe, Cr) precipitate size and distribution, and in Zr-Nb precipitate size and distribution. The E110 grain size was determined by SEM to be 4.7  $\mu\text{m}$ , which is within the acceptable range for M5 (3-5  $\mu\text{m}$ ). The E110 Nb-Fe-rich precipitates were found to be  $>100$  nm, which is consistent with the 100-200 nm reported by Mardon et al. [6] for M5 and measured by ANL. The E110 Nb-rich precipitates were determined to be  $\approx 40$  nm, which is consistent with the 50 nm reported by Mardon et al. [6] for M5 and measured by ANL. A non-uniform cluster of precipitates was found in one location of an E110 TEM sample, while Mardon et al. [6] reported uniform distribution of such precipitates. However, given the very small size of the TEM sample area examined, such non-uniform clusters may not be characteristic of the bulk of E110 tubing and cladding.

Within the limits of what ANL did measure for E110 and M5 alloys, no differences could be found in the characterization to explain the differences in LOCA performance. However, because the early breakaway oxidation could be due to surface as well as bulk effects, ANL tested several surface-modified types of E110: as-received tubing, polished tubing, machined-and-polished tubing, tubing etched in an acid bath containing HF, and cladding that was etched and anodized. The outer surfaces of the as-received (a), polished (b), and etched (c) tubing samples are shown in Figure 83 at low magnification (50X). Figure 83a shows the rough surface of as-received tubing. The tubing exhibited longitudinal and circumferential scratches, as well as high surface roughness. Figure 83b shows the outer surface of polished and machined-and-polished E110 tubing with a reduced roughness of 0.14  $\mu\text{m}$ . Polishing also removed some of the surfaces scratches. Figure 83c shows the outer surface of a sample etched in an HF-containing solution (13.5% HF + 13.5%  $\text{HNO}_3$  + 40%  $\text{C}_3\text{H}_6\text{O}_3$  + 33%  $\text{H}_2\text{O}$  for 30 s). The surface roughness appears to have decreased, but the longitudinal and axial scratches are more readily observed. Preferential etching may have widened and deepened these scratches.

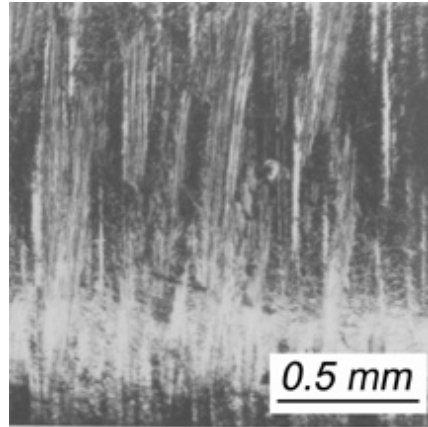


Figure 83a. Outer surface of E110 tubing in the as-received condition (0.35- $\mu\text{m}$  surface roughness). Axial direction is left to right.

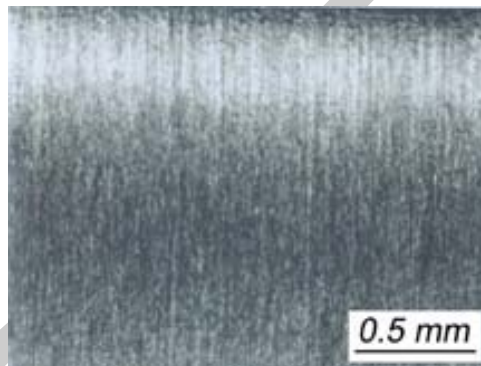


Figure 83b. Outer surface of E110 tubing in the polished condition (0.14- $\mu\text{m}$  outer-surface roughness). Axial direction is left to right.

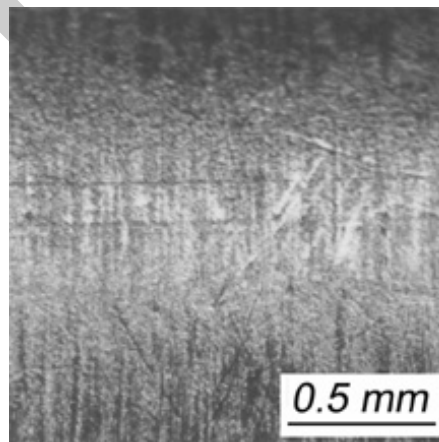


Figure 83c. Outer surface of E110 tubing following etching in HF-containing pickling solution. Axial direction is left to right.

## As-fabricated E110 tubing and cladding oxidized at 1000°C

Because the results of the Russian program indicated very early breakaway at 1000°C oxidation temperature, testing at ANL focused on this temperature. The thermal benchmark for the 1000°C tests is shown in Figure 84. The ramp time from 300°C to 1000°C is 75 s. Hold times of 5 s to 1350 s were investigated. The reference hold time for most tests was 290 s. Table 38 summarizes the test conditions and observations for the more interesting tests conducted with as-received E110 tubing.

Test EU#10 was conducted to observe the behavior of the outer-surface oxide layer following the ramp to 1000°C. The hold time at 1000°C was only 5 s. Although the outer-surface oxide layer appeared to be lustrous black (see Figure 85a), higher magnification images revealed the presence of white or "gray" spots ( $\leq 50\text{-}\mu\text{m}$  diameter) and streaks within the lustrous black matrix (see Figure 85b). It is assumed that these spots and streaks represent monoclinic oxide in a tetragonal matrix. Such behavior was not observed for any other cladding alloy tested. The white spots are not observed until much later times for polished E110 samples.

Test EU#9 was the thermal benchmark test with thermocouples (TCs) welded directly onto the E110 tubing. The TCs resulted in an abrupt change in geometry – much like the change at the ends of the sample – at the cladding surface, which can alter the stress state and induce early breakaway oxidation. This sample had a larger area of gray monoclinic oxide on the outer surface (see Figure 86) than the EU#12 sample (see Figure 87a), which had no welded TCs on the sample. Metallography of the cross section (see Figure 87b) shows that some of the oxide layer has already experienced delamination after only 290-s hold time for the companion EU#13 sample. Breakaway oxidation is both local and extensive. Hydrogen appears to be absorbed locally into E110 at breakaway locations, but it does not have time to diffuse and homogenize during the short hold time at temperature. Sample EU#11 was oxidized at 950°C for 290-s hold time. Breakaway oxidation is evident in Figure 88.

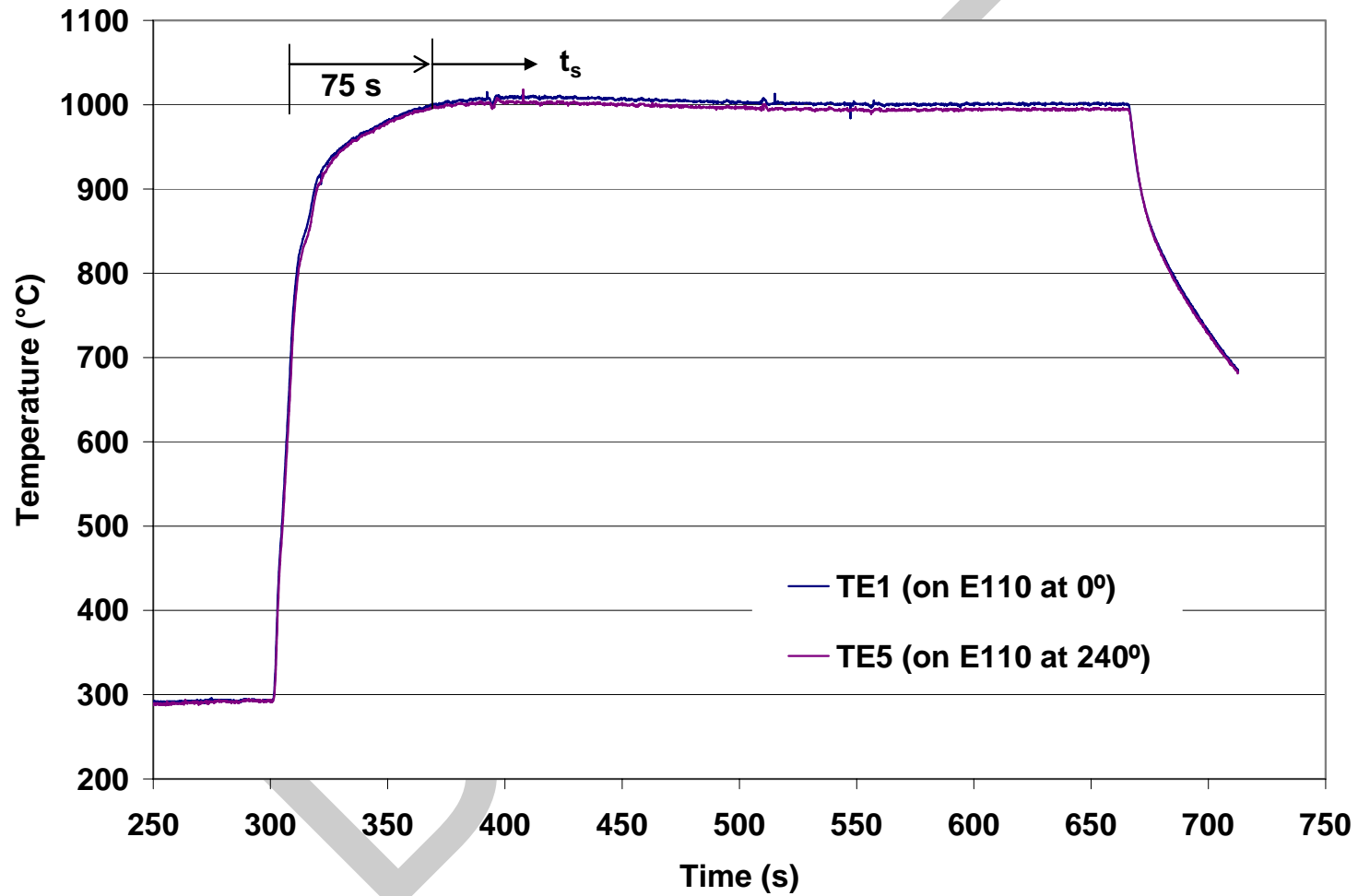
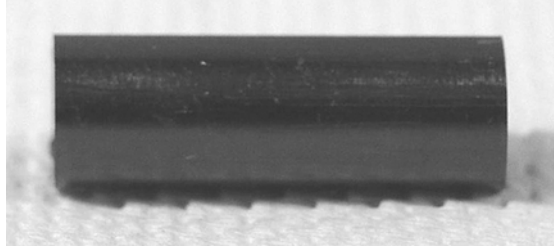


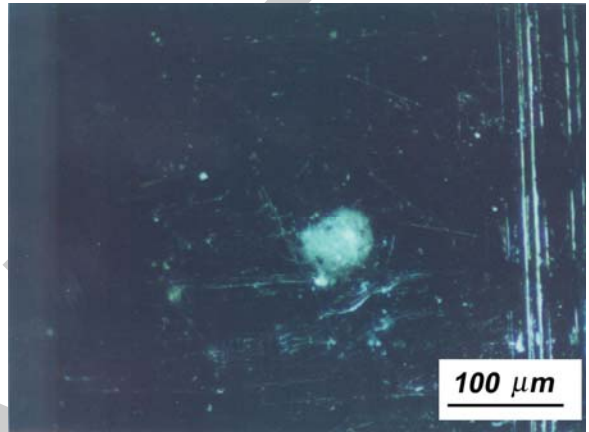
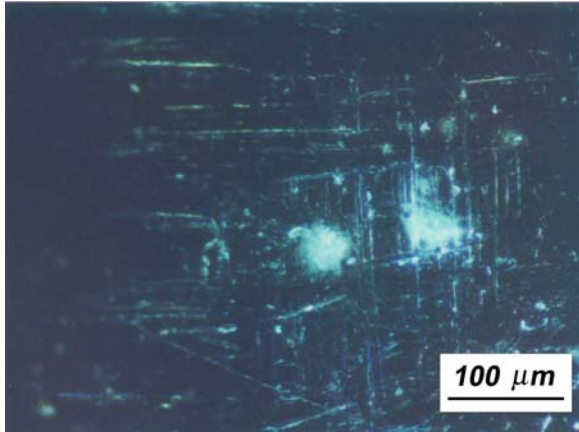
Figure 84. Thermal benchmark results for as-received E110 tubing and cladding oxidized in steam at 1000°C. Ramp time is 75 s.

Table 38 Two-Sided Steam Oxidation Tests Conducted at 1000°C with As-received E110 Tubing. Cladding dimensions are 9.17-mm OD and 0.71-mm wall thickness; CP-ECR = 1.235 CP-Wg; outer-surface roughness = 0.35  $\mu\text{m}$ ; and sample length =  $\approx$ 25 mm. Hydrogen samples were cut from center (C) and off-center (OC) sample locations. Note that Test EU#11 was conducted at 950°C.

Test ID#	Hold Time, s	Total Time, s	CP-ECR, %	H Content, wppm	Sample Condition Observations
EU#10	5	80	1.8	---	Black oxide layer (Fig. 85a); white spots $\leq$ 50 $\mu\text{m}$ (Fig. 85b)
EU#9	290	365	5.0	---	Extensive monoclinic oxide around welded TCs (Fig. 86)
EU#12	290	365	5.0	120 $\pm$ 45 (C)	Nonuniform oxide (Fig. 87a)
EU#13	290	365	5.0	---	Half the sample was as-fabricated; oxide delamination (Fig. 87b)
EU#11	290 at 950°C	365	<5	---	Oxide surface (Fig. 88) may be worse than EU#12 sample
EU#36	395	470	5.8	7 $\pm$ 3 (C) 44 $\pm$ 7 (OC)	Nonuniform oxide layer
EU#38	625	700	7.1	80 $\pm$ 40 (C) 90 $\pm$ 90 (C) 420 $\pm$ 160 (OC)	Significant axial distribution of hydrogen content (Fig. 89)
EU#40	825	900	8.1	540 $\pm$ 80 (C) 1430 $\pm$ 110 (OC)	Delamination-spallation from half the sample
EU#8	1350	1425	10.4	4230 $\pm$ 250 (C)	Extensive delamination-spallation (see Fig. 90)



(a)



(b)

Figure 85. As-fabricated E110 tubing oxidized in steam for a 75-s ramp from 300°C to 1000°C, followed by a 5-s hold at 1000°C and slow cooling: (a) low magnification of lustrous black outer surface oxide and (b) higher magnification of outer surface oxide showing white spots and streaks believed to be monoclinic oxide and oxide-instability initiation sites.

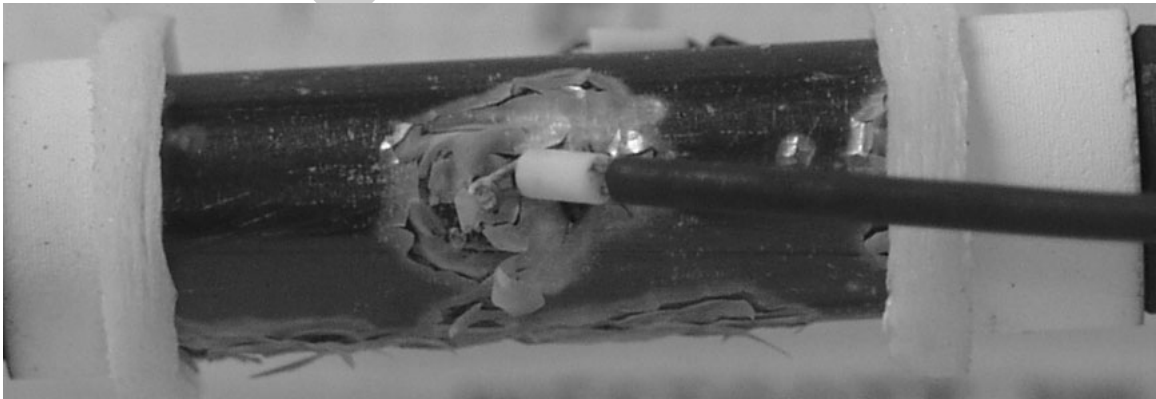
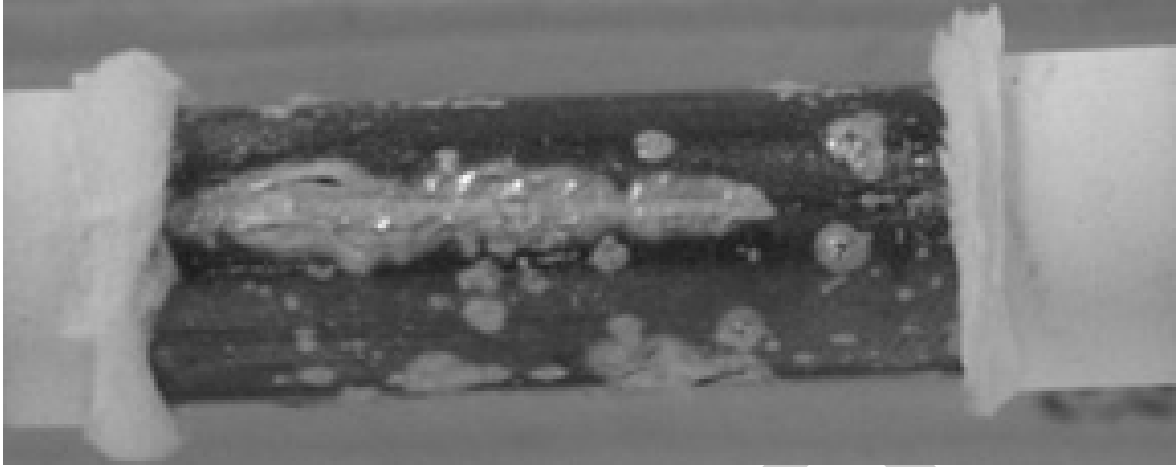
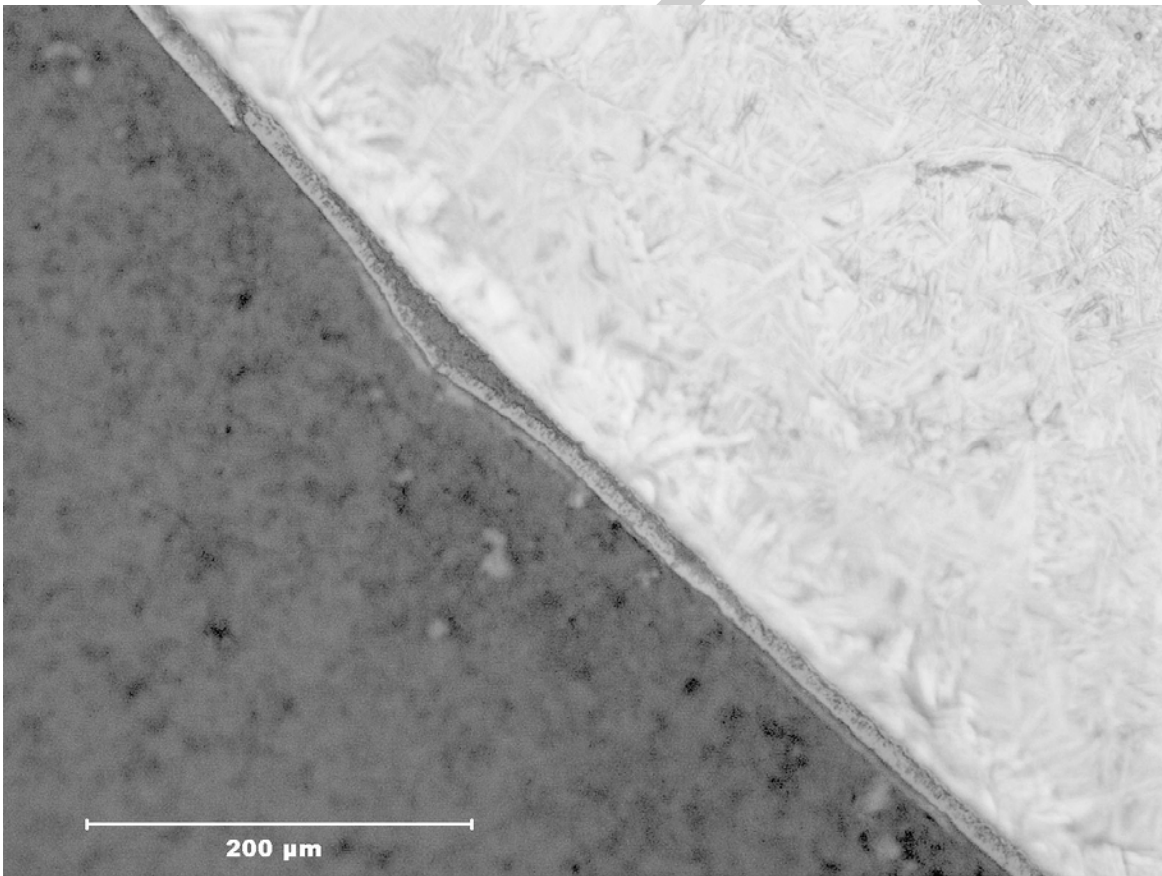


Figure 86. As-fabricated E110 thermal-benchmark (EU#9) sample showing excessive monoclinic oxide formation around the welded thermocouple after 290-s hold time at 1000°C.



(a)



(b)

Figure 87. As-fabricated E110 sample oxidized in steam for a hold time of 290 s at 1000°C: (a) low magnification image of breakaway oxidation on the outer surface oxide of EU#12 sample and (b) higher magnification image of delaminated outer-surface oxide layer on EU#13 sample.

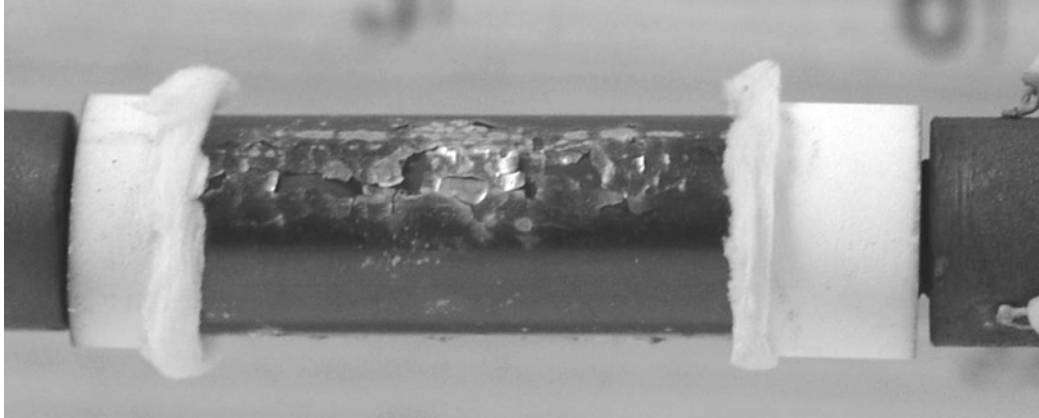


Figure 88. EU#11 sample oxidized for a hold time of 290 s at 950°C. Breakaway oxidation is as extensive as for the EU#12 sample oxidized for the same hold time at 1000°C.

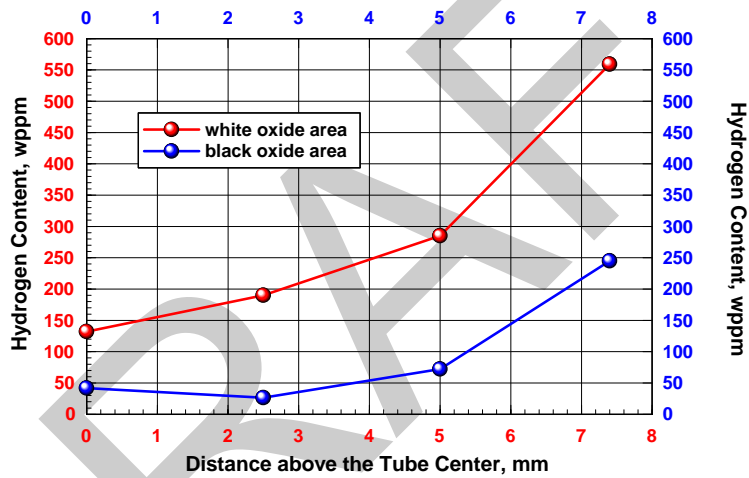


Figure 89. Hydrogen content distribution in E110 after oxidation Test EU#38 with as-fabricated E110 exposed to steam at 1000°C for a hold time of 625 s ( $\approx 7\%$  CP-ECR).

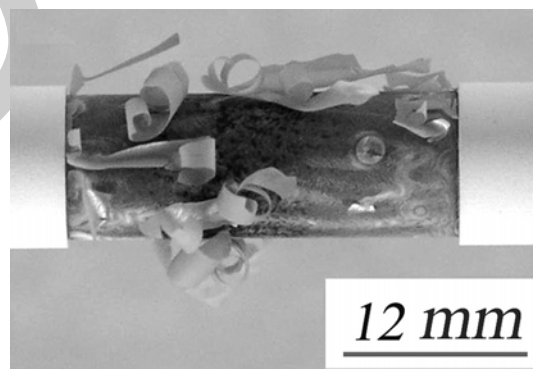


Figure 90. EU#8 sample oxidized for a hold time of 1350 s at 1000°C. Breakaway oxidation, delamination, and spallation are evident. The hydrogen pickup was  $\approx 4200$  wppm.

Sample EU#36 had a hold time of 395 s at 1000°C. However, breakaway was less extensive than for the 290-s hold-time sample. Thus, the hydrogen pickup was low at the sample midplane and <50 wppm in the regions between the midplane and the ends of the sample. These results confirm that breakaway oxidation is an instability phenomenon with variation in the extent of breakaway vs. hold-time at temperature. At the longer hold time of 625 s, sample EU#38 picked up a significant amount of hydrogen. The midplane of the sample had local hydrogen readings ranging from very low values to ≈180 wppm, with the low values occurring under black oxide and the higher values occurring under regions of gray oxide. At the off-center locations, the hydrogen pickup was much higher (420±160 wppm). Even for a longer hold time (625 s), hydrogen does not diffuse enough to homogenize the concentration. Figure 89 shows the axial variation of hydrogen content for the EU#38 test sample.

Samples with hold times of 825 to 1350 s experienced significant oxide delamination and spallation, as well as significant hydrogen pickup. The hydrogen concentration was still highly non-uniform after 825 s, but it was both high and homogeneous after a 1350-s hold time at 1000°C. The 1350-s sample (EU#8) is shown in Figure 90.

Some of the 1000°C-oxidized samples were sectioned into 8-mm-long rings and ring-compressed at RT. The results are summarized in Table 39. The ductile-to-brittle transition CP-ECR was in the range of 6-7% (see Figure 91). The corresponding embrittlement hold time at 1000°C is  $500 \pm 100$  s, with total test times including the ramp from 300°C of  $575 \pm 100$  s. For E110 oxidized under these conditions, embrittlement occurs with hydrogen contents >200 wppm. However, there was significant circumferential and axial variation in hydrogen content (25-560 wppm) for the embrittled sample at ≈7% CP-ECR. Thus, a precise determination between H content and embrittlement could not be made for these samples.

#### Effects of etching E110 tubing prior to oxidizing at 1000°C

The results in Figure 85 suggest that surface and substrate impurities may serve as initiation sites for E110 breakaway oxidation. E110 tubing is pickled and anodized to produce cladding with an increased surface hardness to make it more scratch resistant. The specific acid mixture and pickling time used by TVEL are proprietary. However, based on the Russian program tests and one test conducted by ANL with E110 cladding oxidized at 1100°C for ≈500 s, the extent of outer-surface breakaway oxidation was comparable for the cladding and the tubing.

In an effort to determine the effects of pickling (etching) on breakaway oxidation, E110 tubing was exposed to two types of acid-bath mixtures prior to cleaning and oxidation: (a) a solution used by ANL to clean steel and vanadium surfaces (30-s exposure to 13.5% HF + 13.5% HNO<sub>3</sub> + 40% C<sub>3</sub>H<sub>6</sub>O<sub>3</sub> + 33% H<sub>2</sub>O) and (b) a solution used to etch Zry-2 cladding in the 1980s (180-s exposure to 3.5% HF + 45% HNO<sub>3</sub> + 51.5% H<sub>2</sub>O). Samples were then cleaned and oxidized at 1000°C for a hold time of 290 s. Both (a) and (b) resulted in extensive monoclinic oxide formation and breakaway oxidation of the E110 outer-surface oxide. The results suggest that E110 oxidation behavior is very sensitive to sub-micron-deep F impurities. Figure 92a shows the silver-gray appearance of the outer surface following etching with solution (b) and oxidation. Figure 92b shows the partial, but extensive breakaway oxidation of polished-and-etched (b) E110. Figure 92c shows the lustrous black appearance of an E110-tubing sample that was etched with (b) and then polished. The results of this limited study suggest that pickling (etching) E110 with an acid solution containing HF can promote earlier and more extensive breakaway oxidation, while polishing the sample following etching appears to remove the sub-micron-deep layer containing F impurities.

Table 39 Ring-Compression Test Results for E110 Samples Oxidized at 1000°C and Slow Cooled. Tests were performed on 8-mm-long samples at RT and 0.0333-mm/s displacement rate.

Test ID	Hold Time, s	Total Time, s	ECR, % CP-Model	H Content (Variation), wppm	RT Offset Displacement, mm	RT Offset Strain, %
E110	0	0	0	3	6	66
EU#10	5	80	1.8	---	6.05	66
EU#9	290	365	5.0	---	---	---
EU#12	290	365	5.0	120 (70-170)	5.44	59
EU#36	395	470	5.8	32 (4-84)	5.82	63
EU#38	625	700	7.1	275 (25-560)	0.13	1.4 (brittle)
EU#40	825	900	8.1	925 (440-1500)	0.04	0.4 (brittle)

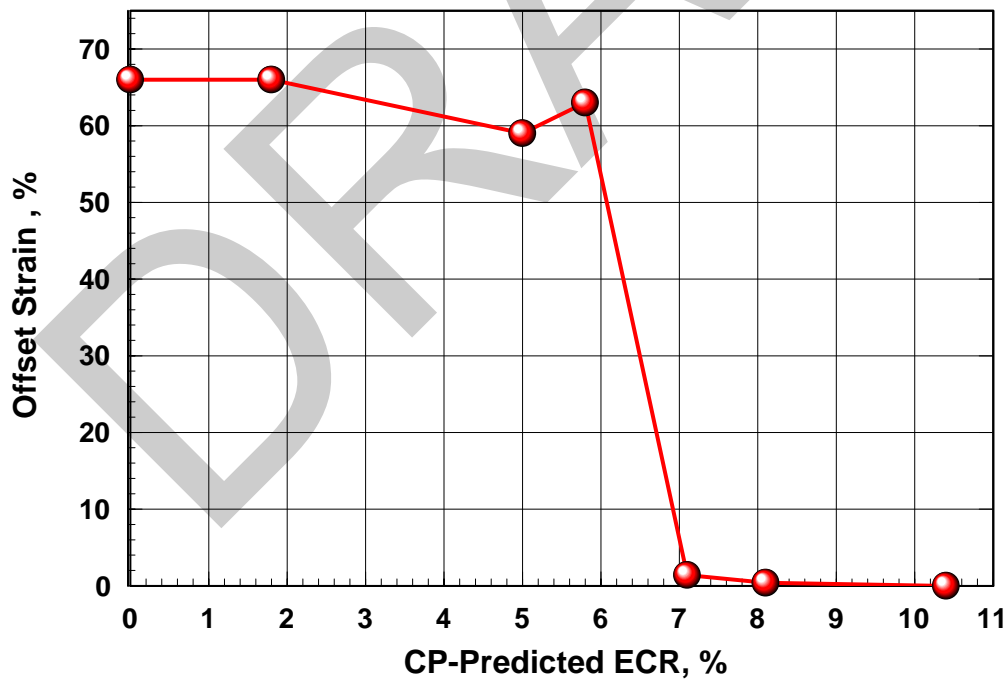
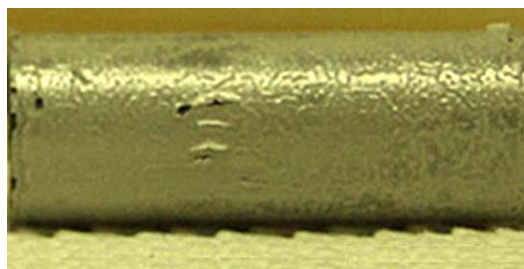
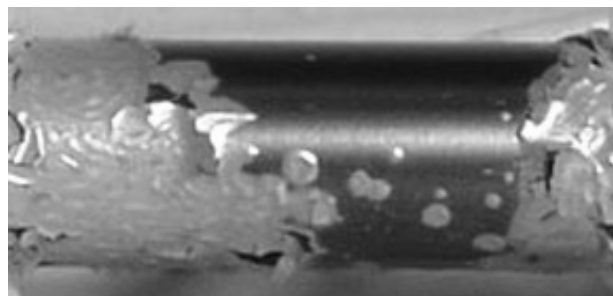


Figure 91. Room-temperature offset strain vs. CP-ECR of as-fabricated E110 tubing oxidized (two-sided) in steam at 1000°C for hold times of 0-825 s. Sample length is 8 mm, and displacement rate is 0.0333 mm/s. Embrittlement is due to excessive hydrogen pickup (>200 wppm).



(a)



(b)



(c)

Figure 92. The effects of pickling (etching) E110 tubing prior to oxidation at 1000°C for 290 s: (a) etched (180-s exposure to 3.5% HF + 45% HNO<sub>3</sub> + 51.5% H<sub>2</sub>O) tubing sample; (b) polished-and-etched E110 sample; and (c) etched-and-polished E110 sample.

### Effects of polishing and machining-and-polishing E110 tubing prior to oxidizing at 1000°C

In Test EU#13, half of the sample was in the as-fabricated condition, and half the sample was machined on the outer surface (38 μm removed) and polished. The hybrid sample was oxidized at 1000°C for 290-s hold time. Based on visual inspection, the oxide on the machined-and-polished segment is lustrous black, while the non-treated segment shows the mix of grayish-white (monoclinic oxide) regions in a matrix of black (tetragonal) oxide observed in all other tests with as-received E110 (see Figure 93).

Test EU#14 was conducted to determine the relative benefits of polishing vs. machining-and-polishing on E110 steam-oxidation performance. The hybrid sample consisted of three axial regions: a) one-half-segment prepared by machining (25 μm removed) and polishing; b) one-quarter-segment prepared by polishing only; and c) one-quarter-segment of as-fabricated E110 tubing. This hybrid sample was also oxidized at 1000°C for 290-s hold time. As shown in Figure 94, both the polished-only and the machined-and-polished regions of the sample exhibited lustrous black outer-surface oxides, while the as-fabricated region exhibited breakaway oxidation. From Figure 94, it appears that polishing alone is sufficient to improve the behavior of E110. Polishing smoothes out the surface roughness by removing <5 μm of material and chemical impurities at the surface and in the substrate.

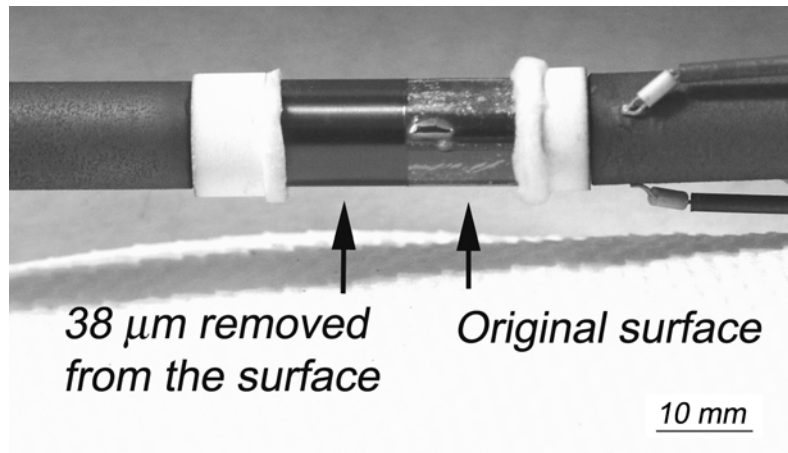


Figure 93. Hybrid E110 sample (EU#13) following oxidation at 1000°C for 290 s. Machined-and-polished section is lustrous black, while as-fabricated E110 section is in breakaway oxidation.

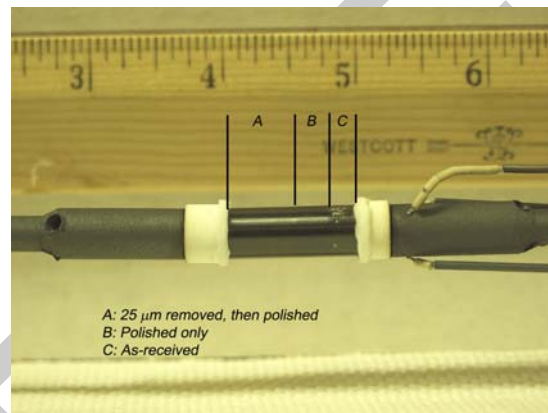


Figure 94. Effects of polishing vs. machining-and-polishing on E110 oxidation at 1000°C for 290 s.

To further investigate the effects of polishing and machining-polishing, higher (200X) magnification photographs were taken of the surfaces of the three regions of the EU#14 sample. Figure 95a shows the outer surface of the as-fabricated material after oxidation with large regions of monoclinic (light-colored) oxide. Figure 95b shows the same magnification of the machined-and-polished outer surface after oxidation with very small, isolated spots of monoclinic oxide. The largest spot diameter in the image is  $\approx 25 \mu\text{m}$ . Figure 95c shows the same magnification of the polished outer surface after oxidation with small – compared to the as-received material – spots of monoclinic oxide. The largest spot diameter in Figure 95c is  $\approx 75 \mu\text{m}$ .

It is clear that the quality of the oxide layer on the polished surface is much better than the as-fabricated tubing surface. This observation suggests that the oxidation behavior of the E110 alloy is sensitive to some combination of surface roughness and surface chemistry. Further improvement may be made by removing some of the near-surface layer, as well as the surface itself. Worth noting is that the untreated inner surface of the whole sample had large regions of monoclinic oxide visible to the eye.

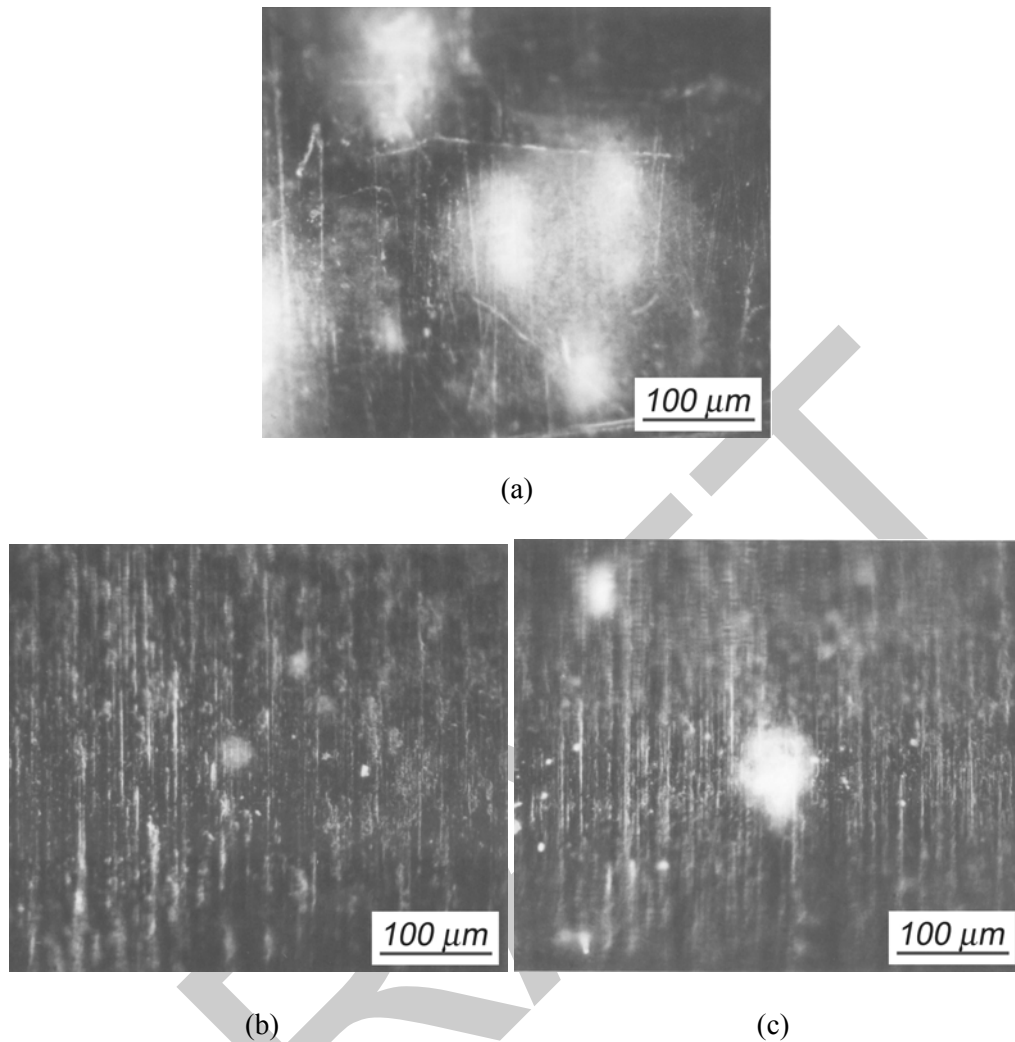


Figure 95. High magnification (200X) image of outer-surface oxide layers following oxidation at 1000°C for 290 s: (a) as-fabricated E110, (b) machined-and-polished E110, and (c) polished E110.

To better compare the E110 oxidation performance to the performance of Western alloys, E110 samples were modified to give the same wall thickness ( $\approx 0.6$  mm) and comparable outer-surface roughness as M5 (see Table 5). The ANL-modified E110 was fabricated by machining about 100  $\mu\text{m}$  from the inner-surface wall, polishing the inner surface, and polishing the outer surface to a roughness level of 0.14  $\mu\text{m}$ . Oxidation tests of these samples were designed to determine breakaway oxidation time in terms of outer-surface oxide appearance and hydrogen pickup. The thermal benchmark results for the M5 oxidation tests were used to plan and interpret the E110 tests (see Figure 63). The E110 results are summarized in Table 40. Not included in Table 40 are tests conducted for 0 to 190-s hold times for which the samples were lustrous black with no hydrogen pickup.

For the machined-and-polished samples, breakaway oxidation initiated at the ends of the sample and progressed towards the middle (Figure 96). Longer breakaway oxidation times could possibly have been achieved with longer, more continuous samples without abrupt changes in geometry (e.g., ends of 25-mm-long ANL samples). However, polishing of the E110 surfaces did significantly delay breakaway

Table 40 Two-Sided Oxidation Tests Conducted on Modified E110 Cladding at 1000°C. Samples had polished cladding outer diameter (9.17 mm), machined and polished inner diameter (7.98 mm), and 0.6-mm wall thickness.

Test ID#	Hold Time, s	Total Time, s	H Content, wppm	Outer-Surface Oxide
EU#22	292	382	---	Lustrous black
EU#24	413	503	11±5	Lustrous black with white ends
EU#37	815	905	6±1	---
EU#16	1025	1115	150 (32-342)	See Figure 96 for variation in outer surface oxide layer
EU#41	2025	2115	1280±100	---

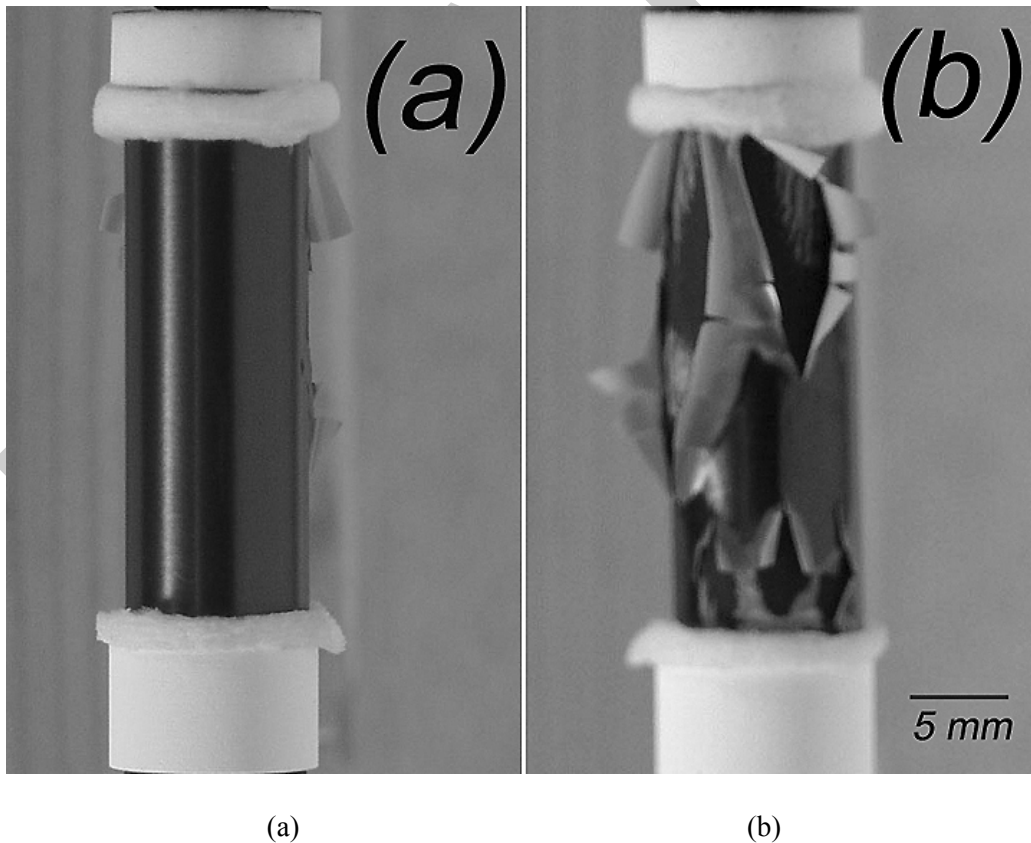


Figure 96. Machined-and-polished E110 sample (EU#16) after 1025-s hold time in steam at 1000°C: (a) lustrous black oxide surface on the other side of the sample and (b) extensive monoclinic oxide formation, delamination, and spallation evident on one side of the sample.

oxidation time in terms of hydrogen pickup. Figure 97 shows the hydrogen pickup vs. time for as-fabricated E110 samples vs. ANL-modified (OD polishing, ID machining-and-polishing) E110 samples. The breakaway oxidation time was essentially double for the polished E110 as compared to the as-fabricated E110 tubing.

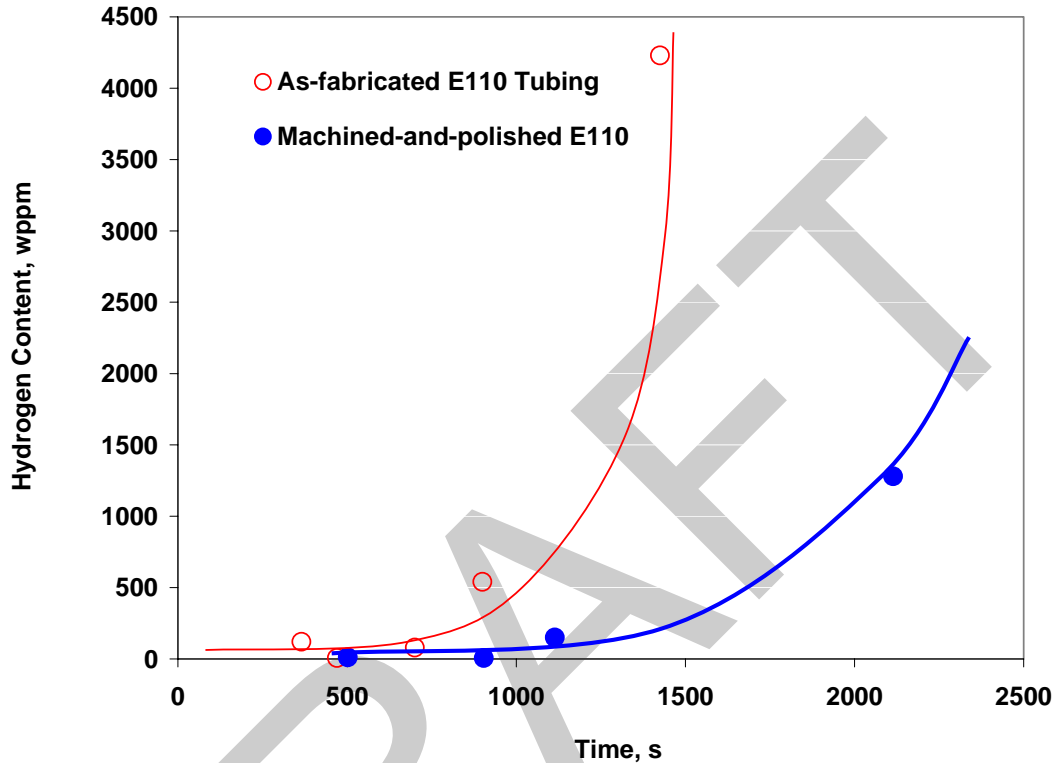


Figure 97. Hydrogen pickup vs. total test time for as-fabricated E110 tubing and ANL-modified machined-and-polished E110. The ramp time from 300°C to 1000°C is 75 s for the as-fabricated tubing (0.70-mm wall) and 90 s for the machined-and-polished samples (0.6-mm wall).

#### Effects of machining-and-polishing E110 tubing prior to oxidizing at 1100°C

A series of tests was conducted with ANL machined-and-polished E110 samples oxidized at 1100°C to determine post-oxidation ductility vs. CP-ECR. The M5 thermal benchmark results for 1100°C were used to plan these E110 tests and interpret the results (see Figure 64). All samples exhibited a lustrous black oxide layer up to the highest hold time (1011 s) at 1100°C. At this hold time, small white spots were observed on the outer-surface oxide layer.

The investigation of ANL-modified post-oxidation ductility was motivated by the results of Bochvar-Institute/TVEL work [25] for the RT ring-compression ductility of seven lots of E110, with varying concentrations of Hf, Fe, and O (all within material specification ranges), as well as different combined impurity levels (Ni, Al, Si, Ca, K, F, Cl, Na, and Mg). The E110 tubing used in the Bochvar/TVEL study had an outer diameter of 9.13 mm after “pickling.” Although not specified, the tubing wall thickness was assumed to be 0.71 mm. It is not clear whether or not the tubing was anodized – standard procedure to convert tubing into cladding – following pickling. For these tests, 30-mm-long tubing segments were exposed to two-sided steam oxidation for 600 s. Both heating (300°C to 1100°C in

≈2 s) and cooling (1100°C to 300°C in 15-20 s) rates were relatively high. The corresponding CP-ECR is 12% for 0.71-mm-wall cladding oxidized (two-sided) to 1100°C for 600 s.

Four of the Bochvar-TVEL lots with a combined impurity level of 110-135 wppm exhibited outer-surface breakaway oxidation, high hydrogen pickup (200-600 wppm), and low RT ring-compression ductility (<5%). Three of the lots with combined impurity levels of 25-45 wppm exhibited stable oxide growth (observed at low magnification), lower hydrogen pickup (60-200 wppm), and higher RT ring-compression offset strain (5-10%). Based on ANL experience with the effects of surface finish (polishing vs. pickling), we hypothesized that the Bochvar-TVEL samples would have exhibited longer-time stable oxide growth, lower hydrogen pickup, and higher ductility if the surfaces had been polished rather than pickled. To test this hypothesis, ANL machined-and-polished (M-P) samples were oxidized at 1100°C and subjected to RT ring-compression tests. The results of these tests are compared to the best of the Bochvar-TVEL results (Lots 2-4) in Table 41 and Figure 98.

Table 41 Comparison of E110 Post-Oxidation RT Ductility between ANL Machined-and-Polished (M-P) Cladding Samples and Bochvar-TVEL (BT) Lots 2-4 Pickled Cladding Samples [25] Following Two-sided Steam Oxidation at 1100°C.

E110 Material	Wall Thickness, mm	CP ECR, %	Meas. ECR, %	Offset Displacement, mm	Offset Strain, %
ANL M-P	0.61	7.5	7.0	5.47	60
ANL M-P	0.69	10.5	9.2	2.86	31
BT Lot 2	0.71	12	≈10	---	10
BT Lot 3	0.71	12	≈10	---	6.6
BT Lot 4	0.71	12	≈10	---	4.4
ANL M-P	0.58	14.4	12.7	1.94	21
ANL M-P	0.58	19.4	16.0	0.58	6.3

Significantly higher post-oxidation ductility was achieved by machining the inner surface to give a wall thickness comparable to M5 and by polishing both inner and outer surfaces. The Bochvar-TVEL samples, which were pickled rather than polished, may have exhibited higher post-oxidation ductility if the surfaces had been polished following pickling or if the surfaces had not been pickled at all. Also, the machined-and-polished E110 post-oxidation ductility results for 1100°C-oxidized samples are comparable to the results obtained for the modern 17×17 alloys (Zry-4, ZIRLO, and M5) used in U.S. reactors.

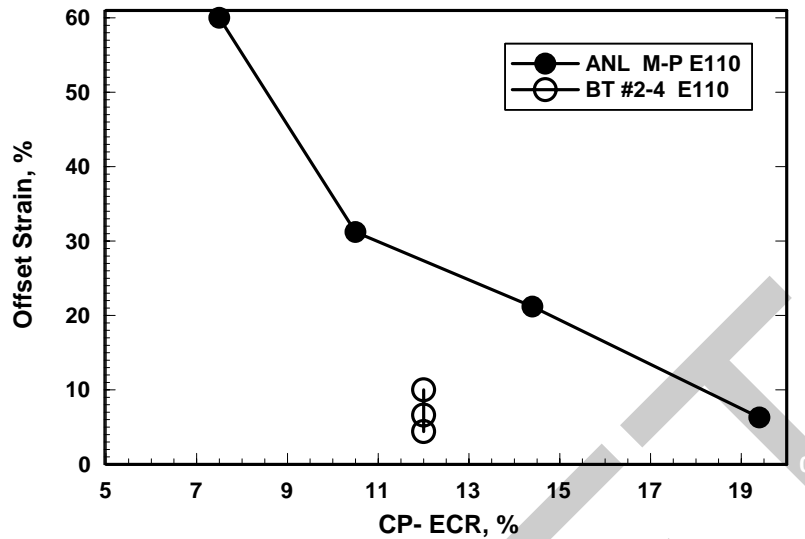


Figure 98. Post-oxidation RT ductility vs. CP-ECR for ANL machined-and-polished (M-P) E110 samples and Bochvar-TVEL (BT) pickled E110 cladding following two-sided steam oxidation at 1100°C.

#### Effects of machining-and-polishing E110 tubing prior to oxidizing at 1200°C

Machined-and-polished E110 samples were oxidized at 1200°C, slow-cooled, and ring-compressed at 135°C. Because the ductility of the ANL-modified E110 was so good following 1100°C, the 1200°C-oxidized samples were tested to see how they compared to the U.S. alloys. The 1200°C thermal benchmark results for M5 (see Figure 72) were used to plan the tests and interpret the results. Table 42 summarizes the results for the oxidation levels and ring-compression offset strains for these E110 samples.

Table 42 Post-oxidation Ductility at 135°C for ANL Machined-and-Polished E110 Samples following Oxidation at 1200°C and Slow Cooling. Samples were fabricated from E110 cladding (etched and anodized); polished outer diameter (9.07 mm), machined-and-polished inner surface, and 0.6-mm wall thickness.

E110 Test #	Wall Thickness, mm	CP ECR, %	Meas. ECR, %	Offset Displacement, mm	Offset Strain, %
EU#53	0.60	7.5	8.6	>5	>55
EU#51	0.60	10.0	10.4	>5	>55
EU#52	0.61	13.0	13.8	1.47	16
	0.61	13.0	13.8	0.66	7

The ductility of ANL-modified E110 oxidized at 1200°C is higher than that of HBR-type 15×15 Zry-4 and modern 17×17 Zry-4 cladding for ≤13% CP-ECR. The post-oxidation ductility of ANL-modified E110 (12%) is comparable to that of 17×17 M5 (14%) at 13% CP-ECR. The ductile-to-brittle transition CP-ECR for ANL-modified E110 was not determined in this program.

### 3.6 Effects quench temperature on post-quench ductility

The protocol for preparing samples for post-quench ductility was the same for 17×17 Zry-4, ZIRLO, and M5: cooling in steam at ≈10-13°C/s from the oxidation temperature to 800°C; and rapid cooling (quench) from 800°C to 100°C. As 800°C is below the (alpha + beta) → alpha phase-transformation temperature for as-fabricated Zry-4, the quench temperature is low enough to allow the phase transformation to occur prior to "freezing" in the microstructure at 800°C. While slower cooling from the oxidation temperature to the quench temperature could result in more redistribution of oxygen between oxygen-rich alpha incursions and low-oxygen beta, there is no clear evidence that this change would affect post-quench ductility. However, for as-fabricated M5 the (alpha + beta) → alpha phase-transformation temperature is ≈650°C. For as-fabricated ZIRLO, this phase transformation temperature is expected to be between 650°C and 800°C. Thus, the phase transformation for M5 and ZIRLO is not complete at the time of the 800°C quench (Q) used in the ANL test program. Additional tests were conducted with samples oxidized at 1200°C. Following cooling at ≈13°C/s to 800°C, samples were further slow cooled (SC) to RT and ring-compressed at 135°C.

#### 3.6.1 Effects of quench temperature on post-quench ductility of 17×17 Zry-4

The post-oxidation ductility results for Zry-4 subjected to slow cooling are presented in Table 43. The slow-cooled samples were oxidized in a separate test train with the thermal history shown in Figure 99. The complete data set presented in Table 11 (Q) is combined with the data set in Table 43 (SC) to generate the graphical results shown in Figure 100 for offset strain vs. CP-ECR.

Table 43 Ring Compression Test Results at 135°C and 0.0333 mm/s for 17×17 Zry-4 Cladding Oxidized at 1200°C and Slow Cooled (SC). ECR = 1.538 Wg for 0.57-mm-wall cladding.

Test Conditions		ECR, %		Plastic Displacement, mm		Plastic Strain, %	
Ox. Test Time, <sup>a</sup> s	Cooling	CP	Meas.	Offset	Permanent	Offset	Permanent
187	SC	13.0	13.2	1.03	---	11	---
187	SC	13.0	13.2	0.61	---	6.5	---
288	SC	17.0	18.5	0.30	0.16	3.2	1.7
288	SC	17.0	18.5	0.12	0.05	1.3	0.5

<sup>a</sup>Includes time for ramp from 300°C and hold time.

At 13% CP-ECR, the slow-cooled Zry-4 samples have an average offset strain of 9% (6.5-11%) as compared to 5.1% for quenched Zry-4. Although ductility apparently increases with slow-cooling at 13% CP-ECR, this effect may be due to data scatter as there is an abrupt decrease in ductility of Zry-4 in the range of 11-15% CP-ECR. At 17% CP-ECR, the ductility strains of the slow-cooled and quenched Zry-4 samples are essentially the same: 2.3% (1.3-3.2%) average offset strain and 1.1% (0.5-1.7%) average permanent strain for slow-cooled Zry-4 samples; and 2.5% (2.0-2.8%) average offset strain and 1.1% (0.7-1.4%) permanent strain for quenched Zry-4. Thus, the ductile-to-brittle transition CP-ECR for 1200°C-oxidized Zry-4 appears to be insensitive to quench at ≤800°C.

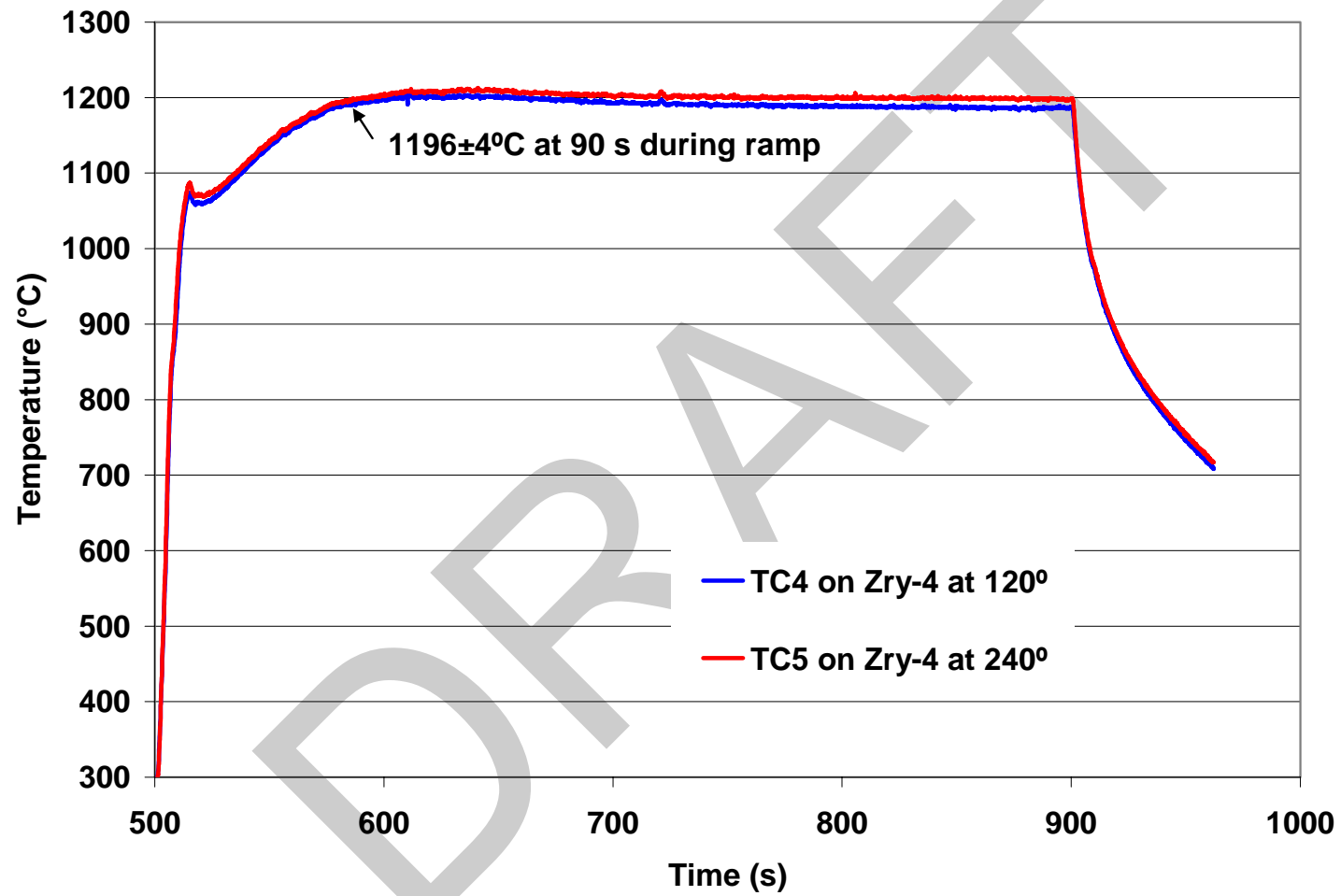


Figure 99. Thermal benchmark test results for slow-cooled 17×17 Zry-4, ZIRLO, and M5 samples oxidized at 1200°C.

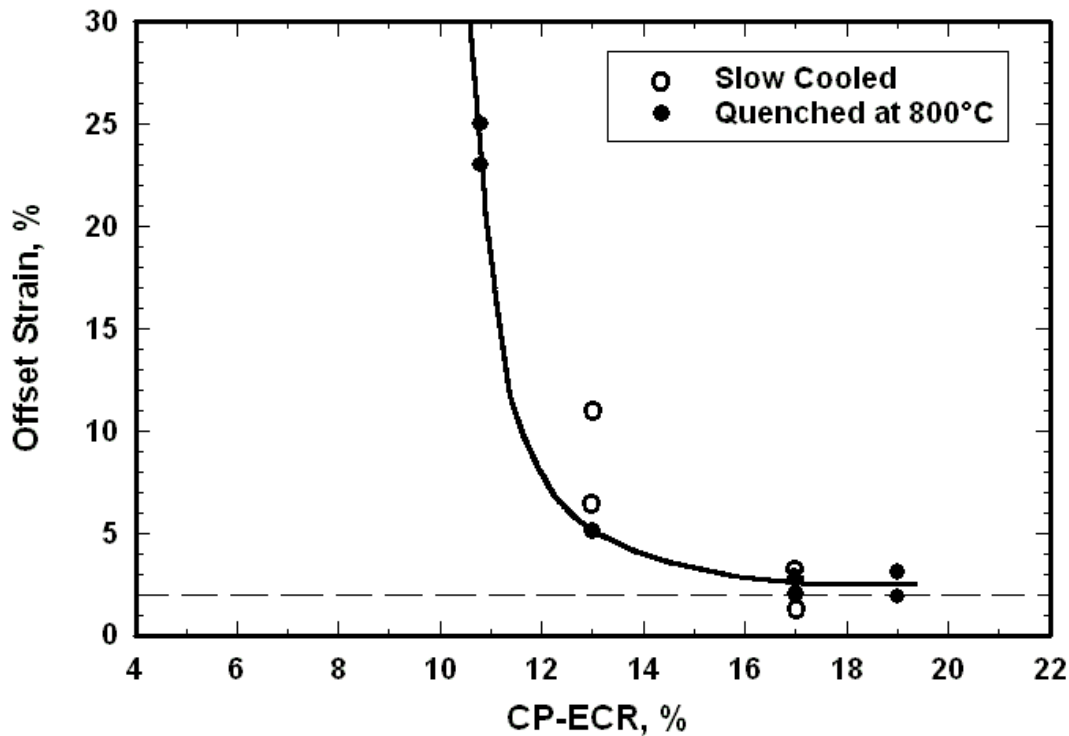


Figure 100. Effects of quench vs. slow cooling on the post-oxidation ductility of 17×17 Zry-4 (0.57-mm wall) oxidized at 1200°C, cooled at ≈13°C/s to 800°C, and either quenched at 800°C or slow cooled from 800°C to RT. Ring-compression tests were performed at 135°C and 0.0333-mm/s displacement rate.

### 3.6.2 Effects of quench temperature on post-quench ductility of 17×17 ZIRLO

The post-oxidation ductility results for ZIRLO subjected to slow cooling are given in Table 44. The slow-cooled samples were oxidized in a separate test train with the thermal history shown in Figure 99. The complete data set presented in Table 27 (Q) is combined with the data set in Table 44 (SC) to generate the graphical results shown in Figure 101 for offset strain vs. CP-ECR.

At 13% CP-ECR, the slow-cooled ZIRLO samples have an average offset strain of 9% (8.1-9.3%) as compared to 27% (21-33%) for quenched ZIRLO. This factor of three reduction in ductility for slow-cooled samples appears to be significant. However, at 17% CP-ECR, the ductility of slow-cooled and quenched ZIRLO are within data scatter: 3.6% (2.0-5.5%) average offset strain and 1.5% (1.2-1.8%) average permanent strain for slow-cooled ZIRLO samples; and 5.7% (3.8-7.0%) average offset strain and 2.3% (1.8-2.8%) permanent strain for quenched ZIRLO. Thus, the ductile-to-brittle transition CP-ECR for 1200°C-oxidized ZIRLO appears to be relatively insensitive to quench at ≤800°C. For <17% CP-ECR, slow-cooled ZIRLO samples may have less ductility than quenched samples at the same CP-ECR (e.g., 13%). However, considerably more data would need to be generated to establish such a trend. Also, data points plotted at 10% and 15% CP-ECR were obtained from shorter rings (5-6 mm) cut from the ends of the oxidation-quench sample. These data points may not be as reliable as the ones for 8-mm-long rings sectioned from within the middle 20 mm of the 25-mm-long oxidation-quench sample.

Table 44 Ring Compression Test Results at 135°C and 0.0333 mm/s for 17×17 ZIRLO Cladding Oxidized at 1200°C and Slow Cooled (SC). ECR = 1.538 Wg for 0.57-mm-wall cladding.

Test Conditions		ECR, %		Plastic Displacement, mm		Plastic Strain, %	
Ox. Test Time, <sup>a</sup> s	Cooling	CP	Meas.	Offset	Permanent	Offset	Permanent
187	SC	13.0	13.5	0.77	---	8.1	---
187	SC	13.0	13.5	0.89	---	9.3	---
288	SC	17.0	17.3	0.32	0.17	3.4	1.8
288	SC	17.0	17.3	0.32	0.14	3.4	1.5
288	SC	17.0	17.3	0.52	---	5.5	---
288	SC	17.0	17.3	0.20	0.11	2.0	1.2

<sup>a</sup>Includes time for ramp from 300°C and hold time.

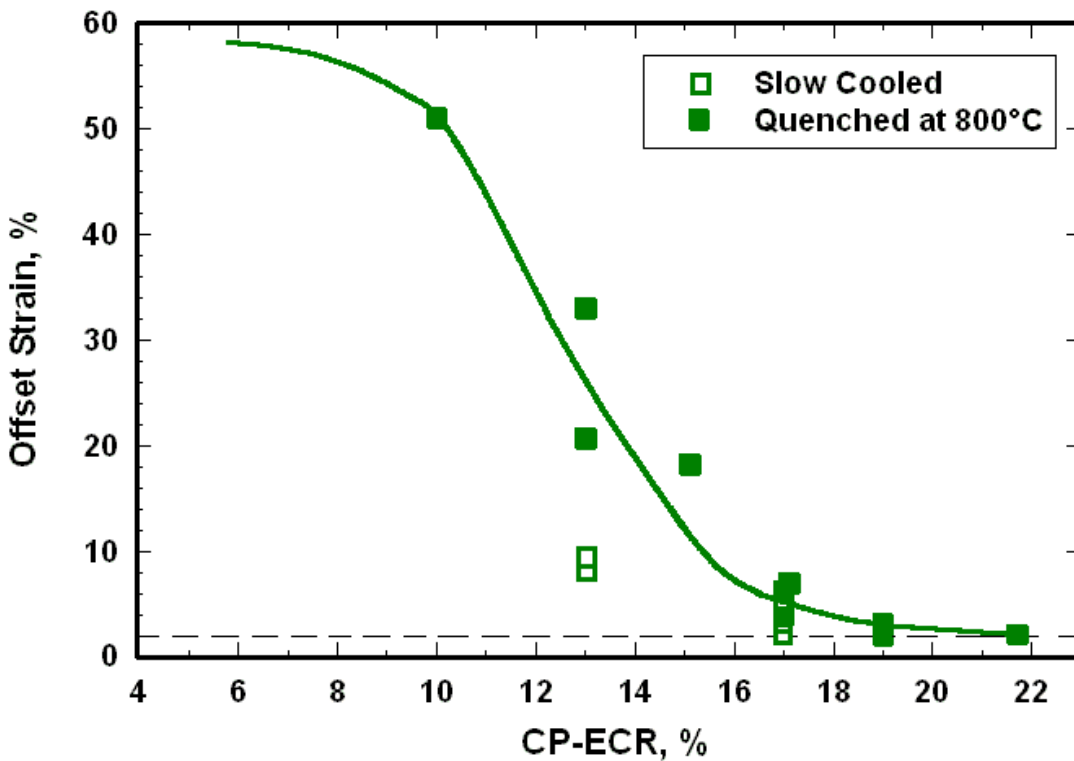


Figure 101. Effects of quench vs. slow cooling on the post-oxidation ductility of 17×17 ZIRLO (0.57-mm wall) oxidized at 1200°C, cooled at ≈13°C/s to 800°C, and either quenched at 800°C or slow cooled from 800°C to RT. Ring-compression tests were performed at 135°C and 0.0333-mm/s displacement rate.

### 3.6.3 Effects of quench temperature on post-quench ductility of 17×17 M5

The post-oxidation ductility results for M5 subjected to slow cooling are given in Table 45. The slow-cooled samples were oxidized in a separate test train with the thermal history shown in Figure 99. The complete data set presented in Table 34 (Q) is combined with the data set in Table 45 (SC) to generate the graphical results shown in Figure 102 for offset strain vs. CP-ECR. The post-oxidation ductility of M5 appears to be insensitive to quench temperatures  $\leq 800^\circ\text{C}$ . The strain data for the slow-cooled samples are within the scatter of the strain data for the samples quenched at  $800^\circ\text{C}$ .

Table 45 Ring-Compression Test Results at  $135^\circ\text{C}$  and  $0.0333\text{ mm/s}$  for  $17\times 17$  M5 Cladding Oxidized at  $1200^\circ\text{C}$  and Slow Cooled (SC). ECR =  $1.437\text{ Wg}$  for  $0.61\text{-mm}$ -wall cladding.

Test Conditions		ECR %		Plastic Displacement, mm		Plastic Strain, %	
Ox. Test Time <sup>a</sup> , s	Cooling	CP	Meas.	Offset	Permanent	Offset	Permanent
192	SC	13.0	13.3	1.54	---	16	---
192	SC	13.0	13.3	1.18	---	13	---
292	SC	16.0	15.6	0.87	---	9.1	---
292	SC	16.0	15.6	0.52	---	5.1	---

<sup>a</sup>Includes time for ramp from  $300^\circ\text{C}$  and hold time.

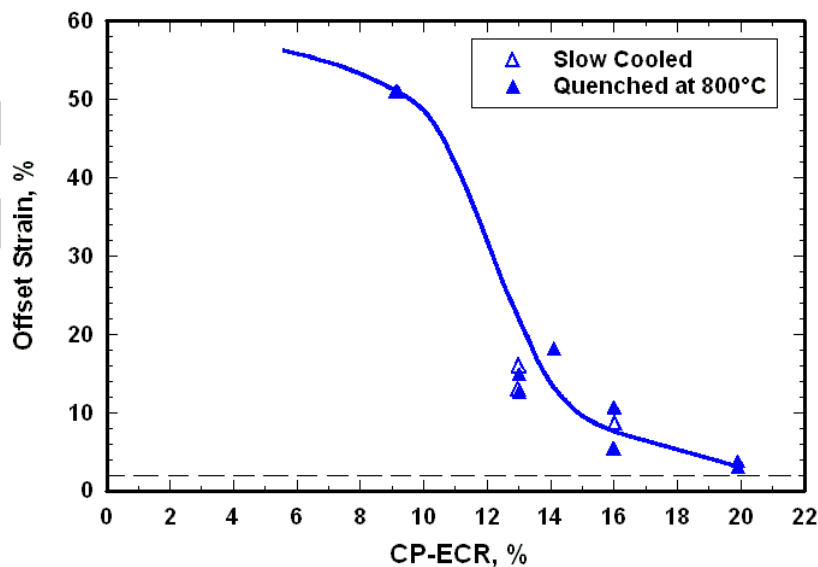


Figure 102. Effects of quench vs. slow cooling on the post-oxidation ductility of  $17\times 17$  M5 ( $0.61\text{-mm}$  wall) oxidized at  $1200^\circ\text{C}$ , cooled at  $\approx 13^\circ\text{C/s}$  to  $800^\circ\text{C}$ , and either quenched at  $800^\circ\text{C}$  or slow cooled from  $800^\circ\text{C}$  to RT. Ring-compression tests were performed at  $135^\circ\text{C}$  and  $0.0333\text{-mm/s}$  displacement rate.

### 3.7 Summary of results for as-fabricated cladding

Modern PWR and BWR cladding alloys are belt-polished on the cladding outer surface to reduce surface roughness to  $\approx 0.1 \mu\text{m}$ . In addition to resulting in a smoother outer surface, the belt-polishing mechanically removes surface and substrate ( $< 0.3 \mu\text{m}$ ) impurities. The cladding inner-surface roughness is also reduced through a variety of techniques, including grit-polishing. Pickling (etching) with an acid mixture containing HF, which was used in the 1970s-1980s to remove surface impurities, is no longer used as a finishing step to convert tubing into cladding. This fabrication change has made the modern alloys more resistant to breakaway oxidation in the temperature range of 800-1000°C. The modern alloys also retain post-quench ductility to higher CP-ECR ( $\geq 17\%$ ) values for oxidation temperatures in the range of 1000-1200°C.

For steam-oxidation temperatures of 1000°C and 1100°C, modern PWR 17×17 alloys (Zry-4, ZIRLO, and M5) retained RT post-quench ductility following two-sided oxidation to 20% CP-ECR, which is the highest oxidation level investigated in the ANL program, and quenching at 800°C. The post-quench ductility of BWR 10×10 Zry-2 was comparable to the PWR alloys following oxidation at 1000°C. Hydrogen pickup for Zry-4, Zry-2, and M5 was very low ( $< 25$  wppm) for samples oxidized to 20% CP-ECR, so hydrogen did not induce embrittlement in these samples. For ZIRLO, hydrogen pickup was low ( $< 20$  wppm) for 1100°C-oxidized samples and  $\approx 100$  wppm for the 1000°C-oxidized sample at 20% CP-ECR ( $\approx 3400$  s). Alloy differences in weight gain vs. time at 1000°C were observed for ZIRLO and M5 as compared to Zry-4. Similar low weight gain, due to the Zr inner liner, was observed for 10×10 Zry-2 cladding. The weight gain for each alloy correlated with the total (OD+ID) oxide layer thickness. However, the post-quench ductility of the four alloys was essentially the same after long-time oxidation at these temperatures and quench. In particular, the low weight gain and ECR (13%) measured for M5 after long-time oxidation at 1000°C did not increase post-quench ductility relative to Zry-4, which exhibited higher weight gain and measured ECR (22%).

For Zry-4, ZIRLO, and M5 oxidized at 1200°C and quenched at 800°C, RT embrittlement was observed at CP-ECR values significantly below 17%. However, when these samples, along with 10×10 Zry-2, were ring-compressed at 135°C, the ductile-to-brittle transition CP-ECR increased to  $\geq 17\%$  (17% for Zry-4, 19% for Zry-2, 19% for ZIRLO, and 20% for M5). Modern 15×15 Zry-4, which was also tested under these conditions, had a ductile-to-brittle transition of 19% CP-ECR. The 17×17 alloys were also tested after cooling from 1200°C with no quench. The slow cooling had no effect on the ductile-to-brittle transition CP-ECR, indicating that lower quench temperatures would not increase ductility. Hydrogen pickup was very low for all three alloys, and the prior-beta layer was thick enough ( $> 0.25$  mm) to preclude hydrogen-induced or beta-layer-thinning-induced embrittlement, respectively. Although the prior-beta-layer microstructures were quite different for ZIRLO and M5, as compared to Zry-4 and Zry-2, post-quench ductility results were comparable and correlated quite well with CP-ECR.

Although two-sided oxidized cladding samples maintain ductility up to 20% CP-ECR following oxidation at 1000°C, the test times are short (3400 s for Zry-4 and ZIRLO, 4100 s for M5) relative to the test times needed to achieve these high CP-ECR levels for one-sided-oxidized cladding. Breakaway oxidation, hydrogen pickup, and embrittlement occur for all Zr-based cladding alloys. However, there is considerable variability in time-at-temperature to initiate this instability and to pick up enough hydrogen to embrittle the cladding. Previous studies have shown minimum breakaway oxidation times, based on weight gain, for Zry-4 oxidized at 800°C and 1000°C. With respect to hydrogen pickup, these studies have also shown that oxidation at 1000°C results in the shortest time to pick up 200-wppm hydrogen relative to other temperatures within the range of 800-1000°C. The ANL criterion for determining breakaway oxidation time is a hydrogen pickup of 200 wppm. It was confirmed that cladding alloys with

200-wppm hydrogen retain ductility at 135°C for these oxidation temperatures. For oxidation temperatures in the range of 950-1000°C, embrittlement occurs at hydrogen levels of 500-700 wppm.

In the ANL test program, two types of Zry-4 cladding alloys were subjected to numerous two-sided-oxidation tests at 985-1015°C to determine breakaway oxidation time: HBR-type 15×15 low-tin Zry-4 and modern belt-polished 15×15 low-tin Zry-4. The differences in the as-fabricated materials were outer-surface roughness (0.32 μm for HBR-type and 0.10 μm for modern Zry-4) and inner-surface finishing (pickled for HBR-type and grit-polished for modern Zry-4). When oxidized in the same test apparatus, the breakaway oxidation time – time to pick up 200 wppm H – for the HBR-type Zry-4 was ≈3800 s, while the breakaway time for the modern Zry-4 was ≈5000 s. Also, the hydrogen pickup rate for HBR-type Zry-4 was much higher than for modern Zry-4. The effects of surface scratches, inadvertently induced during sample sectioning of HBR-type Zry-4, resulted in initiation of breakaway in the scratched region, hydrogen pickup, and ≈200-s reduction in the breakaway time (3600 s vs. 3800 s). For belt-polished 10×10 Zry-2, no breakaway oxidation was observed up to 5000 s in the temperature range of 970-1010 °C. The Zry-2 sample with a 20-μm-deep axial scratch machined into the outer surface showed no signs of breakaway oxidation after 5000 s at 1000°C. For BP 17×17 ZIRLO, breakaway oxidation tests were conducted at 800°C and 950-1015°C. The minimum breakaway oxidation time for ZIRLO was found to occur in the temperature range of 970-985°C: 3000 s for smooth ZIRLO; ≈2800 s for ZIRLO with a 20-μm-deep axial scratch machined into the outer surface; and ≈3300 s for pre-filmed ZIRLO with inner- and outer-oxide layers of <1 μm grown at 360°C. Thus, "normal" surface scratches that may form during handling and loading of rods into assemblies appear to have only a small influence on breakaway oxidation time for the modern alloys.

The Russian Zr-1Nb cladding (E110) was added to the ANL test program to determine why this cladding exhibited such short breakaway oxidation times (500-700 s at 1000°C) as compared to the breakaway oxidation times (>6000 s at 1000°C) for the Zr-1Nb cladding (M5) used in the U.S. The ANL study focused primarily on E110 tubing (0.35-μm surface roughness), although some tests were conducted with pickled-and-anodized E110 cladding (0.19-μm surface roughness). Within the limitations of what ANL could measure and vary, no significant differences were found in chemical composition or microstructure between E110 and M5. Differences in surface roughness, along with possible differences in surface impurities, were considered as plausible reasons for behavior differences. Argonne tests confirmed the poor performance of E110 at 1000°C in terms of early hydrogen pickup and embrittlement and identified instability initiation sites (≤50 μm) on the E110 outer-surface oxide as early as 5 s at 1000°C following a 75-s ramp from 300°C to 1000°C. ANL modified the E110 cladding to be more similar to M5 by polishing the outer surface to 0.14-μm surface roughness and by machining-and-polishing the inner surface to give the same wall thickness (0.6 mm) as for M5. The outer-surface polishing increased the breakaway time from ≈600 s to ≈1200 s for 1000°C oxidation tests. For 1100°C and 1200°C oxidation temperatures, breakaway oxidation was not observed, and post-oxidation ductility of the ANL-modified E110 was as good as Zry-4 and M5. Etching the E110 tubing surface with HF-containing acid baths tended to exacerbate breakaway oxidation for pre-etched samples oxidized at 1000°C for a 290-s hold time. In a parallel study, pre-etched modern Zry-4, M5 and ZIRLO were oxidized at 1000°C for 2400 s. Outer-surface oxidation of these alloys was much less sensitive than E110 to pre-etching with acid mixtures containing HF. However, the inner surface of the alloys, which is rougher than the belt-polished outer surface, exhibited a superficial layer of gray monoclinic oxide following 2400 s at 1000°C. The results support the contention that the combination of higher surface roughness and etching with HF-containing acid mixtures promotes early monoclinic-oxide formation, which can reduce breakaway oxidation time. The less stable the alloy, the more significant the reduction in breakaway-oxidation time.

Although the bulk properties of E110 may certainly make the alloy unstable, the instability is initiated earlier in time by high surface roughness, by deep surface scratches, by abrupt changes in geometry, and by surface-layer impurities (e.g., F). Based on the combined work of the Russian and ANL test programs, it appears that E110 can be fabricated to behave more like Western cladding under LOCA conditions if the Kroll process is used to refine the Zircon ore (rather than electrolytic refining), if pickling is not used to clean the inner surface, and if the outer surface is belt-polished rather than pickled-and-anodized. Pickling can be used in intermediate fabrication steps if belt-polishing (OD) and grit-polishing (ID) are used as final finishing steps to mechanically remove the sub-micron layer of F and other impurities resulting from pickling.

DRAFT

This page is intentionally left blank

DRAFT